Engineering neural cells in implantable materials

Jacqueline Amanda Tickle

Thesis submitted for

Doctor of Philosophy in Neuroscience

June 2017

Keele University

Keele University

Declaration Part 1. To be bound in the thesis

SUBMISSION OF THESIS FOR A RESEARCH DEGREE

Part I. DECLARATION by the candidate for a research degree. To be bound in the thesis

Degree for which thesis being submitted **Doctor of Philosophy in Neuroscience**

Title of thesis **Engineering neural cells in implantable materials**

This thesis contains confidential information and is subject to the protocol set down for the submission and examination of such a thesis.

~~YES~~/NO [please delete as appropriate; if YES the box in Part II should be completed]

Date of submission **03-04-2017** Original registration date **26-09-2011**
(Date of submission must comply with Regulation 2D)

Name of candidate **Jacqueline Amanda Tickle**

Research Institute Name of Lead Supervisor
Research Institute for Science & Technology in Medicine **Professor D.M. Chari**

I certify that:

(a) The thesis being submitted for examination is my own account of my own research
(b) My research has been conducted ethically. Where relevant a letter from the approving body confirming that ethical approval has been given has been bound in the thesis as an Annex
(c) The data and results presented are the genuine data and results actually obtained by me during the conduct of the research
(d) Where I have drawn on the work, ideas and results of others this has been appropriately acknowledged in the thesis
(e) Where any collaboration has taken place with one or more other researchers, I have included within an 'Acknowledgments' section in the thesis a clear statement of their contributions, in line with the relevant statement in the Code of Practice (see Note overleaf).
(f) The greater portion of the work described in the thesis has been undertaken subsequent to my registration for the higher degree for which I am submitting for examination
(g) Where part of the work described in the thesis has previously been incorporated in another thesis submitted by me for a higher degree (if any), this has been identified and acknowledged in the thesis
(h) The thesis submitted is within the required word limit as specified in the Regulations

Total words in submitted thesis (including text and footnotes, but excluding references and appendices) 54668

Signature of candidate ……Date ……

Note
Extract from Code of Practice: If the research degree is set within a broader programme of work involving a group of investigators – particularly if this programme of work predates the candidate's registration – the candidate should provide an explicit statement (in an 'Acknowledgments' section) of the respective roles of the candidate and these other individuals in relevant aspects of the work reported in the thesis. For example, it should make clear, where relevant, the candidate's role in designing the study, developing data collection instruments, collecting primary data, analysing such data, and formulating conclusions from the analysis. Others involved in these aspects of the research should be named, and their contributions relative to that of the candidate should be specified (*this does not apply to the ordinary supervision, only if the supervisor or supervisory team has had greater than usual involvement*).

Abstract

A key goal in regenerative therapy is to improve outcomes following the devastating consequences of spinal cord injury. Yearly, between 250,000 to 500,000 people suffer permanent injury to the spinal cord. The cost to the individual, their families and society is substantial. Modest success in clinical trials has offered hope. However, there remain a number of challenges still to be met in respect of a combinatorial approach that offers safe delivery of grafts, to promote recovery and regeneration in the injured spinal cord.

In this context astrocytes have shown promise as a cell transplant population. This project aimed to develop strategies to engineer astrocytes to improve their repair capacity as a cell transplant population for regenerative applications. Specifically, methods were attempted using applied magnetic fields to *i*) enhance magnetic nanoparticle mediated gene delivery in primary-derived cortical astrocytes, and *ii*) achieve high levels of magnetic particle loading and long term retention in cells by tailoring particle magnetite content, improving utility for non-invasive imaging applications. Further, high cell loss during surgical delivery of transplant cells has prompted the need to develop protective cell delivery systems for neural cells. Use of a 3-dimensional collagen hydrogel was investigated for this purpose, and the capacity to image particle labelled intra-gel astrocytes evaluated.

The findings show that a tailored combination of magnetic field parameters increased transfection efficiency, and enhanced transgene expression in astrocytes. Second, astrocytes showed rapid, highly efficient but safe accumulation and long term retention of high magnetite content particles. Third, collagen hydrogels offered a protective environment conducive to cell transplant delivery. Finally, within the hydrogel, magnetic particle labelled astrocytes retained their utility for cell tracking by MRI over an extended time frame.

Contents

Abstract **I**

Contents **II**

List of tables and figures **X**

Acknowledgements **XIV**

Abbreviations **XVI**

Chapter 1 General Introduction **1**

1.1 Overview of spinal cord injury **2**

1.1.1 What is SCI? **4**

1.2 The hope from emerging cell therapy **10**

1.2.1 Cell therapies in clinical trials **16**

1.3 What are astrocytes? **22**

1.3.1 Astrocytes – origin and development in the CNS **24**

1.3.2 Astrocytes are a major player in the homeostatic function of the healthy CNS **25**

1.3.3 Astrocytes are intrinsic to neuroprotection in SCI **27**

1.3.4 Astrocytes play a major role as a transplant population for SCI **28**

1.3.5 Cortical astrocytes as a cell transplant population in injured spinal cord **36**

1.4 The need to develop better cell therapies **38**

1.4.1 The need for safe, effective genetic engineering of the cell transplant population **38**

1.4.2 The critical need to develop a means of non-invasively detecting and tracking transplant populations, fundamental to translational applications **42**

1.4.3 The low survival rate of cell transplant populations necessitates a protected cell transplant delivery system **44**

1.5 Emerging technologies offer the hope for development of better cell therapies **46**

1.5.1 Magnetic platforms as potential tools in basic and clinical neurobiology **46**

Magnetic (nano) particles are ideal candidates for delivery of therapeutic biomolecules to the spinal cord **47**

Astrocytes show efficient magnetic particle uptake **47**

Magnetic assistive technology to enhance cell:particle interaction **48**

Knowledge gaps **50**

1.5.2 3-dimensional hydrogels as potential constructs for delivery of cell transplant populations **52**

Substrate differentially affects cellular function and morphology **52**

3-dimensional constructs are beneficial to clinical application **53**

Collagen as an ideal carrier for cell transplant **53**

Knowledge gaps **57**

Chapter 2 Materials and Methods **59**

2.1 Materials **60**

2.2 Preparation of mixed glial culture and isolation of cortical astrocytes **62**

2.2.1 Preparation of mixed glial culture **62**

2.2.2 Isolation of astrocytes from mixed glial culture **62**

2.2.3 Sub-culturing of astrocytes **63**

2.3 Oscillating magnetic array device for MP-labelling of and MNP-mediated gene transfer to astrocyte monolayers **64**

2.4 MP - labelling (magnetolabelling) of astrocyte monolayers **66**

2.4.1 Particle characterisation **66**

2.4.2 Magnetolabelling of astrocytes utilising the magnefect-nano oscillating magnetic array device **68**

2.4.3 Magnetolabelling of astrocytes as monolayers in preparation for use in hydrogel constructs **69**

2.5 Processing of astrocyte monolayers **70**

2.5.1 Particle inheritance by daughter cells of dividing astrocytes **70**

2.5.2 EdU as a measure of proliferation in cell monolayers **70**

2.5.3 Termination of monolayer experiments **70**

2.6 MNP-mediated gene transfer (magnetofection) to astrocyte monolayers **72**

2.6.1 Particle characterisation **72**

2.6.2 Plasmid characteristics **72**

2.6.3 MNP-mediated gene transfer to astrocytes using the magnefect-nano oscillating magnetic array device **75**

2.7 Collagen I hydrogel experiments **77**

2.7.1 Preparation of a Collagen I hydrogel for use in supraconstruct experiments **78**

2.7.2 Supraconstruct hydrogels with MP-labelled astrocytes **80**

2.7.3 Preparation of a Collagen I hydrogel for use in intraconstruct experiments **81**

2.7.4 Intraconstruct hydrogels with MP-labelled astrocytes **81**

2.8 Processing of hydrogels **83**

2.8.1 Analysis of supraconstruct hydrogels **83**

Particle uptake **83**

Particle inheritance in daughter cells of dividing astrocytes **83**

Ultrastructural membrane features associated with endocytotic activity **83**

2.8.2 Analysis of intraconstruct hydrogels **84**

Particle uptake **84**

Intracellular features and endocytotic activity associated with particle uptake **84**

MP-5x particles as a contrast agent **84**

EdU as a measure of proliferation **85**

Viability **85**

2.9. Immunocytochemistry **86**

2.9.1 Immunolabelling of cells seeded as monolayers **86**

2.9.2 Immunolabelling of supraconstruct hydrogels **86**

2.9.3 Immunolabelling of intraconstruct hydrogels **87**

2.10 Imaging **88**

2.10.1 Imaging of cell monolayers **88**

Fluorescence microscopy **88**

Dynamic time-lapse microscopy **88**

2.10.2 Imaging of supra- and intraconstruct hydrogels **89**

Z-stack microscopy **89**

Dynamic time-lapse microscopy **89**

Field emission scanning electron microscopy of supraconstruct hydrogels **89**

Transmission electron microscopy of intraconstruct hydrogels **90**

Magnetic resonance imaging of intraconstruct hydrogels **90**

2.11 Histological analyses of culture properties **91**

2.11.1 Cell monolayer experiments **91**

2.11.2 Supraconstruct hydrogels **91**

2.11.3 Intraconstruct hydrogels **92**

2.12 Analyses of magnetic (nano) particle uptake and transfection **93**

2.12.1 Analysis of MP-labelling of astrocytes in cell monolayers and intraconstruct hydrogels **93**

2.12.2 Analysis of MNP-mediated gene transfer to astrocytes in cell monolayers **93**

2.13 Viability and proliferation assays for cell monolayers and intraconstruct hydrogels **94**

2.13.1 Cellular assessment **94**

2.13.2 MTS Assay in cell monolayer transfection experiments **94**

2.13.3 EdU proliferation assay in cell monolayers and intraconstruct hydrogels **94**

2.13.4 Cellular viability assay in intraconstruct hydrogels **95**

2.14 Statistical analyses **96**

Chapter 3 Endocytotic potential governs magnetic particle loading in dividing neural cells **97**

3.1 Introduction **98**

3.2 Objectives **102**

3.3 Experimental procedures **103**

3.3.1 Reagents and equipment **103**

3.3.2 Development of a robust methodology for quantification of particle accumulation within astrocytes **103**

3.3.3 Influence of tailoring particle magnetite content on astrocyte loading **105**

3.3.4 Studying the retention of particles over an extended time period **106**

3.3.5 Safety evaluation of procedures **107**

3.3.6 Investigating profiles of particle inheritance in daughter cells of MP-labelled astrocytes **107**

3.3.7 Immunocytochemistry **108**

3.3.8 Imaging **108**

3.3.9 Analyses **108**

3.3.10 Statistical analysis **108**

3.4 Results **109**

3.4.1 Evaluating the robustness of quantitative PI analysis **109**

3.4.2 Influence of tailoring particle magnetite content on astrocyte loading **113**

3.4.3 Studying the retention of particles over an extended time period **117**

3.4.4 Safety evaluation of long-term particle retention **120**

3.4.5 Investigating profiles of particle inheritance in daughter cells of MP-labelled astrocytes **124**

3.5 Discussion **126**

Chapter 4 Non-invasive tracking of neural cells in implantable materials **133**

4.1 Introduction **134**

4.2 Objectives **138**

4.3 Experimental procedures **139**

4.3.1 Reagents and equipment **139**

4.3.2 Establishing MP-labelled astrocyte monolayers on a collagen substrate **139**

Preparation for FESEM **139**

Modification of step-wise dehydration **140**

4.3.3 Developing an MP-labelled cellular intraconstruct hydrogel with the utility for non-invasive tracking of the neural cell population using MRI **141**

Exogenous particle-labelling approach **142**

In-situ particle-labelling approach **143**

Promoting homogeneity of cellular distribution **143**

Preparing the intraconstruct hydrogels for MRI **144**

4.3.4 Assessing cellular viability and safety of the protocols used **145**

4.3.5 Investigating cellular characteristics of cortical astrocytes in a 3-dimensional environment **146**

4.3.6 Investigation of endocytotic features associated with particle uptake **147**

4.3.7 Immunocytochemistry **148**

4.3.8 Imaging **148**

4.3.9 Analyses **148**

4.3.10 Statistical analysis **149**

4.4 Results **150**

4.4.1 Establishing MP-labelled astrocyte monolayers on a collagen substrate **150**

Pre- MP-labelled supraconstruct hydrogels show high levels of cell clumping **150**

In-situ MP-labelled supraconstruct hydrogels show high particle uptake and accumulation **150**

MP-5x particle uptake and accumulation in pre- MP-labelled versus in-situ MP-labelled supraconstruct hydrogels **153**

Results from supraconstruct gels inform the development of intraconstruct hydrogels **153**

4.4.2 Assessment of cellular viability and the safety of the protocols with intraconstruct hydrogels **155**

4.4.3 Characterisation of cellular and endocytotic features of cortical astrocytes within an intraconstruct hydrogel: comparison to astrocyte monolayers **160**

4.4.4 Endocytotic features associated with particle uptake in an intraconstruct hydrogel **166**

Ultrastructural membrane features visualised under FESEM **166**

Ultrastructural membrane and subcellular features visualised under TEM **167**

4.4.5 Development of exogenous MP-labelled cellular intraconstruct hydrogel: utility for non-invasive tracking of the neural cell population using MRI **170**

Particle inheritance in daughter cells of dividing astrocytes **172**

MP-labelled intraconstruct gel at 37 d post-construct **173**

4.5 Discussion **174**

Chapter 5 Influence of amplitude of oscillating magnetic fields on MNP-mediated gene transfer to astrocytes **181**

5.1 Introduction **182**

5.2 Objectives **186**

5.3 Experimental procedures **187**

5.3.1 Reagents and equipment **187**

5.3.2 Area and Feret's Diameter (FD) as representative measures of cell size **187**

5.3.3 MNP-mediated gene (gfp) transfer **188**

5.3.4 Investigating the correlation between MNP uptake versus transgene expression **189**

5.3.5 Pilot study: Investigating effect of coverslip depth on gene (gfp) transfer **189**

5.3.6 Magneto-multifection MNP-mediated gene (gfp) transfer **190**

5.3.7 Investigating proportions of cells showing repeat uptake **191**

5.3.8 Immunocytochemistry **191**

5.3.9 Imaging **191**

5.3.10 Analyses **191**

5.3.11 Statistical analysis **192**

5.4 Results **193**

5.4.1 Measure of cell size to inform amplitude parameters **193**

5.4.2 Pilot study: Investigating effect of coverslip depth on gene (gfp) transfer **194**

5.4.3 Safety assessment of MNP-mediated gene (gfp) transfer to astrocytes **196**

5.4.4 Influence of amplitude of oscillating magnetic fields on MNP-mediated gene (*gfp*) transfer to astrocytes **199**

5.4.5 Safety assessment of magneto-multifection MNP-mediated gene (*gfp*) transfer to astrocytes **202**

5.4.6 Magneto-multifection MNP-mediated gene (*gfp*) transfer **205**

5.4.7 Correlation between MNP-uptake and transgene expression **208**

5.5 Discussion **210**

Chapter 6 Future direction and concluding comments **217**

6.1 Summary of key research findings **218**

Chapter 3 Endocytotic potential governs particle uptake in dividing neural cells **218**

Chapter 4 Non-invasive tracking of neural cells in implantable materials **219**

Chapter 5 Influence of amplitude of oscillating magnetic fields on MNP-mediated gene transfer to astrocytes **219**

6.2 Future direction **221**

6.3 Concluding comment **226**

References **227**

Appendices **247**

Appendix 1 EdU protocol **248**

Appendix 2 Tickle et al., 2015 Influence of amplitude of oscillating magnetic fields on magnetic nanoparticle-mediated gene transfer to astrocytes **249**

Appendix 3 Tickle et al., 2016 Endocytotic potential governs magnetic particle loading in dividing neural cells: studying modes of particle inheritance **250**

List of tables and figures

Chapter 1 General Introduction

Tables

1.1 Cell Therapies in Rodent SCI Models **13**

1.2 American Spinal Injury Association Classification Criteria for SCI **19**

1.3 Astrocyte Cell Transplant Studies in Rodent SCI Models **29**

Figures

1.1 Characterisation of the different regions of the spinal column and the areas of the body affected by spinal cord injury to that region **4**

1.2 The metabolic relationship between astrocytes and neurons in the adult brain **23**

Chapter 2 Materials and Methods

Tables

2.1 Physical characterisation of magnetic particles **68**

Figures

2.1 Schematic diagram of magnefect-nano oscillating magnetic array device (NanoTherics, UK) **65**

2.2 Transmission electron micrographs of the MP-0x – MP-5x particles **67**

2.3 pmaxGFP plasmid map **74**

2.4 Structural composition of collagen I hydrogel substrate **77**

2.5 Schematic of Collagen I hydrogel construct **79**

2.6 Schematic outlining the two approaches used in MP-5x labelling of supraconstruct hydrogels **80**

2.7 Schematic of z-stack imaging through an intraconstruct hydrogel **92**

Chapter 3 Endocytotic potential governs magnetic particle loading in dividing neural cells

Figures

3.1 Development of parameters for PI analysis **104**

3.2 Schematic illustrating the transfer of coverslips **106**

3.3 Intracellular particle density in individual cells was assigned a PI value and categorised according to the semi-quantitative method of ‘low’, ‘moderate’ or ‘high’. The PI value was then binned according to its corresponding category. **110**

3.4 Intracellular particle density measured using semi-quantitative visual analysis and quantitative PI analysis **111**

3.5 Culture characteristics of MP-labelling of astrocytes **114**

3.6 MP-labelling of astrocytes at 4 h and 24 h post-particle exposure, with and without magnetic field application **116**

3.7 Larger wells facilitate the spread of astrocytes from the coverslip onto the base of the well plate **117**

3.8 Long-term particle retention following 30 min application of an oscillating magnetic field **119**

3.9 Cellular viability evaluation of long-term particle retention in astrocytes *in vitro* **121**

3.10 Identification of pyknotic cells in astrocyte cultures **123**

3.11 Particle inheritance in MP-labelled astrocytes **125**

3.12 Factors influencing cellular particle uptake **131**

Chapter 4 Non-invasive tracking of neural cells in implantable materials

Figures

4.1 A schematic outlining the formation of an intraconstruct hydrogel **141**

4.2 A schematic outlining formation of an exogenous MP-labelled intraconstruct hydrogel **142**

4.3 Schematic of modified paddle spatula and transfer technique **144**

4.4 Characteristic morphologies of cortical astrocytes **146**

4.5 Pre- MP-labelled supraconstruct hydrogels over 14 days **151**

4.6 In-situ MP-labelled supraconstruct hydrogels over 14 days **152**

4.7 Viability assessments show a high level of cellular viability and safety of protocols over time **156**

4.8 Safety assays show homogenous nature of cellular distribution in gels over time **157**

4.9 Gels show contraction of size over time **159**

4.10 Intraconstruct hydrogels at 14 d post-construct **160**

4.11 Cortical astrocytes grown within a 3-dimensional hydrogel show morphological characteristics different to that of astrocyte monolayers cultured on glass **162**

4.12 Comparative measures of cells grown in either a 2- or 3-dimensional environment show significant differences in morphology **165**

4.13 Ultrastructural membrane features of cortical astrocytes **166**

4.14 A number of endocytotic features were observed, associated with particle uptake and trafficking **168**

4.15 MP-5x labelled astrocytes within intraconstruct hydrogels provide a hypointense signal under MRI **171**

4.16 Particle inheritance between daughter cells of dividing astrocytes **172**

4.17 Hypointense signal recorded from MP-5x labelled cells within intraconstruct hydrogels at 37 d post-construct **173**

Chapter 5 Influence of amplitude of oscillating magnetic fields on MNP-mediated gene transfer to astrocytes

Figures

5.1 Schematic of experimental setup investigating effect of coverslip depth on gene transfer **189**

5.2 Schematic of time course of magneto-multifection protocol **190**

5.3 Measure of cell size **193**

5.4 Effect of coverslip depth on gene (*gfp*) transfer **195**

5.5 Influence of amplitude on proportions of astrocytes and on astrocyte phenotype **197**

5.6 Cell viability analyses report no acute toxicity **198**

5.7 Influence of amplitude of oscillation on transfection efficiency and extent of transgene expression in astrocytes **200**

5.8 Safety assessment of magneto-multifection protocols **203**

5.9 Magneto-multifection and transfection efficiency **206**

5.10 Relationship between particle uptake and transgene expression **209**

5.11 Schematic illustrating the putative interaction between cell cycle dynamics and MNP-mediated gene transfer **214**

Chapter 6 Future direction and concluding comments

Tables

6.1 Barriers to recovery and proposed mechanism **221**

Acknowledgements

If there be any good thing that you can do, any kindness that you can show – do it now – for you will not pass this way again.

The ultimate goal in regenerative therapy is that of overturning the devastating consequences of spinal cord injury. It has been a privilege to undertake this research. I hope it counts.

Research is often referred to as a 'body of science'. There is good reason for this; as scientists we collaborate - we work independently and yet remain dependent on the work of others to focus and challenge our research. No one part of the body can function independently of the other. In the same manner, this thesis would not have been possible without the assistance, support and guidance generously given by those infinitely more knowledgeable than I.

First and foremost, I owe a debt of gratitude to my supervisors, Professor Divya Chari and Dr. Mark Pickard, without whom I would not have had this opportunity to study for my PhD – thank you, for everything along the way, thank you.

Professor Dave Furness and Professor Carole Hackney – you gave me the opportunity to take this path and inspired me to do great things and I thank you.

I also wish to thank the Faculty of Health and the Post Graduate Research Committee for their assistance with funding throughout this time. I am very grateful. I also wish to acknowledge Dr. Boris Polyak for providing the magnetic particles evaluated in this research; Professor Harish Poptani and Dr. Arthur Taylor of the University of Liverpool for the magnetic resonance imaging of the intraconstruct hydrogels, and Dr. Joshua Price for the confocal imaging of the intraconstruct hydrogels.

For Dr. Stuart Jenkins, there has to be a special mention – you have been my mentor (and me, your tormentor!). You have trained me as a scientist and modelled the three most important qualities required – thoroughness, conscientiousness, and humour when it all goes wrong – you have trained this Padawan well, Obi-Wan.

A special thank you also to Mrs. Karen Walker for your help, guidance and seemingly infinite patience with electron microscopy, and without whose help, chapter 4 would not be a part of this thesis.

My friends and colleagues at Keele, you have welcomed me into the wonderful world of research. Thank you to Síls and Alinda – lovely ladies and fabulous friends. Thank you Alinda, for proof-reading chapter 5. Thank you to Arwa, my friend and colleague for your knowledge, wisdom and kindness, and thank you to Noor and Ysr for filling our office with beautiful pictures and supporting us with your patience.

James (a 'truepenny' and a fellow scholar to boot), Andrew (you indulged my penchant for Latin), Alan (a patient, skilled scientist from whom I learned much), Janet (where would I be without you), Sarah (a true friend), Lyns & Doug, Lynne & Tobias, Chris, Tim, Rawaa – friends one and all. Your friendship has kept me sane throughout.

And to my family go my greatest, heartfelt thanks. My sons and my gorgeous daughters-in-law - Leigh & Ali, Craig & Gemma – I am truly blessed.

And to my gorgeous (long-suffering) husband Pete. Thank you, a thousand times thank you! Your support, love, encouragement and sheer bravery at bowling along with this fiery, passionate, crazy redhead means the world to me – grow old with me Pete, the best is yet to come.

Thank you to my Mum; you have always believed in me and encouraged me to keep going. And to my Dad, although you've not seen me achieve any of this - you were the instigator of it all. Nean, John, Jess and Jo – you have surrounded me with love and hugs and brought me my own special little mug for the endless cups of tea, thank you!

Thank you to Nean and Johnnie B. for proof-reading my chapters – your diligence and keen eye have prevented many a mistake. Errors that remain, dear reader, are mine.

Linda, you helped me find my voice … there are not enough words.

Lord, you have blessed me beyond measure, I stand in awe.

- Nunc est bibendum, nunc pede libero pulsanda tellus –

Now is the time to drink, now the time to dance footloose upon the earth

- Homer

Abbreviations

AAV	adeno-associated viral vector
ANOVA	analysis of variance
BDNF	brain-derived neurotrophic factor
BFGF	basic fibroblast growth factor
BLBP	brain lipid binding protein
BMP	bone morphogenetic protein
BSA	bovine serum albumen
Ca^{2+}	calcium
$CaCl_2$	calcium chloride
Cdc2	cell division cycle 2
CNS	central nervous system
CNTF	ciliary neurotrophic factor
CPD	critical point dryer
CSPGs	chondroitin sulphate proteoglycans
DAPI	4',6-diamidino-2-phenylindole
dH_2O	deionised water
DIV	days in vitro
DMEM	Dulbecco's modified eagle's medium
DNA	deoxyribonucleic acid
ECM	extra cellular matrix
EDU	5-ethynyl-2´-deoxyuridine
ERK	extracellular signal regulated kinase
ESCs	embryonic stem cells
ETOH	ethanol
F	frequency
FBS	foetal bovine serum
FD	Feret's diameter
FESEM	field emission scanning electron microscope
FITC	fluorescein isothiocyanate
FTIR	fourier transform infrared spectroscopy
GABA	γ-aminobutyric acid
GDNF	glial cell-line derived neurotrophic factor

GFAP	glial fibrillary acidic protein
GFP	green fluorescent protein
GLAST	glutamate transporters
GLT	glutamate
GM-1	monosialotetrahexosylganglioside
GRP	glial restricted precursor cell
(h)GPC	human glial restricted progenitors
(h)GRP	human glial restricted precursor
(h) iPSC	human induced pluripotent stem cell
ID	integrated density
iPSC	induced pluripotent stem cells
K^+	potassium
LV	lentiviral vector
MCT	multiple comparison test
MEM	modified eagle's medium
M-Mfect	magneto-multifection
MNPs	magnetic nanoparticles
MP	magnetic particles
MPRED	Methylprednisolone
MRI	magnetic resonance imaging
MSCs	mesenchymal stem cells
MTS	3-(4,5-Dimethylthiazol-2-yl)-5-(3-carboxymethoxyphenyl)-2-(4-sulphophenyl)-2H-tetrazolium, inner salt
Na^+	sodium
NaOH	sodium hydroxide
NdFeB	neodymium iron boron
NDS	normal donkey serum
NF	no field
NINDS	*National Institute of Neurological Disorders and Stroke*
NRP	neuron restricted precursor cells
NSCs	neural stem cells
OECs	olfactory ensheathing cells
OPCs	oligodendrocyte precursor cells
PBS	phosphate buffered saline

PDL	poly-D-lysine
pDNA	plasmid deoxyribonucleic acid
PFA	paraformaldehyde
PI	pixel intensity
PLA	poly lactic acid
PVA	poly vinyl alcohol
RFP	red fluorescent protein
RGB	red; green; blue
RT	room temperature
RV	retroviral vector
SCI	spinal cord injury
TEM	transmission electron microscopy
WHO	World Health Organisation

Chapter 1
General Introduction

1.1 Overview of spinal cord injury

There are at present, approximately 2.5 million people globally affected by spinal cord injury (SCI). Up to 200,000 people are affected each year, with an incidence rate of 16 per million in Western Europe, of which 40,000 occur in the UK. Of these numbers globally, approximately 82% are male (*Fitzharris et al., 2014; Lee et al., 2014*). The major causes of SCI are motor accidents, falls (work or sport-related), or the result of violent attacks [*Lee et al., 2014*; *World Health Organisation, 2013*(*WHO*)]. The severity of the injury determines the long-term outcome. Incomplete injury, where the spinal cord has sustained moderate bruising (contusion) or pressure (compression), has a greater chance of recovery. Complete injury refers to full or partial severance of the spinal cord, and results in loss of sensory and motor function (paralysis) below the level of injury. Classification of the severity of SCI is scored according to the American Spinal Injury Association (ASIA), with function evaluated on a score of A –E [A refers to a complete loss of sensory/motor function below sacral level 4/5; E refers to normal levels of function (*Table 1.2*)]. Coincident with paralysis are a range of secondary pathologies, such as the inability to breathe unaided, the loss of urinary and bowel control, the inability to control body temperature, the loss of sexual function and the onset of continual chronic pain in the paralysed limbs [*National Institute of Neurological Disorders and Stroke, 2016* (*NINDS*)]. The cost of ongoing treatment in the US alone is approximately $3 billion each year with the cost of treatment, in the US, averaging $105 – 400,000 over a patient's lifetime (*NINDS, 2016*). Not every country provides excellent health care provision, or health care that is free at the point of use; irrespective the overall cost of health care, assisted living and assistive aids is mostly met by the patient and their family. Even where access to excellent health care is guaranteed, the mortality rate is much higher for those living with a SCI (*WHO, 2013*). The severity of this type of injury, coupled with the unlikely probability

of subsequent regeneration and neurological recovery, places a substantial emotional and financial burden on the patient and their families, with an ever increasing socio-economic cost.

1.1.1 What is SCI?

SCI is classified by type (contusion, compression or crush); location and extent (complete or incomplete), with the majority of SCI occurring in the cervical and thoracic regions and therefore, these are the focus of SCI models (*Siebert et al, 2015*) (*Figure 1.1*).

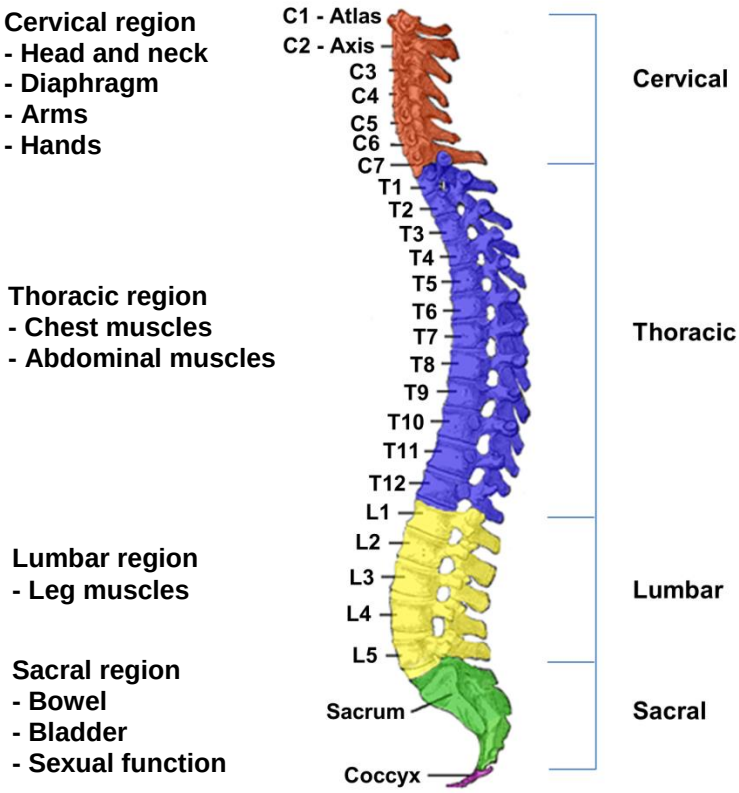

Figure 1.1 Characterisation of the different regions of the spinal column and the areas of the body affected by spinal cord injury to that region *The spinal column is made up of a continuous length of vertebrae that surround and protect the spinal cord. Severe impact to the spine risks damage to the cord, with the possibility of permanent paralysis below the level of injury. Severe damage to the spinal cord at the thoracic level results in paraplegia (trunk and lower limbs), with damage at the cervical level resulting in tetra- or quadriplegia (upper and lower body) (Figure adapted from www.spinal-research.org).*

Axonal rupture in SCI tends to be located at the nodes of Ranvier, as these are the weakest point in the spinal cord due to non-myelination of the axon (*Maxwell, 1996*). Rapid extracellular Ca^{2+} influx activates phospholipase A_2 which is a Ca^{2+}-dependent enzyme involved in modulation of inflammation and "host defence" (*Murakami & Kudo, 2002*). This triggers re-sealing of the cut end of the axon (*Yawo & Kuno 1985*). Ca^{2+} also determines whether the damaged end develops into a functional growth cone or a non-functioning end bulb (*Kamber et al., 2009*). Different responses occur at either end of the severed axon. While the distal end degenerates, chromatolysis (disintegration of the Nissl bodies) occurs at the proximal end, with the nucleus moving to the periphery of the neuron cell body (*Kandel et al., 1991*). Injury to the spinal cord initiates an immediate graded neuroinflammatory response from neutrophils, macrophages and microglia; a response that continues over a number of months. It is this response that triggers reactive astrogliosis. Reactive astrocytes become hypertrophic and upregulate glial fibrillary acidic protein (GFAP) expression, leading to extensive proliferation and overlapping of the astrocyte matrix, resulting in formation of a glial scar (*Fawcett & Asher, 1999*).

This glial scar forms a barrier which effectively seals the, by now, hypoxic injury site, preventing widespread inflammation, cell necrosis and neurite outgrowth into the surrounding healthy tissue. Moreover, dependent on the severity of the SCI, fibroblast infiltration can result in a dense fibrous scar that has a greater inhibitory effect on regeneration than the glial scar itself, due to its density and proclivity in binding "growth inhibitory molecules" (*Macaya & Spector, 2012*). Loss of oligodendrocytes following injury results in neuron demyelination, resulting in lack of myelin support for regenerating axons and a release of growth inhibitors from the degrading myelin (*Hannila & Filbin, 2008; Mukhopadhyay et al., 1994*). The high level of chondroitin sulfate proteoglycans (CSPGs) within the injury site, also act as inhibitors for axonal regrowth by activating the

RHO-Rock inhibitory signalling cascade, which causes growth cone collapse and subsequent retraction, effectively halting neuronal regeneration (*Siebert et al., 2015*). Over time the lesion site develops into a fluid-filled cyst called a syrinx, and together with the tightly meshed astrocytic scar, prevents axonal ingrowth, limiting regenerative capacity (*Norenberg et al., 2004; Goetz & Mummanemi, 2015*). **This remains the biggest challenge in spinal cord repair.** Even if axonal ingrowth beyond the scar tissue were possible, the void within provides no trophic or structural support for regenerating axons. Indeed, degeneration continues beyond the initial response to injury, with infiltration of Schwann cells (SCs) into the injured spinal cord over the following 6-12 months, causing pain and spasticity alongside the paralysis (*Macaya & Spector, 2012*).

Beyond inflammation and the astroglial scar lie further difficulties. Descending axonal tracts are dependent on activity from corticospinal motor circuits for their initial development. Following SCI, the severing of these pathways result in loss of voluntary motor skills, thus, the potential for regeneration is limited as the bi-directional circuits that corticospinal pathways depend on, are now no longer active. Further, prolonged motor inactivation results in subsequent axonal withdrawal (*Martin, 2016*). The incomplete nature of the majority of SC injuries can, however, result in some sparing of these pathways (*Raineteau & Schwab, 2001*). It is increasingly postulated that reorganisation of these pathways (i.e. synaptic plasticity) may be the underlying cause behind the 'spontaneous functional recovery' (*Renault-Mihara et al., 2008*) seen in the immediate timeframe following SCI (*Nakagawa et al., 2015*), and recovery seen following cell transplant, where regeneration of severed pathways was absent (*Yamamoto et al., 2009*).

Nevertheless, full functional recovery is rare, with the glial scar, the syrinx void, the high prevalence of axonal growth inhibitors and the subsequent infiltration of

peripheral neural cells, all contributing to the non-regenerative environment of the injured spinal cord.

Initial interventions to alleviate the severity of SCI involve decompressive surgery to relieve pressure on the spinal cord from internal haemorrhaging and leaking of cerebrospinal fluid. Vasopressors and intravenous crystalloids are administered to increase blood pressure, thus ensuring an adequate blood supply. Intravenous delivery of corticosteroids act as anti-inflammatory agents, working to reduce inflammatory factors and Ca^{2+} influx, and facilitating increased blood flow to the spinal cord (*Ahuja et al., 2016*). The most commonly used anti-inflammatory is methylprednisolone (MPRED), which also acts to promote survival of endogenous tissue through decrease of oxidative stress (*Ahuja et al., 2016; Silva et al., 2014*). This particular corticosteroid has been shown in numerous clinical trials to improve outcomes if administered within 8 h of injury (*see Bracken, 2012 for review*). However, the use of MPRED has proved controversial due to its serious side effects, most notable of which is sepsis, with high infection rates reported primarily in the wound site due to avascular necrosis, but also in the respiratory and urinary tracts (*Matsumoto et al., 2001; Suberviola et al., 2008*). "Worsening neurological function" (*Hurlbert, 2000*), and alteration to the immune response have also been reported with high doses of MPRED (*Galandiuk et al., 1993*).Therefore stringent guidelines have been devised on the rate and dose of delivery (*Silva et al., 2014*), although its use is still considered as standard care for initial intervention in SCI (*Pandya et al., 2010*). In order to develop a safe, effective pharmacological agent, other drugs have been subjected to clinical trials, for example monosialotetrahexosylganglioside (GM-1; formulated under the brand name Sygen®). Use of this drug reported a small improvement in bowel and bladder function, and increased safety in its use (*Geisler at el., 2001*), although the level of improvement reported with the use of GM-1 was not sufficient to continue clinical trials.

The authors argued that greater benefit would have been seen had GM-1 been administered within an earlier timeframe. As it was MPRED was administered within 8 h of injury (as standard intervention), with GM-1 administered approximately 55 h later (*Hawryluk et al., 2008*). However, findings prior to the Geisler study raised concerns regarding the drugs immunogenic potential and its associated link with Guillain-Barré syndrome (*Bradley, 1990; Lacomblez et al., 1989; Nagai et al., 1976; Yuki et al., 1991*), resulting in its eventual withdrawal from market pending Phase III trials. Hence, as yet, no drug offers similar clinical benefit as MPRED. The side effects associated with its use though, have raised the suggestion that a delivery system utilising nanoparticles (*Cerqueira et al., 2013)* may facilitate a targeted, slower rate of delivery to the injury site, thus circumventing the side effects related to the high therapeutic dose of MPRED (*Silva et al., 2014*).

Following the initial medical intervention, once the patient is stabilised, the main priority is mobilisation. This involves aggressive rehabilitation therapy to, at the very least, strengthen muscles (*Behrman & Harkema, 2000*), but has also been shown to exert beneficial effects on functional recovery (*Sandrow-Feinberg & Houle, 2015*). In this respect, it is hypothesised that manual manipulation i.e. through aggressive rehabilitation therapy, and/or neural stimulation of motor circuits (*Song et al., 2016*), may induce synaptic plasticity in the spared pathways, resulting in localised sprouting and new connections (*Oudega & Perez, 2012*); any level of functional recovery however, is very much dependent on the location and the severity of the injury (*Fink & Cafferty, 2016 for review*).

Rehabilitation training will almost certainly involve the teaching of communication skills, together with fine motor skills and coping strategies for bladder/bowel toileting, and management of spasticity and chronic pain (*Ahuja et al., 2016; NINDS, 2016*). **While these interventions are critical for the management of SCI, in that they are aimed at**

limiting the initial damage and increasing quality of life, in the majority of SC injuries, they unfortunately lack the potential to promote regenerative processes in the injured cord.

1.2 The hope from emerging cell therapy

Research into overturning the outcome of SCI goes back over a century (*Thompson, 1890*), with many aspects of the injury 'cascade' targeted in pursuit of repair. The role of the astrocytic scar has long been in dispute as to its 'neuro-preventative' or neuroprotective role in SCI. The barrier formed by the glial scar, their release of CSPGs to halt neuronal regeneration and the resultant void within the injury site (*Goetz & Mummanemi, 2015; Norenberg at el., 2004; Siebert et al., 2015*) proposed the glial scar as an inhibitory force preventing axonal regeneration (*Liuzzi & Lasek, 1987*). While this is indeed so, what has traditionally been perceived as a negative event is beginning to be understood as a major neuroprotective feature within SCI to prevent widespread injury (*Sofroniew, 2015*). For example, using a transgenic mouse model that expressed GFAP-herpes simplex virus-thymidine kinase transgene, following moderate crush or stab injury to the spinal cord, anti-viral agent ganciclovir was administered to ablate reactive "transgene-expressing" astrocytes, thus preventing formation of the glial scar. Injury was followed by blood-brain-barrier failure, demyelination, tissue damage, cell death and subsequent motor impairment. By contrast, where ganciclovir was not administered, the subsequent formation of a glial scar following similar injuries, resulted in low levels of SCI and only temporary motor and functional impairment (*Faulkner et al., 2004).* Following the same protocol, a further study from this group caused a severe crush injury in the same transgenic mouse model, and compared the resulting consequences between mice where ganciclovir was administered to ablate reactive astrocytes and prevent scar formation, and control transgenic mice where a glial scar was allowed to form. The findings showed that, following severe SCI, there was no difference to the level of tissue loss and cell death (*Myer et al., 2006*). Taken together, the findings of these studies advocate the neuroprotective role of the glial scar, but suggest this protection is limited by the severity of the injury in that, with moderate SCI, reactive

astrocytes and the subsequent formation of the glial scar played a major neuroprotective role. However, in the severe SCI mice, there was little further tissue damage in the absence of reactive astrocytes, than that occasioned in the control mice where a scar was allowed to form, suggesting that where injury is severe, little can effectively be done to *limit* the damage (*Faulkner et al., 2004; Myer et al., 2006*). In support of these findings, recent *in vivo* studies using differing transgenic strategies, either prevented or attenuated astrocyte reactivity following induced severe thoracic (T10) crush injury, or 5 weeks after such injury, ablated the scar tissue. Subsequent delivery of hydrogels loaded with axon-specific growth factors neurotrophin-3 (NT-3 - proven to be beneficial to regeneration of injured spinal cord axons) and brain-derived neurotrophic factor (BDNF - shown to promote regeneration of spinal cord tracts) to the lesion site, stimulated robust axonal growth across the glial scar, but only in mice where a scar was allowed to form. Where scar formation had been modified, initial axonal dieback was significantly increased compared with control wild-type mice, and despite delivery of NT-3/BDNF – loaded hydrogels, there was no axonal regrowth at all. Moreover, prevention and attenuation of reactive astrocytes increased the level of CSPGs in the lesion site, with the increase associated with influx of non-GFAP^{+ve} cells. The study reported that contrary to being perceived as a barrier to regeneration, reactive astrocytes and the subsequent presence of the glial scar are proactive in neuroprotection through inhibition of overall CSPG expression, and continued expression of molecules supportive to axonal growth (*Anderson et al., 2016*). These findings reinforce the neuroprotective role of the astrocytic response and, more importantly the continuing protective role of astrocytes within the lesion site (*discussed further in 1.3.3*). Thus, it is proposed that the target for regeneration is not the inhibition of the astrocytic response within the injured spinal cord, but rather in facilitating an environment within the void that is conducive to regeneration. **In this respect, a key point to note in**

transplant strategies is that cell transplant does not infer the capacity to replace damaged cells, but rather, to facilitate a regenerative environment through the neuroprotective and immunomodulatory mechanisms inherent within the transplant (*Li & Leung, 2015*). Further, it is postulated that these mechanisms may also confer a more advantageous environment for synaptic plasticity in spared pathways.

In a bid to promote this, research has targeted the lesion site. A diverse number of strategies have shown promise, including use of chondroitinase ABC to neutralise the inhibitory effects of CSPGs, and antibody IN-1 to neutralise Nogo. Anticancer drugs have been found to aid in stimulating axonal regeneration, as have specific molecular signalling targets, transcription factors and neurotrophic factor supplements (*Siebert et al., 2015 for review*). In an endeavour to promote neuronal regeneration, functionalised scaffolds containing proteins that neutralise axon inhibitors have also seen modest success in axonal regrowth, and subsequent motor locomotion (*Li et al., 2016*). These strategies hold promise. However the probability of one type of strategy being sufficient for regeneration is unlikely, the greater likelihood being that of a combinatorial approach, of which this would play a part. For example, genetic engineering of cell transplants to deliver therapeutic biomolecules or growth factors to an injured spinal cord, and utilising a scaffold to act as a carrier for delivery of such a cell transplant.

To address this challenge, cell replacement therapies have become a key strategy (*Willerth & Sakiyama-Elbert, 2008*). The difficulty here is in choosing the cell population that offers the most potential for regeneration within the injured spinal cord. The criteria for such a therapy are *i)* cell integration into the lesion site that *ii)* encourages axonal ingrowth, and *iii)* offers both trophic and structural support to the regenerating neurons. In this respect, a number of cell types have been tested in animal studies and shown modest success (*Table 1.1*).*

Table 1.1 Cell Therapies in Rodent SCI Models				
Cell transplant population	**Injury model**	**Combinatorial approach**	**Outcome**	**Study**
(h) Adult bone marrow-derived multipotent progenitor cells (BMmPCs)	Thoracic contusion (T8) – rat	-------	IV delivery of BMmPCs 24 h following SCI had immunomodulatory effect, decreasing inflammation and modulating macrophage activation. BMmPCs targeted the spleen rather than the site of injury, resulting in a marked increase of spared SC tissue, and improved urinary and locomotor recovery	DePaul et al 2015
Neural stem cells (NSCs)	Thoracic contusion – rat	-------	Neurogenesis within the SC; improved fore limb movement	Ogawa et al., 2002
	Thoracic contusion (T9-10) – rat	(h)NSCs + Olig2 differentiated into OL in vivo and in vitro prior to transplant	(h)NSCs differentiated into OL in vivo; however, (h)NSCs differentiated prior to transplant showed protective & restorative effect on myelin; migration from lesion; improved hind limb function	Hwang et al 2009
	SC lesion – mice	NSCs + BMP signalling inhibitor resulting in expression of Noggin	Inhibition of BMP facilitated differentiation into neurons, OL & astrocytes; improved functional recovery	Setoguchi et al 2004
Mesenchymal stem cells (MSCs)	Thoracic contusion (T10-11) – rat	-------	Improved hind limb function	Karaoz et al 2011
	Hemi-sected SC- rat	MSCs/BMCs	Reduced lesion size; faster recovery (MSCs/BMCs); improved function with MSCs c/w BMCs	Syková et al 2006
	Compression lesion (T8-9) - rat	-------	Cell migration to lesion site; improved function	Syková & Jendolová 2005

Table 1.1 Cell Therapies in Rodent SCI Models				
Cell transplant population	**Injury model**	**Combinatorial approach**	**Outcome**	**Study**
Oligodendrocyte progenitor cells (OPCs)	Thoracic contusion – rat	MRF-expressing OPCs & SchCs	Increased myelination; addition of MRF stimulated differentiation into OL; improved locomotor function	Xie et al 2016
	Thoracic (T8-T11) contusion – rat	(h)ESC-derived OPCs	Differentiated into OL in SC; migrated; enhanced remyelination; improved locomotor function	Keirstead et al 2005
	Cervical contusion (C5) - rat	(h) ESC-derived OPCs	Protective effect on motor neurons; improved fore limb function	Sharp et al 2010
Olfactory ensheathing cells (OECs)	Cervical lesions (C1-2) - rat	Mucosal OECs	Restoration of fore limb retrieval associated with localised axon sprouting	Yamamoto et al 2009
	Upper cervical lesion Cervical hemi-section - rat	-------	Migrated from graft into host SC; functional recovery of fore-paw retrieval task; climbing & respiratory function	Li et al 1998;2003;2004
	Transected spinal cord (T8-9) – rat	-------	Motor axonal regeneration over long distances; improved locomotor and sensory function	Ramon-Cueto et al 2000
	Contusion and transected SC – rat	-------	Increased nerve innervation; improved locomotor function	Sun et al 2005

Table 1.1 Cell Therapies in Rodent SCI Models				
Cell transplant population	**Injury model**	**Combinatorial approach**	**Outcome**	**Study**
Schwann cells (SchCs)	Thoracic contusion (T8) – rat	SchCs & cAMP & Rolipram	Promoted axon sparing & myelination; improved locomotor function	Pearse et al 2004
	Thoracic contusion (T8-9) – rat	SchCs & OECs	Low cell survival rate; endogenous SchCs influx; combinatory therapy reported increased locomotor ability c/w control	Pearse et al 2007
	Transected SC - rat	SchCs & BFGF-2	Increased neuronal survival with addition of BFGF-2; no axon regeneration or functional recovery	Meijs et al 2004
	Transected SC - rat	SchCs in hydrogel	Axonal regeneration; improved hind limb locomotion	Williams et al 2015
	Demyelinated SC lesion –rat	SchCs & OECs	Cells retained ability to remyelinate	Dunning et al 2004
	Thoracic contusion (T9) - rat	SchCs/OECs	Greater myelination, migration & improved hind limb function with SchCs c/w OECs	Takami et al 2002

Abbreviations

BFGF-2 basic fibroblast growth factor
BMCs bone marrow cells
BMmPCs bone marrow-derived multipotent progenitor cells
BMP bone morphogenetic protein
cAMP cyclic adenosine monophosphate
c/w compared with
(h)ESCs human embryonic stem cells
IV intravenous
(h)NSCs human neural stem cells
MRF myelin gene regulatory factor
MSCs mesenchymal stem cells
NSCs neural stem cells
OECs olfactory ensheathing cells
OPCs oligodendrocyte progenitor cells
OL oligodendrocytes
SC spinal cord
SchCs Schwann cells

** This table refers to the main cell types used, and is an illustrative, and by no means exhaustive, list.*

Of the animal studies, of note is the intravenous delivery of bone marrow-derived multipotent progenitor cells (BMmPCs) to rodents with thoracic contusion SCI (*De Paul et al., 2015*). Interestingly, the cells did not home to the injury site but instead, targeted the spleen. The authors concluded that the recovery observed in these animals was not due to cell 'replacement', but rather to the neuroprotective and immunomodulatory benefits induced by the transplant population, with recovery associated with marked sparing of the tissue in the SC (*De Paul et al., 2015*). These findings could suggest a greater role for cell transplant strategies than has been initially perceived.

Not all cell transplant populations have been found to be advantageous to regeneration though. Transplant of undifferentiated NSCs in the injured spinal cord have revealed that the lesion site is non-conducive to stem cell expression (*Cao et al., 2010; Teng et al., 2009*); a limiting factor in neuronal repair. More recent studies have found that NSC transplants migrate from the lesion site and begin to proliferate in an uncontrolled manner throughout the spinal cord, highlighting an ever-increasing concern for prospective tumorigenesis with this cell type (*Steward et al., 2014*). Indeed, for translational application, the use of *undifferentiated* stem cells is being increasingly deemed unfit for purpose, as the developmental signals that would drive typical stem cell differentiation are absent in the adult CNS (*Dunnett & Rosser, 2014*).

1.2.1 Cell therapies in clinical trials

Certain cell therapies have been utilised in clinical trials, such as Schwann cells (SchCs - *Saberi et al., 2008);* olfactory ensheathing cells (OECs - *Granger et al., 2012; Tabakow et al., 2014*); mesenchymal stem cells (MSCs - *Dai et al., 2013*) and bone marrow cells

(BMCs - *Syková et al., 2006*) with others, such as oligodendrocyte precursor/progenitor cells (OPCs - *Li & Leung, 2015*) currently recruiting for phase I/II clinical trials (*Asterias Biotherapeutics, Inc., 2016).* Variable success rates have been reported. SchCs have been regarded as safe for transplant, but their inability to migrate beyond the lesion site has resulted in low levels of success (*Pearse et al., 2004; Xu & Onifer, 2009*). The majority of animal studies found that utilising SchCs *in a combinatorial approach* offered higher levels of regeneration and improvement in functional recovery (*Pearse et al., 2004; 2007; Takami et al., 2002*). Of their use in clinical trials in patients with chronic thoracic or cervical SCI (ASIA grade A-B), a 2-year follow up study reported no toxicity with SchC transplant; "subtle" improvement in light touch/pinprick, but no gain in ASIA score. While some patients reported bladder and sphincter sensation, with two patients reporting a level of faecal control, SchC transplant was found to be ineffective in functional recovery and for 3 of the 33 patients, actually worsened the symptoms (*Saberi et al., 2008; 2011*).

In recent years, clinical studies transplanting OECs have reported promising results, with restoration of fore-hind leg co-ordination in dogs with severe SCI (*Granger et al., 2012*). OEC transplant to a patient with complete transected spinal cord resulted in restoration of "trunk stability", touch sensitivity, visceral sensation and improved blood flow to the lower limbs. Of major consequence, a level of voluntary lower body movement was recovered, with evidence of long tract restoration (*Tabakow et al., 2014*). This is the first reported clinical evidence of long tract restoration; all other studies of functional recovery have reported only short tract axonal sprouting, interestingly even with OECs (*Granger at el., 2012*).

A number of mechanisms are suggested for OECs success in SCI. One is their migratory capacity. It is thought that they migrate alongside growing axons and therefore, as they have been shown to ameliorate the astrocytic response and subsequent CSPG expression

(*Takami et al., 2002*); OECs modulate the non-permissiveness of the spinal cord lesion (*Xu & Onifer., 2009*). This 'mechanism' could offer plausible explanation for long tract restoration. Results such as these, while highly promising, are moderated by the low overall success rate, with a number of earlier studies reporting no benefit at all, with considerable doubts surrounding claims of success (*Hawryluk et al., 2008*). Indeed, of the more recent studies, Tabakow *et al.* state that the nature of the spinal cord transection facilitated, to a large extent, the success of the repair (*Tabakow et al., 2014*), with Granger *et al.* finding that low efficacy of surgical techniques was a major factor in prevention of repair and subsequent recovery, resulting in only a 50% success rate (*personal communication – N. Granger*); a finding echoed in a number of studies utilising OECs (*Guest et al., 2011; Pearse et al., 2004*).

Bone marrow-derived MSCs have also shown promise in clinical trials, with a number of studies reporting modest recovery in sub- acute and acute SCI, but not in chronic injuries (*Hawryluk et al., 2008 for review*). Although, a recent clinical study has reported significant motor and sensory improvement in patients with chronic cervical SCI. Urodynamic improvement was also observed, in that bladder hyperreflexia improved, although voluntary control and bladder perception showed no improvement (*hyperreflexic bladder refers to an overactive bladder that holds less urine).* Moreover, some level of respiratory muscle strength recovery has also been reported in these patients (*Dai et al., 2013*). Importantly, at 6 month follow-up there was no evidence of tumour formation or adverse side effects at the lesion site, suggesting, at least in the short term, the safety of these cells. Despite these promising reports, measures of improvement were only seen in 50% of the treatment group, and the measures did not translate into functional benefit for these patients.

Clinical studies utilising bone marrow-containing nucleated cells have also shown improvement in motor and sensory function, although this was mostly seen in patients with sub-acute SCI where cell transplant was conducted within 1 month post-SCI. Of the patients with chronic SCI, cell transplant was conducted between 2 and 18 months following injury. Of this latter group (12 patients), modest improvement was seen in 1 patient (*Syková et al., 2006*). It is unclear, considering the difference in severity of SCI between the two groups, whether earlier intervention is more conducive to recovery, or whether the earlier intervention (within 1 month) 'masked' spontaneous recovery. Further, the majority of the 'improvement' reported in this study related to electrophysiological recordings of motor and somatosensory potentials, which do not necessarily confer functional recovery. Notwithstanding, increases in ASIA classification changed for a number of patients from A to B, with one patient recording a classification change from B to D (*Table 1.2 for ASIA classification*).

Table 1.2 American Spinal Injury Association (ASIA) Classification Criteria for SCI

Class	Classification	Prognosis criteria
A - Complete	No motor or sensory function in sacral segment (S4-5)	**SENSORY - 28 key sensory points** (light touch & pin prick) 0 – absent 1 – present but impaired 2 - normal
B - Incomplete	Sensory function below injury and in S4-5 but no motor function	**MOTOR – 10 key muscles** Scale of 0 – 5; 0 = total paralysis and 5 = active movement; full range of motion
C - Incomplete	Motor function below injury; >50% key muscle groups have muscle grade < 3	**COMPLETE INJURY PROGNOSIS** No voluntary anal contraction S4-5 sensory score is zero No anal sensation
D - Incomplete	Motor function below injury; 50% key muscle groups have muscle grade > 3	
E - Normal	Normal sensory and motor function	

Criteria adapted from ASIA

OPCs in animal studies showed evidence of differentiation into mature oligodendrocytes, and migration and enhanced remyelination, all of which appeared to facilitate a neuroprotective effect on motor neurons. This would suggest a plausible mechanism underpinning the improvement in locomotor function seen with transplant of these cells (*Keirstead et al., 2005; Sharp et al., 2010; Xie et al., 2016*). However, one of the major considerations with the use of OPCs is that of "autologous availability", with extensive immunosuppressive drugs required following donor transplant (*Li & Leung, 2015*). To circumvent this, iPSC-derived OPCs have been utilised in cell transplant studies. Initial findings reported decreased cavitation and increased axonal remyelination following SC contusion, and myelin initiation when transplanted into myelin-deficient mice. (h)ESC-derived OPCs have also been suggested as a clinical - but not autologous - alternative, having also proved beneficial in animal studies (*Li & Leung, 2015 for review*). A major, albeit now regarded as controversial study, utilising a low dose of (h)ESC-derived OPCs was the Geron trial. Financial instability was the reason given for its cancellation, although of the four patients who underwent cell therapy, no benefits were reported (*Wilcox et al., 2012 for review*). Notwithstanding these findings, a second clinical study is currently recruiting for phase I (cervical SCI) and phase II (spinal injury & spinal cord trauma) clinical trials investigating the safety of "escalating OPC dose" (*Asterias Biotherapeutics, Inc., 2016*).

One particular cell that has proved highly successful in animal models but that has, until relatively recently been mostly overlooked, is the astrocyte. This neural cell is highly specific to neuroprotection in both healthy and injured spinal cord, with a growing body of evidence supporting astrocyte involvement in axonal regeneration. Far from being the main inhibitory factor in the injured spinal cord, there is now a wider realisation of their

involvement in neuroprotection and "spontaneous functional recovery" (*Renault-Mihara et al., 2008*).

For example, following SCI, astrocyte-induced cell division cycle 2 (Cdc2) and vimentin activity facilitated neuronal outgrowth in co-culture (*Toy & Namgung, 2013*). Similar neuron regrowth was observed from Cdc2-vimentin activity in astrocytes *in vivo* (*Seo et al., 2013*). β3-Integrin has also been shown to play a role in axonal regeneration, with the linked mechanism of Cdc2, vimentin and integrin, mediating communication between astrocytes and regenerating axons (*Toy & Namgung, 2013*). Thus, utilising astrocytes as a transplant population may be beneficial in mitigating regeneration in the spinal cord. In this context, it has also been posited that ingrowth of astrocytes into the injury site may be a mechanism for functional regeneration (*Joosten et al., 2004; Macaya et al., 2013*). So, it could be postulated, that as well as having a major role in the healthy spinal cord for neuroprotection and homeostasis, astrocytes may offer the promise of regeneration and consequent functional recovery to the injured spinal cord; as such, they are now emerging as a major candidate as a transplant population for SCI. In this respect, it has to be made clear from the outset that cell transplants are not intended as a direct replacement of damaged astrocytes, but rather to confer the neuroprotective and neuro-immunomodulatory benefits inherent to endogenous astrocytes (*Li & Leung, 2015*).

1.3 What are astrocytes?

Within the central nervous system (CNS), glial cells provide physical and trophic support for neuronal cells. Of these supporting cells, astrocytes are the most predominant and their contribution to continued CNS function is of critical importance. Astrocytes are a highly heterogeneous cell population displaying morphological, functional, molecular and chemical differences with distinct roles dependent on the brain region they inhabit (*Freitas-Andrade & Naus, 2016*). Astrocytes and neurons form a structural and communicative network in the brain with a ratio of one astrocyte to eight neurons, five blood vessels and in excess of 100,000 synapses (*see Chu et al., 2014 for review*), facilitating extensive signalling 'cross-talk' with neurons, which influences the functional characteristics of both (*Fellin & Carmignoto, 2004; Van den Bosch & Robberecht, 2008*). For example, through end-feet contact, astrocytes mediate between neurons and the basal lamina of blood vessels, modulating neuronal activity and cerebral blood flow. This neuron-astrocyte-bloodstream relationship facilitates the key role astrocytes play in regulating the barriers between brain, blood and cerebrospinal fluid and in turn, CNS metabolic homeostasis (*Abbot et al., 2006; Maragakis & Rothstein, 2006*). This involves the glutamate-glutamine cycle (*Danbolt, 2001*), and the glucose-lactate shuttle which transports glucose (amongst other substances) into the brain, converting it to lactate to meet the energy demands of the neuron (*Magistretti & Pellerin, 1999*). Astrocytes also regulate the intra- and extracellular ion concentrations of the by-products of these metabolic functions (*Kofuji & Newman, 2004*) (*Figure 1.2*).

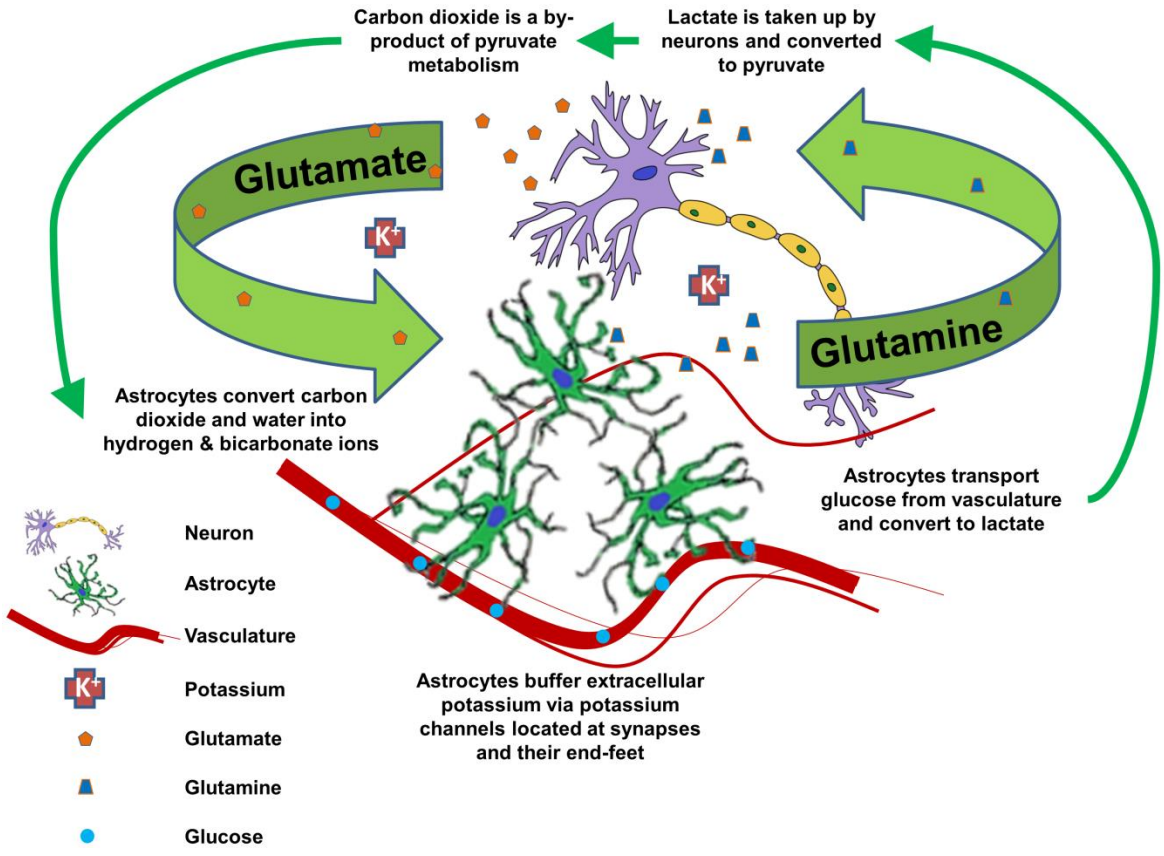

Figure 1.2 The metabolic relationship between astrocytes and neurons in the adult brain *A schematic of the glutamate-glutamine cycle and the glucose-lactate shuttle. When glutamate is released from neurons, the excess glutamate is taken up from the synaptic cleft by the plasma membrane glutamate transporters expressed on astrocytes. Conversion of glutamate to glutamine is undertaken by astrocytes before returning it back via the presynaptic terminals of the neuron. Astrocytes also convert glucose taken up from the vasculature into lactate, which is then taken up by the neurons and converted into pyruvate for energy metabolism. Astrocytes regulate the intra- and extracellular ion concentrations of the by-products of these metabolic functions via their synapses and end-feet.*

1.3.1 Astrocytes – origin and development in the CNS

Astrocytes have differing lineage, dependent on their subtype and relationship with other neural cell types. Mammalian astrocytes and neurons (together with other main CNS cells) originate from the same precursor cell, radial glia (*Malatesta et al., 2008*). Astrocytic differentiation (astrogliogenesis) is marked by the onset of astrocyte-specific markers, the main ones being GFAP (widely used for identification); brain lipid binding protein (BLBP); S-100 and M1 antigen (*Barry & McDermott, 2005*). Two further astrocyte subtypes are derived from these glial-restricted precursor cells. Exposure to different signalling molecules, bone morphogenetic protein-4^{BMP}, or ciliary neurotrophic factor^{CNTF}, facilitates differentiation into two specific astrocyte sub-populations, now regarded as of key importance to cell transplant populations due to their regenerative (-BMP), or inhibitory (-CNTF) effect in SCI (*Davies et 2011; Liu et al., 2015*). During differentiation, the continued expression of neuronal markers by radial glia-derived astrocytes facilitates neuronal growth and migration in the developing brain and spinal cord (*Joosten & Gribnau, 1989*).

Comparative studies of human, primate and rodent astrocytes highlight differences and similarities in astrocyte subtype, morphology, activation state, ion channel pharmacology and role in intercellular communication, related to the differing level of complexity required for CNS function across species (*Oberheim et al., 2006*). Notwithstanding these differences, astrocyte morphology across species is broadly characterised as protoplasmic (predominant within grey matter) or fibrous (principally found in white matter). However, in light of biomedical applications involving astrocytes based on rodent experimental models, as is the case here, it is needful to address the difference in astrocyte morphology between human and rodent cortical astrocytes *in vivo* and those observed in rodent models *in vitro*.

It is important to note that the origin and development of astrocytes in rodent brain differs from that of human. Neuroepithelial stem cells in the rodent brain generate *neuron*-restricted precursor cells, and from rodent spinal cord, *glial*-restricted precursor cells (*Barry & McDermott, 2005; Hirano & Goldman, 1988; Mayer-Proschel et al., 1997*). Human cortical astrocytes, both protoplasmic and fibrous, are larger and have an extensive process network not seen in rodent cortex. Moreover, the uniform nature of rodent astrocytes *in vivo*, while similar to the uniformity and even distribution observed in human hippocampal regions (*Ogata & Kosaka, 2002*), differs notably from the subtype distribution observed in human cortex. Interlaminar astrocytes, observed in both primate and human cortex, extend long glial processes through cortical layers II and IV, from somas contained within cortical layer I (*Columbo & Reisin, 2004; Columbo et al., 2002; 2005*). Protoplasmic astrocytes are found in layers II to VI, with fibrous astrocytes localised to white matter. A further subtype, specific to human cortex layers V and VI, are polarised astrocytes, characterised by long varicose processes (*Oberheim et al., 2009*). This variation differs greatly from morphologies observed in monolayers of primary rodent astrocytes cultured on glass, whereby cortical astrocyte subtypes are characterised by their morphology (flattened, unbranched membraneous cells with truncated processes, or small soma and highly branched) and classified by phenotype – type 1 and type 2, respectively (*Pickard et al., 2011*).

1.3.2 Astrocytes are a major player in the homeostatic function of the healthy CNS

The homeostatic role of astrocytes in the mature CNS is intrinsic to continued neuronal function. Homeostatic membrane channels, sodium (Na^+), potassium (K^+) and calcium (Ca^{2+}) differ dependent on subtype and location, *in vivo* or as a cell culture. *In vitro* studies have shown only 30% of astrocytes in culture express Na^+ current, with cultured astrocytes showing no expression of Ca^{2+} current unless co-cultured with neurons (*Schipke &*

Ketenmann, 2004). By comparison, Ca^{2+} shows significant increase *in vivo* in the presence of glutamate and purinergic receptor agonists, and rapidly propagates in the presence of glutamate release (*Oberheim et al., 2009*). This is an important consideration when proposing clinical applications of experimental models, highlighting the gulf between 2-dimensional culture and the 3-dimensional, functional environment of the CNS.

Astrocytes form a neuronal trophic support network within the CNS facilitating the astrocyte-neuronal signalling complex; their physical coupling isolating synapses (*Schipke & Kettenmann, 2004*). Electrical coupling is facilitated by an extensive astrocyte-neuronal gap junction communication network. This highly interactive network is instigated by astrocytes. Their high expression of gap junction protein molecules, connexin -43 and -30, establish astrocyte-neuronal communication, the subsequent regulation of which is tightly controlled, in turn, by neurons (*Fellin & Carmingnoto, 2004; Rouach et al., 2004*). Of importance to translational application, *in vitro* studies of co-culture with neurons have shown similar extensive physical and electrical coupling typically observed *in vivo* (*Nagy & Rash, 2000; Rouach et al., 2004*).

The astrocyte matrix also enables neuroprotection. Astrocytes are fundamental to homeostasis of glutamate and γ-aminobutyric acid (GABA) neurotransmission within the CNS (*Yu et al., 1983*). Their high expression of glutamate transporters (GLAST) and GABA receptors for neurotransmitters and modulators are crucial to synaptic transmission, enabling uptake and transport of excess glutamate, GABA and glycine (amongst others) from the synaptic cleft, and thus preventing neurotoxicity from overexpression of these Ca^{2+} dependent processes (*Danbolt, 2001; Sattler & Tymianski, 2001).* Astrocytic synthesis and release of neurotrophic and growth factors also facilitate neuronal survival and function.

It has been widely held that astrocytes possess negligible regenerative properties following maturation. However, recent evidence is highlighting a level of regenerative capability in healthy adult astrocytes. The use of specific transcription factors have proved successful in promoting neurogenesis of murine and human astrocytes. In the adult mouse brain, SOX2 generated proliferative neuroblasts from adult and aged astrocytes, with the addition of BDNF and Noggin to SOX2 promoting neuroblast development into functional neurons (*Niu et al., 2013).* The individual addition of OCT4, SOX2 or NANOG to cultured human cortical astrocytes induced cells expressing neural precursor markers, with the resulting NSCs giving rise to astrocytes, neurons and oligodendrocytes. Further, transplantation of these NSCs into mouse lateral ventricles generated neuronal and glial phenotypes, with some migration into the cortical area (*Corti et al., 2012*). The generation of neuronal precursors from foetal human astrocytes, when exposed to medium supplemented with basic fibroblast growth factor (BFGF) has also been reported, with maturation into neurons occurring following subsequent BFGF withdrawal (*Aziza & Krynska, 2013*). Although modest, the regenerative potential of mature astrocytes is beginning to be realised.

1.3.3 Astrocytes are intrinsic to neuroprotection in SCI

In the injured spinal cord, coincident with glial scar formation, reactive astrocytes release a plethora of neurotrophic factors to promote neuronal survival, and signalling molecules that mediate both neuroprotective and neurotoxic effects (*Freitas-Andrade & Naus, 2016*). Interleukin-1 β and tumour necrosis factor-α (astrocyte derived cytokines) are released into the area of insult, promoting neurotoxicity to phagocytose necrotic tissue, with Interleukin-6 and transforming growth factor-β (also astrocyte derived cytokines) promoting neuroprotection (*John et al., 2003; Liberto et al., 2004*). CSPGs are produced by reactive astrocytes, with the influx of macrophages and microglia into the injury site further increasing CSPG expression (*Viapiano & Matthews, 2006*). OPCs, triggered by

demyelination of the severed axon, also increase CSPG expression following injury (*Asher et al., 2002*). To limit tissue damage, reactive astrocytes also take up from the synapse the glutamate and ions released from dying neurons, and remove the metabolic by products (*Chen & Swanson, 2003; Sofroniew et al., 2001*).

1.3.4 Astrocytes play a major role as a transplant population for SCI

The co-dependency of the astrocyte-neuron relationship suggests the continuation of astrocytes' role as critical to repair and restored function within the injured spinal cord. In this regard, there are a number of properties that propose them as ideal candidates. Unlike transplantation of undifferentiated NSCs into the lesion site, the transplantation of astrocytes appears to mitigate the astroglial response to injury. In this context, it has been postulated that the reduction of proliferation and the consequent reduction of glial scar density, facilitates axonal regeneration (*Wang et al., 1995*). Interestingly, regeneration appears dependent on astrocytes' developmental stage at the point of transplantation. Astrocyte precursor cells (glial-restricted) transplanted into rat spinal cord, reduced glial scarring and induced low levels of improvement to the surrounding tissue. Autonomic function was enhanced, as observed by penis pressure tests, although no effect on functional erectile recovery was observed (*Nout et al., 2011*). By contrast, differentiating these cells into astrocytes *prior* to transplantation, enabled extensive regeneration and repair to axons and neurons, with restoration of mobility function as assessed by grid-walk foot placement (*Noble et al., 2011*).

It has also been observed that regeneration appears to be dependent on a specific population of differentiated astrocytes. The two signalling molecules (BMP or CNTF) that facilitated differentiation of these cells during mammalian development, have been found to confer different regenerative properties to the mature sub-populations when used for cell

transplant (*Davies et al., 2011; Liu et al., 2015*). Use of BMP^{-4} resulted in an astrocyte sub-population that facilitated extensive regeneration and functional recovery, whereas use of CNTF resulted in the similarly low levels of regeneration observed with precursor cells (*Davies et al., 2011; Liu et al., 2015; Noble et al., 2011*).

Their therapeutic benefits following SCI have prompted a number of astrocyte transplant studies which have subsequently provided a broad knowledge base for the further development of this cell to translational application (*Table 1.3*).

**Astrocyte transplant studies not in the context of SCI are not included*.

Table 1.3 Astrocyte Cell Transplant Studies in Rodent SCI Models

Transplant population characteristics	Injury model	Outcome	Study
SC embryonic astrocytes	Crush injury - rat	Limited inflammatory response; axonal regrowth	Kliot et al 1990
Embryonic whole SC (graft) or SC embryonic astrocytes (EmA)	Cervical aspiration (C3) - rat	Improved hind limb placement with graft; worsening of hind limb placement with EmA	Bernstein & Goldberg 1991
Type 1 astrocyte culture	EB SC lesion - rat	Promoted host OL integration into the lesion site resulting in increased OL remyelination	Franklin et al 1991
Neonatal cortical	Hemi-sected lumbar (L3) - rat	Astrocyte migration; reduction in glial scar; nerve fibre regrowth	Wang et al 1995
Embryonic whole SC	Thoracic transection (T8-9) - rat	Integration of host axons with transplant; regeneration and recovery of foot placement and weight-supported stepping	Coumans et al 2001

Human adult astrocytes	Non-injured SC (T9) - mice	Migration and integration into the host SC tissue; absence of tumour formation	Ridet et al 2003
Neonatal cortical astrocytes	Thoracic hemi-section (T7-9)	No migration from implant into host tissue led to significant corticospinal axon fibre ingrowth; resulted in modest (temporary) locomotor recovery	Joosten et al 2004
GRP cells	SC contusion - rat	Differentiated into astrocytes & OL *in vivo*; reduction of glial scar; reduction of CSPGs; altered axon stumps to growth cones	Hill et 2004
NRP + GRP	Thoracic contusion (T8-9) - rat	*In vivo* differentiation into neurons and astrocytes; accelerated recovery from bladder areflexia vs control; improved hypersensitivity to heat; greater recovery of hind limb function; no difference in locomotor grid walk function vs control	Mitsui et al 2005
Primary adult rat cortical astrocytes	Thoracic transection (T8) - rat	Cells genetically modified to express *gfp* – cells migrated from injection site & integrated with host tissue	Pencalet et al 2006
Embryonic GRP cells	Cervical transection (C1-2 or C3-4) - rat	No suppression of glial scar formation; no axonal growth; no locomotor recovery	Davies et al 2006
Pre-differentiated astrocytes from embryonic GRP cells		Promotion of axonal growth into and beyond the lesion; improved locomotor function	

GRP-derived astrocytes (+BMP or CNTF)	Cervical transection (C1-2 or C3-4) - rat	Astrocytes+CNTF – no axonal regeneration or functional recovery; onset of neuropathic pain Astrocytes+BMP – promoted axonal regeneration and functional recovery; no pain syndrome exhibited	Davies et al 2008
Embryonic (h)GPC-derived astrocytes (+BMP or CNTF)	Cervical transection (C3-4)	Astrocytes+CNTF – failure of axonal growth, neuronal survival and behavioural recovery Astrocytes+BMP – promoted axonal growth; increased neuronal survival; significant recovery of voluntary foot placement	Davies et al 2011
iPSC-derived astrocytes	Thoracic contusion (T9-10) - rat	Despite process elongation, no integration with host cells was observed; no tumorigenesis; no locomotor recovery; increased sensitivity (pain)	Hayashi et al 2011
(h)GRP vs (h)GRP-derived astrocytes	Thoracic contusion (T10) -rat	Both cell transplants migrated into host tissue; (h)GRP differentiated into astrocytes *in vivo*; cyst & scar formation was reduced; axonal growth; no increased sensitivity (pain); no improvement in motor function recovery; (h)GRP-derived astrocytes promoted normal recovery of sensory function	Jin et al 2011
GRP-derived astrocytes	Thoracic contusion (T9) - rat	Integration with host tissue; axonal regeneration; decreased injury size; improved locomotor function	Fan et al 2013

(h)GRP-derived astrocytes (+BMP/CNTF)	Cervical transection (C4-5) - rat	Both astrocyte-BMP and astrocyte-CNTF promoted regeneration of long ascending tracts into lesion site	Haas & Fischer 2013
GRP-derived astrocytes+BMP+ (hr)-decorin	Thoracic contusion (T8)-rat	Reduced SC inflammation; inhibited astrogliosis and glial scar formation; axonal regeneration; improved functional recovery	Wu et al 2013
(h)iPSC-derived astrocyte progenitors	Cervical laminectomy (C6) - rat	Limited cell survival (<5%); *In vivo* differentiation to astrocytes; upregulation of mature astrocyte genetic markers	Haidet-Phillips et al 2014
GRP-derived astrocytes+BMP – periostin$^{+/-}$	Cervical transection (C1-2)	GRP-A periostin^{+} cells reported axonal growth & motor functional recovery. GRP-A periostin^{-} cells inhibited axonal growth	Shih et al 2014
(h)iPSC-derived astrocytes+GLT	Cervical contusion (C4) - rat	*In vivo* differentiation into astrocytes; long term survival; increased expression of GLT transporters and functional GLT uptake; reduced lesion size; improved functional diaphragm denervation (aiding respiration)	Li et al 2015a
GRP-derived astrocytes+AAV8	Cervical hemi-contusion (C4) -rat	GRP-derived astrocytes+AAV8 overexpressed GLT transporters in SCI; significant increase in GLT transporter protein expression and subsequent GLT uptake; reduced lesion size; reduction in diaphragm dysfunction	Li et al 2015b

SVZ-NPCs	Cervical hemi-section (C2) - rat	50% cell survival; *in vivo* differentiation into astrocyte phenotype; increased phrenic nerve output (improvement in respiratory recovery)	Sandhu et al 2015

BMP–bone morphogenetic protein; **C3**–cervical region; **CNTF**–ciliary neurotrophic factor; **CSPGs**–chondroitin sulfate proteoglycans; **EB**–ethidum bromide; **EmA**–embryonic astrocytes; **GLT**–glutamate; **GRP**–glial restricted precursor; **GRP-A**–glial restricted precursor-derived astrocytes; **(h)GPC**–human glial restricted progenitors; **hr**–human recombinant; **iPSC**-induced pluripotent stem cell; **L3**–lumbar region; **NRP**–neuron restricted precursor cells; **OL**–oligodendrocytes; **SC**–spinal cord; **SVZ-NPCs**–sub-ventricular zone neural progenitor cells; **T9**–thoracic region.

As can be seen from the above studies, astrocytes as a transplant population have been showing consistently promising results in the repair of SCI for over a decade. The field has shown development from basic rodent cell transplant (*Bernstein & Goldberg, 1991; Coumans et al., 2001; Davies et al., 2006; Franklin et al., 1991; Kliot et al., 1990; Wang et al., 1995*) to that of a combinatorial approach, delivering functionalised and/or genetic engineered cells as a transplant to the injured spinal cord (*Davies et al., 2008; 2011; Haas & Fischer, 2013; Joosten et al., 2004; Li et al., 2015a; 2015b; Shih et al., 2014; Wu et al., 2013*). They have been tested across a wide developmental range, from GRP cells (*Davies et al., 2006; Hill et al., 2004; Jin et al., 2011; Mitsui et al., 2005; Sandhu et al., 2015*) through to mature adult astrocytes (*Pencalet et al., 2006; Ridet et al., 2003*), with both rat and human origin proving beneficial to recovery (*Davies et al., 2011; Haas & Fischer, 2013; Haidet-Phillips et al., 2014; Jin et al., 2011; Li et al., 2015a; Ridet et al., 2003*).

It is interesting to note that differentiating precursor cells to astrocytes *prior* to transplant (*Davies et al., 2006; 2008;2011; Fan et al., 2013; Haas & Fischer, 2013; Jin et al 2011;*

Li et al., 2015b; Shih et al., 2014; Wu et al., 2013), appears to exert greater functional recovery and regeneration than allowing cells to differentiate *in vivo* (*Hill et al., 2004; Jin et al., 2011; Li et al., 2015a; Sandhu et al., 2015*). The benefit though of the latter approach appears to be in mitigating the non-permissiveness of the lesion environment (*Hill et al., 2004; Jin et al., 2011*). From this a combinatorial strategy could be postulated for the transplant of differentiated astrocytes *alongside* precursor/progenitor cells, to gain the benefits attributed to both when transplanted separately.

While a number of cell types in both animal and clinical trials have reported improved sensory, motor and to some degree, functional recovery, unlike astrocytes relatively few cell types have reported any improvement to urodynamics. This has physical, psychological and social consequences. Erectile dysfunction related to SCI has been shown to be mediated by pharmacological intervention (*Giuliano et al., 1999; Khorrami et al., 2010; Lombardi et al., 2012).* However, the major impact on 'quality of life', as reported consistently by SCI patients during clinical trials (*Professor Steven Conlan; Swansea University - personal communication*), has been the loss of urodynamic control (loss of bladder/bowel control). Hyperreflexia and areflexia impact kidney function, preventing adequate filtering of the blood with the potential consequences of kidney failure and dialysis. (*Bladder areflexia refers to a flaccid bladder that overfills and leaks due to non-contraction*). Incontinence without proper management, can lead to breakdown of the surrounding skin tissue, resulting in pressure ulcers and infection. Loss of bowel control can lead to faecal impaction and/or sudden ejection of faecal matter from an overloaded bowel (*UPMC, 2016*).

In this regard, NRP+GRP-derived astrocytes reported beneficial effect following cell transplant (*Mitsui et al., 2005*). In this study, both treatment and control groups acquired bladder areflexia immediately following SCI, however, the treatment group showed a

significantly accelerated and improved recovery compared with control (*Mitsui et al., 2005*). Coupled with the extensive regeneration seen within the lesion site and the subsequent translation of this regeneration into functional recovery (i.e. sensory and motor function; improved and recovered locomotor function; improvement in respiratory recovery; improvement in urodynamics), astrocytes as a cell transplant appear to be offering high promise in regenerative treatment of SCI.

Notwithstanding, it has to be recognised that a number of cell types that showed promise in animal studies have not translated favourably into the clinic. In the context of translatable application, the use of (h)iPSCs have been promoted as having high potential, although, there appears to be an inordinate number of complications surrounding their use (*Nakamura & Okano, 2013; Ruff et al., 2012; Yamanaka, 2009*). Indeed, of all the precursor cell types differentiated into astrocytes both prior to transplant and *in vivo*, the use of (h)iPSCs showed the least promise, with very low cell survival (<5%), no motor recovery and increased hypersensitivity (worsening of pain symptoms) (*Haidet & Phillips., 2014; Hayashi et al., 2011*). Of interest, these cells appear to be more promising when used as part of a combinatorial approach, in that survival *in vivo* was significantly increased, although it may be that they are functioning only as a vehicle for transport of glutamate, and that the therapeutic benefits seen are due only to the presence of this neurotransmitter (*Li et al., 2015a*). Thus, at present, these findings do not promote them sufficiently as a transplant population.

By contrast, human (h) adult astrocytes, embryonic (h)GPC-derived astrocytes^{BMP} and (h)GRP-derived astrocytes report cell migration and integration into host tissue; axonal growth and regeneration into and beyond the lesion site; neuronal survival and recovered urodynamics. Coupled with improved "volitional" (*Davies et al., 2011*) functional

recovery, and reports of high levels of safety, astrocytes represent an ideal candidate for translational application into clinic.

Autologous transplantation is a distinct possibility with this cell type, obviating the need for extensive immunosuppression (*Ridet et al., 1999; 2003*). Ridet *et al.,* reported obtaining human adult cortical astrocytes and maintaining them *in vitro* for approximately 10 months, prior to lenti-viral modification of the cells to express *gfp.* To "mimic an autologous human transplant", the cells were transplanted into adult nude mice (*Ridet et al., 2003*). They reported cell survival and migration of the cell transplant, together with sustained expression of the *gfp* transgene. There was complete absence of tumorigenesis, suggesting the safety of these cells for clinical application. Ridet *et al.,* argue the obvious biological advantage to autologous transplant, compared with the ethical and safety considerations concerning embryonic and cloned cells (*Ridet et al., 2003*).

1.3.5 Cortical astrocytes as a cell transplant population in injured spinal cord

In respect of clinical application, and with regard to the series of studies detailed within this research, a key point to note is the well-documented use, and potential feasibility of, cortical astrocytes (as opposed to SC astrocytes) as a transplant population in the injured SC, due to their subsequent survival and integration into host tissue, coupled with the consequent functional improvement observed in animal studies (*Joosten et al., 2004; Pencalet et al., 2006; Ridet et al., 2003; Wang et al., 1995*). This in contrast to the use of embryonic SC astrocytes which showed significantly worse outcomes and 'highly variable regeneration' when transplanted into injured SC (*Bernstein & Goldberg, 1991; Kliot et al., 1990*). While it is recognised that more recent studies have utilised (h)GRP-differentiated astrocytes as a transplant population, the ethical challenges remain, as does the challenge to move towards translational and/or autologous use.

Astrocytes 'tile' the entire CNS (*Sofroniew et al., 2010*), and are classified at present, not by region, but by phenotype (Type 1 or 2), and morphology [protoplasmic (located predominantly in grey matter) or fibrous (white matter)]. Putative regional heterogeneity has been suggested, based on differing neuronal characteristics when cultured with astrocytes from different regions, however, in respect of astrocyte molecular markers, while onset may differ, expression itself does not (*Molofsky et al., 2012 for review*). Moreover, irrespective of location astrocytes are similarly characterised (*Kerstetter & Miller, 2012, and as elucidated previously – section 1.3*); for example, cortical and SC astrocytes show no difference in Ca^{2+} conductance for intercellular communication (*Scemes et al., 2000*). Fundamentally, astrocytes' role in the CNS is to provide a structural and supportive environment for neuronal networks and axonal growth (*Chu et al., 2014 for review).*

Hence, in respect of utilising cortical – as opposed to SC - astrocytes as a cell transplant in the injured spinal cord, the key points remain *i*) astrocytes throughout the CNS are similarly characterised; *ii*) their use as a transplant population in injured spinal cord has been well-documented; *iii*) for the purposes of translational/autologous use, cortical astrocytes can be feasibly derived and therefore, *iv*) circumvent ethical challenges. Importantly, the fundamental purpose of a cell transplant is not to replace damaged cells, but rather to confer the neuroprotective and neuro-immunomodulatory benefits of a cell transplant to facilitate a conducive environment for regeneration (*Li & Leung., 2015*).

It is therefore postulated that astrocytes propose an excellent strategic approach to regeneration within the injured spinal cord; nonetheless there remains a major challenge still represented in pursuit of translational application (*Ridet at al., 2003*).

1.4 The need to develop better cell therapies

While it is clear then, that astrocytes as a cell therapy are advantageous for regeneration within the injured spinal cord, in order to *enhance* their promise, there is a critical need to address the fundamental issues surrounding the development of a more select cell therapy. In the drive for improvement there are a number of approaches that could be considered, three of which are the focus of this research.

1.4.1 The need for safe, effective genetic engineering of the cell transplant population

The first approach considered is that of genetically engineering the cell transplant population. Varied therapeutic approaches have been utilised to deliver drugs/genes to the injured spinal cord. Strategies deployed to inhibit degenerative processes and promote neural repair are considered of greater efficacy when delivered within specific timeframes, i.e. the administration of corticosteroid within 8 h of injury (*Bo et al., 2011 for review*). However, a number of concerns have been expressed regarding the *mode* of delivery; its effectiveness and its safety.

Drug delivery at SCI onset is either systemic or direct. Each method has limitations. Systemic delivery faces two main challenges in crossing the "blood-spinal cord barrier" (*Kabu et al., 2015*). Firstly, while this barrier is more permissible than the blood-brain barrier, pharmacokinetic studies have shown that the damage occasioned by SCI (and disease) alters its dynamic activity in gap-junction and receptor expression (*Ge & Pachter, 2006; Li et al., 2004; Whetstone et al., 2003*). The second challenge with systemic delivery is that of retaining sufficient dose to be effective on arrival at the injury site. By contrast, direct administration is targeted, but entails a number of puncture wounds due to the overall volume required (an average of 8 sites were required for delivery in animal studies), inducing tissue damage and potentially further inflammation (*Guest et al., 2011*).

The use of slow release intrathecal catheters has been suggested to address this. However, they incur further problems such as infection, and the extended time frame required to deliver the dose (*Jones et al., 2001*). Moreover, and of clinical relevance, doses delivered in the lab are not tolerated in the clinic, presenting a major challenge to translational therapies (*Kabu et al., 2015*).

It is increasingly clear that a combinatorial approach offers the most promise for recovery and regeneration in the injured spinal cord, with therapeutic molecules delivered *alongside* cell transplants seeing effective results (*Coumans et al., 2001; Shih et al., 2014*). However, the low effectiveness and rapid degradation of neurotrophins, growth factors or inhibitory molecules when delivered *utilising standard approaches*, represents an obstacle to the development of such an approach. This demonstrates a need to genetically engineer transplant populations, **to augment cells to facilitate delivery of therapeutic molecules**.

There are two main strategies for transducing genes to astrocytes (and indeed, most cell therapies). The less common strategies are non-viral approaches to genetic engineering, such as Lipofectamine (*Tinsley et al., 2004*). For example, to upregulate BDNF and glial cell-line derived neurotrophic factor (GDNF), Lipofectamine was used to introduce a vector containing the cDNA for Pitx3 to primary-derived astrocytes; Pitx3 protein being a transcription factor critical to dopamine neuron development (*Yang et al., 2008*). Following introduction of these cells into a dopamine neuron injury model, the study found the significant upregulation of GDNF and BDNF attenuated dopamine neuron injury (*Yang et al., 2008*). Although these particular results are promising, the low transfection efficiency (10-15%) and transient expression (24 h) associated with this approach has discouraged development (*de Lima et al., 2005*). Other non-viral approaches, such as electroporation, where DNA is introduced into the cells using an electrical pulse to disrupt

the cell membrane, are also disadvantageous due to the high cell death occasioned with such a forceful strategy (*de Lima et al., 2005*).

The more common strategy has been the use of viral vectors – notably lentiviral (LV); retroviral (RV) and adeno-associated viral vectors (AAV) (*Merienne et al., 2013*). A large proportion of earlier studies utilising RV (*Selkirk et al., 2002*) or LV vectors (*Ericson et al., 2002; Filous et al., 2010; Pencalet et al., 2006; Ridet et al., 2003*), genetically engineered astrocytes to express a reporter protein (green fluorescent protein – *gfp*). These studies proved its safety and efficacy in gene transfer, and its capacity to facilitate tracking of a cell transplant population. Moreover, use of viral methods for transgene expression in astrocytes in neurological disease has proved highly beneficial. For example, using a recombinant AAV, primary adult human astrocytes were transduced to carry (h)β-glucuronidase cDNA – an enzyme whose deficiency in the developing CNS leads to growth and mental retardation (*Serguera et al., 2001*). Transplant of the genetically engineered cells to mouse striatum, resulted in long term survival and expression of the enzyme (*Serguera et al., 2001*). Use of an AAV-5 vector for delivery of GDNF transgene-expressing neurons into the brain of Parkinson's disease animal models, reported serious side effects due to mis-targeting and entry to the unaffected part of the brain (*Drinkut et al., 2011*). However, use of this vector for GDNF transgene expression *in astrocytes*, facilitated efficient and specific targeting to the affected area only (*Drinkut et al., 2011*).

A number of studies have investigated the development of a combinatorial approach of genetically engineering astrocytes as a vehicle for delivery within the injured spinal cord. One particular study, utilising a retroviral approach, engineered astrocytes to express a novel, multiple neurotrophin -'D15A', which possesses the combined benefits of NT-3 and BDNF. Following transplant into a contusion SCI, apart from the reduced lesion size and low expression of CSPG, an increased level of spared white matter was observed,

suggesting a neuroprotective effect with this cell transplant. Functional recovery showed significant improvement, and as evidenced with other astrocyte transplants, hypersensitivity did not increase (*Fan et al., 2013*).

Loss of glutamate transporters in the injured spinal cord results in high levels of excess glutamate, leading to disrupted glutamate homeostasis. This has been found to have a highly negative effect on phrenic nerve function in cervical SCI (i.e. it impacts on respiratory recovery) (*Li et al., 2015a*). To ameliorate "diaphragm dysfunction" (*Li et al., 2015b*), (h)iPSC-derived astrocytes (*Li et al., 2015a*) and GRP-derived astrocytes (*Li et al., 2015b*) were genetically engineered using LV and AAV-8, respectively, to overexpress glutamate transporters. Following transplant into a cervical hemi-contusion (C4) animal model, glutamate protein expression and uptake was significantly increased, with a significant reduction seen in denervation and "diaphragm dysfunction", resulting in a level of improvement in muscle action potentials within the diaphragm (*Li et al., 2015a; 2015b*).

Although promising, viral-mediated strategies have their limitations. While they are highly efficient in targeting the lesion site, and show high and sustained expression, they are restricted to small plasmid size, making them inefficient carriers of larger therapeutic molecules. RV has little efficiency in post-mitotic cells, with both RV and LV showing random integration (*de Lima et al., 2005*). By contrast, AAVs are more precise and target-selective and therefore, represent the safest option in vivo. They are however, the least efficient of the viral vectors (*Lentz et al., 2012*). Of major concern is the level of safety associated with these approaches. They can represent an unpredictable immune response *in vivo,* and have been linked with insertional mutagenesis and oncogene activation (*Blits & Bunge, 2006; Ryan & Federoff, 2007*). Moreover, the inability to monitor or control their level of expression within the lesion site, suggests a high potential for tumorigenesis (*Costantini et al., 2000; de Lima et al., 2005; Siebert et al., 2015*).

Thus, there has arisen **a critical need for a safe, effective mode of delivery** that has to fulfil a number of criteria: *i*) it can be accurately targeted to the site of injury without incurring tissue damage or increased inflammation; *ii*) the delivery vector should be capable of retaining sufficient dose to be clinically effective and have the capacity to remain at the injury site long enough for efficient delivery, and *iii*) be biocompatible and biodegradable to ensure no toxicity to the host tissue. In this respect, magnetic nano-particles (MNPs) - used extensively in clinical application for contrast under magnetic resonance imaging (MRI) - have emerged as excellent delivery vectors for transgene expression in cell transplant populations (*Cerqueira et al., 2013*). Moreover, and discussed more extensively in Chapter 5, MNPs have been suggested as a "safer and more efficient" approach, due to their biodegradability, capacity to target the lesion site and to facilitate slow and sustainable release of therapeutic drugs/genes (*Hans & Lowman, 2002; Silva et al., 2014*). Until recently, the limiting factor with this approach was their low transgene efficiency when compared with the high transfection efficiencies reported with the use of viral vectors. Nucleofection, RV and LV routinely achieve transfection efficiencies of 60-90% in astrocyte cultures, with 100% seen with certain viral vectors (*see Pickard & Chari, 2010 for review*). However – and discussed further in Chapter 5 – the deployment of magnetic fields in conjunction with MNPs, is proving highly advantageous in overcoming the barriers to MNP-mediated gene transfer.

1.4.2 The critical need to develop a means of non-invasively detecting and tracking transplant populations, fundamental to translational applications

The second approach requiring development is for non-invasive tracking of the cells for transplantation, in order to correlate their distribution in host tissue with any observed functional neurological recovery. Cell tracking of transplant populations in host tissue, have shown heavy reliance on dyes such as Hoechst 33342, fast blue (*Joosten et al., 2004*)

or fluorescent dyes (*Frampton et al., 2011; O'Shaughnessy et al., 2003*). Other methods include DNA identification of Y-chromosome probes (*Pearse et al., 2007*); retrograde tracing (*i.e. Fluoro-Gold – Kushchayev et al., 2016*), radiolabelling or reporter protein expression (*Bulte et al., 2001; Filous et al., 2010; Kircher et al., 2011*). Each of these strategies have a number of limitations in respect of imaging, toxicity and rapid decay of the label (*Hossain et al., 2014; Mertens et al., 2014; Pearse et al., 2007).* The biggest obstacle with these methods is that the end point of each of these strategies still remains histological analysis, a major barrier to translational use.

Thus, there is **a requirement for a non-invasive approach to** *in-vivo* **detection and tracking** of a cell transplant population. This approach requires a high level of safety, both to the transplant population and to the endogenous cells. It must offer a high imaging contrast that is not subject to rapid degradation, and yet remain both biocompatible and biodegradable to offer potential for clinical application. In this respect, superparamagnetic (nano) particles have shown themselves to be a highly effective contrast agent for non-invasive MRI, and have been used as such for the tracking of cell suspensions. For example, NSC-derived OPCs showed efficient labelling of magnetodendrimers (magnetic tags); sufficient to be tracked using MRI in intracerebral regions of rodent neonatal brains (*Bulte et al., 2001*). MSCs loaded with silica-coated magnetic particles were suspended in a dense collagen gel and injected into an *ex vivo* cartilage slice prior to imaging under MRI (*Harrison et al., 2016*). Adipose-derived stem cells showed uptake of oleic-acid modified MNPs which were seen to be localised to vesicles within the cytoplasm. Following injection of these labelled cells into murine subcutaneous tissue, they could be visualised under MRI for up to 9 days (*Cen et al., 2009*). However, the biggest challenge that still remains is ensuring a sufficient high initial loading of particles into the cell transplant to

promote high imaging sensitivity over an extended time frame, as loss of signal is the major limitation in clinical application (*Bernsen et al., 2015*).

1.4.3 The low survival rate of cell transplant populations necessitates a protected cell transplant delivery system

The third area for development entails addressing the low efficacy of surgical techniques in cell delivery. A number of approaches are used in delivery of the cell transplant population to the site of injury. However limitations to the transplant's subsequent effectiveness in the injury site have been reported. The main consideration is the initial major surgery required to expose the spinal cord. Percutaneous surgery has been suggested as a less invasive alternative, although the adjunct here is that, in comparison to animals, human SCI would require a number of needle penetrations to cover the entire length of the lesion, increasing the invasive nature of this approach (*Granger et al., 2012*). Further to this is the highly invasive nature of implanted pumps or catheters, all of which have the potential to increase the inflammatory response in the lesion site. There is a high risk of infection with implanted devices, which also carry the threat of failure or breakdown (*Jones et al., 2001*). Moreover, delivery of growth factors or protein inhibitors *alongside* cell transplants is unable to be successfully monitored to ensure safety and prevent tumorigenesis (*Siebert et al., 2015*). Delivery of cell transplant populations via fine bore needles, the more common route, involves either a series of injections, or one large dose to ensure the high cell numbers required are delivered, resulting in a high incidence of "injection injury" (*Guest et al., 2011*). In this context, the autonomic pulsing nature of the spinal cord around the infiltrating needle can result in cavitation, triggering a further neural response and increased neuronal degradation (*Guest et al., 2011*). Potentially the major factor underlying the low success rate in clinic and laboratory is the use of fine bore needles. These place shearing stresses on the cell membrane during delivery, with the majority of cell death

reported as occurring at the time of transplant (*Hill et al., 2007; Pearse et al., 2007*). To allow for this, a high cell density is used. To reduce 'injection injury', one large dose is delivered. However, this higher volume impacts on the pressure that can be sustained by the spinal cord lesion, causing injury due to overexpansion of an already highly damaged area (*Dai et al., 2013; Guest et al., 2011*). Circumventing this problem would require slower release, however, it has been reported that a therapeutic dose of cells would require a delivery rate of 1 µl over approximately 2 hours; an unsustainable timeframe for clinical application (*Guest et al., 2011*).

A lesion site is an irregular 3-dimensional space (*Siebert et al., 2015*). A second major factor fundamental to the lack of efficacy in surgical techniques, is the delivery of a transplant cell population in a 2-dimensional construct i.e. cell suspension. The cells, following injectable delivery, flow in an uncontrolled manner into the cavity and, in the absence of a structure, settle disproportionately. This heterogeneous distribution of dead, dying and surviving cells leads to high proportions of cell clumping. The high level of cell mortality occasioned by delivery and subsequent clumping of surviving cells leads to further infiltration by macrophages, increasing the already hostile environment and, in turn, lowering survival of the remaining cells (*Pearse et al., 2007*). It is being increasingly realised that **the technical difficulties associated with surgical delivery of transplant cells would be attenuated by the use of a 3-dimensional protective cell construct** (*i.e. Siebert et al., 2015; Vater et al., 2010*).

1.5 Emerging technologies offer the hope for development of better cell therapies

To meet these challenges, two technological approaches have emerged that offer promise for cell therapies to realise their full potential in SCI.

The first approach is that of utilising MPs. These have *i*) been proved as a safe, efficient delivery vector for the genetic engineering of a cell transplant population, and *ii*) through particle labelling of the cell transplant, have shown themselves as an ideal contrast agent for non-invasive tracking under MRI.

The second approach is the delivery of the engineered cell transplant population within a 3-dimensional hydrogel construct. This would offer a protected cell delivery system, which would circumvent the low efficacy of surgical techniques seen with transplant of 2-dimensional cell suspension to the spinal cord. It is the further development of these two approaches that is addressed within this project.

1.5.1 Magnetic platforms as potential tools in basic and clinical neurobiology

The disadvantages inherent within non-viral and viral-mediated delivery systems i.e. their immunogenic response; insertional mutagenesis; potential oncogene activation and their questionable safety (*Ryan & Federoff, 2007*), have brought to the fore the need to develop a non-viral mediated strategy that provides for safe, efficient gene delivery to, and cell:particle labelling of, a cell transplant applicable to clinical applications. In this regard, magnetic assistive technologies offer considerable promise.

Magnetic (nano) particles are ideal candidates for delivery of therapeutic bio-molecules to the spinal cord

Magnetic (nano) particles (MPs) propose themselves as ideal candidates for delivery of therapeutic drugs/genes to the injured spinal cord on a number of counts. One, they possess superparamagnetic (SP) properties, meaning they are only magnetic when in the presence of a magnetic field gradient. Superparamagnetism in these particles is facilitated by the iron oxide - magnetite or maghemite - crystallites which make up their composition (*Hofmann-Amtenbrink et al., 2010*). These SP properties allow MPs to be administered and targeted to the site of interest via an external magnet. Two, they can be functionalised to deliver a therapeutic molecule. Three, for tracking purposes, they have proved themselves as a safe, effective contrast agent under MRI, and as such, are used extensively in clinic.

MPs are typically formulated with a magnetite core, and overlaid with a positively charged surface coating that can be functionalised through attachment of a variety of biomolecules (*Mykhaylyk et al., 2007*). Conjugated fluorophores enable microscopy visualisation, with the magnetite loading acting as a contrast agent for non-invasive tracking under MRI.

Astrocytes show efficient MP uptake

Astrocytes show efficient uptake of various types of particles (*Hohnholt et al., 2013*). However, certain particle formulations have induced a level of toxicity in these cells. For example, silver nanoparticles show a concentration-dependent toxicity (*Haase et al., 2012*), as do other metallic oxide particles i.e. titanium dioxide, zinc oxide and magnesium oxide (*Lai et al., 2008*). By contrast, use of iron oxide MPs have shown themselves to have a high safety profile (*Geppert et al., 2012; Hohnholt et al., 2013; Hohnholt & Dringen., 2013*). Although, particle addition to astrocytes has been shown to be dependent on the cell's developmental age, where addition to immature astrocytes, or to astrocytes that have

not attached to the culture substrate, has prevented cell adherence and subsequently, cell growth (*Au et al., 2007*). Further to this, particle *uptake* in astrocytes appears to be temperature, concentration and time–dependent, with increased uptake of higher iron oxide particles over time (24 h *vs.* 4 h), being markedly reduced at lower temperatures (4° C), showing the uptake mechanisms of this cell to be energy-dependent (*Pickard et al., 2011*).

Astrocytes also show higher and increased uptake of positively charged MPs (*Harush-Frenkel et al., 2007; Sun et al., 2013*), with uptake of negatively charged particles linked to toxicity (*Sun et al., 2013*). There are a number of probable explanations for this. One is the attraction of the positively charged MP to the relative negative charge of the cell (*Ito et al., 2005*). Another explanation offered is that particle charge has a preference for specific endocytotic mechanisms (*Harush-Frenkel et al., 2007*). This then has implications to particle size, as endocytotic mechanisms are also known to be size-dependent (*Oh et al., 2009; Rejman et al., 2004; Zhu et al., 2013*).

Of particle retention in astrocytes, particle accumulation has been shown to be intact up to 21 days post-particle exposure (*Hossain et al., 2014; Pickard et al., 2011*), with a putative link between surface coating and a cell's capacity for particle retention being reported. It was found that dextran-coated particles 'leaked' from healthy MSCs, significantly truncating the timeframe for tracking. However, changing the surface coating to, in this instance, aminopropyltriethoxysilane, facilitated longer term particle retention (*Hossain et al., 2014*).

Magnetic assistive technology to enhance cell:particle interaction

In order to be of functional use in clinical applications, sufficient particle uptake in a cell transplant population is critical to therapeutic gene delivery, and subsequent tracking of the cell (*Bernsen et al., 2015*). However, the major obstacle for particle, and by definition

particle:plasmid uptake is thought to be the cell's endocytotic capability (*Fernandes & Chari, 2015*). To overcome this obstacle, an innovative strategy has been the deployment of static magnetic fields beneath cell monolayers to promote the sedimentation of particle:pDNA complexes onto cells, thereby enhancing complex interaction with, and subsequent uptake by, the cell (*Laurentt et al., 2011*). This process of magnetically assisted gene delivery is referred to as 'magnetofection' (*Plank et al., 2011*). 'Magnetolabelling' refers to the use of this strategy to enhance MP-labelling of cells for tracking purposes. Such an understanding can aid the development of both robust experimental protocols, and state-of-the-art devices, to optimise the use of magnetic assistive technology with astrocytes.

Indeed, use of magnetic fields deployed beneath astrocyte cultures has significantly increased particle uptake in these cells. For example, it has been widely reported that astrocytes show greater uptake of positive compared with negatively charged MPs (*Harush-Frenkel et al., 2007; Ito et al., 2005; Sun et al., 2013).* Yet, application of a magnetic field enhanced particle accumulation of both positive and negatively charged particles (*Sun et al., 2013*). It has also been reported that particle uptake in astrocytes is temperature-dependent, with reduced uptake at 4° C *vs.* 37° C (*Pickard et al., 2011*). However, deployment of a magnetic field beneath the cells circumvents this limitation, with increased particle uptake even at this low temperature, suggesting this strategy plays a role in enhancing endocytotic mechanisms (*Lamkowsky et al., 2012*).

Magnetic field arrays have been further developed to increase their capacity for magnetofection and magnetolabelling purposes. Oscillating, rotating, pulsing and directional-alternating magnetic field arrays have been investigated for enhanced efficiency in magnetofection (*Baryshev et al., 2011; Dahmani et al., 2013; Fouriki et al., 2010; Kamau et al., 2006; McBain et al., 2008; Subramanian et al., 2013*). One particular

array - oscillating magnetic fields - which impart a lateral motion to the MPs, has been postulated to increase cell particle contact across the *whole* cell population (*Pickard & Chari, 2010*). Exposure of cells to oscillating fields has shown significant enhancement of transgene expression in a number of cell types, including in astrocytes (*McBain et al., 2008; Pickard & Chari, 2010*). In this respect, investigation of a *range* of oscillating frequencies found enhanced magnetofection in astrocytes to be frequency-dependent (*Pickard & Chari, 2010*).

Knowledge gaps

In addressing this first approach, that of utilising MPs for genetic engineering and labelling of astrocytes, there appears to be a number of knowledge gaps.

1). It is becoming widely acknowledged that a combinatorial approach to SCI offers the most promise. Therefore with regard to genetically engineering astrocytes as a cell transplant population, transgene expression in astrocytes (and cell lines) has been reported as being frequency-dependent. However, extrapolating the benefits of magnetic oscillating fields to their fullest extent raises further questions:

i) How does the *amplitude* of oscillation affect transgene expression in this cell?

i) How does repeat application of a gene affect transgene expression in this cell?

2). The major limitation with the use of MPs as a contrast agent under MRI is the loss of imaging signal, requiring high MP-loading into the cell transplant to confer utility for tracking (*Bernsen et al., 2015*). To address this, use of high magnetite-loaded MPs may offer the potential for the high sensitivity required for MRI over an extended timeframe. Astrocytes show efficient uptake of MPs, and show a high resistance to iron, being complicit in iron homeostasis in the brain (*Moos, 2002; Moos et al., 2007; Hohnholt &*

Dringen, 2013). This raises a number of questions regarding cell tracking and the factors that govern this in this particular cell type.

i) **How will astrocytes deal with such high magnetite-loaded particles required for clinical application?**

ii) **Further to this, how will astrocytes deal with magnetolabelling strategies that *enhance* uptake of such particles?**

iii) **Astrocytes are a highly proliferative neural cell, what are the factors governing their conferred utility for tracking?**

iv) **With regard to the use of magnetolabelling strategies and their putative role in *enhancing* cellular trafficking of particles, how will this affect particle retention in astrocytes?**

1.5.2 3-dimensional hydrogels as potential constructs for delivery of cell transplant populations

The second approach, of delivering an engineered, trackable cell transplant population within a 3-dimensional construct, has the potential to offset the lack of efficacy of surgical techniques seen with delivery of cell suspension transplants to the injured spinal cord.

Substrate differentially affects cellular function and morphology

The use of 3-dimensional constructs are an emerging field for therapeutic cell transplantation, with the now widely accepted understanding that cells removed from their *in vivo* environment display atypical morphologies *and* functional behaviour when cultured on flat substrates (*Hu et al., 2014; Moshayedi et al., 2010*). For example, on a 2-dimensional substrate, postnatal astrocytes mostly possess a rounded morphology with a small subpopulation of bipolar cells. However, when cultured within the 3-dimensional environment of a hydrogel, these cells developed into a population of equal proportions of round, stellate and perivascular morphologies (*Balasubramanian et al., 2016*). Adult astrocytes show similar comparison between 2-dimensional culture and 3-dimensional *in vivo* environment. They display a flattened, membraneous morphology with truncated processes and a highly proliferative reactive behaviour when plated on a hard substrate, in clear contrast to their highly ramified morphology, and their typically quiescent state *in vivo*.

Of importance to clinical application, functional homeostatic behaviour of astrocytes has been observed to be affected dependent on the substrate on which they are grown (*Lee et al., 2008; Miron-Mendoza et al., 2013*). For example, astrocytes and brain endothelial cells were co-cultured on a 2-dimensional substrate and within a 3-dimensional hydrogel. TGF β1, which is a transforming growth factor responsible for cell growth and development,

was added to the co-cultures to stimulate reactive astrogliosis, i.e. to mimic an injured spinal cord. Modulation of brain endothelial cells was much greater in the hydrogel than in the 2-dimensional culture, suggesting a putative explanation for the increased permeability of the blood-brain barrier observed in SCI. The study highlights the differing results that would have been reported, had this experiment only been conducted on a flat substrate (*Hawkins et al., 2015*). Thus, they present a strong argument that 2-dimensional cell cultures may not fully represent their *in vivo* counterparts (*Hawkins et al., 2015*).

3-dimensional constructs are beneficial to clinical application

So what are these 3-dimensional constructs and what are their benefits to clinical application? Hydrogels are a highly hydrated network of cross-linked polymers with their hydrophilic properties facilitating high water content (*Frampton et al., 2011*). Their protein composition self assembles *in vitro* into a highly fibrous structure that closely approximates an *in vivo* environment (*Trappmann & Chen, 2013*). They have shown themselves to be implantable and mouldable for ease of delivery to various lesion shapes (*Hejcl et al., 2008; Perale et al., 2008*), and show no effect on cell viability (*Frampton et al., 2011*). Indeed, the specific tuneable properties of hydrogels facilitate a cell's typical *in vivo* behaviour (*Trappmann & Chen, 2013*). Development of 3-dimensional constructs such as hydrogels, show promise to the combinatorial approach required for successful regeneration in SCI. They offer the potential to incorporate therapeutic molecules or growth factors, structure to support ingrowing axons, and delivery of cell transplant populations to offer trophic support and recovery of a homeostatic environment.

Collagen as an ideal carrier for cell transplant

The formulation of carrier for delivery of the therapeutic cell transplant is critical to translational application. A hydrogel implant has to be biocompatible and biodegradable,

and yet offer a sufficient time scale for tissue formation, for example, to allow ingrowth of host axons. A number of polymers, synthetic and natural (biologically-derived) have been used for the formulation of hydrogels. Biologically-derived polymers have been classified as superior due to their biocompatibility and the existence of these proteins within the ECM (*Alovskaya et al., 2007*); therefore these will be the focus.

Various formulations of biologically-derived polymers have been used as tissue engineered grafts, scaffolds and *in vitro* models, with hydrogels emerging as a key component for clinical application. However, a number of limitations have been reported with the use of certain gel formulations.

Agarose and methylcellulose hydrogels have shown cell growth, nerve guidance and successful delivery of neurotrophic factors (*Perale et al., 2011 for review*). However, their major limitation is their lack of bioactivity and biodegradability (*Tate et al., 2001; Wells et al., 1997*). Adhesion of cells is prevented within the negatively charged environment of alginate gels. Negatively charged hyaluronan hydrogels do not pose the same problem, having been shown to support viability of encapsulated SCs, although the gel formulation has impeded their success as an implant (*Tian et al., 2005*). Chitosan has been linked with increasing the inflammatory response of a SCI, as its properties activate macrophages and microglia within the lesion site (*Crompton et al., 2006*). Matrigel™, a commercially available hydrogel formulation, does not appear to have the limitations seen with other hydrogels. However, tissue loss has been associated with its use, requiring addition of MPRED to aid in regeneration of infiltrating axons (*Chen et al., 1996*). The use of MPRED, as discussed above, has serious side effects associated with its use, raising concern regarding its use within an implant.

Collagen type IV is the major protein and component of the ECM, and is the most prolific collagen within the brain. However, it is collagen I – found in more than 90% of the body - that is more commonly used in SCI, both for *in vitro* and *in vivo* work (*Hawkins et al., 2015; Di Lullo et al., 2002*). This preference is mainly due to the structural properties of each of the collagen types. Collagen IV is a non-fibrillar protein which forms the basal lamina and thus, is found in basement membrane. Following SCI, because of the disruption caused to the endothelial cells, it shows increased accumulation at the lesion site (*Assuncao-Silva et al., 2015; Stitchel et al., 1999*). Collagen I is a fibrillary protein and therefore, has the properties necessary to form a structural and supportive fibril construct for the purposes of a 'scaffold' or 'bridge' within the lesion site (*Han et al., 2010; Kaneko et al., 2015; Li et al., 2015; 2016; Nam et al., 2010*). For the purposes of the series of experiments reported here, unless otherwise stated, it is collagen type I that is referred to.

Collagen implants used as carriers for neurotrophic or growth factors - 'functionalised scaffolds' - have been shown to promote neurological recovery and spinal cord regeneration. For example, addition of BDNF to a collagen gel implant into a T7-10 crush SCI, showed a slower and more extended release rate than BDNF injection alone. Moreover, this translated into functional improvement over a 6-week period (*Liang et al., 2010*). Similar levels of recovery and regeneration have been reported with addition of BDNF and 151IgG, which is an antibody that neutralises epidermal growth factor receptor (EGFR). EGFR is a precursor of myelin inhibitory factors and CSPG upregulation, therefore targeting EGFR effectively halts these "regeneration inhibitors" (*Han et al., 2010*). Implant into a complete thoracic (T7-10) transected spinal cord prevented glial scarring and promoted regeneration of neurons and electrical synapse transmission (*Han et al., 2010*). Moreover, reports of locomotor recovery and regeneration have been reported

with implant of unfunctionalised gels, which act as a bridging tissue in thoracic transection SCI (*Kaneko et al., 2015*).

Collagen I has been used extensively as a 3-dimensional hydrogel in a number of *in vitro* studies with astrocytes (*e.g. Al Ahmad et al., 2010; East et al., 2009; 2010; 2012; Hawkins et al., 2015; Seyedhassantehrani et al., 2016; Winter et al., 2016*). In comparison to other formulations, collagen offers a homogeneous, consistent composition (*Hawkins et al., 2015*) made up of a porous, fibrillary network that offers structure to encapsulated cells (*Alovskaya et al., 2007; Macaya & Spector, 2012*). These gels possess tuneable characteristics, for example, pore size is concentration-dependent, allowing for ingrowth of neurites (*Willits & Skornia, 2004*). Applying tension to the gel can induce alignment of the encapsulated cells, with "mechanical elongation" producing longer length "stretch-growth" of astrocytic processes cultured on top of collagen gels; both mechanisms facilitating guidance for axonal growth (*East et al., 2010; Katiyar et al., 2016*).

Collagen gels are biodegradable and yet retain sufficient function within the lesion site for ingrowth of sprouting axons. For example, collagen degradation time is approximately 3 - 4 weeks, yet can be extended up to 6 months with the addition of additives (*Kaneko et al., 2015; Macaya & Spector, 2012*). Rodent axonal sprouting within collagen implants has been observed as early as 3-4 weeks post implant (*Hill et al., 2001; Yoshii et al., 2004*), proposing these gels as functional implants for the regenerating spinal cord. In the context of axonal ingrowth, again collagen has been shown to provide a permissive environment, as endogenous proteases released from the tips of neuronal growth cones possess the ability to degrade collagen, thus facilitating axonal regeneration through the implant (*Seeds et al., 1997*). Of further importance to the use of these hydrogels as a carrier for astrocytes as a cell transplant, collagen type I has been shown to inhibit glial proliferation of the

encapsulated astrocytes, *and* inhibit endogenous astrocyte response in host tissue (*Eccleston et al., 1989*).

Considering the large body of evidence regarding the regenerative benefits of astrocytes as a transplant population in the injured spinal cord, there are relatively few studies utilising astrocytes as a cell transplant population within a hydrogel, as an implant into a SCI. One such study transplanted neonatal astrocytes encapsulated within a collagen hydrogel, into a bilateral transection of the dorsal half of the spinal cord at the thoracic level (T7-9) (*Joosten et al., 2004*). The study reported survival and localisation of the astrocytes to the implant, and significantly increased ingrowth of neurofilament positive fibres and cortico-spinal axons. Of consequence to the beneficial influence of astrocytes, the axonal and fibre ingrowth was closely associated with the transplanted cells. Moreover, regeneration within the lesion site translated into functional recovery, with modest improvement of locomotor recovery and fore-hind limb co-ordination (*Joosten et al., 2004*). What is interesting is that cell tracking was facilitated with fast blue dye and subsequent histological analysis.

Knowledge gaps

Taken together, these findings highly promote the benefits conferred by 3-dimensional hydrogels to bridging the gap between bench and clinic. However, as this is an emerging field, and as astrocytes have until relatively recently been overlooked, there are a number of major knowledge gaps.

1). While the combination of astrocytes and hydrogels as an implant is still relatively unexplored, it is clear that use of a 3-dimensional substrate offers greater knowledge applicable to an *in vivo* environment than cultures grown on 2-dimensional substrates. Moreover, the use of a combinatorial approach offers greater promise to SCI than separate procedures. Of major consequence to cell transplant is the survival of the cells to be able to

offer any regenerative purpose. In this respect, hydrogels may offer the potential for a protective cell delivery system as a carrier for cell transplants. This raises a number of questions:

i) **How will a 3-dimensional environment affect astrocyte characteristics, compared with cultures grown on a 2-dimensional flat substrate?**

ii) **How will a collagen hydrogel offer potential as a carrier of a cell transplant, in terms of addressing the challenges presented by lack of efficacy in surgical technique?**

2). The tracking of cell transplants utilising MPs as a contrast agent, has proved successful with cell suspensions. However, as astrocytes are a highly proliferative neural cell, this may present specific challenges.

i) **How will this affect the *utility* for tracking with this cell when grown within a 3-dimensional construct?**

ii) **Moreover, how will the *capacity* to track a MP-labelled cell transplant be affected when grown within a hydrogel construct?**

In further developing these two main approaches, 1) utilising magnetic particles for magnetofection and magnetolabelling of astrocytes, and 2) the delivery of an engineered cell transplant within a 3-dimensional construct, the knowledge gaps that have arisen have informed the main aims of this research.

Chapter 2
Materials and Methods

2.1 Materials

All tissue culture-grade plastics were from Greiner bio one Ltd (Stonehouse, UK). Media, media supplements (including foetal bovine serum [FBS-Ref. 11573397]) and reagents, excepting where stated, were from Fisher Scientific (Loughborough, UK) and Sigma-Aldrich (Dorset, UK).

Reagents used in the transfection experiments were pmax:GFP plasmid which was from Amaxa Biosciences (Cologne, Germany) and prepared using Endofree® Plasmid Maxiprep Kit which was from Qiagen (UK). The NeuroMag and NeuroMag Fluo particles used for transfection were obtained from Oz Biosciences (Marseilles, France). The magnetic particles used for cell labelling experiments were prepared by the Boris Polyak Laboratory, Drexel University, Philadelphia using published procedures *(MacDonald et al., 2012).*

For immunocytochemistry, the primary antibody used was polyclonal rabbit anti-glial fibrillary acidic protein (GFAP; Z0334), which was from DakoCytomation (Ely, UK). The secondary antibodies, fluorescein isothiocyanate (FITC) and Cy3-conjugated AffiniPure donkey anti-rabbit, IgG, were both sourced from Jackson Laboratories (Pennsylvania, USA). Normal donkey serum was from Stratech Scientific (Suffolk, UK) and Vectashield mounting medium containing DAPI (4',6-diamidino-2-phenylindole) was from Vector Laboratories (Peterborough, UK).

For the 3-dimensional collagen hydrogel experiments collagen type I, rat tail, high concentrate (H/C; Corning - No. 354249; 100 mg) was sourced from VWR (Lutterworth, UK). Agarose type VII: low gelling temperature (A4018), was from Sigma-Aldrich (Dorset, UK). Hoechst 33342 (used as a nuclear counterstain as it emits blue fluorescence when bound to double stranded DNA) was from ThermoFisher Scientific (Loughborough,

UK). The CELLview™ glass bottom dish (No. 627 899) was from Grenier bio-one (Stonehouse, UK).

Reagents for safety assays were CellTiter 96 Aqueous One Solution Reagent MTS [3-(4,5-Dimethylthiazol-2-yl)-5-(3-carboxymethoxyphenyl)-2-(4-sulphophenyl)-2H-tetrazolium, inner salt] assay from Promega UK (Southampton, UK) and Click-iT® Plus EdU Alexa Fluor® 488 Flow Cytometry Assay Kit from Life Technologies (Paisley, Scotland, UK). For the live-dead studies propidium iodide (penetrates compromised membranes of dead cells) was from Fisher Scientific (Loughborough, UK) and calcein AM [fluoresces when metabolised in live cells (80011-10)] was sourced from VWR (Lutterworth, UK).

2.2 Preparation of mixed glial culture and isolation of cortical astrocytes

The care and use of animals used in the production of cell cultures was in accordance with the Animals (Scientific Procedures) Act of 1986 (UK), and with approval by the local ethics committee.

2.2.1 Preparation of mixed glial culture

Mixed glial cultures [microglia; OPCs; astrocytes] were derived from disaggregated cortex of Sprague-Dawley rat pups (postnatal day 1-3) with dissection procedure conducted following established protocols (*Cole & de Vellis, 2001*). Cell suspension was diluted with D10 medium (Dulbecco's modified Eagle's medium plus 2 mM glutaMAX-I, 1 mM sodium pyruvate, 50 U/mL penicillin, 50 µg/mL streptomycin, and 10% FBS) and routinely seeded at a cell density of ≻ 0.75 x 106 viable cells/mL into poly-D-lysine [PDL (10 µg/mL working solution – 7.5 mL/flask]-coated T75 flasks. Cultures were maintained in D10 medium with a 100% D10 medium change at 24 h, and a 50% D10 refresh every 2-3 days. All cultures were incubated at 37° C in 5% CO2/95% humidified air

2.2.2 Isolation of astrocytes from mixed glial culture

At day 7-8, sequential shaking of the culture flasks facilitated the isolation of a high purity astrocyte culture for sub-culturing. Briefly, the flasks were shaken for 2 h and the medium (containing largely microglia and OPCs) discarded. The flasks were then rinsed with phosphate buffered saline (PBS), then fresh D10 medium (10 mL) was added before being incubated at 37° C (5% CO_2/95% humidified air) for 2 h to re-gas (restore physiological pH and a 5% CO_2 flask headspace). To remove all OPCs and microglia, this step was repeated sequentially over the following 2-3 days, with the flasks shaken for 22 h each day followed by a 100% medium change and 2 h to re-gas. Visualisation of ≤ 10 OPCs per

microscopic field (100 x magnification) was considered indicative of sufficient astrocyte purity for subculturing.

2.2.3 Sub-culturing of astrocytes

Following the sequential shakes, the astrocyte monolayer was washed with PBS to remove traces of medium, as FBS inhibits trypsin. TrypLE™ (a dissociation reagent; 2.5 mL/flask) was added to the cell culture and the flask placed on an orbital shaker for *ca*. 5 min @ 100 rpm. Dissociated cells were centrifuged (1000 rpm; 4 min) and cell counts were performed by mixing 10 µl of cell suspension with 10 µl of 0.4% trypan blue (an exclusion dye that selectively stains dead cells blue), and adding 10 µl of the cell mixture into one chamber of the haemocytometer. Viable cells appeared bright and round. Cells were seeded at 1-2 x 10^5 cells/mL D10 in PDL-coated T75 flasks. Since OPCs adhere more slowly and less avidly than astrocytes, a 100% medium change performed *ca*. 1 h post-seeding helped to further reduce any OPC contamination.

Subsequent passages of the astrocyte flasks were conducted while cultures were subconfluent (*ca*. 2-3 d post-plating), up to a maximum of two passages per culture. For all 2-dimensional monolayer experiments cells were seeded at 2.7 x 10^5/mL D10 either on PDL-coated coverslips in a 24-well plate (0.3 mL/well), directly on a PDL-coated 6-well plate (0.9 mL/well) or on a PDL-coated 96-well plate (0.07 mL/well) for use in MTS assays.

In preparation for hydrogel studies, cells were seeded at 2.7 x 10^5/mL D10 either directly on a PDL-coated 6-well plate (0.9 mL/well) or in PDL-coated T175 flasks (20 mL/flask). Cultures were maintained in D10 medium (incubated at 37° C in 5% CO_2/95% humidified air) with a 50% medium refresh every 2-3 days.

2.3 Oscillating magnetic array for MP-labelling of and MNP-mediated gene transfer to astrocyte monolayers

All magnetofection protocols were conducted using the magnefect-nano oscillating magnetic array device (nanoTherics Ltd., Stoke-on-Trent, UK). The device utilises high gradient neodymium iron boron (NdFeB) magnets with lateral oscillation capability having both programmable frequency (F = 1 – 4 Hz) and amplitude (100 – 1000 µm), with a field strength at the magnet face of 421 ± 20 mT (24-magnet array) and 303 ± 5 mT (96-magnet array) (*Pickard & Chari, 2010*). The interchangeable 24-well and 96-well magnetic arrays facilitated the use of different size culture plates but having similar experimental configurations. *(Figure 2.1)*

Unless otherwise stated, each experiment utilising magnetofection consisted of three conditions; no magnetic field (NF), static magnetic field (F0) or oscillating magnetic field with specific frequency and amplitude of displacement. Within the experiments, the cells were subjected to 30 min application of either the static or the oscillating magnetic field.

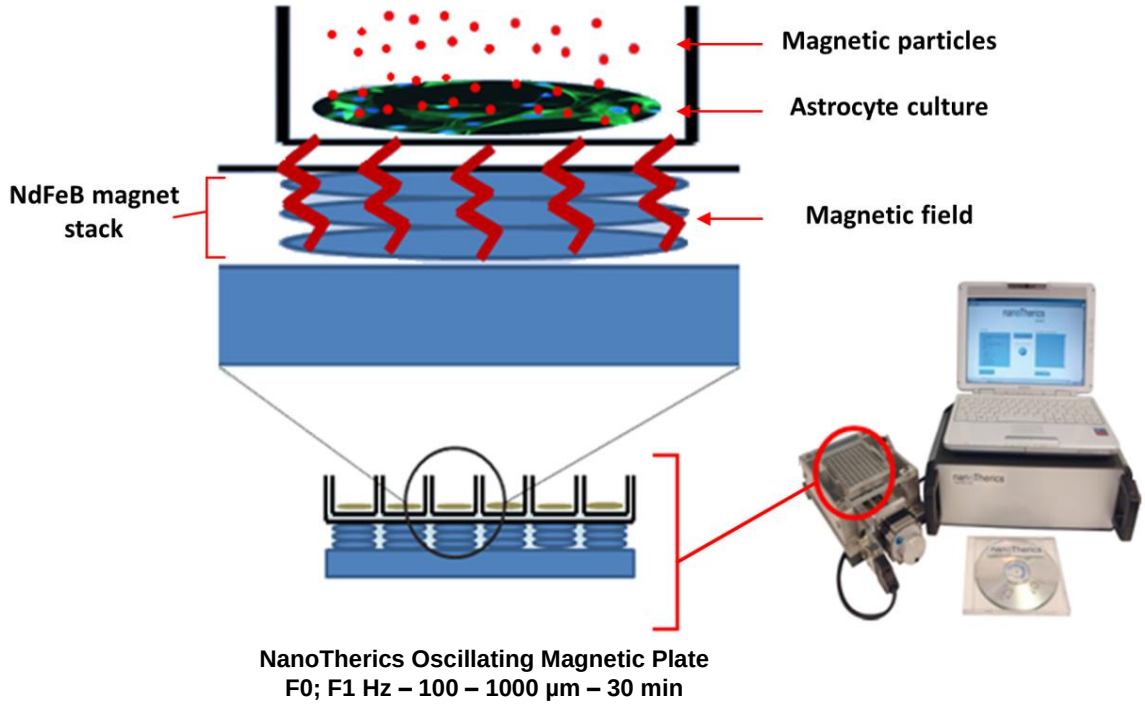

Figure 2.1: Schematic diagram of magnefect-nano oscillating magnetic array device (NanoTherics, UK) *The magnefect-nano oscillating magnetic array device utilises static or oscillating magnetic fields with a programmable combination of frequency and amplitude. Interchangeable arrays of 24 and 96 magnets enabled similar experimental configurations to be used for both 24- and 96-well plates. Frequency and amplitude used in transfection experiments was F0 or F1 Hz and 100-1000 µm, with F0 or F1 Hz and 200 µm amplitude used for the labelling experiments.*

2.4 MP – labelling (magnetolabelling) of astrocyte monolayers

2.4.1 Particle characterisation

Four types of magnetic particles (MPs) of differing magnetite content were used for uptake experiments and were evaluated for their labelling efficiency (percentage of cells labelled) and extent of accumulation in astrocytes. All four types were prepared using published procedures by the Boris Polyak Laboratory, Drexel University, Philadelphia, *(MacDonald et al., 2012)* with extensive characterisation having been undertaken previously *(Adams et al., 2015; Johnson et al., 2010; MacDonald et al., 2012).*

The superparamagnetic MPs were composed of a matrix of magnetite, poly (lactic acid; PLA) and poly (vinyl alcohol; PVA) with a BODIPY® 564/570 fluorophore-PLA coating. Differences in magnetite loading in the three types of magnetite-loaded particles resulted in MPs with magnetite *weight percent* ratios of 1:3:7, from which the nomenclature MP-1x; MP-3x and MP-5x originated and to which they are hereinafter referred. This increase in magnetite loading altered their magnetic responsiveness and weight but not their size (hydrodynamic diameter range of 262-278 nm), their shape (as imaged under transmission electron microscopy [TEM]; *see Figure 2.2*) or their surface charge (-8.98 to -14.4 mV). A non-magnetic control particle with no magnetite (having the nomenclature MP-0x) was also synthesised, its size, shape and surface charge similar to the magnetite-loaded particles *(Table 2.1).* Use of fourier transform infrared spectroscopy (FTIR) has previously confirmed the overall similarities in composition of these particles, irrespective of their differing magnetite loading *(Adams et al., 2015).*

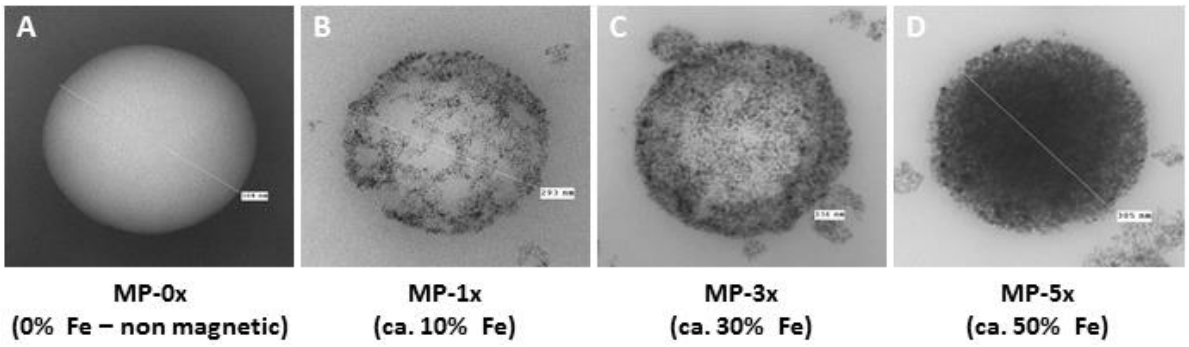

Figure 2.2 Transmission electron micrographs of the MP-0x – MP-5x particles *All four particles can be clearly visualised under TEM with the differing magnetite content of each particle (Non-Mag; MP-0x; MP-1x; MP-3x and MP-5x) a defining characteristic. Note also the similarity in shape and size of all four particles. Images courtesy of Boris Polyak Laboratory and adapted from Johnson et al., 2010*

The superparamagnetic nature of the particles allows for magnetic responsiveness only when particles are exposed to a magnetic field gradient. Therefore use of these particles in combination with the deployment of a magnetic field gradient (e.g. permanent NdFeB magnets used throughout this series of studies) beneath the culture plate attracts the particles down to the cell monolayer, while the application of an oscillating field/gradient may cause particles to (*i*) move laterally with the movement of the magnets, enhancing the likelihood of contact with cells, and/or (*ii*) vibrate *in situ* when attached to cell membrane, potentially stimulating endocytotic mechanisms and enhancing cellular MP uptake (*Adams et al., 2013; Fouriki et al., 2010; McBain et al., 2008; Pickard et al., 2011*).

All MPs were stored at 4° C in a lyophilised state and re-suspended in 100 µl of sterile deionised water as required. Once re-suspended, the MPs were kept at 4° C and protected from light until use. For experiments, 1 µl of MPs per mL of D10 was used, a concentration that corresponded to 13 µg/mL dry weight for MP-0x, 15 µg/mL for MP-1x,

19 µg/mL for MP-3x and 26.5 µg/mL dry weight for MP-5x; each corresponding to an identical number of particles per mL (*Adams et al., 2015*).

Table 1. Physical characterisation of magnetic particles

Magnetic particle	Weight corresponding to magnetite (%)	Magnetite content w/w	Hydrodynamic diameter (nm)	ζ-potential (mV)
MP-0x	-	Non-magnetite	267 ± 1	-8.98 ± 0.16
MP-1x	6.7	11.5 ± 1.0	262 ± 10	-9.46 ± 0.14
MP-3x	19.2	27.7 ± 3.1	254 ± 3	-11.05 ± 0.07
MP-5x	35.4	46.0 ± 1.1	278 ± 2	-14.40 ± 0.34

Table 2.1 Physical characterisation of magnetic particles *Magnetic particles of differing magnetite content were used for all uptake experiments, and evaluated for their labelling efficiency, and extent of accumulation in astrocytes. There was little difference in physical characteristics between the particles. The increase in magnetite loading altered their magnetic responsiveness but not their size, shape or surface charge* (*data taken from Adams et al., 2015; MacDonald et al., 2012)*

2.4.2 Magnetolabelling of astrocytes utilising the magnefect-nano oscillating magnetic array device

At 24-48 h post-plating (allowing for cell adherence and growth of processes), the MPs were added to the cells; diluted per weight ratio (*see 2.4.1*) in fresh D10 (1 µL/mL D10) in a final volume of 0.3 mL/well for 24-well plates. Following particle addition, the plates were immediately placed on the magnefect-nano device *(see 2.3)* for 30 minutes using

either a static magnetic field (F0) or an oscillating magnetic field having a frequency of F1 Hz and an amplitude of 200 µm (F1; 200 µm). The cells under the NF condition were incubated in the absence of a magnetic field. All magnetolabelling was carried out at 37° C in the 5% CO_2/95% humidified air incubator. After 30 minutes, the cell plates were removed from the device and incubated at 37° C (5% CO_2/95% humidified air). Controls consisted of unlabelled cells (no particles) which were subjected to the same magnetofection protocols. For all magnetolabelling experiments, at 24 h post-particle addition the cells were rinsed once with PBS to remove any extracellular particles and subsequently maintained in D10 medium, incubated at 37° C. For long term experiments (21 days) cells were maintained in D10 medium with a 50% refresh every 2-3 days (incubated at 37° C).

2.4.3 Magnetolabelling of astrocytes as monolayers in preparation for use in hydrogel constructs

In preparation for the hydrogel experiments, as detailed above monolayer cultures were grown in T175 flasks (*see 2.2.3*). MP-5x labelling of these cell monolayers was carried out 24 -48 h post-plating with MP-5x particles added to the cells in fresh D10 (1 µl/mL D10) in a final volume of 20 mL/flask. The cells were exposed to a static magnetic field (F0) for 30 minutes. As with well plates, controls consisted of unlabelled cells (no particles) and were subject to the same magnetofection protocol. Following 24 h post-particle addition, cells were rinsed once with PBS to remove any particles not internalised by the cells. Control and MP-labelled cells were then enzymatically detached and used for hydrogel experiments.

2.5 Processing of astrocyte monolayers

2.5.1 Particle inheritance by daughter cells of dividing astrocytes

Particle inheritance by daughter cells of dividing labelled astrocytes was assessed using dynamic time-lapse microscopy. Time-lapse images were captured over at least 48 h. Cells were incubated at 37° C in D10 medium with 5% CO_2.

2.5.2 EdU as a measure of proliferation in cell monolayers

A Click-iT® EdU (5-ethynyl-2´-deoxyuridine) cell proliferation assay was used as a measure of proliferation. Briefly, 10 µM EdU in a final volume of 0.3 mL D10 was added over the coverslip followed by incubation at 37° C for 18 h. This incubation time was determined by the cell growth rate for astrocytes which is acknowledged to be between 14 – 24 h (*Pedram et al, 1998*). The cells were then fixed in 4% PFA for 30 min at RT, followed by 2 washes with 3% bovine serum albumen (BSA). Incubation for 20 min in 0.3% Triton-X 100 in PBS (0.5 mL) permeabilised the cells facilitating access to the internalised cell DNA. Following permeabilisation, the cells were washed twice in 3% BSA and the reagent cocktail for EdU detection was distributed over the cells (0.3 mL final volume/well; see Appendix 1). Following incubation at RT for 30 min (protected from light), the cells were washed twice with 3% BSA. In preparation for imaging and analysis, the coverslips were mounted on slides using mounting medium containing DAPI, with the coverslips sealed with nail varnish to prevent dehydration. Imaging took place immediately.

2.5.3 Termination of monolayer experiments

To terminate the monolayer experiments, at the indicated time (4 – 48 h post-particle addition for short-term experiments; 21 days for long-term), cells were rinsed twice with

PBS before being fixed with 4% PFA for 30 min at RT. Following fixation cells were washed three times with PBS to remove fixative, and stored at 4° C prior to immunolabelling.

2.6 MNP-mediated gene transfer (magnetofection) to astrocyte monolayers

2.6.1 Particle characterisation

NeuroMag and NeuroMag Fluo transfection-grade magnetic particles are patented by Oz Biosciences and have a proprietary formulation involving iron oxide and polyethylenimine. Our laboratory has characterised the physicochemical properties of these particles. Briefly, the positively-charged (ζ-potential +40.3 mV) particles range in size from 140-200 nm with an average size of 160 nm for NeuroMag *(Pickard & Chari, 2010)* and 200 nm for NeuroMag Fluo (*Fernandes & Chari, 2014).* The positive charge facilitates binding of nucleic acids, allowing the particles to serve as transfection vectors. NeuroMag-based protocols have resulted in high transfection efficiencies (*ca*. 60%) in astrocytes (*Pickard & Chari, 2010*), demonstrating their suitability for use here. Both NeuroMag and NeuroMag Fluo are biodegradable within cells over 96 h. NeuroMag Fluo are NeuroMag particles with a tetramethylrhodamine-conjugate that can be visualised under fluorescence microscopy (excitation peak 555 nm; emission maximum 580 nm); the covalent coupling of this label to the particles ensuring non-disruption during cellular internalisation *(OZ BIOSCIENCES: Pers. Comm.).* These fluorophore-labelled particles were used to study the co-localisation of MP-labelling with transgene expression.

2.6.2 Plasmid characteristics

To assess transfection efficiency a plasmid encoding a reporter transgene was used (pmaxGFP; 3486bp; Figure 2.3) which encodes green fluorescent protein (*gfp*). Large scale plasmid DNA preparations (Maxipreps) were generated using the Endofree® Plasmid Maxiprep Kit following the manufacturer's instructions. Briefly, pmaxGFP transformed bacteria were cultured overnight at 37° C on agar containing Kanamycin (50 mg/mL). The

following day colonies were transferred to LB broth and incubated overnight (37° C, 180-200 rpm on an orbital shaker) to prepare precultures. Minipreps were carried out in order to verify the presence of the pmaxGFP plasmid prior to carrying out maxipreps. For minipreps, the following protocol was used in accordance with Qiagen Qiaprep® Miniprep kit. 1 mL of the bacterial precultures was transferred into eppendorfs and centrifuged for 5 min (1000 rpm). The supernatant was removed and 250 µL of P1 added to the pellet followed by 250 µL of P2, the eppendorf gently inverted to mix the two solutions. Addition of Buffer N3 was followed by centrifugation for 10 min (13000 rpm). The resulting supernatant was poured into a filter column tube and centrifuged for 30-60 s. The supernatant in the tube was discarded and Buffer PB (0.5 mL) added on top of the filter and the contents centrifuged for 1 min (13000 rpm). The supernatant was again discarded and Buffer solution PE (750 µL) added and centrifuged for *ca*. 1 min. The column was then emptied and re-centrifuged to remove all traces of ethanol. The column containing the DNA was transferred to a fresh eppendorf and 50 µL of EB Buffer added to the centre of the filter and incubated at RT for *ca*. 1 min and then centrifuged for 1 min (12-13000 rpm) to retrieve the maximum yield of DNA. For Maxipreps, the remaining preculture was used to inoculate 400 mL of LB broth (containing Kanamycin)

For Maxipreps, a similar protocol to minipreps was carried out. For resuspension and lysis of the bacterial pellet, Buffers P1 and P2 were added respectively. For neutralisation the lysis reaction Buffer P3 was added. This mixture was filtered to obtain a clear lysate to which Buffer ER (endotoxin removal) was added and incubated for 30 min. This mix was then added to a DNA purification column, washed (Buffer Q3) and eluted (Buffer QN). DNA was precipitated with the addition of isopropanol, the resulting DNA pellet washed with 70% ethanol and dissolved in Buffer TE. This yielded high quality plasmid DNA without contaminating endotoxins from the *E.coli* host.

(*P1; P2; Buffer N3; Buffer PB; Buffer PE; EB Buffer referred to above are all proprietary components of the Qiaprep® Miniprep Kit. P1; P2; P3; ER; Q3; QN; TE referred to above are all proprietary components of the Endofree® Plasmid Maxiprep Kit*)

Figure 2.3 pmaxGFP plasmid map *pmaxGFP plasmid encodes for green fluorescent protein (GFP) facilitating the scoring of transfected cells using fluorescence microscopy. Plasmid map image adapted from amaxa Nucleofactor® technology literature.*

2.6.3 MNP-mediated gene transfer to astrocytes using the magnefect-nano oscillating magnetic array device

The transfection protocol was performed in 24- and 96-well plates at 24-48 h post-plating to allow for cell adherence and growth of processes. In the use of lipofection for gene transfer, adverse effects on transfection efficiency were reported with the use of antibiotics in the medium (*Asgharian et al., 2014*), therefore 1 h prior to particle addition, all wells were refreshed with antibiotic-free D10 (24 well, 0.225 mL; 96 well, 0.054 mL).

For each well of the 24-well plate, 60 ng of pmaxGFP plasmid was mixed with 0.21 µL NeuroMag or NeuroMag Fluo in a final volume of 75 µL DMEM, and for each well of the 96-well plate, 12 ng of pmaxGFP was mixed with 0.042 µL NeuroMag or NeuroMag Fluo in a final volume of 15 µL DMEM. The plasmid:particle solution was triturated gently to mix and allowed to complex for 20 min. The complexes were then gently added dropwise to the cells while gently moving the plate in a circular manner to help disperse the complex over the cell monolayer. DMEM alone or DMEM plus plasmid were added to the control wells. The plate was then placed on the magnefect-nano device *(see 2.3)* with cells:particles and controls exposed to an oscillating magnetic field (F = 1 Hz; at a 100 – 1000 µm amplitude of displacement) for 30 min. All magnetofection was conducted at 37° C within the 5% CO_2/95% humidified air incubator. As the term suggests, plates containing cells under the no magnetic field (NF) condition were incubated in the absence of a magnetic field.

After removal from the magnefect-nano device, the cells were incubated without a magnetic field for 30 min followed by a 100% medium change of antibiotic-free D10 to remove any extracellular particles. The cells under the NF condition also received a 100% antibiotic-free medium change at this time point. All cells were incubated for a further 47 h

(48 h in total), as previous studies have bracketed this time point at which *gfp* expression is maximal in 2-dimensional cell monolayers *(Guo et al., 1996; Pickard & Chari, 2010; Rubio et al., 2004).*

At 48 h, the cells in the 24-well plate were rinsed twice with PBS before fixing with 4% paraformaldehyde (PFA) for 30 min incubation at RT. Following fixation the cells were washed three times to remove any residual fixative and stored at 4 °C prior to immunolabelling. In contrast, the cells in the 96-well plate were immediately subjected to an MTS assay.

Controls for the experimental plate and the MTS assay consisted of cells only and cells+plasmid, with further controls for the MTS assay consisting of blanks (no cells) containing medium; medium+plasmid; medium+plasmid+MNPs. A key point to note here is that cells+MNPs and medium+MNPs were not classed as viable controls as unfunctionalised MNPs (without plasmid) are considerably smaller and have a substantially different charge to that of a functionalised MNP (in this case, NeuroMag+plasmid). As unfunctionalised MNPs would not be used to engineer cells it was more pertinent to measure any potential toxicity of functionalised NeuroMag.

2.7 Collagen I hydrogel experiments

Collagen I hydrogels were used as a substrate for 2-dimensional monolayer surface seeding and for 3-dimensional internal seeding of astrocytes (hereinafter referred to as 'supraconstruct' and 'intraconstruct' hydrogels respectively). Hydrogels were assembled using a published protocol (*Phillips & Brown, 2011*) producing a collagen substrate with a multi-layered and porous fibrillary collagen network (*Figure 2.4).*

Supraconstruct – astrocytes seeded as monolayers on top of a collagen I hydrogel

Intraconstruct – astrocytes seeded within a collagen I hydrogel

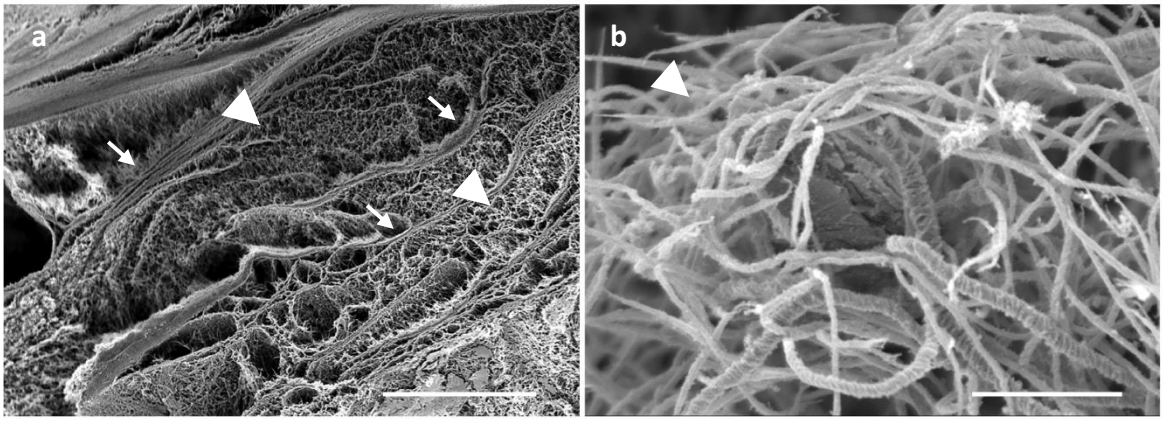

Figure 2.4 Structural composition of collagen I hydrogel substrate *Scanning electron micrographs show the structural composition of the hydrogels. Note the multi-layered construction of the gels (a; arrow) and the open fibrillary network (a & b; arrow head). Scale of images (a = 74.4 µm); (b = 7.5 µm)*

2.7.1 Preparation of a Collagen I hydrogel for use in supraconstruct experiments.

All preparation of hydrogels was conducted under aseptic conditions, keeping all components at 4° C until ready for use. Collagen I, rat tail, high concentrate was used to assemble the hydrogels, diluted in 0.6% acetic acid to a 2 mg/mL concentration for use in both supra- and intraconstruct hydrogel experiments. Each hydrogel had a final volume of 0.5 mL. The composition of the assembled hydrogel was 80% 2 mg/mL Collagen I; 10% Modified Eagle's Medium (MEM) Alpha (10x) and 10% D10 medium for supraconstruct hydrogels; the latter constituent replaced with 10% cell suspension (at 1 x 10^6 cells/gel) in D10 for intraconstruct hydrogels. For both types of gel, prior to addition of D10 or cell suspension in D10, sodium hydroxide (NaOH; 1x) was used to obtain neutral pH.

In preparation to forming supraconstruct hydrogels, coverslips were placed into the 24-well plates and kept hydrated in D10 which was aspirated off just prior to dispensing the hydrogel solution. Placement of coverslips in the well was to ensure the correct orientation of the hydrogels when removing them for imaging purposes. The following technical procedures were adhered to during formation of the supraconstruct hydrogels - the hydrogel solution and the D10 were prepared in separate 50 mL falcon tubes to permit gentle addition of the different components, with a 10 mL pipette used when dispensing the hydrogel solution into the well plate to prevent shearing of the collagen fibres or addition of bubbles to the viscous collagen solution.

The hydrogel solution was prepared by adding the MEM Alpha to the collagen, gently swirling the tube to mix. To bring the solution to neutral pH, NaOH was added in a dropwise manner while gently swirling the tube, until the hydrogel solution turned red, the colour change indicating neutral pH. This colour change is due to the phenol red contained within the MEM Alpha. Upon neutral pH, the hydrogel solution was immediately added to

the D10, again gently swirling to mix. To form the hydrogel, a 10 mL pipette was used to dispense 0.5 mL of the hydrogel solution into each well of a 24- well plate (0.5 mL/gel). The hydrogels were incubated at RT for 15 min before incubating at 37° C (5% CO_2/95% humidified air). This 15 min step allowed for a gradual increase in temperature facilitating the setting process. After 1 h D10 medium was gently added over the top of the hydrogels to keep them hydrated (*Figure 2.5*).

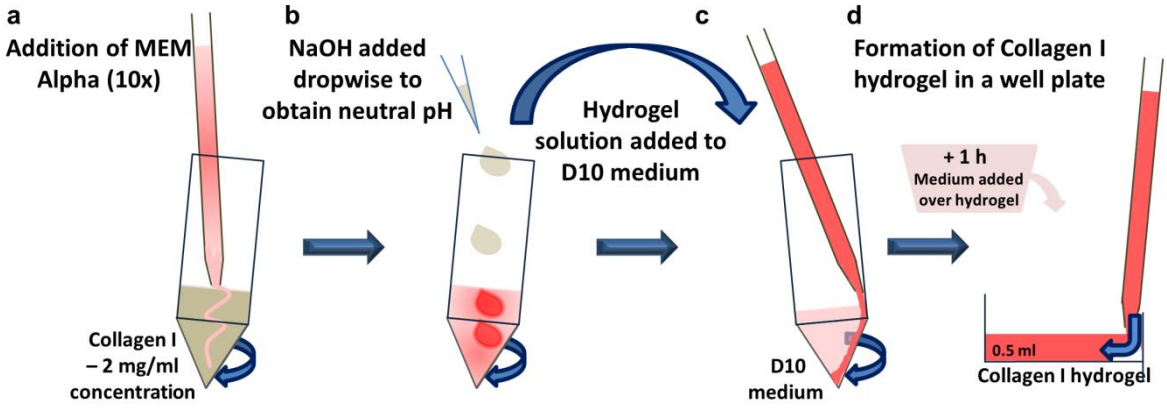

Figure 2.5 Schematic of Collagen I hydrogel construct *MEM Alpha (10x) is added to the (a) 2 mg/mL Collagen I in a 50 mL falcon tube and the two liquids swirled gently to mix. Dropwise addition of (b) sodium hydroxide brings the hydrogel solution to neutral pH indicated by a colour change of the solution to red. Using a 10 mL pipette (c), the hydrogel solution is added gently to D10 medium before (d) dispensing 0.5 mL hydrogel solution per gel/well in a 24-well plate. After 1 h incubation, D10 medium is added gently over the top of the hydrogel to prevent dehydration.*

2.7.2 Supraconstruct hydrogels with MP-labelled astrocytes

After further 2 h incubation, cell monolayers at 2.7 x 10^5 cells/mL were seeded on top of the hydrogel, following one of two labelling approaches (*Figure 2.6*).

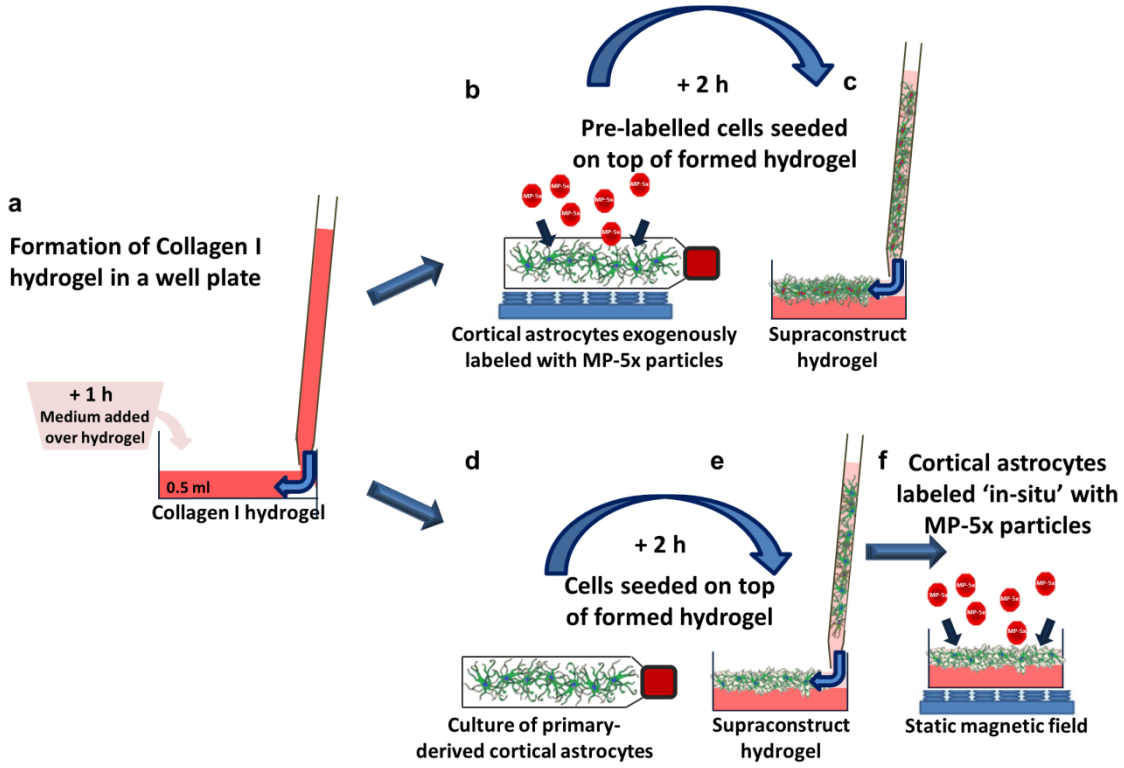

Figure 2.6 Schematic outlining the two approaches used in MP-5x labelling of supraconstruct hydrogels *Following (a) formation, astrocytes were seeded as a monolayer to form a supraconstruct hydrogel. Cells were either (b) pre- labelled with MP-5x particles as a monolayer culture before (c) seeding onto the formed hydrogel, or (d) unlabelled (no particles) cells from monolayer cultures were (e) seeded onto the hydrogel, and after 24 h (f) were labelled 'in-situ' with MP-5x particles following the same protocol as for cell monolayers on coverslips.*

One approach was to pre-label the cells with MP-5x particles as a monolayer culture (*see 2.4.2*), enzymatically detach and seed these pre-labelled cells on top of the gel, forming an '*pre-labelled'* supraconstruct hydrogel. The second approach was to seed cells as a monolayer on top of the gel and, following 24 h to allow cell growth and adherence, label the cells with MP-5x particles in-situ, using a static magnetic field to draw the particles down to the cell monolayer, forming an *'in-situ labelled'* supraconstruct hydrogel. In-situ labelling followed the same protocol as for cell monolayers on coverslips, as detailed above (*see 2.4.2*)

Supraconstruct hydrogels were maintained in D10 medium, incubated at 37° C (5% CO_2/95% humidified air), with a 50% D10 refresh every 2 days. Samples were subject to different processes as detailed below (*see 2.8.1*).

2.7.3 Preparation of a Collagen I hydrogel for use in intraconstruct experiments

The hydrogel assembly for the intraconstruct hydrogels used the same protocol and the same concentration as used previously (*see 2.7.1*) with the 10% D10 medium replaced with 10% cell suspension in D10 at 1 x 10^6 cells per hydrogel. Final volume of the assembled hydrogel was 0.5 mL as detailed previously (*see 2.7.1*).

2.7.4 Intraconstruct hydrogels with MP-labelled astrocytes

In addition to intraconstruct seeding of gels with unlabelled (no particles) cells, particle labelling of cells associated with an intraconstruct hydrogel required two different protocols; exogenous particle-labelling and in-situ particle labelling, both of which are detailed further within each experimental chapter. Briefly, exogenous particle-labelling refers to cells pre-labelled (MP-5x) as monolayers in T175 flasks. These exogenously labelled cells were added as cell suspension when forming an intraconstruct hydrogel, as

detailed above (*see 2.7.1; 2.7.3*). In-situ particle labelling refers to addition of magnetic particles (MP-5x) to the cell suspension prior to association with the hydrogel solution. In-situ labelling allowed observation of endocytotic activity in intraconstruct hydrogels, i.e. intracellular particle uptake and trafficking.

Following assembly of the intraconstruct hydrogels, incubation was carried out in two steps as for the supraconstruct gels as detailed above (*see 2.7.1*). After 1 h post-construct, D10 (0.5 mL) was gently added over the hydrogels with a 100% refresh at 30 min intervals over 90 min to replenish protein/nutrients taken up by the internalised cells. Following 3 h incubation, the hydrogels were transferred from a 24-well plate to a 12-well plate (*detailed further within the experimental chapter*), and maintained in D10 at 37° C (5% CO_2/95% humidified air) with a 50% D10 refresh every 2 days. Samples were subject to different processes as detailed below (*see 2.8.2*).

2.8 Processing of hydrogels

At termination of the experiments hydrogels were fixed at different time points as indicated by the separate experiments. **Unless otherwise stated**, all hydrogels were rinsed *briefly* in PBS and fixed with 4% PFA for 3 h at RT, followed by three PBS washes (5 min/wash) before being stored at 4° C prior to immunolabelling and imaging for analysis.

2.8.1 Analysis of supraconstruct hydrogels

Particle uptake

For the particle uptake experiments, sample gels were fixed at different time point's post-particle addition (24 h – 14 DIV).

Particle inheritance in daughter cells of dividing astrocytes

Particle inheritance in supraconstruct hydrogels was assessed from dynamic time-lapse images as detailed above (*see 2.5.1*).

Ultrastructural membrane features associated with endocytotic activity

To investigate ultrastructural membrane features associated with endocytotic activity, MP-5x particles were added to supraconstruct hydrogels following the same protocol as for cell monolayers *(see 2.4.2)* and fixed in glutaraldehyde at 24 h post-particle addition. To fully dehydrate the hydrogels for visualisation in a field emission scanning electron microscope (FESEM) they were prepared using the Osmium-Thiocarbohydrazide step-wise procedure with the samples further dehydrated in a critical point dryer *(detailed further within the experimental chapter).* Following critical point drying, the samples were mounted onto carbon pads on aluminium stubs, with the sample edges sealed with silver conducting paint (Agar Scientific) to improve electron conductivity.

2.8.2 Analysis of intraconstruct hydrogels

Particle uptake

For the particle uptake experiments, sample gels were fixed at different time point's post-particle addition (24 h – 37 DIV).

Intracellular features and endocytotic activity associated with particle uptake

To investigate intracellular features and endocytotic activity associated with particle uptake in intraconstruct hydrogels, MPs were added to the astrocytes 'in-situ' (*see 2.7.4*). At 15 days the hydrogels were glutaraldehyde fixed and prepared for transmission electron microscopy (TEM). In brief, following glutaraldehyde fix and first Osmium step and washes, the hydrogels were taken through a series of dehydration steps and embedded in Spurr resin (*detailed further within the experimental chapter*). Ultrathin sections (100 nm) of the resin-embedded hydrogel were cut using a Reichert Ultracut E Microtome with the sections collected on 200-mesh thin bar grids. The grids were stored in a grid box prior to imaging.

MP-5x particles as a contrast agent

To investigate the potential of the MP-5x particles as a contrast agent under magnetic resonance imaging (MRI), astrocytes were exogenously pre-labelled with MP-5x particles and at 24 h post-particle addition, were added to collagen solution to form an intraconstruct hydrogel. Sample intraconstruct hydrogels were fixed with 4% PFA *(see 2.8)* following 24 h, 14 days and 37 days incubation and were prepared for MRI imaging *(detailed further within the experimental chapter).* Controls, which were fixed at the same time points, consisted of intraconstruct hydrogels containing unlabelled cells (no particles).

EdU as a measure of proliferation

Sample intraconstruct hydrogels were processed for EdU labelling at indicated time points (24 h; 7 DIV; 14 DIV) using a Click-iT® EdU (5-ethynyl-2´-deoxyuridine) cell proliferation assay as a measure of proliferative capacity of intraconstruct hydrogels over time. Briefly, the same protocol was followed as detailed above (*see 2.5.2*) with increases to volumes and incubation timings (*East et al., 2009*). Specifically, 10 µM of EdU in a final volume of 1 mL D10 was added over the hydrogel followed by incubation at 37° C for 18 h. The hydrogels were then fixed in 4% PFA for 3 h at RT, followed by 4 washes with 3% bovine serum albumen (BSA). To permeabilise the hydrogel, the concentration of Triton-X 100 was increased to 0.5% Triton-X 100 in PBS and the hydrogels incubated for 40 min at RT. Permeabilisation was followed by four washes in 3% BSA prior to the reagent cocktail being distributed over the hydrogel (1 mL/gel; see Appendix 1). The hydrogels were then incubated for 1 h, protected from light, at RT followed by 2 washes in 3% BSA. Nuclei were counterstained with Hoechst 33342 as detailed below (*see 2.9.2*) and imaged immediately.

Viability

To assess cellular viability, sample hydrogels (control and exogenous MP-labelled) were subjected to a live/dead assay at defined time points (24 h; 7 DIV; 14 DIV). Hydrogels were incubated in a mixed solution of propidium iodide (5 µM), calcein (4 µM) and Hoechst 33342 (5 µg) in a final volume of 2 mL D10 medium per gel/well. Following 30 min incubation at 37° C (5% CO_2/95% humidified air), the hydrogels were fixed with 4% PFA for 3 h at RT, followed by 3 PBS washes and imaging for analysis.

2.9. Immunocytochemistry

2.9.1 Immunolabelling of cells seeded as monolayers

Following fixation and PBS washes, cell monolayers on coverslips were immunolabelled in preparation for imaging. The blocking solution used throughout was 5% normal donkey serum (NDS) diluted in 0.3% Triton-X 100 in PBS. The primary antibody (diluted in blocker solution) was polyclonal rabbit anti-GFAP (1:500), with the secondary antibody (diluted in blocker solution) being FITC- or Cy3-labelled donkey anti-rabbit IgG (1:200).

The cells were blocked for 30 min at RT (0.2 mL/well), after which the primary antibody was added (0.2 mL/well) and the cells incubated overnight at 4° C. Following overnight incubation the cells were washed twice in PBS at RT for 15 min per wash before being incubated in blocker solution (0.2 mL/well) for 30 min at RT. The secondary antibody was then added (0.2 mL/well) and the cells incubated, protected from light, at RT. Following 2-3 h incubation, the cells were washed three times with PBS for 5 min per wash. Cells on coverslips were mounted on slides in mounting medium containing DAPI, and the coverslips were sealed with nail varnish prior to fluorescence microscopy.

2.9.2 Immunolabelling of supraconstruct hydrogels

Supraconstruct hydrogels were subject to the same immunolabelling protocol as detailed above for cell monolayers (*see 2.9.1*), with some alterations to the protocol. Namely, the volume of blocking solution, primary and secondary antibodies was increased to 0.5 mL/gel. Following immunolabelling, nuclei were counterstained with Hoechst 33342 rather than DAPI mounting medium. Hydrogels were incubated in Hoechst 33342 at a concentration of 5 µg/mL PBS (0.5 mL/well) for 30 min at RT, protected from light, followed by three 5 min PBS washes (1 mL/well). For imaging purposes, the hydrogel

was gently transferred from the coverslip to a glass slide ensuring that the correct orientation of the gel was maintained. The hydrogel was then imaged under an inverted fluorescence microscope.

2.9.3 Immunolabelling of intraconstruct hydrogels

For protein detection and labelling of cellular architecture in intraconstruct hydrogels the primary and secondary antibodies used, and their respective dilutions, were the same as those used for cell monolayers and supraconstruct hydrogels as detailed above (*see 2.9.1*), with some alterations to the protocol. Specifically, all incubation times were doubled. Also, to facilitate permeabilisation of the hydrogel, the 5% NDS blocker solution was diluted in 0.5% Triton-X 100 in PBS; these alterations to the standard protocol were based on published procedures for immunolabelling of hydrogels (*Phillips & Brown, 2011*).

Briefly, following fixation and PBS washes, the intraconstruct hydrogel was blocked for 1 h at RT (0.75 mL/gel) followed by addition of the primary antibody (0.75 mL/gel) and incubation for 24 h at 4° C. The hydrogel was then washed three times in PBS (2 mL/gel) for 15 min/wash at RT before addition of the blocker solution (0.75 mL/gel) and incubation at RT for 1 h. The secondary antibody (0.75 mL/gel) was added and the hydrogel incubated at RT, protected from light, for at least 4 h. Incubation was followed by three PBS washes (2 mL/gel) for 10 min per wash. To counterstain for nuclei, Hoechst 33342 was added at a concentration of 5 µg/mL PBS at a final volume of 1 mL/gel, and incubated for 1 h at RT, protected from light. To remove residual stain, the hydrogels were washed three times in PBS for 10 min per wash (1 mL/gel) before being imaged.

2.10 Imaging

2.10.1 Imaging of cell monolayers

Fluorescence microscopy

Analysis of each experimental condition was conducted using fluorescence images captured at 200-400 x magnification, from four random fields per coverslip/hydrogel. Three different microscopes were used to capture the fluorescence images. A Leica DM IL LED inverted microscope fitted with a DFC 420 C digital camera and a *p*E-300 W CoolLED fluorescence unit, was used to capture images from well-plates using the Leica Application Suite imaging software, version 3.3.1. Fluorescence images from cell monolayers on coverslips were captured using an AxioScope A1 microscope fitted with an AxioCam ICc1 digital camera, and utilising Axiovision imaging software by Carl Zeiss MicroImaging, GmbH (Germany). Fluorescence Z-stack images of supraconstruct hydrogels were captured using a Nikon Eclipse 80i microscope, fitted with a Hamamatsu ORCA camera utilising NIS-Elements imaging software, version Br3.2.

All images were captured using fixed exposure settings to allow for consistency and accuracy in analysis of fluorescence intensity measures of *gfp* expression and particle accumulation in cells.

Dynamic time-lapse microscopy

Particle inheritance in daughter cells of dividing astrocytes cultured on coverslips was assessed from dynamic time-lapse images captured at a frequency of 1 frame/120 s over a period of at least 48 h. Images were captured from the transmitted light (16 ms exposure) and BODIPY® 564/570 (420 ms exposure) fluorescence channels using an Axio Zoom

V16 microscope fitted with an AxioCam ICm1 camera and utilising Blue Edition ZEN software, version 1.1.1.0.

2.10.2 Imaging of supra- and intraconstruct hydrogels

Z-stack microscopy

Intraconstruct hydrogels were transferred into a CELLview™ glass-bottom petri dish for imaging. Quantification and subsequent analysis of culture characteristics, experimental outcomes and cellular assessments using intraconstruct hydrogels was assessed from four (RGB fluorescence and phase) z-stack images. These were captured at 100-200x magnification from four random fields of the hydrogel using a Zeiss Axio Observer.Z1 microscope fitted with a Zeiss AxioCam MR R3 digital camera and a *p*E-300 CoolLED fluorescence unit and utilising the Blue Edition ZEN 2 software, version 2.0.

Dynamic time-lapse microscopy

Particle inheritance in daughter cells from in-situ MP-5x particle-labelled supraconstruct hydrogels were assessed from time-lapse images taken at a frequency of 1 frame/120 s over a period of at least 48 h. Images were captured from the transmitted light (23 ms exposure) and BODIPY® 564/570 (20 ms exposure) fluorescence channels using hardware and software as detailed above (*see 2.10.1*). Particle inheritance from in-situ MP-5x particle-labelled intraconstruct hydrogels were assessed from images taken at a frequency of 1 frame/180 s with transmitted light exposure set at 97 ms and BODIPY® 564/570 set at 500 ms exposure.

Field emission scanning electron microscopy of supraconstruct hydrogels

Observation of the cell ultrastructure on supraconstruct hydrogels was visualised using a Hitachi S4500 FESEM operating at an accelerating voltage of 5 kV.

Transmission electron microscopy of intraconstruct hydrogels

Cell cytoskeletal and subcellular features were visualised from the ultrathin sections using a JEOL-100CX TEM operating at an accelerating voltage of 100 kV.

Magnetic resonance imaging of intraconstruct hydrogels

The MRI imaging of the intraconstruct hydrogels was conducted at the Centre for Pre-Clinical Imaging (Liverpool, UK) using a Bruker 9.4 T Avance III HD instrument (Bruker, Coventry, UK) utilising a 40 mm transmit/receive quadrature volume coil. High resolution three-dimensional TurboRARE T_2 weighted and T_2* images were captured using a 25 x 25 x 4 mm field of view with 8 slices in total taken of each hydrogel. Each hydrogel took an acquisition time of 2 h 37 min with a calculated resolution of 256 x 256 x 41 pixels per hydrogel, with an echo time (TE) of 8 ms and a repetition time (TR) of 400 ms. T_2-weighted images are a 'true' or 'natural' image of the sample, weighted to accentuate the local magnetic homogeneity effect to give a greater degree of contrast. The T_2* images have a greater degree of 'observed' resolution accuracy as they reflect the 'true' T2 image and account for any magnetic field inhomogeneities within the sample (*H. Poptani; University of Liverpool – Pers. Communication.*).

2.11 Histological analyses of culture properties

Culture characterisation within each experimental condition was quantified by cell counts (the number of nuclei/image), culture purity (percentage of nuclei co-localised with GFAP+ expression) and incidence of pyknosis (as a percentage of healthy plus pyknotic nuclei), which was categorised by shrunken, fragmenting nuclei. Astrocyte phenotype was classified as type 1 or type 2 based on their morphology. Type 1 astrocytes have flat, membranous unbranched morphology compared with the small soma and highly branched, more complex morphology seen with type 2.

2.11.1 Cell monolayer experiments

All culture characteristics, experimental outcomes and cellular assessments in cell monolayer experiments were quantified from fluorescence images taken from four random fields per coverslip with at least 100 counterstained nuclei assessed from each experiment. Prior to counting, images were triple merged using Adobe Photoshop CS5 Extended, version 12 x32 with all quantification carried out using ImageJ image analysis software (NIH USA). Using this approach to analyses enabled quantification of experimental outcomes while simultaneously assessing for cell health, for example cell adherence, atypical cell morphologies or prevalence of pyknosis.

2.11.2 Supraconstruct hydrogels

Observations of culture characteristics, experimental outcomes and cellular assessments from supraconstruct hydrogels were visualised from images taken from four random fields per hydrogel and as such, were used as proof-of-concept findings to validate experimental outcomes and to inform subsequent intraconstruct hydrogel protocols.

2.11.3 Intraconstruct hydrogels

In intraconstruct hydrogels culture characteristics, experimental outcomes and cellular assessments were quantified from z-stack images taken from four random fields per hydrogel, one field captured through the centre of the gel with the other three fields captured from at least 1-2 mm in from the outer edge of the gel (*Figure 2.7*) with all counterstained nuclei counted per z-stack image/field of view. To investigate homogeneity of cell distribution and cell growth throughout the hydrogel, the data obtained from the centre of the gel was compared with that obtained from the edge. Quantification was carried out using Blue Edition ZEN 2 software, version 2.0 and ImageJ.

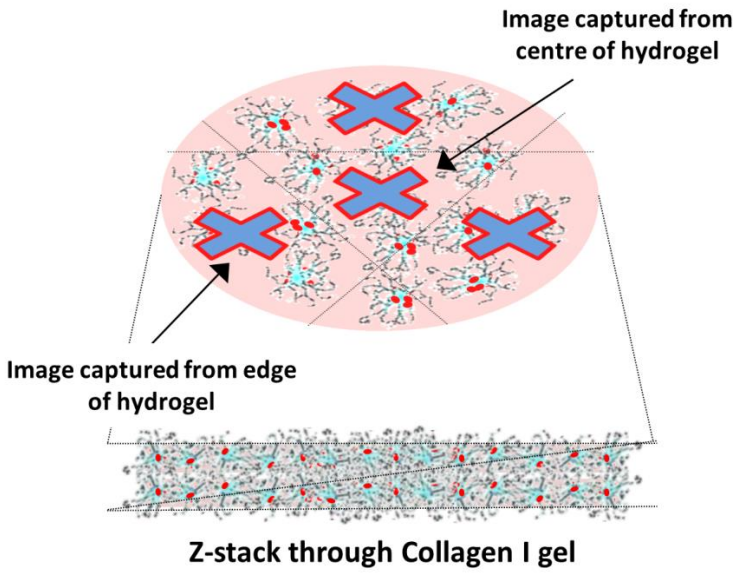

Figure 2.7 Schematic of z-stack imaging through an intraconstruct hydrogel *Culture characterisation and experimental outcomes were evaluated from z-stack images captured from four random fields of a hydrogel. To investigate homogeneity of cell distribution and growth, comparisons were made between data taken from the centre and data taken from the edge of the hydrogel (see arrows).*

2.12 Analyses of magnetic (nano) particle uptake and transfection

2.12.1 Analysis of MP-labelling of astrocytes in cell monolayers and intraconstruct hydrogels

Labelling efficiency in astrocytes was quantified by the proportion of GFAP+ cells showing particle uptake. All data were expressed as a percentage of the total number of cells per field. The extent of particle accumulation per cell was evaluated using pixel intensity. Briefly, using ImageJ software pixel intensity readings were taken from each cell showing particle uptake. As with fluorescence intensity (*see 2.12.2*) readings were taken to correct for background fluorescence with the resulting value representing the extent of particle accumulation per cell *(detailed further within the experimental chapter).* The data for each condition was averaged to allow comparisons across experimental conditions.

2.12.2 Analysis of MNP-mediated gene transfer to astrocytes in cell monolayers

Transfection efficiency in astrocytes was classified as the proportion of GFAP/*gfp*+ cells and expressed as a percentage of the total cells. In the cell monolayer experiments, fluorescence intensity was used as a representative measure of *gfp* expression, with particle accumulation classified semi-quantitatively as low, moderate and high. Briefly, using ImageJ software, fluorescence images were converted to grayscale, inverted and calibrated using an optical density step tablet before fluorescent intensity readings were taken from each cell expressing *gfp*. Readings were taken to correct for background fluorescence, these values then subtracted from the mean fluorescence intensity value taken from the cells, with the resulting value representing a measure of the extent of *gfp* expression in a transfected cell. The data for particle accumulation vs. *gfp* expression was then correlated to allow for comparisons across experimental conditions.

2.13 Viability and proliferation assays for cell monolayers and intraconstruct hydrogels

2.13.1 Cellular assessment

Assessment of cell health within the experimental conditions was quantified through culture characterisation i.e. average cell count; culture purity and prevalence of pyknosis across conditions *(see 2.11).*

2.13.2 MTS Assay in cell monolayer transfection experiments

At 48 h post-transfection, an MTS assay was conducted to measure mitochondrial dehydrogenase activity in the astrocyte monolayer, as an indicator of metabolic activity, and consequently as a safety assessment of the transfection protocols. Briefly, additional D10 medium was added to each well (cells; cells+plasmid; cells+plasmid+MNPs) to equal a final volume of 0.2 mL and 20 µL/well of MTS reagent added. Following 3 h incubation at 37° C (5% CO_2/95% humidified air) absorbance was measured at 490 nm (A490 - VICTOR^2 Multi-label Counter, PerkinElmer). The 'blank' (no cells) absorbance readings were subtracted from the appropriate test readings with the resulting values expressed as a percentage of cellular viability relative to the control incubations minus MNPs.

2.13.3 EdU proliferation assay in cell monolayers and intraconstruct hydrogels

Click-iT® EdU (5-ethynyl-2´-deoxyuridine) cell proliferation assay was used to assess the proliferative capacity of astrocytes in cell monolayers and within intraconstruct hydrogels, as detailed above (*see 2.5.2 & 2.8.2 respectively*). For cell monolayers, fluorescence images were captured from four random fields of the coverslip, and for intraconstruct hydrogels, Z-stack images were captured from four random fields of the gel. Counts of nuclei co-expressing the EdU marker and nuclear counterstain (DAPI or Hoechst 33342)

were classified as proliferating cells (proliferation expressed as a percentage of the total cells counted). For intraconstruct hydrogels, data were evaluated to provide a comparison of proliferative capacity at the hydrogel centre, with that seen at the edge.

2.13.4 Cellular viability assay in intraconstruct hydrogels

Alongside culture characterisation assessments, cell viability in hydrogels was assessed by live/dead assays as detailed above (*see 2.8.2*). Fluorescence z-stack imaging captured images from four random fields of the hydrogel, one from the centre and three from the edge. Cellular viability was determined as the percentage of cells expressing calcein (live) from the total number of cells per field. The data obtained from the centre of the hydrogel was compared with that obtained from the edge to investigate homogeneity of cellular viability throughout the gel.

2.14 Statistical analyses

Experimental data were analysed by one-way analysis of variance (ANOVA) with *post-hoc* analysis carried out using Bonferroni's multiple comparison test (MCT). Equality of variance across cell samples was verified using Bartlett's Test. All data are expressed as mean ± standard error of the mean (s.e.m) with *'n'* referring to the number of different experiments within each particular study, each derived from a different rat litter. Analysis was conducted using Prism statistical analysis software, version 7 (GraphPad Software Inc.).

Chapter 3
Endocytotic potential governs magnetic particle loading in dividing neural cells

3.1 Introduction

The use of MPs with cell therapies is becoming an established field for magnetic cell localisation and imaging applications. In turn, this is paving the way for safe and efficient delivery of cell transplant populations to sites of injury and allowing for non-invasive monitoring of grafts (*Chen et al ., 2013; Jenkins et al., 2014; Riegler et al., 2010; Yanai et al., 2012*). As discussed previously within the main introduction, to address the limitations inherent to the regenerative capacity of the CNS, an emerging area for such applications is that of cell transplantation to facilitate repair of neurological injury. In this regard, a number of studies have utilised astrocytes as a transplant population (*Nicaise et al., 2015 for review*). Despite the safety of MNPs for labelling of this particular neural cell (*Pickard et al., 2011*), in transplant populations it has been neglected in favour of heavy reliance on histological findings (*Davies et al., 2006, 2011; Fan et al., 2013; Filous et al., 2010; Pencalet et al., 2006; Selkirk et al., 2002; Wang et al., 1995; Zhang et al., 2016).* This, then, remains a clear oversight when furthering the use of this neural cell type for cell therapies.

Labelling cells prior to transplantation requires a cell-particle combination that results in rapid and safe particle uptake by the majority, if not all cells. However, the regenerative capacity of most transplant populations relies partially on their proliferative capacity which results in rapid dilution of intracellular particle accumulations in labelled cells (*Kim et al., 2012*). Particle loss can also occur via exocytosis, potentially compromising magnetic cell localisation and imaging capacity (*Jin et al., 2009*). Although, it has been disputed that particles, once internalised by the cell are not released from healthy cells, but instead their accumulation is diluted through cell division (*Harrison et al., 2016*). In this respect the high proliferative capacity of cultured astrocytes (*Errington et al., 2010; Kim et al., 2011*)

may rapidly dilute particle accumulation. Therefore, a further requirement for transplant cell labelling is long-term retention of sufficient particles per cell to facilitate its continued utility in imaging and tracking approaches. To counter the proliferative nature of this cell, one way that long-term particle retention could be achieved is by initial high loading of MP-label into graft cells.

The factors that govern MP loading are varied and dependent on the particular cell:particle combination (*Kettler et al., 2014 for review*). Astrocytes display high levels of membrane activity. It has been shown in a recent ultrastructural study using high resolution SEM that astrocytes are the dominant neuroepithelial population in terms of particle uptake. Relative to other major neural cell types such as neurons and oligodendrocytes, astrocytes display extensive membrane ruffling with numerous filopodia and membrane pits in line with greater particle uptake/transfection (*Fernandes & Chari, 2014*). Moreover, it is well established that uptake of nanoparticles is mediated via a range of endocytotic mechanisms (*Canton & Battaglia, 2012; Kou et al., 2013; Verma & Stellacci, 2010; Yameen et al., 2014; Zhao et al., 2011*). In this context, astrocytes employ a number of endocytotic pathways for nanoparticle uptake which, in turn, are mostly determined by the size of the particle employed (*Rejman et al., 2004; Chaudhuri et al., 2011*). The predominant MP-uptake pathways reported in astrocytes are receptor-mediated (caveolae and clathrin) with macropinocytosis playing a greater endocytotic role in uptake of larger particles (*Megias et al., 2000; Pickard et al., 2011; Walz, 2000*). In respect of particle properties, while size is a factor determining the uptake pathway (*Zhao et al., 2011*), it has also been reported that stiffer particles result in more *rapid* uptake due to their interaction with the plasma membrane (*Oh & Park, 2014*). Enhanced particle loading appears to be dependent on surface coating (*Alexis et al., 2008*), biomolecular corona (*Lesniak et al., 2013*) and surface charge (*Alexis et al., 2008; He et al., 2010; Harush-Frenkel et al., 2007*). However, the

benefits conveyed by particle properties appear to be highly dependent on the particle:cell combination (*Alexis et al., 2008*). A clear understanding, then, is required of both the physico-chemical and the biological parameters that govern particle loading in this particular neural cell. Indeed, in the use of MPs with astrocytes there is still a knowledge gap regarding the factors that contribute to successful magnetolabelling and label retention.

A recent study investigated the uptake of particles with tailored magnetite concentration. These particular particles are formulated using biocompatible and biodegradable components; properties that highlight their translational potential and justify their use in this study (*Adams et al., 2015*). It was recently proved that systematic tailored increases in the magnetite content of these particles could significantly enhance cell labelling (>95% cells labelled) in the typically 'hard-to-label' transplant population of NSCs (*Adams et al., 2015*). However, this study did not evaluate the longer-term retention of these particles by the labelled cells, or establish the pattern of 'inheritance' of particles by daughter NSCs post-proliferation. **It is unclear how astrocytes, with their high level of endocytotic activity, will handle such high magnetite content MPs.** The aim therefore of this study is to investigate the effect of different combinations of magnetite particle and magnetic field condition, on particle uptake and extent of accumulation in cortical astrocytes – a primary-derived neural cell. The hypothesis is that optimal particle/magnetic field combination can result in greater enhancement of cell labelling for neural transplant populations.

In realising this aim, a consistent and accurate approach is needed to quantify cellular particle accumulation. Previously, particle accumulation – in a range of neural cells – has been assessed semi-quantitatively and categorised as 'low', 'moderate' or 'high' based on visual assessment of the area ratio of particles to cell nucleus [NSCs *(Adams et al., 2013*); OPCs (*Jenkins et al., 2013*) and astrocytes (*Pickard et al., 2011*)]. The major disadvantages

in other approaches considered (i.e. plate readers; flow cytometry) are their reliance on culture-wide assays rather than single-cell quantification. In turn, they assume homogeneity in particle uptake, contrary to the heterogeneity reported in primary neural cells (*Adams et al., 2013; Jenkins et al., 2013; Pickard et al., 2011*). Moreover these approaches are unable to discriminate between intracellular and extracellular particles, and in respect of astrocytes, this could be up to 50% of the signal, resulting in an unacceptable level of 'false-positives'.

Of key importance in respect of the assessment of uptake and safety, use of enzymatically detached cells do not maintain the morphological features that are pertinent to these assessments as conducted within the present study. Furthermore, none of the aforementioned approaches are able to distinguish intracellular particle localisation, a determinant of particle trafficking. Thus, an approach is required that will *i*) quantify particle uptake and extent of accumulation on a cell-by-cell basis, *ii*) will exclude extracellular and membrane-adherent particles with consistent accuracy, *iii*) will be able to identify cells with unhealthy morphologies and *iv*) will yield measures that are representative of the heterogeneity in particle uptake seen within a primary-derived neural cell population.

3.2 Objectives

1) **Develop a robust and simple methodology for quantification of particle accumulation in astrocytes**

2) **Investigate the effect of combinations of tailoring particle magnetite content and magnetic field, on particle uptake by astrocytes**

3) **Study particle retention by astrocytes over an extended time period (21 days)**

4) **Investigate the profile of particle inheritance in daughter cells of MP-labelled astrocytes**

3.3 Experimental procedures

3.3.1 Reagents and equipment: All reagents and equipment used are as described previously in sections *2.1; 2.2.3; 2.3; 2.4 & 2.5*. Three types of MPs of differing magnetite content [MP-0x (non-magnetite); MP-1x; MP-5x] were used for uptake experiments and were evaluated for their labelling efficiency and extent of accumulation in cortical astrocytes. The nomenclature used to refer to the different MPs is indicative of their weight percent ratio (*as characterised in 2.4.1*).

3.3.2 Development of a robust methodology for quantification of particle accumulation within astrocytes: To devise a quantitative analytical method that offered a robust measure of particle accumulation, a methodology was developed based on the pixel intensity (**PI**) exhibited by the dense accumulation of particles. This density prevented exact particle counts per cell; however integrated density (**ID**) values provided a measure of **PI** (ImageJ software, NIH USA). A measure such as this would prevent operator bias; a concern when utilising semi-quantitative visual assessment categories of low, medium and high particle accumulation. The **PI** method could then be extrapolated to particle uptake in other cell types, and, as such, used laboratory wide.

Prior to taking any measures, triple-merged fluorescence micrographs and their un-merged counterparts were scaled to show measurements per micron (µm) and, for each MP-labelled astrocyte, the total area per cell occupied by intracellular MPs was outlined. This outline was then transferred to the unmerged particle channel image from which a cellular ID measure was obtained. Five background ID readings were taken from the same unmerged particle channel image, the mean of which was subtracted from the cellular ID measure, resulting in a PI measure relative to the accumulation of particles in an individual

cell; using the formula: - **PI** = **ID** – (**A** * **Br**) where **ID**=integrated density, **A**=cell area, **Br**=mean background reading and **PI**=pixel intensity.

A major consideration during development of this methodology was taking accurate measures from overlapping cells (*Figure 3.1*).

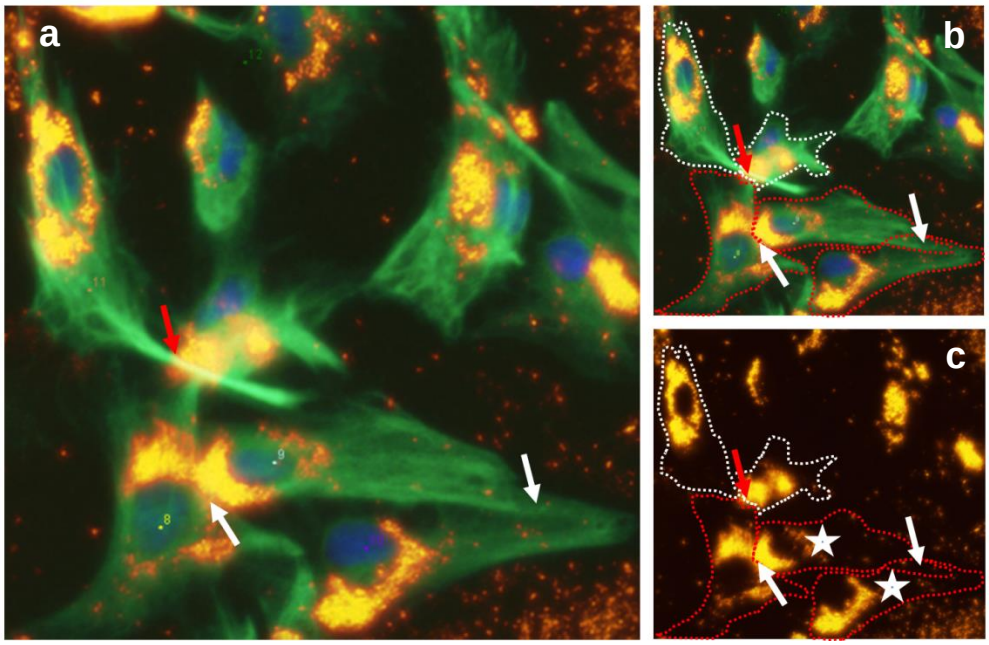

Figure 3.1 Development of parameters for PI analysis *Representative fluorescence images of MP-loaded cells (a) and (b) with corresponding particle image (c). Cell boundaries are outlined (b) for the purposes of measuring particle density from the particle image (c). For overlapping cells (b and c; white outline) where the corresponding particle image showed a clear association with the underlying cell (b and c; red arrow) particles could be confidently ascribed to that cell. Where particles were coincident (b and c; red outline, white arrow), both cells were measured with coincident particles assigned to the cell to the right (c; star).*

Where clear boundaries could be ascertained, and there were no particles in the overlying cell, the measure from the particle image captured only the particles from the underlying target cell [*red arrow; Figure 3.1 (a and b) and corresponding particle image (c)*]. Where particles from two cells were coincident on the particle image [*white arrow; Figure 3.1 (b) and (c)*], and could not be definitively ascribed to either cell, then both cells were measured, with the coincident particles assigned to the right-hand cell [*Figure 3.1 (c)*]. This deliberation was chosen to prevent any bias in assigning coincident particles.

The robustness of this method was tested with a number of data sets and the results compared with those of semi-quantification categorisation.

3.3.3 Influence of tailoring particle magnetite content on astrocyte loading: The MPs used in this study were evaluated for cellular labelling efficiency and extent of cellular accumulation over time. Use of these superparamagnetic particles was in combination with a magnetic field/gradient.

For the particle uptake experiments cortical astrocytes were routinely plated on PDL-coated coverslips in a 24-well plate and incubated for 24-48 h to allow for cell adherence and growth of processes prior to addition of the MPs (MP-0x (non-magnetite); MP-1x or MP-5x) (*as detailed in 2.4.2*). For each condition, particles were added at a dilution of 1 µl/mL D10 medium in a total volume of 0.3 mL, and exposed to either a static [0 Hz (F0)] or an oscillating [1 Hz; 200 µm amplitude (F1)] magnetic field for 30 min before being incubated for 4 or 24 h at 37° C (5% CO_2/95% humidified air). For the no field condition (NF), cells were incubated in the absence of a magnetic field. At the determined time-point, cells were subject to two PBS washes to remove any free particles (two PBS washes have been found to be sufficient in removing free particles, as verified by fluorescence/z-

stack microscopy). Following the washes, cells were fixed in 4% PFA and prepared for imaging and analysis.

3.3.4 Studying the retention of particles over an extended time period: In trialling the long-term studies it was clear that the proliferative nature of the cell population resulted very rapidly in over-confluent cultures within the well-plate, highlighting the possibility of density-dependent inhibition (*Davies & Ross, 1980*). Therefore, to facilitate continued viability, coverslips containing MP-loaded cells were transferred to PDL-coated 6-well plates at 96 h post-particle addition. At day 7 in culture, the coverslip containing cells was transferred to a fresh PDL-coated 6-well plate, cultured up to day 14 before being transferred again, and cultivated up to 21 days (*Figure 3.2*).

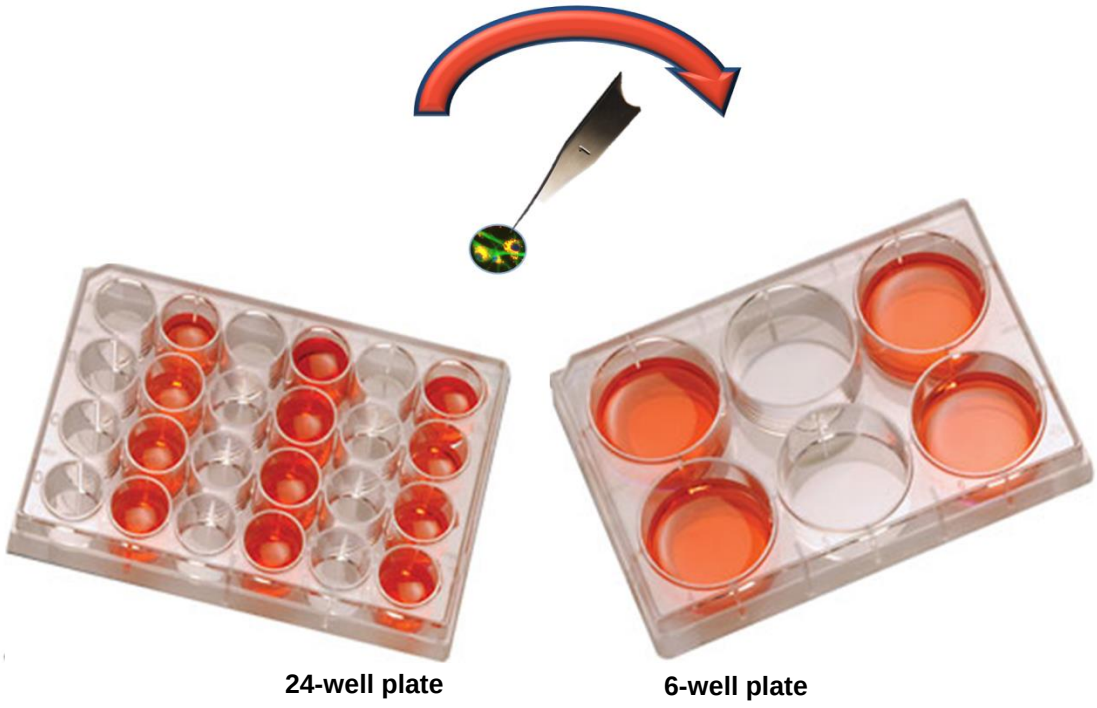

Figure 3.2 Schematic illustrating the transfer of coverslips *Schematic illustrating the transfer of coverslips, containing MP-loaded cells, from 24-well plate to 6-well plate to facilitate continued viability over long term culture of astrocytes. Coverslips were transferred to fresh wells at 96 h; day 7 and day 14 and cultivated up to day 21.*

Long-term experiments were conducted over a 21-day period. Informed by the results of the shorter-term experiments, astrocytes in the long term experiments were labelled with MP-1x or MP-5x particles and exposed to an applied oscillating magnetic field at a frequency of 1 Hz and an amplitude of 200 µm for 30 min. At 24 h post-particle addition, cells were washed twice in PBS to remove any free particles, and maintained in D10 medium with a 50% refresh every 2-3 days, incubated at 37° C (5% CO_2/95% humidified air). A proportion of the cultures were fixed (washed twice in PBS and fixed with 4% PFA for 25 min at RT) at 6 different time points - day 1 and every 4 days thereafter up to day 21.

Assessment of long-term particle retention was quantified by percentage of MP-labelled cells (MP-labelling efficiency); extent of particle accumulation (as quantified by **PI**), and particle safety.

3.3.5 Safety evaluation of procedures: Safety was of primary concern with the use of these procedures and to this end cellular viability was assessed by average cell counts, culture purity, phenotype distribution and levels of pyknosis. All safety analyses were assessed from triple-merged fluorescence micrographs.

3.3.6 Investigating profiles of particle inheritance in daughter cells of MP-labelled astrocytes: Dynamic time-lapse imaging over 48 h allowed determination of the pattern of particle inheritance in daughter cells of dividing astrocytes (*as detailed in 2.5.1 & 2.10.1*). Visual observation of time-lapse imaging videos provided counts of symmetrical/non-symmetrical particle inheritance events. A total of 30 mitotic events were recorded (60 daughter cells), with each classified as ‘symmetric’ or ‘asymmetric’ depending on the proportions of total MP inherited by each daughter cell as determined for both daughter

cells. Events were classified as symmetrical inheritance when each daughter cell contained 40-60% of the total MP, with asymmetric defined as > 60% in one daughter cell.

3.3.7 Immunocytochemistry: Immunolabelling of cells in uptake experiments was as detailed in section *2.9.1*, with FITC secondary antibody used in these experiments due to the BODIPY® 546-570-PLA fluorophore coating of the particles.

3.3.8 Imaging: Imaging of these experiments was conducted as detailed in section *2.10.1*

3.3.9 Analyses: Triple-merged fluorescence micrographs allowed quantification of culture and particle uptake characteristics and safety assessments across each experimental condition. MP-labelling efficiency (% labelled cells) and the extent of particle accumulation within cells (PI) were quantified using triple-merges of DAPI, GFAP and particle images/channels.

3.3.10 Statistical analysis: Data were analysed using one-way analysis of variance (ANOVA) with post-hoc analysis conducted using Bonferroni's multiple comparison test (MCT); the results expressed as mean ± s.e.m. For the trial analysis data only (*Section 3.4.1*), equality of variance as tested by Bartlett's Test showed the data to be non-parametric, therefore this data set was analysed using Kruskal-Wallis.

The number of cultures used in this series of experiments was 3 ($n = 3$) unless otherwise noted, each derived from a different rat litter.

3.4 Results

3.4.1 Evaluating the robustness of quantitative PI analysis

Particle density within a cell was represented by **PI**. To test the validity and the robustness of this method a trial analysis was first conducted followed by analysis of a number of data sets from this study, the results of which were compared with those of semi-quantitative categorisation.

Trial analysis entailed each individual cell being categorised as 'low', 'moderate' or 'high' for extent of particle accumulation and simultaneously assigned a **PI** value (representative of intracellular particle density). The resulting **PI** value was then binned according to its corresponding visual categorisation (i.e. **PI** value to 'low', 'moderate' or 'high') to determine whether the two measures were in any respect comparable. Results from the trial data reported significant differences between the categories suggesting **PI** values are comparable to the visual observations typically used within the semi-quantitative method i.e. low **PI** values correspond to 'low' visual observation of particle accumulation [*Figure 3.3 (a)*]. Based on the interquartile range [*Figure 3.3 (b)*] this preliminary data reported a distinct range of **PI** values for each category, although some overlap was noted. The findings also reported no difference in **PI** values between particle types across the categories [*Figure 3.3 (a and b*)].

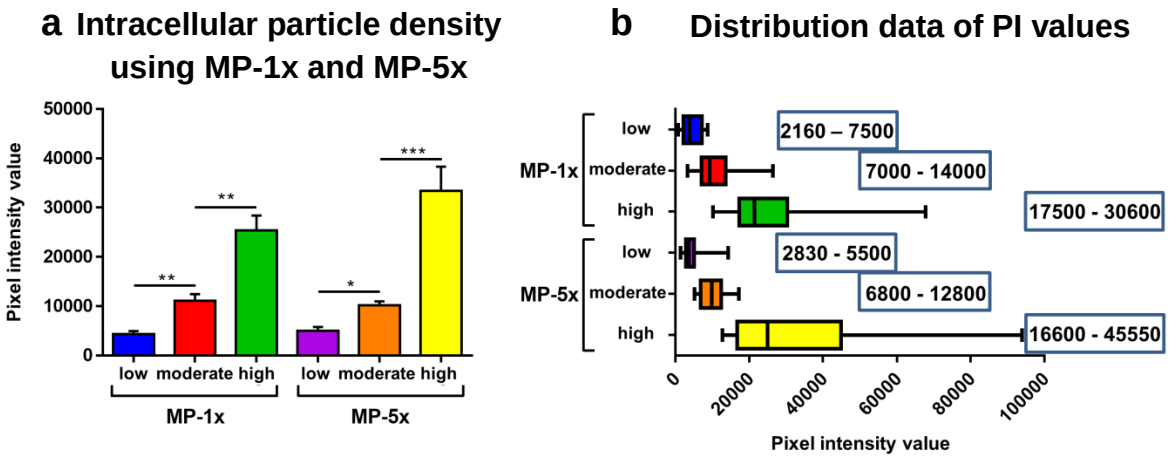

Figure 3.3 Intracellular particle density in individual cells was assigned a PI value and categorised according to the semi-quantitative method of 'low', 'moderate' or 'high'. The PI value was then binned according to its corresponding category. *Bar graph (a) showing a significant difference between categories for intracellular particle density as measured by* ***PI*** *(*p < 0.05; **p < 0.01; ***p <0.001; Kruskal-Wallis). Box and whisker plot (b) showing the distribution of the* ***PI*** *values when used as a measure of intracellular particle density. Based on the interquartile range [denoted in graph (b)] distinct* ***PI*** *ranges for each category were reported, although some overlap is noted. Results expressed as mean ± s.e.m.* **PI** = Pixel Intensity

In evaluating the trial analysis, consideration was given to whether binning the **PI** values into categories may be biasing the results. Therefore to further test the validity of this method, the **PI** values were not binned during the following set of analyses.

Hence, to validate the method and test the robustness of this approach, a number of data sets from the current study were analysed for internalised particle accumulation. Two analytical methods were simultaneously employed here –semi-quantitative visual analysis and quantitative **PI** analysis (*Figure 3.4*).

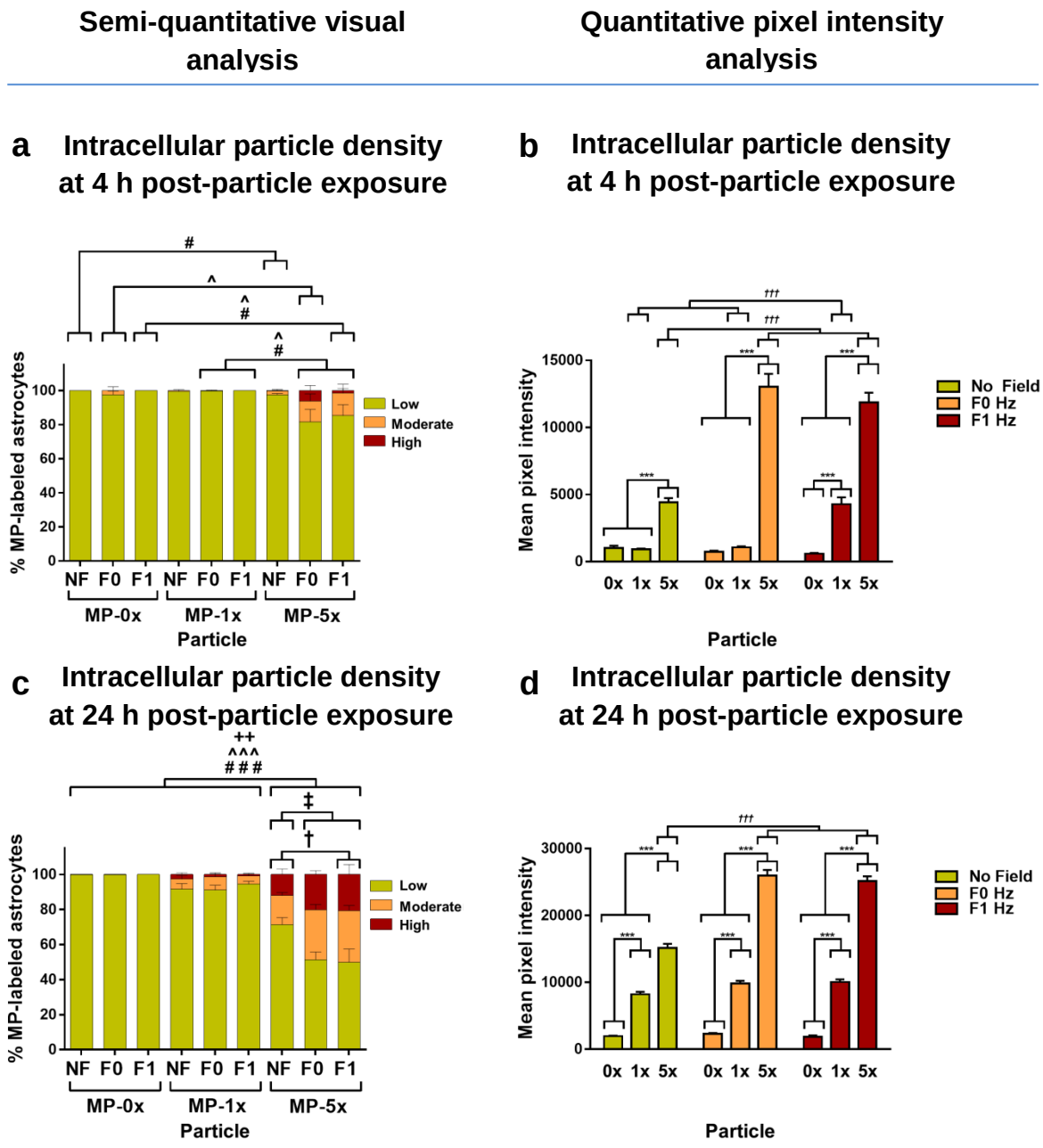

Figure 3.4 Intracellular particle density measured using semi-quantitative visual analysis and quantitative PI analysis *Following addition of MP-0x, -1x or -5x particles to astrocytes, and subsequent 30 minute application of one of three differing magnetic field conditions [no field (NF); static field (F0) or oscillating field (F1 Hz: 200µm amplitude)], the extent of intracellular particle density was measured at 4 h and 24 h post-particle exposure. Bar graphs displaying extent of intracellular particle density at 4 h (a & b) and at 24 h (c & d) post-particle exposure. The data sets were analysed using both semi-*

quantitative visual analysis (a & c), which is based on area of particle density relative to the cross-section of the nucleus and categorised as 'low', 'moderate' or 'high' and quantitative ***PI*** *analysis (b & d), which is a measure of the pixel intensity of the area coverage of particles within the cell Similar significant findings were reported by the two analytical methods employed, although* ***PI*** *analysis reported the data in greater detail [compare (a) versus (b); (c) versus (d)]. Significant differences are indicated in terms of magnetic field ($^{\dagger}p$ <0.05; $^{\dagger\dagger\dagger}p$ <0.001) and particle (***p <0.001) and 'low' ($^{\#}p$ <0.05; $^{\#\#\#}p$ <.001); 'moderate' (^p <0.05; ^^^p <0.001) and 'high' (^{++}p <0.01). Results expressed as mean ± s.e.m.* **MP**: magnetic particle; **PI**: pixel intensity

Both analytical approaches reported similar findings. Significant differences in extent of particle accumulation were reported between MP-5x and MP-1x across the applied magnetic field conditions, and between MP-5x and MP-0x across all field conditions, for both 4 h and 24 h post-particle exposure [*compare Figure 3.4 (a and b); (c and d)*]. However, **PI** analysis reported the results in greater detail. In this regard, at 4 h post-particle exposure significant increases in intracellular particle density were shown for MP-1x *versus* MP-0x (at F=1 Hz); MP-5x (F=1 Hz & F=0 Hz) *versus* MP-5x (NF) and MP-1x (F=1 Hz) *versus* (MP-1x F=0 Hz & NF) [*Figure 3.4 (b)*]. At 24 h, use of **PI** analysis also showed significant increases in particle density for MP-1x *versus* MP-0x across all field conditions [*Figure 3.4 (d)*], again a finding not reported under semi-quantitative visual analysis [*compare Figure 3.4 (c and d)*].

Taken together the findings indicate that use of **PI** is a valid tool as a representative measure of intracellular particle density, and as such, provides a quantifiable and unbiased

measure of particle accumulation within the cell. Therefore, all subsequent data of intracellular particle accumulation were analysed using this quantitative approach.

3.4.2 Influence of tailoring particle magnetite content on astrocyte loading

Particles of varying magnetite content, in combination with differing magnetic fields, were evaluated for cellular labelling efficiency and extent of accumulation over time. Visual analysis of MP-labelling at 4 and 24 h showed widespread cellular uptake throughout cultures for all three particle types, and revealed cellular heterogeneity in terms of relative particle accumulation showing low, moderate or high uptake [*Figure 3.5 (a - c)*]. Both peri-nuclear and cytoplasmic distributions of MPs were observed post-labelling (cytoplasmic as opposed to peri-nuclear localisation; nomenclature not intended to preclude possibility that particles may be localised to endosomes within the cytoplasm). The astrocyte cultures used in this study were of high purity as judged by expression of the astrocyte marker GFAP (99.4 ± 0.2 % of cells were GFAP+ve; n =6) [*Figure 3.5 (d)*], with cells displaying healthy morphologies typical of type 1 and type 2 astrocytes [*Figure 3.5 (a and inset)*], with type 1 cells dominating (97.1 ± 1.6 % of GFAP+ve cells) [*Figure 3.5 (e)*].

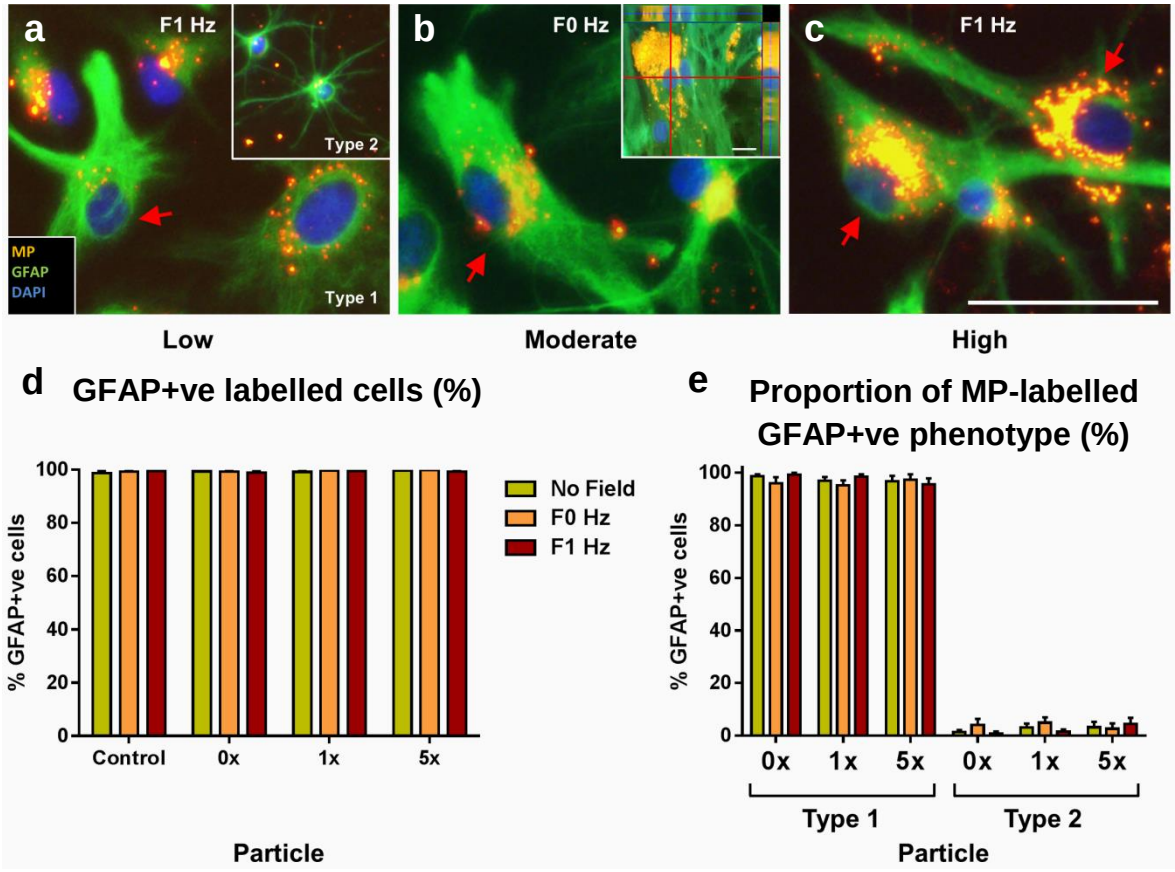

Figure 3.5 Culture characteristics of MP-labelling of astrocytes *Representative fluorescence images (a – c) of MP-5x uptake in type 1 and type 2 astrocytes at 24 h post-particle addition [(a) and inset]. Arrows indicate (a) 'low', (b) 'moderate' and (c) 'high' levels of intracellular particle accumulation. Z-stack fluorescence micrograph [(b) inset] demonstrating intracellular localisation of particles. Bar graphs displaying (d) the high purity of this cell population (99.4 ± 0.2% of the cells were GFAP+ve), and (e) the proportions of astrocyte phenotype represented within the cell population (97.1 ± 1.6%; 2.9 ± 1.6% - type 1 & type 2 respectively). Results expressed as mean ± s.e.m (Number of replicates = 6). Scale of main and inset images = 50 µm* **MP**: magnetic particle.

Particle uptake was rapid, and for magnetite-loaded cells a substantial proportion (*ca.* 50%) of cells was MP-labelled at 4 h post-particle addition. MP-5x particles showed

significantly increased labelling efficiency compared with the other particle types, and in turn, MP-1x showed significantly increased MP-labelling compared with MP-0x [*Figure 3.6 (a)*]. By contrast, application of a magnetic field had no effect on labelling efficiency with either MP-0x or MP-1x at 4 h. Furthermore, magnetic fields had no effect on the proportion of cells labelled with the MP-5x particles, which was very high (> 90%) even under the no magnetic field condition [*Figure 3.6 (a)*].

In respect of the extent of particle accumulation at 4 h, cells labelled with MP-5x particles showed significantly higher particle accumulation compared with MP-0x and MP-1x particles for both magnetic field conditions [*Figure 3.6 (b)*]. Application of a magnetic field also resulted in significantly greater accumulation of MP-5x particles compared with the no field condition [*Figure 3.6 (b)*].

At 24 h post-particle exposure, a greater proportion of cells were MP-labelled compared with 4 h for all particle types [*compare Figure 3.6 (a and c)*]. Of note, for MP-1x and MP-5x particles virtually all of the astrocytes (>98%) were MP-labelled [*Figure 3.6 (c)*] and notably, magnetic field application at both frequencies was without effect at this time point as would be expected given the near complete labelling of the cells.

The extent of particle accumulation was also much greater at 24 h compared with 4 h for all magnetite containing particles [*compare Figure 3.6 (b and d)*]; please note scale difference of y-axes, with particle accumulation significantly higher versus MP-0x [*Figure 3.6 (d)*]. Interestingly, for MP-5x particles application of a magnetic field promoted particle accumulation [*Figure 3.6 (d)*], an effect not observed for MP-1x particles.

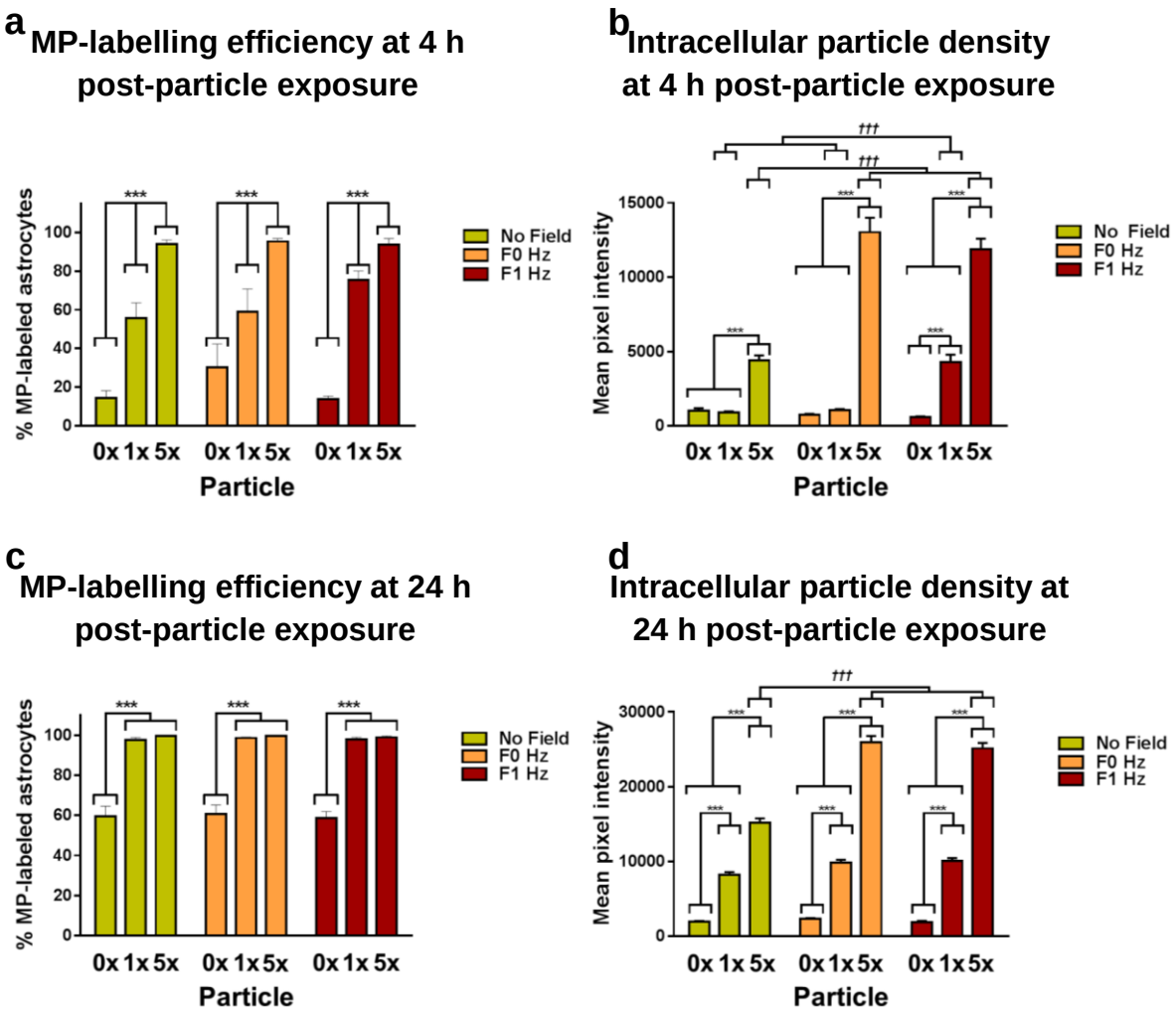

Figure 3.6 MP-labelling of astrocytes at 4 h and 24 h post-particle exposure, with and without magnetic field application *Bar graph (a) displaying MP-labelling efficiency (proportion of cells showing particle uptake) in astrocytes at 4 h. Bar graph (b) showing intracellular particle density (extent of particle accumulation per cell) in astrocytes across magnetic fields at 4 h. Bar graph (c) showing MP-labelling efficiency at 24 h. Bar graph (d) showing extent of intracellular particle density across magnetic fields at 24 h. Differences are indicated in terms of magnetic field (†††p < 0.001) and particle (*p < 0.005; **p < 0.01; ***p < 0.001) Results expressed as mean ± s.e.m. Number of replicates = 6. Bar graphs b & d previously referred to in Fig. 3.4* **MP**: magnetic particle.

3.4.3 Studying the retention of particles over an extended time period

Over the extended time period, transfer of coverslips containing MP-loaded cells into larger wells facilitated the proliferative spread of astrocytes (*Figure 3.7*), thus helping prevent over-confluency of cultures and subsequent growth contact inhibition. As can be seen from the long term analyses below, the increase in cell numbers over the 21 days suggested little inhibition of cell growth. And likewise, the decrease in intracellular particle retention over this extended time period also implied that growth contact inhibition was not mediating particle retention.

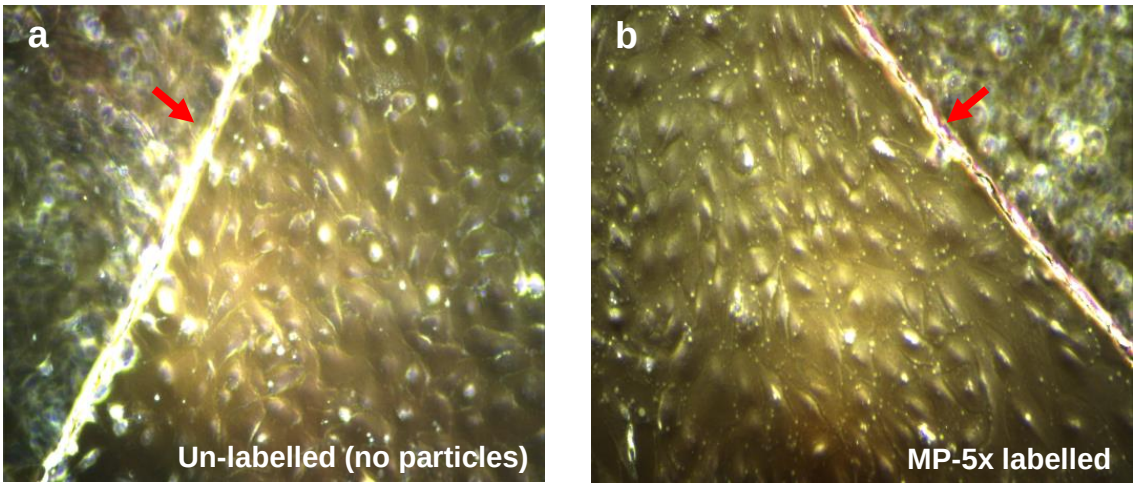

Figure 3.7 Larger wells facilitated the spread of astrocytes from the coverslip onto the base of the well plate *Phase contrast images (a & b) showing that, for long term culturing, placement of coverslips into larger well plates facilitated the spread of astrocytes from the coverslip onto the base of the well plate (red arrow denotes coverslip edge). Over long term culturing, no difference in spread was observed between (a) un-labelled (no particles) and (b) MP-labelled (MP-5x) astrocytes.* **MP**: magnetic particle.

Utilising the parameters which yielded optimal MP-loading at 24 h (*F=1 Hz; 200 µm amplitude; see Figure 3.6*), long-term particle retention was studied for magnetite-containing particles in combination with applied oscillating fields. For both MP-1x and MP-5x particles, substantial label retention (> 50%) was evident over 21 days. For MP-1x particles, approximately 92% of cells were labelled at day 1, with this value declining significantly by day 17 to *ca.* 51% of cells [*Figure 3.8 (a)*]. For MP-5x particles, in contrast, a greater labelling efficiency (*ca.* 99% of cells) was obtained at day 1 which declined significantly by day 21, albeit with > 78% of cells remaining labelled at this time point [*Figure 3.8 (b)*].

A steady reduction in particle retention was noted over the 21-day time period, with considerable heterogeneity observed among cells in terms of extent of particle retention. Visual observations over time for MP-1x showed a clear transition from peri-nuclear clustering of particles [*Figure 3.8 (c; inset)*] to a more cytoplasmic distribution (again, termed as such only as opposed to peri-nuclear localisation; nomenclature not intended to preclude possibility that particles may be localised to endosomes within the cytoplasm) [*Figure 3.8 (c; main image)*] suggesting reverse trafficking of particles. While a similar pattern was seen overall with MP-5x particles [*Figure 3.8 (d; inset)*], it was noticeable that a subpopulation of astrocytes retained large particle accumulations clustered around the nucleus even at 21 days [*Figure 3.8 (d; main image)*].

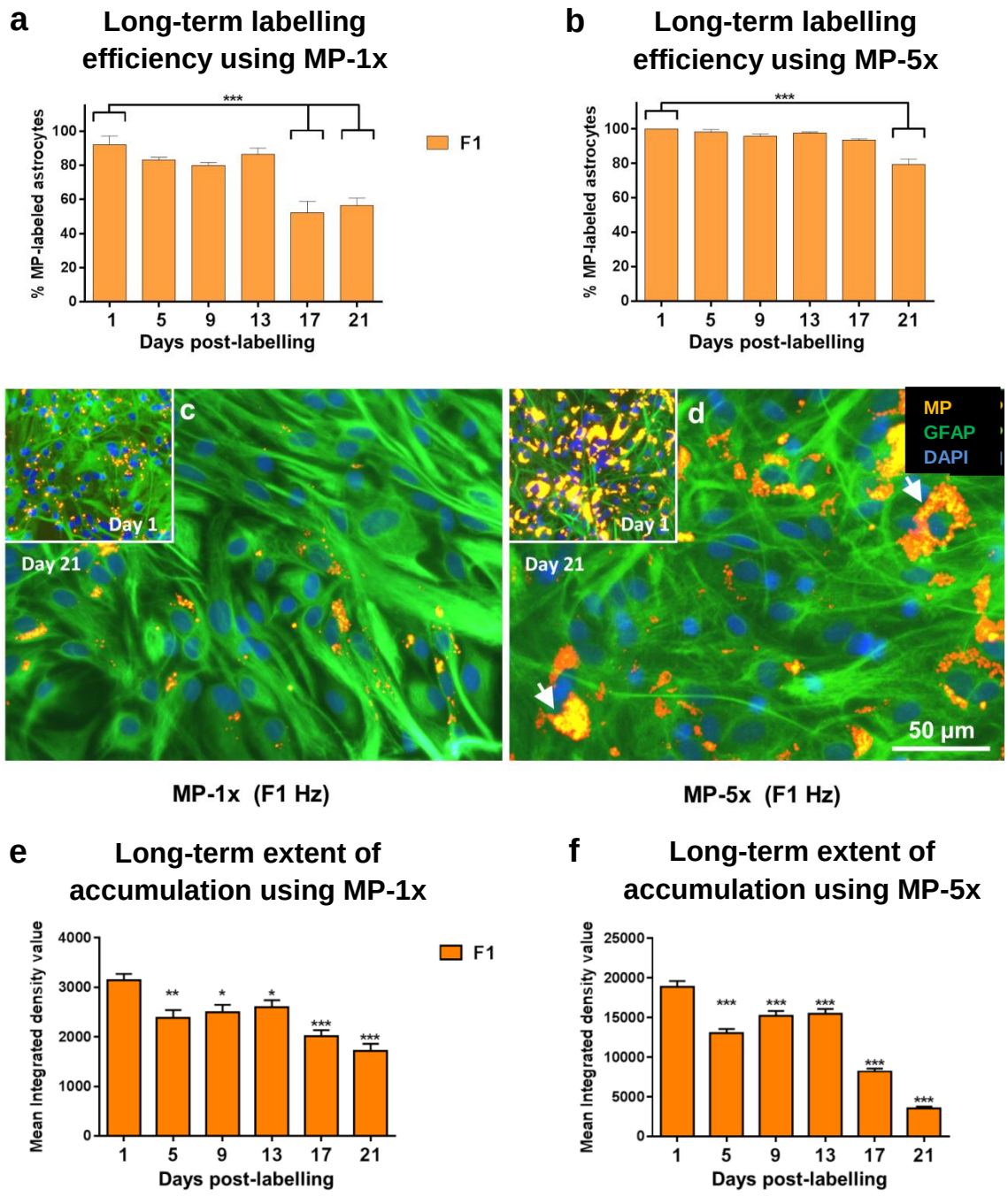

Figure 3.8 Long-term particle retention following 30 min application of an oscillating magnetic field *Following addition of particles and 30 min application of a magnetic field, long-term particle retention [MP-labelling efficiency (proportions of MP-labelled cells) and intracellular particle density (extent of particle accumulation per cell)] was assessed at six time-points over 21 days. Bar graphs showing MP-labelling efficiency post-exposure to (a) MP-1x and (b) MP-5x particles (***p < 0.001). Representative triple-merged*

*fluorescence images (c & d) showing differences in extent of intracellular particle density seen at day 1 (insets) and day 21 (main images) post-labelling with (c) MP-1x and (d) MP-5x particles. Arrows indicate 'high' levels of peri-nuclear labelling at day 21 with MP-5x particles. Bar graphs displaying extent of (e) MP-1x and (f) MP-5x intracellular particle density accumulation over 21 days, following application of an oscillating magnetic field. Within each particle condition versus day 1 (*p < 0.05; **p < 0.01; ***p < 0.001) Results expressed as mean ± s.e.m (Number of replicates = 3). Scale = 50 µm* **MP**: Magnetic particle

3.4.4 Safety evaluation of long-term particle retention

Safety of these protocols was of paramount importance, specifically with regard to particle retention over an extended period of time. Safety assessments indicate long-term retention of the particles did not impair the proliferative capacity of astrocytes. Average cell numbers showed a significant increase by day 9 for both MP-1x and MP-5x particles and for both magnetic field conditions, with no significant differences compared with untreated (no particles) controls at 21 days [*Figure 3.9 (a and b)*]. Culture purity remained at >99% over the 21 days [*Figure 3.9 (c and d)*].

There was no effect of either particles or magnetic field condition on astrocyte phenotype distribution (84.6 ± 0.7% type 1 compared with 15.4 ± 0.7% type 2, average across all conditions) [*Figure 3.9 (e and f)*].

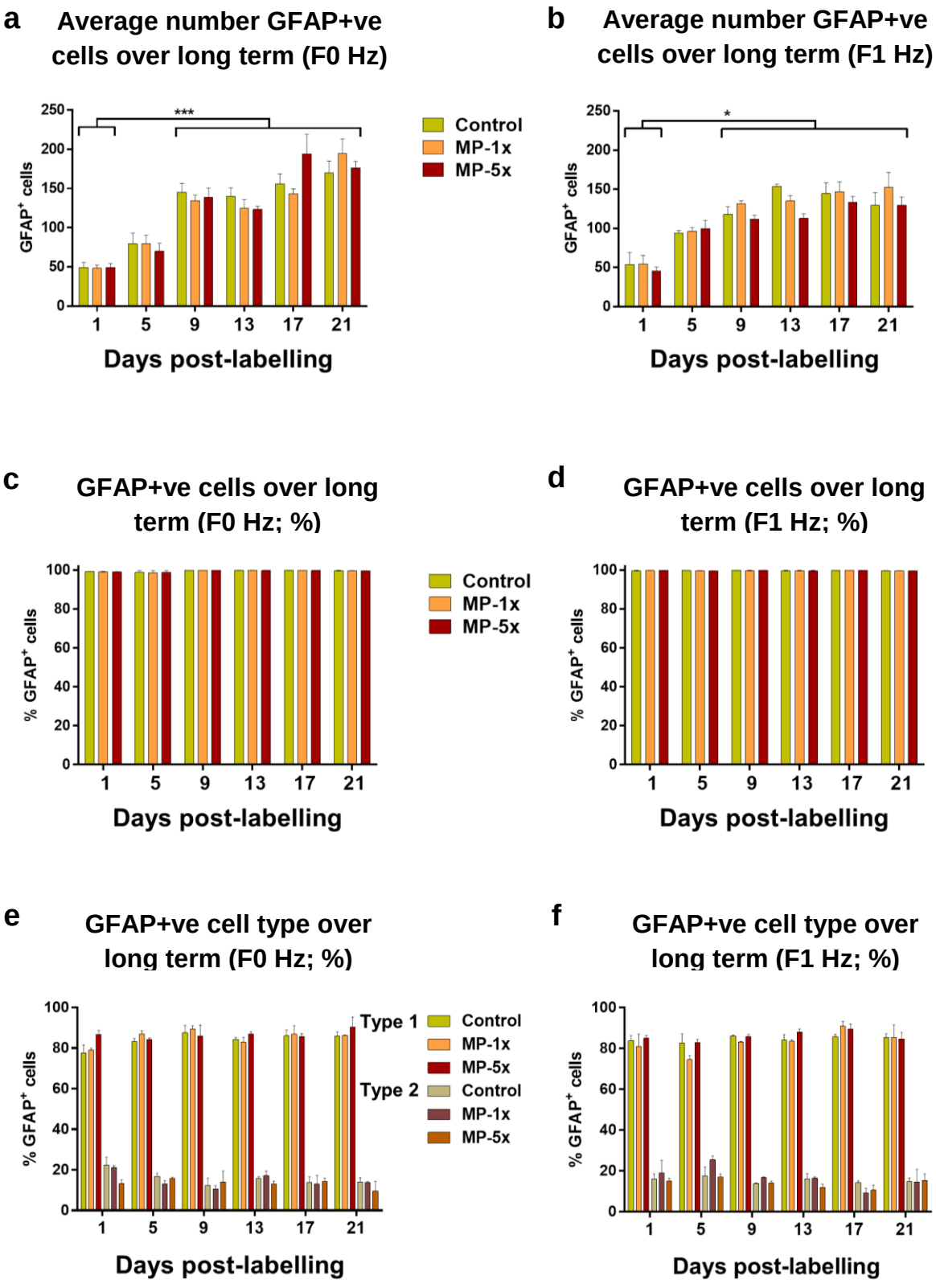

Figure 3.9 Cellular viability evaluation of long-term particle retention in astrocytes *in vitro* *The safety of long-term particle retention in astrocytes in vitro was evaluated over 21 days, with assessment of average cell counts, culture purity (%) and phenotype distribution*

*(%) assessed at six time-points over the term of the experiment. Bar graphs displaying astrocyte number per microscopic field post-labelling under (a) static (F=0 Hz) and (b) oscillating (F=1 Hz; 200 µm) magnetic field conditions (*p < 0.05; ***p < 0.001 versus day 1). Bar graphs displaying proportions of GFAP+ve cells post-labelling under (c) static field and (d) oscillating field conditions. Bar graphs showing the distribution of astrocyte phenotypes (Type 1; Type 2) post-labelling under (e) static field and (f) oscillating magnetic field conditions. Results expressed as mean ± s.e.m (Number of replicates = 3)*

MP: Magnetic particle

Across all time points a small proportion (<2%) of nuclei were observed as pyknotic, with pyknosis associated with aberrant intense GFAP staining, indicative of membrane detaching from the substrate [*Figure 3.10 (a and b)*]. By contrast, using histological analyses, the majority of labelled cells showed no obvious aberrations in GFAP staining or in astrocyte morphologies compared with controls.

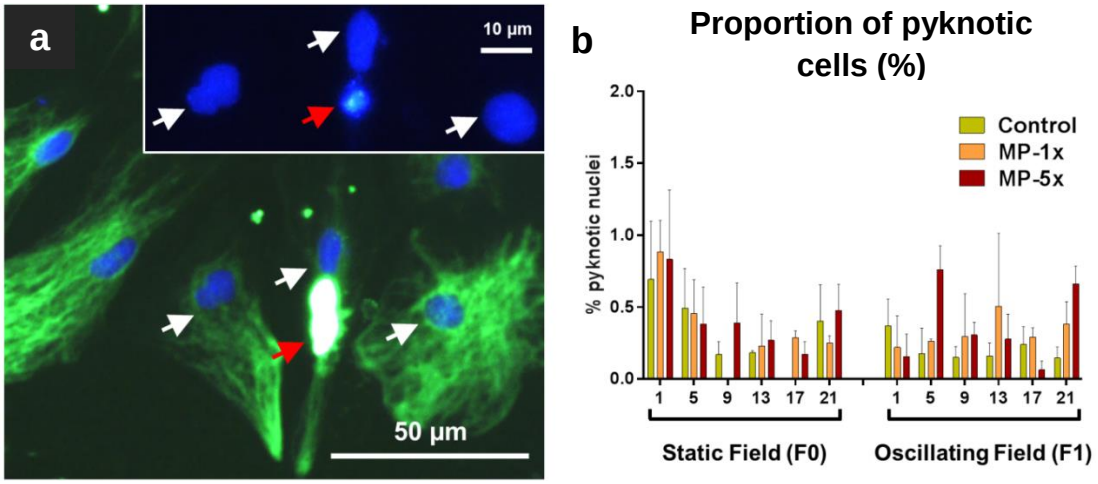

Figure 3.10 Identification of pyknotic cells in astrocyte cultures *The viability of astrocyte cultures was assessed by identifying cells with fragmenting and condensing nuclei, frequently associated with aberrant GFAP staining and evidence of membrane detachment from the substrate, all features indicative of pyknosis (red arrows indicate same pyknotic cell in main image and inset). Healthy nuclei were associated with adherent cells and normal GFAP staining (white arrows indicate same cells in main image and inset). Bar graph (b) displaying the percentage of pyknotic nuclei. Results expressed as mean ± s.e.m (Number of replicates = 3)* **MP**: Magnetic particle

3.4.5 Investigating profiles of particle inheritance in daughter cells of MP-labelled astrocytes

To gain further insight into the pattern of particle distribution into daughter cells, astrocytes labelled with MP-5x particles were studied using dynamic time-lapse imaging of proliferating cells (*Figure 3.11; Please see Supplementary Video 1 – disc 1*). This revealed that daughter cells exhibited a predominantly asymmetric profile of particle inheritance. From observation of 30 mitotic events, 21 were asymmetric compared with 9 showing symmetrical inheritance [*Figure 3.11 (a)*]. Of note, it was also observed that distribution of particles within the parent cell prior to division [*Figure 3.11 (b and f)*] was a predictor of the inheritance profile in the daughter cells. Namely, parent cells exhibiting a symmetric peri-nuclear distribution of particles [*Figure 3.11 (b - d)*] gave rise to daughter cells with symmetric inheritance of particles [*Figure 3.11 (e)*], and mitosis of parent cells with asymmetrically distributed particles [*Figure 3.11 (f - h)*] resulted in asymmetric inheritance [*Figure 3.11 (i)*].

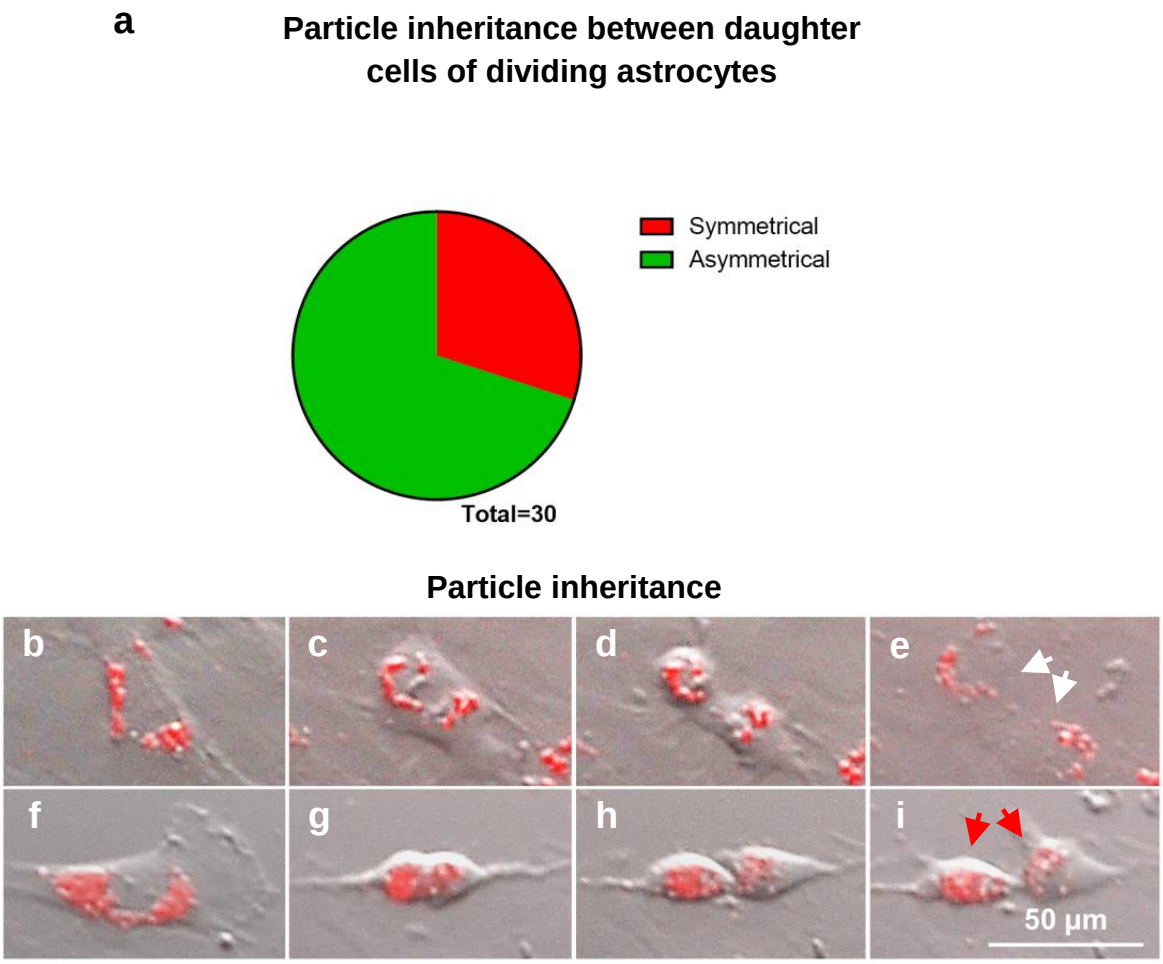

Figure 3.11 Particle inheritance in MP-labelled astrocytes *Particle inheritance in astrocytes was assessed from observation of 30 mitotic events, captured over 48 h, using dynamic time-lapse imaging. Symmetric or asymmetric classification was dependent on the proportion of particles inherited by each daughter cell as determined for both daughter cells. Symmetrical inheritance was determined when each daughter cell contained 40-60% of the total particles, with asymmetric defined as > 60% in one daughter cell. Pie chart (a) displaying quantification of particle inheritance profiles in MP-labelled astrocytes. Representative sequential still images (b – i) from dynamic time-lapse imaging (please see Supplementary Video 1 – disc 1) of dividing astrocytes post-labelling with MP-5x particles without application of a magnetic field, showing examples of (b – e) symmetric and (f – i) asymmetric particle inheritance between daughter cells (arrows).* **MP**: Magnetic particle

3.5 Discussion

This study has investigated the interaction between the physico-chemical properties (namely, magnetite content) of polymeric iron oxide particles and a highly endocytotic neural cell (primary-derived cortical astrocytes). In consideration of astrocytes as a transplant population and looking to achieve intracellular particle uptake prior to transplant, two delivery routes have been typically considered; exploitation of the cell's intrinsic 'engulfing' behaviour or the temporary disruption of the cell membrane, for example by electroporation or ultrasound bubble stimulation (*Chaudhuri et al., 2011*). The former approach relies on natural biological mechanisms and thus offers a safer labelling approach as it causes less cell death and therefore limits immunogenicity, particularly when long-term safety is a critical consideration (i.e. post-transplantation into host tissue) (*Guo et al., 1996; Krueger et al., 1998*).

The novel development of the PI analytical methodology applied within this study provided an unbiased objective approach for the quantification of nanoparticle uptake. Used at the single-cell level it allowed for simultaneous evaluation of cellular morphological features and subcellular particle localisation – the latter a determinant of particle trafficking within the cell. Of key benefit to the wider research field, this methodology is low cost as it is used in combination with easily accessible open access software. Due to its provision for non-bias, it can used across operators, laboratory-wide offering determination of particle accumulation in all cell types. However, this methodology requires further development, as **PI** values are only relative to the measures within each specific experiment. They are not representative of the number of particles or the level of iron within a cell. To address this disadvantage, flow cytometry could be used to isolate a specific number of particles and provide an iron content analysis; the **PI** of

which could then be assessed through fluorescent microscopy. A robust measure of iron content/particle number per cell could thus be elucidated from **PI** values.

The findings of this current study demonstrate that enhanced magnetite concentration in particles leads to greater particle loading in highly endocytotically active cells. In turn, this initial high loading is associated with longer particle retention (≥ 21 days) versus cells loaded with particles of lower or no magnetite content. It can be argued from these findings that greater labelling efficiency with high magnetite particles within a short time frame (i.e. 4 h), is most likely attributable to accelerated gravitational particle sedimentation onto the cells, namely due to the increased magnetite density of the MP-5x particles. However the compatibility of magnetolabelling with a wider range of MPs for use as clinical contrast agents [i.e. imaging and tracking with magnetic resonance imaging (MRI)] or with polymeric particles for drug delivery/magnetic cell targeting, is still relatively unexplored.

With the MPs studied here, application of static or oscillating magnetic fields did not influence the proportions of labelled cells, but notably, significantly enhanced the extent of intracellular particle accumulation. Taken together, the data suggest that a tailored combination of high magnetite content particles, magnetic field application and longer particle exposure times (24 h) provided the ideal combination (for this particular cell/particle) for greater labelling efficiencies and intracellular particle loading to be achieved.

Key to the labelling of a cell transplant population for imaging and tracking purposes is that of label dilution. In this respect the prolonged retention of the higher magnetite particles (21 days) is of high relevance as proliferative dilution/exocytosis and label loss present major challenges to translational applications (*Errington et al., 2010; Kim et al., 2012*). It is possible that the longer retention is simply relative to the higher initial loading

of particles into the cells. It has also been considered that cell-contact inhibition may be 'trapping' the particles within the cells. From this it could be reasoned that this high level of particle retention is an artefact of an overly confluent culture. However, the increase in cell growth and the decrease in particle density over this extended time period, would dispute this. Effects such as slower exocytosis of higher magnetite content particles cannot be ruled out, although some studies suggest label dilution is due to proliferating cells and division of particles into daughter cells rather than exocytotic activity (*Kim et al., 2012; Harrison et al., 2016*). What can be noted however is that the combination of high survival of such cells post-labelling, in conjunction with such slower excretion, may serve to limit the availability of free particles for secondary uptake by resident cells in the host tissue.

The overall trend in labelling seen here was similar to that seen in NSCs, although, in the latter, magnetic field application significantly enhanced labelling efficiency with low magnetite particles (*Adams et al., 2015*). It can, however, be speculated that it is the higher levels of endocytotic activity in astrocytes that results in rapid particle uptake and that it is this characteristic that outweighs the benefits of field application, particularly for higher magnetite content particles with more rapid sedimentary profiles. Moreover, in comparison of intracellular label in astrocytes versus NSCs, a greater level of accumulation is noted in the former (*Adams et al., 2015; Tickle et al., 2016*). This may be related to the morphological features and intrinsic endocytotic profiles of the cells. For example, scanning electron micrographs show broad flattened morphologies for astrocytes (in culture) with elaboration of large amounts of cell membrane, and surface features suggestive of high cellular membrane activity. In contrast, NSCs are bipolar cells with smaller cell bodies, relatively quiescent membranes and considerably less surface area available for particle uptake (*Fernandes & Chari., 2014*). Together, these findings

highlight the importance of studying the interactions of neural cell type and its intrinsic endocytotic behaviour in conjunction with particle tailoring strategies.

A less obvious point to note here is the importance of controlling cell densities for such work; indeed in some populations containing actively dividing cells, there is a density-dependent inhibition of endocytosis which could negatively impact particle uptake processes (*Davies & Ross, 1980*). As can be seen with the neural cell utilised for this study, the majority of neural transplant populations are highly proliferative and are typically (although not in this case) propagated under growth factor drive. It remains important therefore that optimal cell densities for each cell type are established, with cellular confluence carefully monitored prior to particle addition in labelling protocols for biomedical application.

The safety of the procedures utilised here was of paramount concern, given the combined variation of multiple parameters (particle properties, magnetic field application and duration of particle exposure). The procedures did not result in acute or long-term alterations in MP-labelled cells, as determined by an array of safety assays which assessed cell survival, proliferative capacity and cell phenotype. The findings here parallel observations seen with NSCs, highlighting the neurocompatibility of the particles used (*Adams et al., 2015*). The safety profile of these particles could be attributable to the slow degradation profile of the PLA matrix component which limits the rate at which iron leaches from degrading particles; rapid leaching is widely recognised as a major factor in MP toxicity (*Petters et al., 2015; Soenen et al., 2010*). Moreover, the safety profile featured here is also consistent with the observed stability of intracellular particles in astrocytes when part of a mixed glial population (*Jenkins et al., 2013*).

Use of dynamic, live cell imaging is a novel approach in studying the distribution (inheritance) of particles into the progeny of neural cells derived from primary cultures. The observations here show that particle inheritance is largely asymmetric (namely, particle distribution is uneven between daughter cells). These findings are consistent with previous studies utilising cell lines, where particle uptake and redistribution to daughter cells after mitosis has been typically reported as being a 'random' and asymmetric process (*Errington et al., 2010; Kim et al., 2012; Rees et al., 2014; Summers et al., 2013*). The reasons for this uneven distribution are unclear, but may relate to the non-uniform distribution of particles around the nuclear poles in the parent cell, a feature that was consistently observed in the majority (*ca.* 75%) of labelled astrocytes. In turn, the reasons for this polarised initial distribution are unknown, although it has been suggested that intracellular particle distribution may be dependent on particle size/shape and/or particle interaction with signalling pathways (*Chaudhuri et al., 2011; Gratton et al., 2008; Hussain et al., 2014*).

Nonetheless, these findings suggest significant implications for the use of a tailored MP strategy for biomedical applications involving astrocytes, and indeed other proliferative neural transplant populations. Label dilution with cell division contributes to reduced efficacy of particle labelling for imaging, tracking and targeting applications, although the results indicate that not all cells would be affected to the same extent. Unequal inheritance would imply that with each division the usefulness of the intracellular particle load would exponentially diminish for a subpopulation of daughter cells. Conversely, useful levels of label would be retained and persist in a larger subpopulation of daughter cells for a longer period of time. This would not be the case with symmetrical inheritance. Hence, asymmetrical loading of particles in daughter cells would result in the ability to track overall biodistribution of the cellular graft for an extended period of time (in relation to

symmetrical loading), even where a small sub population would be lost to the imaging/tracking process.

Overall, an understanding and characterisation of the mode of particle inheritance in the daughter cells of a labelled transplant population are important parameters contributing to particle detection for tracking/targeting purposes. Moreover, in this regard, what is also needed is a clear understanding of the biological and chemical factors influencing cellular particle uptake (*Figure 3.12*).

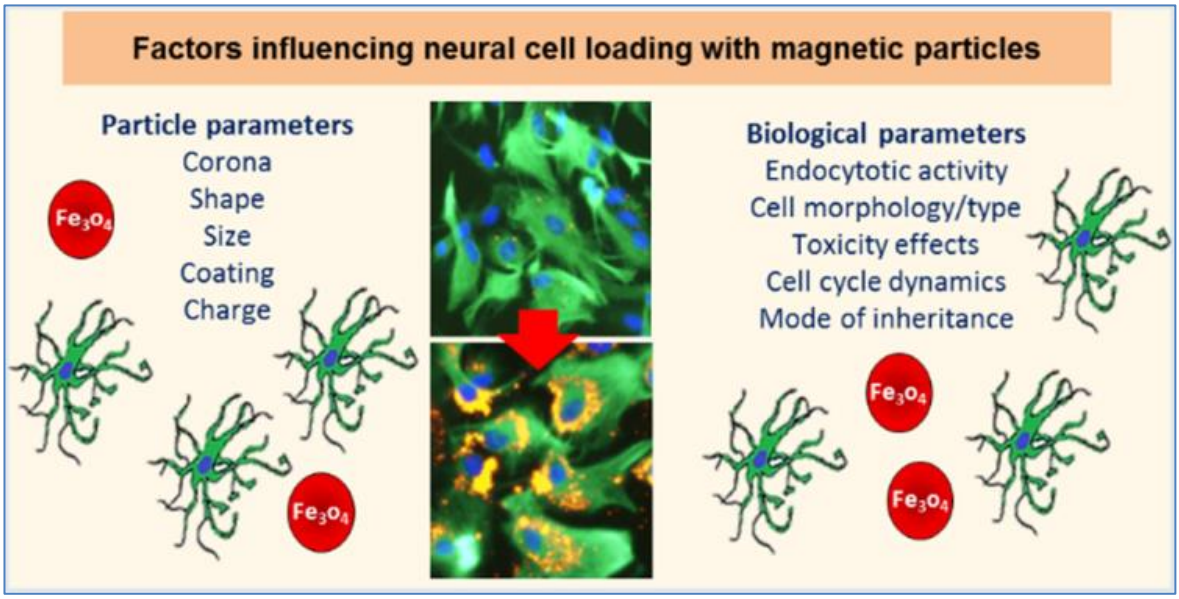

Figure 3.12 Factors influencing cellular particle uptake *Schematic diagram showing factors that influence cell loading with particles, illustrating the combined dynamics of the physicochemical characteristics of MPs and the biological function of the cell. Fluorescence micrograph shows MP-5x labelled astrocytes (Chaudhuri et al., 2011; El-Sayed et al., 2005; Errington et al., 2010; Gratton et al., 2008; Hussain et al., 2014; Kettler et al., 2013; Kim et al., 2011; Lesniak et al., 2013; Ruoslahti et al., 2010).* **MP**: Magnetic particle

Astrocytes participate in complex signalling pathways and secrete several biomolecules needed for homeostatic functions (*Abbott et al., 2006; Chu et al., 2014; Walz, 2000*). What is not clearly understood is the influence exerted on these pathways by the physicochemical factors of the particles themselves, although studies have gone some way to elucidating this (*Hussain et al., 2014*). Systematic investigation of each of these parameters (for example utilising proteomic and bioinformatics pathway analyses) and their relative importance to neural transplant therapies would allow for the tailored development of optimal labelling protocols for translational applications.

Chapter 4
Non-invasive tracking of neural cells in implantable materials

4.1 Introduction

There are two main considerations, each with its own challenges that are key to the utility of a neural cell transplant for regeneration of the damaged spinal cord. The first is enhancing the efficacy of neural cell transplant delivery into the host parenchyma, achievable through use of a protective 3-dimensional construct. The second consideration, particularly in respect of its clinical relevance, is the ability to non-invasively track the transplant cell population over time (*as discussed previously within the main introduction*).

Regenerative medicine following spinal cord injury is moving apace. Research has moved into clinical trials, with the implantation of OECs into the lesion site seeing functional regeneration within the spinal cord, coincident with some restoration of sensory and locomotor function (*Granger et al., 2012; Tabakow et al., 2014*). However, as already discussed, success rates are modest, being hampered by the lack of efficacy in surgical delivery of the cell population (*Guest et al., 2011; Pearse et al., 2007*); a challenge that demands a protective delivery system for cell transplant populations, to build on the success seen so far.

Hydrogels are emerging as a viable solution to address this challenge (*Perale et al., 2011 for review*), with a growing number of studies implanting 3-dimensional constructs as an acellular bridge/scaffold within the lesion cavity, resulting in significant axonal regeneration (*Han et al., 2010; Kaneko et al., 2015; Li et al., 2015; Nam et al., 2010*). These constructs are also widely utilised in combination with stem cells *(Cen et al., 2009; Heymer et al., 2008; Syková et al., 2006)* and SchCs (*Woerly et al., 1996; Xu et al., 1997; Xu et al., 1999*); each cell:construct promoting a conducive environment for regeneration , putatively due to the neuroprotective and neuro-immunomodulatory mechanisms of the cell transplant.

Studies delivering primary neural cells as a cell construct into injured spinal cord are, to date, few (*Joosten et al., 2004; Tian et al., 2005*). In this respect, use of astrocytes as a transplant population for spinal cord repair, despite reporting significant regenerative success in locomotor function when delivered as a cell suspension (*i.e. Davies et al., 2006, 2011; Fan et al., 2013; Filous et al., 2010; Pencalet et al., 2006; Selkirk et al., 2002; Wang et al., 1995*), appears to have been neglected as a transplant population within the protective environment of a hydrogel. One such study reports the transplant of neonatal astrocytes encapsulated in collagen into the lesion site of a hemi-sected spinal cord (*Joosten et al., 2004*). Although successful axonal regeneration led to a level of restoration in locomotor function, the utility of this cell:collagen construct does not appear to have been developed further. Indeed, astrocyte characterisation within a 3-dimensional construct has only recently begun to be explored (*Balasubramanian et al., 2016; Frampton et al., 2011; Placone et al., 2015; Seyedhassantehrani et al., 2016; Winter et al., 2016*). MP-labelling of astrocytes report high uptake with no adverse effects on viability in both *in vitro* and *ex-vivo* studies (*Pickard et al., 2011*). Despite this, as yet no study has furthered the possibility of MP-labelling astrocytes to facilitate non-invasive tracking of this potential cell transplant population. There still remains a heavy reliance on the use of histological analyses to determine transplant cell localisation/migration.

In this regard the second consideration, non-invasive tracking of the transplant cells, is achievable through the use of MRI. In clinic this imaging technique is widely used, facilitated by a number of clinically relevant gadolinium-based contrast agents (*e.g. Omniscan*). In this regard, MPs are ideally suited as a contrast agent in MRI as they present a strong negative signal that addresses the low sensitivity associated with this imaging technique (*Bulte & Kraitchman., 2004*).

MR imaging of neural cell suspensions labelled with superparamagnetic nanoparticles has been extensively undertaken (i.e. OPCs – *Bulte et al., 1999;* NSCs – *Bulte et al., 2001;* ESCs – *Hoehn et al., 2002; Jendelová et al., 2004*), as has MR imaging of mesenchymal; bone-marrow and adipose-derived stem cells within hydrogels (*Cen et al., 2009; Heymer et al., 2008; Syková et al., 2006*). Although interestingly, the majority of these studies, including the few studies combining primary neural cells and hydrogels as a spinal cord implant (*i.e. Joosten et al., 2004; Tian et al., 2005*), have still shown a heavy reliance on histological findings to report cell localisation and integration.

In progressing the use of cell transplant to clinical trials (*i.e. Granger et al., 2012; Saberi et al., 2008; Tabakow et al., 2014*) it is of note that no consideration was given to the labelling of the transplant cells for subsequent tracking. Animal and clinical trials utilising SCs as a transplant population for SCI, have acknowledged this 'oversight' as a significant limitation (*Pearse et al., 2007; Saberi et al., 2008*). Consequently, the concept of utilising MRI to non-invasively track a neural cell transplant population within a hydrogel is, thus far, **an under acknowledged area in this emerging field of regenerative therapy.**

This chapter aims to find a viable solution to this challenge facing regenerative applications. It aims to develop a robust protocol for the synthesis of *i*) a protective delivery system for *ii*) a MP-labelled *iii*) neural cell transplant population (astrocytes). The combination of these three elements offers a 3-dimensional collagen hydrogel, containing a MP-labelled cortical astrocyte transplant population – a cell type that has shown considerable success in regeneration of the spinal cord – and moreover, due to the high concentrate magnetite particle employed in the labelling of these cells, has the potential to be tracked non-invasively using MRI.

In order to further develop this area in regenerative therapy there are a number of technical issues that first need to be considered. The argument for a 3-dimensional environment over 2D monolayer cultures has already been addressed as has the argument for the use of a collagen construct over a number of other biologically derived hydrogels (*General introduction; section 1.5.2*). However, the challenges inherent to the development of a cell-viable 3-dimensional collagen construct are varied.

The first challenge involves optimising particle uptake and accumulation within the cells to ensure an intense signal under MRI (*Bernsen et al., 2015; Wang & Shan, 2012*). Of equal importance is utilising an optimal approach to ensure a viable 3-dimensional cellular construct for potential use as an implant for regenerative application.

In this respect, the second challenge to be addressed is the porosity of the construct to ensure cellular viability (*Melchels et al., 2010*). Too tight a matrix results in cell death from *i*) inhomogeneous cell distribution and *ii*) pockets of necrosis within the construct due to oxygen and nutrients being unable to penetrate through to the centre of the hydrogel (*Malda et al., 2004*), and metabolic waste products unable to be removed from the hydrogel (*Mertens et al., 2014b*).

The third challenge, and one of the major challenges faced in clinic, is the inhomogeneity of the cell transplant following delivery (*Guest et al., 2011; Pearse et al., 2007*). This represents a major challenge within a 3-dimensional construct (*Unsworth et al., 2003*). Inhomogeneous cell distribution results in cell death leading to subsequent inhibition of a cellular network conducive to a regenerative environment (*Wakatsuki & Elson, 2003*). It is these challenges that have informed the objectives for this study.

4.2 Objectives

1) To establish MP-labelled astrocyte monolayers on a collagen substrate, the findings of which will inform development of intraconstruct gels

2) To assess cellular viability and homogeneity within the gels, and assess the safety of the protocols used

3) To characterise the cellular and endocytotic features of cortical astrocytes within the 3-dimensional environment of an intraconstruct hydrogel and to evaluate comparable features of astrocyte monolayers

4) To develop a 3-dimensional MP-labelled astrocytic hydrogel with the utility for non-invasive tracking of the neural cell population using MRI

4.3 Experimental procedures

4.3.1 Reagents and equipment: All reagents and equipment used are as described previously in sections *2.1; 2.2.3; 2.3 & 2.4.* MP-5x particles were used throughout the hydrogel experiments. Use of this particle, due to its enhanced magnetite concentration, has proved the most effective in cellular uptake and long-term particle retention in cortical astrocytes as a monolayer culture. Moreover, for the purposes of non-invasively tracking a MP-labelled transplant population, a particle with such high magnetite concentration promises a strong hypointense signal under MRI.

4.3.2 Establishing MP-labelled astrocyte monolayers on a collagen substrate: Following formation and MP-labelling of a supra-construct hydrogel (*as detailed in 2.7.1-2*), sample gels were fixed at different time-points post-particle addition (24 h – 14 DIV), with culture characteristics, outcomes and cellular assessments used as proof-of-concept findings to inform subsequent intraconstruct hydrogel experiments.

To investigate the ultrastructural membrane features associated with endocytotic activity, at 24 h post-particle addition in-situ labelled supraconstruct hydrogels were fixed for 2 h at RT with 2.5% glutaraldehyde solution, diluted with 0.1 M sodium cacodylate buffer with 2 mM $CaCl_2$ at pH 7.4. This was followed by a further overnight fixing step at 4 °C in 0.25% glutaraldehyde solution diluted in 0.1 M sodium cacodylate buffer.

Preparation for FESEM: Following this, the gels were prepared for FESEM imaging using the osmium-thiocarbohydrazide step-wise procedure (*Vriend & Geissinger, 1980*) followed by critical point drying of the samples. Modifications were made to the protocols to prevent shrinkage and distortion of the gels during the dehydration steps.

Following glutaraldehyde fixation, the gels were rinsed in 0.1 M sodium cacodylate buffer (3x) and then rinsed in deionised water (dH_2O) (6x) before being steeped in osmium and incubated for 2 h at RT. Following 6 further rinses in dH_2O the gels were covered with thiocarbohydrazide and incubated for 20 min at RT, followed by 6 rinses with dH_2O and stored overnight in dH_2O at 4 °C. The osmium and thiocarbohydrazide steps were repeated with 6 dH_2O rinses between each step before the final addition of an osmium layer over the gels. Following 2 h incubation at RT and six rinses in dH_2O, the gels were placed in 70% ethanol (ETOH) for 4 h at RT, before being transferred and stored in 80% ETOH overnight at 4 °C.

Modification of step-wise dehydration: The gels were then stored at 4 °C for a period of 7 days during which time they were subject to an extended series of dehydration steps. After 24 h in 80% ETOH, they were transferred to 90 % ETOH for 48 h, with a 100% refresh at 24 h. The gels were then transferred to 100% ETOH for a further 48 h with a 100% refresh at 24 h, before being transferred to 100% DRY ETOH. At 4 h, a 100% refresh was followed by a further 48 h 100% DRY ETOH dehydration step. The gels were then subject to full dehydration in a Critical Point Dryer (CPD) following the standard procedure. Briefly, keeping gels immersed in 100% DRY ETOH, they were wrapped in vellum tissue and placed in the CPD tray, also filled with 100% DRY ETOH, and the tray inserted into the machine. With the machine cooled to 12 °C, three changes of liquid CO_2 (to facilitate removal of ETOH from the sample) were immediately performed with three further changes performed every 15 minutes over the following 2 h. At 2 h, 4 additional changes of liquid CO_2 were performed with a further 2 full changes made following the complete absence of moisture. Following the final change, the samples were heated to 34 °C and the pressure elevated to 1200 psi to remove all final traces of ETOH and fully dehydrate the

gels. The samples were cooled to 12 °C before removal and mounting onto carbon pads for visualisation under FESEM.

4.3.3 Developing an MP-labelled cellular intraconstruct hydrogel with the utility for non-invasive tracking of the neural cell population using MRI: Achieving an intraconstruct hydrogel followed the same protocol used for hydrogel assembly (*as detailed in sections 2.7.1 & 2.7.3*) with the addition of 10% cell suspension replacing 10% D10 medium (*Figure 4.1*).

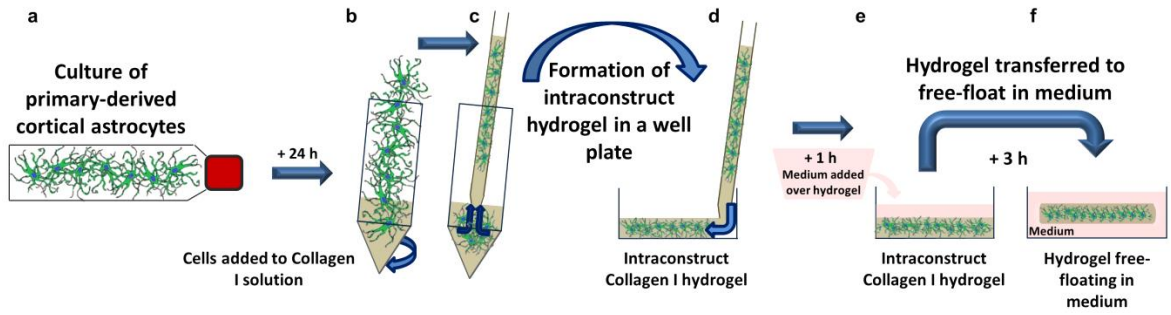

Figure 4.1 A schematic outlining the formation of an intraconstruct hydrogel *Primary-derived cortical astrocytes (a) were cultured in flasks for 24 h, with the cell suspension (b) added to collagen solution. An intraconstruct hydrogel (c & d) was formed in a well plate and allowed to set for 1 h before addition of D10 medium. At 3 h post-construct the hydrogel (e) was transferred to (f) a larger well plate to allow it to free-float in medium.*

Exogenous particle-labelling approach: Addition of MP-5x particles to form intraconstruct hydrogels utilised two approaches; 'exogenous' MP-labelling and 'in-situ' MP-labelling. The former approach consisted of particle addition to astrocyte monolayers cultured in T175 flasks, the cells then exposed to a static magnetic field for 30 mins as MP-labelling of astrocyte monolayers showed that exposure to a magnetic field enhanced levels of particle accumulation. Control cells (no particles) were also exposed to a static field. At 24 h post-particle addition the cells were rinsed with PBS to remove any free particles and dissociated with TrypLE™; the resulting MP-labelled cell suspension then added to the collagen solution (*protocol detailed in 2.7.1 & 2.7.3-4*) (*Figure 4.2*).

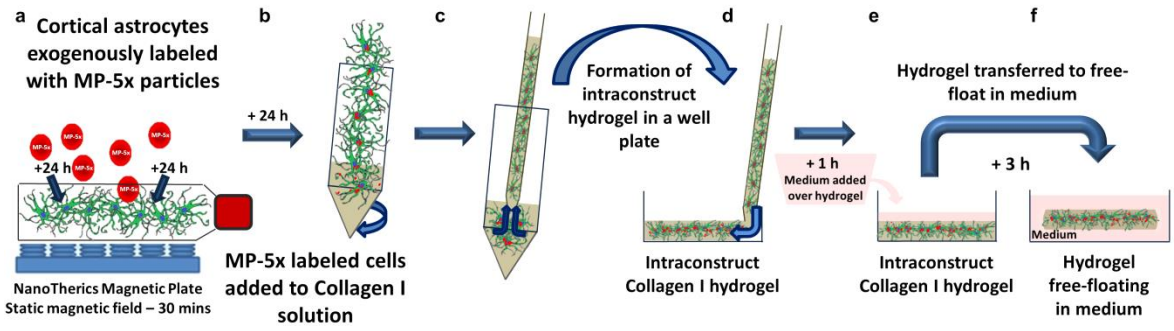

Figure 4.2 A schematic outlining formation of an exogenous MP-labelled intraconstruct hydrogel *Cortical astrocyte monolayers (a) were labelled with MP-5x particles and exposed to a static magnetic field for 30 mins. At 24 h post-particle addition (b) the MP-5x labelled cell suspension was added to the hydrogel solution, followed by (c & d) formation of the intraconstruct hydrogel. At 1 h post-construct (e) medium was added to the gel, and at 3 h post-construct (f) the gel was transferred to a larger well plate and free-floated in D10 medium to prevent inhomogeneous cell distribution.* **MP**: Magnetic particle

Quantification of particle uptake, particle accumulation and long-term particle retention was conducted from these gels.

In-situ particle-labelling approach: The latter approach, that of in-situ MP-labelling of astrocytes, consisted of MP-5x particles being added directly to the cell suspension prior to association with the hydrogel solution (*as detailed in 2.7.1; 3-4*). This approach allowed observation under FESEM, TEM and dynamic live imaging of ultrastructural membrane features and particle inheritance, together with observations of endocytotic activity in intraconstruct hydrogels i.e. intracellular particle uptake and trafficking.

Promoting homogeneity of cellular distribution: In developing the intraconstruct hydrogel, using either approach, it became apparent that the gels were subject to contact-tension from the culture plastic (*Buxboim et al., 2010; Discher et al., 2005*), inducing inhomogeneous cell distribution i.e. cells were drawn towards the edge and the bottom of the gel. This phenomenon also influenced cell morphology in that cells at the base of the gel took on a flattened membranous morphology more typical of monolayer cultures, with clumping of cells a prominent feature at the gel edge where it contacted with the plastic. To address this, at 3 h post-construct, the hydrogels were transferred from the 24-well plate into a larger well-plate using a modified paddle spatula (*Figure 4.3*). Modification of the angle of the paddle head enabled careful transfer of the gels without damage to the collagen substrate or the internalised cells. Once transferred into a well containing 4 mL of D10 to facilitate free-floating of the gel, they were incubated at 37 °C (5% CO_2/95% humidified air) and maintained over the course of the experiment with a 50% D10 refresh every 2 days.

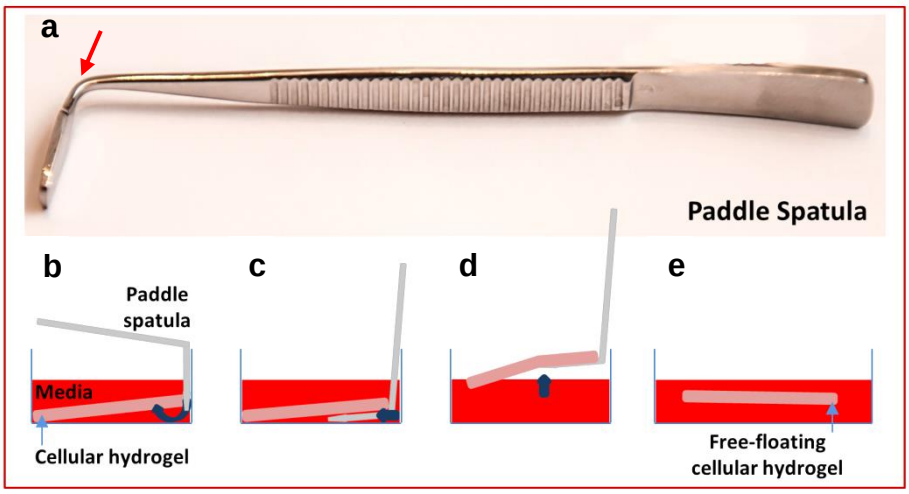

Figure 4.3 Schematic of modified paddle spatula and transfer technique *Image showing (a) the modified angle head (arrow) of the paddle spatula. This modification enabled (b) gentle insertion of the paddle spatula between the cellular hydrogel and the wall of the well. This allowed media flow beneath the hydrogel (c) lifting the gel sufficiently from the base of the well to insert the paddle spatula under the hydrogel without exerting any force. The hydrogel (d) could then be transferred to the (e) larger well plate to free-float in medium. Free-floating the gels helped promote a homogenous 3-dimensional cellular network, unaffected by the tension forces from the culture plastic.*

Preparing the intraconstruct hydrogels for MRI: Exogenous MP-labelled intraconstruct hydrogels facilitated investigation of the utility of the MP-5x particle as a contrast agent for non-invasive tracking of the cell population under MRI. Due to the small size of the gel, it was necessary to place them within a carrier tube for insertion into the machine, for which a 30 mL universal tube was ideally suited. The gel was sandwiched between layers of agarose gel within the tube to prevent air pockets distorting the MR image resolution. A low-gelling temperature agarose gel (A4018 – Sigma) was used due to its gelling temperature of <30 °C – the majority of agarose gels form at temperatures in excess of 37

°C, which would cause degradation of the collagen hydrogel and potentially disrupt the internalised cells.

Briefly, a 1% *w/v* agarose solution with PBS buffer was heated to its melting point of >65 °C to dissolve the agarose before being placed on a heat plate to cool to *ca*. 32-35 °C. The consumables used i.e. 10 mL pipettes and universal tubes, were also maintained at this temperature to prevent premature setting of the agarose gel during dispensing. Once cooled *ca*. 7 mL gel solution was added to the tube and allowed to set at 4 °C, whereupon the intraconstruct hydrogel was placed on this bottom layer before being sandwiched by a further layer of cooled (*ca*. 32-35 °C) agarose gel, and stored at 4 °C until imaged under MRI.

4.3.4 Assessing cellular viability and safety of the protocols used: Safety of the protocols was of paramount importance in ensuring high cellular viability within the intraconstruct hydrogels. In this respect, cell health was quantified by cell counts and live/dead assays. EdU cell proliferation assays were conducted to assess the proliferative capacity of the cells (*as detailed previously in 2.8.2*). Each of these culture characteristics was measured from acquired z-stack images from the centre and edges of the gels. The homogeneity of cell distribution throughout the gels was investigated by comparative cell counts from the base, middle and top of the gel at the centre and the edges of the gel. Proliferation counts and live/dead assays were also quantified in this manner to determine homogeneity throughout the gel construct.

In this respect, account was taken of the effect of cell growth within the collagen substrate itself as formation of the cellular network causes gel contraction. To determine any adverse effect of gel contraction on cellular viability, culture characteristics were assessed across the time-frame of the experiments.

4.3.5 Investigating cellular characteristics of cortical astrocytes in a 3-dimensional environment: Differences in *in vitro* cellular morphology have been linked to the substrate on/in which they are cultured. 2-dimensional substrates force cell attachment and subsequently perfusion to opposing cell faces (*East et al., 2010*), unlike cells grown within a 3-dimensional gel construct which display morphological characteristics closer to their *in vivo* counterparts (*Hu et al., 2014*). As discussed previously in the introduction (*see 1.5.2*), functional behaviour of astrocytes has also seen alteration dependent on the substrate on which the cells were grown [2-dimensional hard substrate compared with 3-dimensional hydrogel (*Hu et al., 2014; Moshayedi et al., 2010*)]. From this, a putative link has been suggested between altered morphology and consequent altered cellular function (*Hu et al., 2014; Lee et al., 2008; Miron-Mendoza et al., 2013; Mohayedi et al., 2010*).

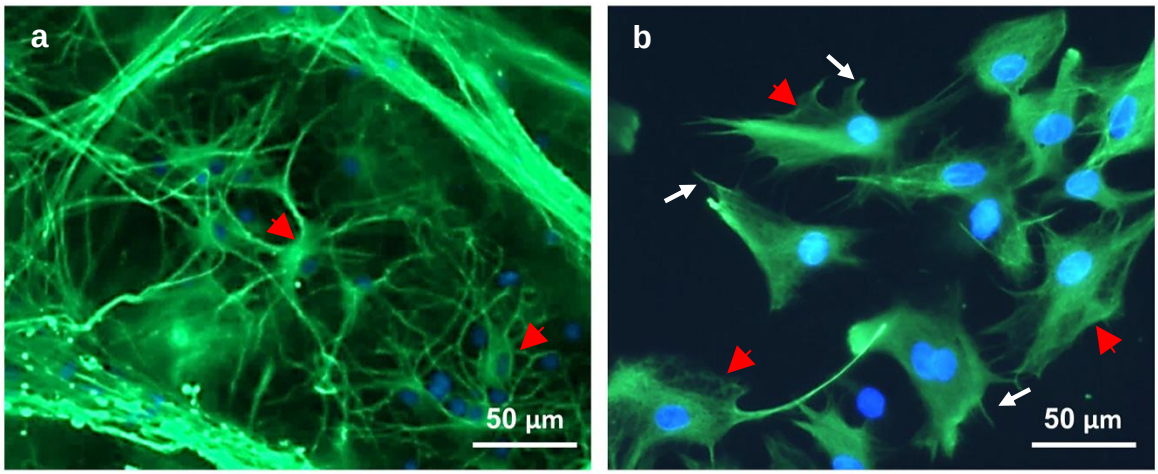

Figure 4.4 Characteristic morphologies of cortical astrocytes *Fluorescence images displaying the characteristic morphologies of cortical astrocytes observed within (a) an intraconstruct hydrogel and (b) a monolayer culture. Note the small cell soma (a; arrowhead) and highly branched complexity of cells grown within a 3-dimensional collagen substrate. Compare this with the flattened, membranous morphology (b; arrowhead) typical of astrocyte monolayers cultured on coverslips, and the truncated processes of these cells (b; arrow). Scale of images = 50 µm*

In these series of studies, observation of cell morphologies within the exogenously MP-labelled intraconstruct gels, were uncharacteristic of those observed in monolayer cultures of cortical astrocytes. The former display a complexity of primary, branched processes and a smaller cell soma and nucleus than the latter, which displayed flattened, membranous morphology with, where present, truncated processes (*Figure 4.4*).

These observations informed the array of morphological/morphometric analyses described below to quantify astrocyte morphology within a 3-dimensional collagen structure in comparison with monolayer astrocyte cultures grown on a hard substrate. Fluorescence images were scaled to show measurements per micron (µm) with the following morphological features quantified on a single cell basis; area of the cell soma; the size of the nucleus, and a measure of the ramified nature (branch-like processes) of astrocytes using the formula: - $\mathbf{4} \times \boldsymbol{\pi} \times \mathbf{A}/\mathbf{P}^2$ where **A**=cell area and **P**=cell perimeter. This formula denotes the spherical nature of a cell, with a calculated value of 1 denoting a rounded cell morphology, and a value of <1 indicative of the level of complexity of the cell i.e. more branched (*East et al., 2009*).

The number of primary processes was quantified, with process length calculated as a length ratio of the cell size, based on the formula: - **L/D** where **L**=*length of the process (µm)* and **D**=*distance from the nucleus to the tip of the process* (*Hu et al., 2014*)

This measure provided a further indicator of the ramified nature of the cell, and the length of process compared to the size of the cell soma.

4.3.6 Investigation of endocytotic features associated with particle uptake: To investigate these features, a novel approach was developed to facilitate visualisation of in-situ MP-labelled intraconstruct hydrogels under TEM. The approach entailed embedding of the gels

within Spurr resin. Following glutaraldehyde fix and initial steeping in osmium (*as previously detailed in 4.3.2*), the gels were rinsed in dH_2O (6x) and immediately taken through a modified series of ETOH dehydration steps as detailed above (*Section 4.3.2*) before embedding in Spurr resin.

The conventional Spurr embedding protocol which is generally used for infiltration into non-decalcified tissue or single cells (*Spurr, 1969*) was modified for use with the collagen gels. Briefly, at RT in the appropriate fume cupboard, gels were infiltrated in 3:1 100% DRY ETOH:Spurr resin mix overnight. The following day the gels were infiltrated in 1:1 Spurr resin:100% DRY ETOH for 4 h. After 4 h, gels were infiltrated in 3:1 resin:100% DRY ETOH for a further 4 h before being infiltrated in pure Spurr resin overnight. The next day the gels were infiltrated in fresh pure Spurr resin for 8 h with a 100% change every 2 h, and then placed in an appropriate embedding mould and covered with fresh pure Spurr resin. The samples were then placed in a heated oven at 60 °C and the resin polymerised for 24 h.

4.3.7 Immunocytochemistry: Immunolabelling of the cells using a modified protocol was as detailed in sections *2.9.2 and 2.9.3*, with FITC secondary antibody used in these experiments due to the BODIPY® 546-570-PLA fluorophore coating of the particles.

4.3.8 Imaging: Imaging of this series of experiments was conducted using Z-stack microscopy; Dynamic time-lapse imaging; FESEM; TEM and MRI (*please refer to section 2.10.2 for detailed information)*

4.3.9 Analyses: Quantification of culture characteristics and safety assessments were conducted from Z-stack triple-merged fluorescent micrographs. Dynamic time-lapse imaging allowed observation of particle inheritance. Ultrastructural membrane features and gel characteristics were visualised from FESEM micrographs, with cell cytoskeletal and

subcellular features visualised from TEM micrographs. Endocytotic activity such as intracellular particle uptake and trafficking and associated membrane features were also visualised from TEM micrographs. The utility of MP-5x particles as a suitable contrast agent for tracking of a cell transplant population, were visualised from MRI images.

4.3.10: Statistical analysis: Data were analysed by one-way analysis of variance (ANOVA) with post-hoc analysis carried out using Bonferroni's multiple comparison test (MCT). All data are expressed as mean ± s.e.m. The number of cultures used in this series of experiments was 3 ($n = 3$) unless otherwise stated, each derived from a different rat litter.

4.4 Results

4.4.1 Establishing MP-labelled astrocyte monolayers on a collagen substrate

Pre- MP-labelled supraconstruct hydrogels show high levels of cell clumping

Extensive cell clumping was observed throughout the supraconstruct gels using this approach [*Figure 4.5 (a)*], a feature which did not alter over the time-frame studied [*Figure 4.5 (c & d)*]. Individual cells, albeit a small minority (*ca*. 5%), displayed small cell soma with numerous fine processes [*Figure 4.5 (b & c)*]. Particle uptake and cellular accumulation were evident although difficult to assess due to the high level of cell clumping observed with these gels.

In-situ MP-labelled supraconstruct hydrogels show high particle uptake and accumulation

In contrast, in-situ supraconstruct gels showed lower levels of cell clumping with individual cells (*ca*. 70%) making up the larger proportion of the cell population. At 24 h post-particle addition, cells displayed small cell soma and long processes [*Figure 4.6 (a)*], and over the following 14 d, cells developed a highly ramified morphology [*Figure 4.6 (b – d)*] and the beginnings of a complex network [*Figure 4.6 (d)*]. Tight spheres of cells were still evident at 7 d [*Figure 4.6 (b; inset)*] with areas of clumped cells prevalent at 14 d, with levels of pyknosis - characterised by high levels of fluorescence indicative of detaching cell membrane - localised to the clumped cells [*Figure 4.6 (e)*]. High levels of particle uptake and accumulation were observed within the individual cells of these gels, with peri-nuclear localisation featuring strongly, both at 24 h and at 14 d [*Figure 4.6 (c & d)*]. A high level of free particles were observed adherent to the collagen substrate [*Figure 4.6 (e)*]

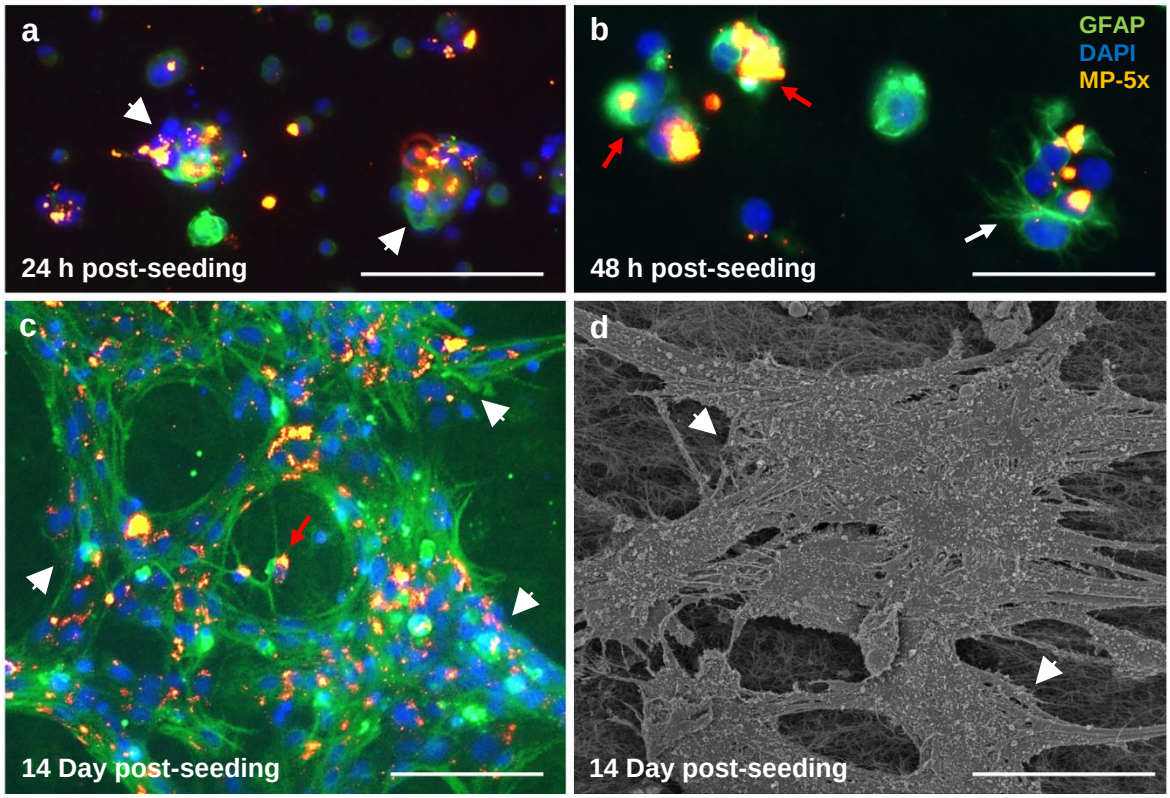

Figure 4.5 Pre- MP-labelled supraconstruct hydrogels over 14 days *Fluorescence images showing pre-labelled supraconstruct gel at (a) 24 h and (b) 48 h post-seeding. Note the inhomogeneous distribution of the astrocyte monolayer (a; arrowhead). Note also the differing morphologies apparent at 48 h whereby the majority of cells have remained rounded (b; red arrow), by contrast, note the ramified nature of a minority of cells at this same time point (b; white arrow). Fluorescence image (c) and FESEM micrograph (d) at 14 d. Note the highly clumped nature of the cell population (c & d; arrowhead). Note the differing morphology displayed by the individual cells not in contact with others (c; arrow) Scale of images (a & c = 100 µm); (b = 50 µm); (d = 300 µm).* **FESEM:** Field Emission Scanning Electron Microscopy; **MP**: Magnetic particle

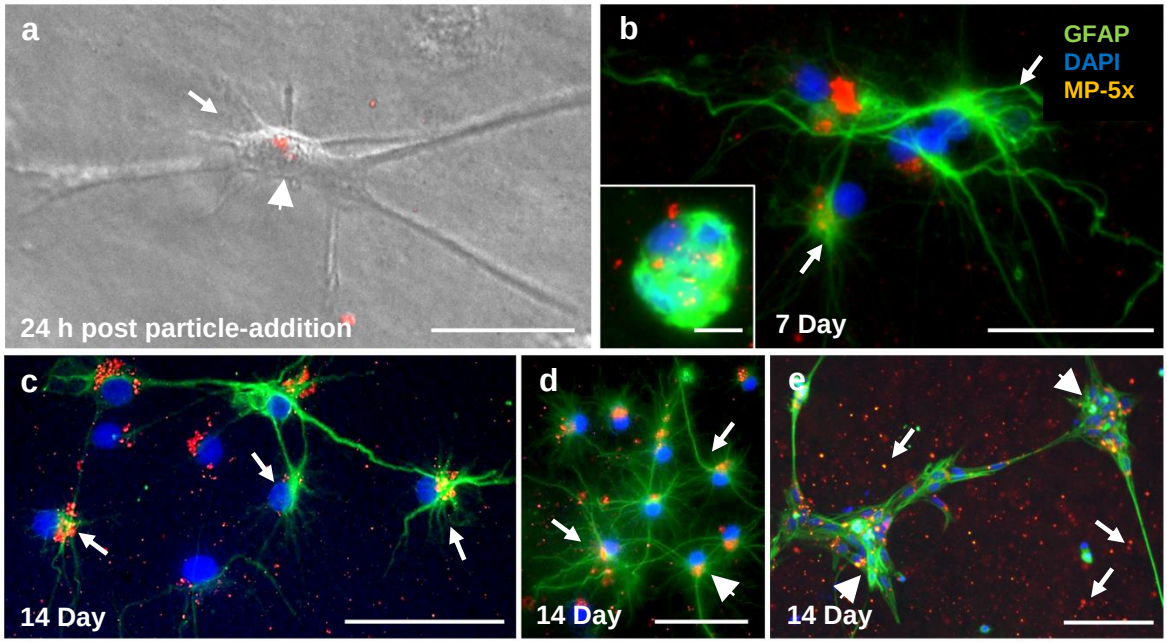

Figure 4.6 In-situ MP-labelled supraconstruct hydrogels over 14 days *Phase image (a) showing in-situ labelled cortical astrocytes at 24 h post-MP-5x particle addition. Fluorescence images showing typical cell morphology at (b) 7 and (c – e) 14 days post-MP-5x-particle addition. At (b) 7 days a large proportion of the culture was made up of individual cells although (b; inset) tight spheres of cells were evident. At 14 days the culture was made up of similar proportions of (c) individual cells, (d) cell networks and (e) areas of cell clumping with localised pyknosis (e; arrowhead). Note the highly ramified nature of the cortical astrocytes (a – d; arrow) and the peri-nuclear localisation of particles at 24 h (a; arrowhead) and at 14 days (d; arrowhead). Note the high level of free particles adherent to the collagen substrate (e; arrow) Scale of images (a – e = 50 µm); (b; inset = 10 µm).* **MP**: Magnetic particle

MP-5x particle uptake and accumulation in pre- MP-labelled versus in-situ MP-labelled supraconstruct hydrogels

Comparative observations of MP-5x particle uptake and cellular accumulation between pre-labelled (*Figure 4.5*) and in-situ labelled (*Figure 4.6*) supraconstruct gels, revealed higher levels of particle uptake and accumulation in the latter condition. The high level of cell clumping observed on the pre-labelled gels though, prevented accurate analysis of particle uptake and accumulation [*Figure 4.5 (c)*]. This overall pattern of cell clumping was observed from 24 h onwards [*Figure 4.5 (a - d*)]. In contrast, a very low level of cell clumping was observed with the in-situ labelled approach [(*i.e. figures 4.5 (c & d) and 4.6 (e)*].

Under the in-situ labelled condition, a high level of 'free' particles were observed adherent to the collagen substrate, a characteristic not observed with pre-labelled gels [*Compare figures 4.5 (c) and 4.6 (e)*]. Notably with the in-situ gels, fewer particles were observed where individual cells or cellular networks were prevalent; this in contrast to areas of highly clumped cells [*Figure 4.6 (c; d; e respectively)*].

Results from supraconstruct gels inform the development of intraconstruct hydrogels

The findings from supraconstruct hydrogels informed the development of intraconstruct hydrogels as a 'protective' environment for a neural cell transplant population. Cell clumping was an issue for both seeding approaches in supraconstruct gels, being more prevalent in the pre- MP-labelling approach. The cells may be responding to the topography and the surface tension of the collagen substrate, in that the MP-labelled cells may have settled within the fibril 'troughs' of the construct. However, this characteristic was less prevalent when cells were labelled in- situ, suggesting that the pre-labelled cells were heavier due to their particle load, and therefore, may have settled deeper into the

construct topography than cells that were seeded particle-free. This possibility is in line with the increased weight of the MP-5x particles. Indeed, in 2D monolayer cultures, rapid cell:particle contact was observed with MP-5x particles (*see Chapter 3*). Cell clumping appears pertinent to supraconstruct gels and therefore, utilising an intraconstruct approach delivers the potential to address this.

A further key consideration noted from the resultant findings of the two MP-labelling approaches was the high level of free particles observed adherent to the collagen substrate with the in-situ MP-labelling approach, a feature not observed with pre- MP-labelling. This high level of particles potentially presents a two-fold disadvantage for tracking purposes. Firstly, free particles themselves would lead to a high frequency of false-positive signal. Secondly, free particles could be taken up by the host cells i.e. macrophages and microglia, resulting in erroneous recordings in tracking of the transplant population. Taken together, it was considered that the formation of intraconstruct hydrogels utilising pre- MP-labelled cortical astrocytes (termed 'exogenous MP-labelled' in regard to intraconstruct gels) would be the more effective approach (*detailed in section 4.4.5*).

4.4.2 Assessment of cellular viability and the safety of the protocols with intraconstruct hydrogels

The average number of cells for both control and MP-labelled gels showed a significant drop in cell numbers at 7 d post-construct, although no difference was noted between the time-points at 14 d [*Figure 4.7 (a)*]. Cell viability remained constant at *ca*. 82% over the 14 d in both control and MP-labelled gels [*Figure 4.7 (b)*]. Comparable proliferation rates were seen at 24 h between cells cultured as monolayers on glass [*Figure 4.7 (c)*] and cells within intraconstruct gels. The proliferative capacity of the cells was significantly reduced at 7 and 14 d post-construct suggesting a more quiescent culture over time [*Figure 4.7 (c - e)*].

Gel thickness was ~ 1000 µm at time of construct. Distribution of cells was observed to be homogenous throughout the gel at 24 h and 14 days post-construct [*Figure 4.8 (a and b); please see Supplementary Video 2 & 3 – disc 1*]. Investigation of homogeneity of cell distribution found no difference in cell counts across the width of the gel [*Figure 4.8 (c)*] and throughout the depth of the gel in both control and MP-labelled gels over the 14 d time frame [*Figure 4.8 (d)*]. No difference was found in cellular viability across the width [*Figure 4.8 (e)*] and throughout the depth [*Figure 4.8 (f)*] of the gel.

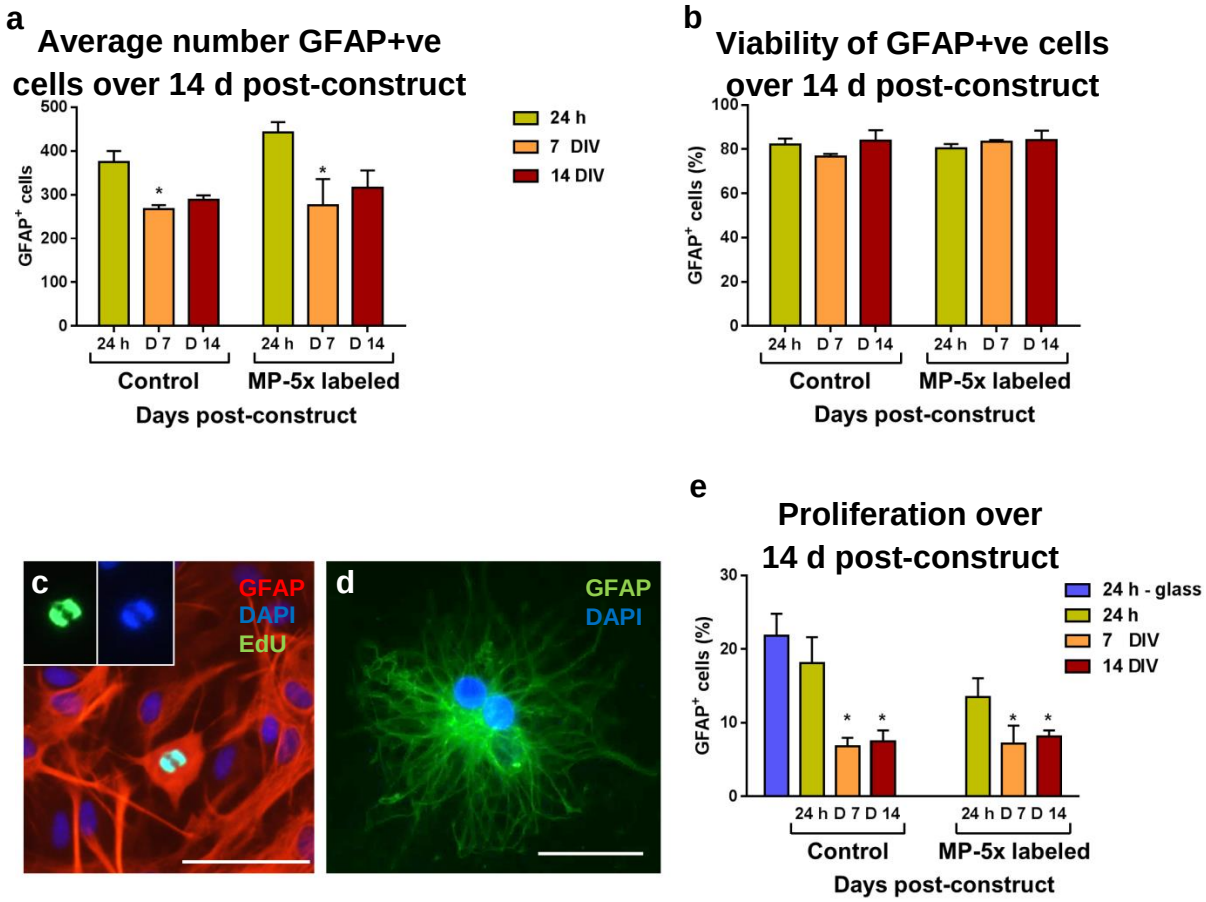

Figure 4.7 Viability assessments show a high level of cellular viability and safety of protocols over time *Bar graph (a) displaying the average number of cells in control and MP-5x labelled gels over 14 d post-construct. A significant difference in cell number was noted between 24 h and 7 d (*p < 0.05) in both control and MP-labelled gels. Bar graph (b) shows cellular viability to be ca. 82% over 14 d. Representative fluorescence micrographs of (c) a pair of EdU-identified dividing astrocytes at 24 h, cultured on glass (c; inset shows un-merged images), and (d) a pair of dividing astrocytes within an intraconstruct gel at 14 d. Bar graph (e) showing EdU-identified proliferative capacity of the cells over 14 d. At 24 h no difference in proliferative capacity was reported between cells in the two different environments. Proliferation was significantly higher at 24 h post – construct versus 7 d and 14 d in both control and MP-labelled gels (*p < 0.05). Scale of image = 50 µm (n = 3) Results expressed as mean ± s.e.m.* **MP**: Magnetic particle

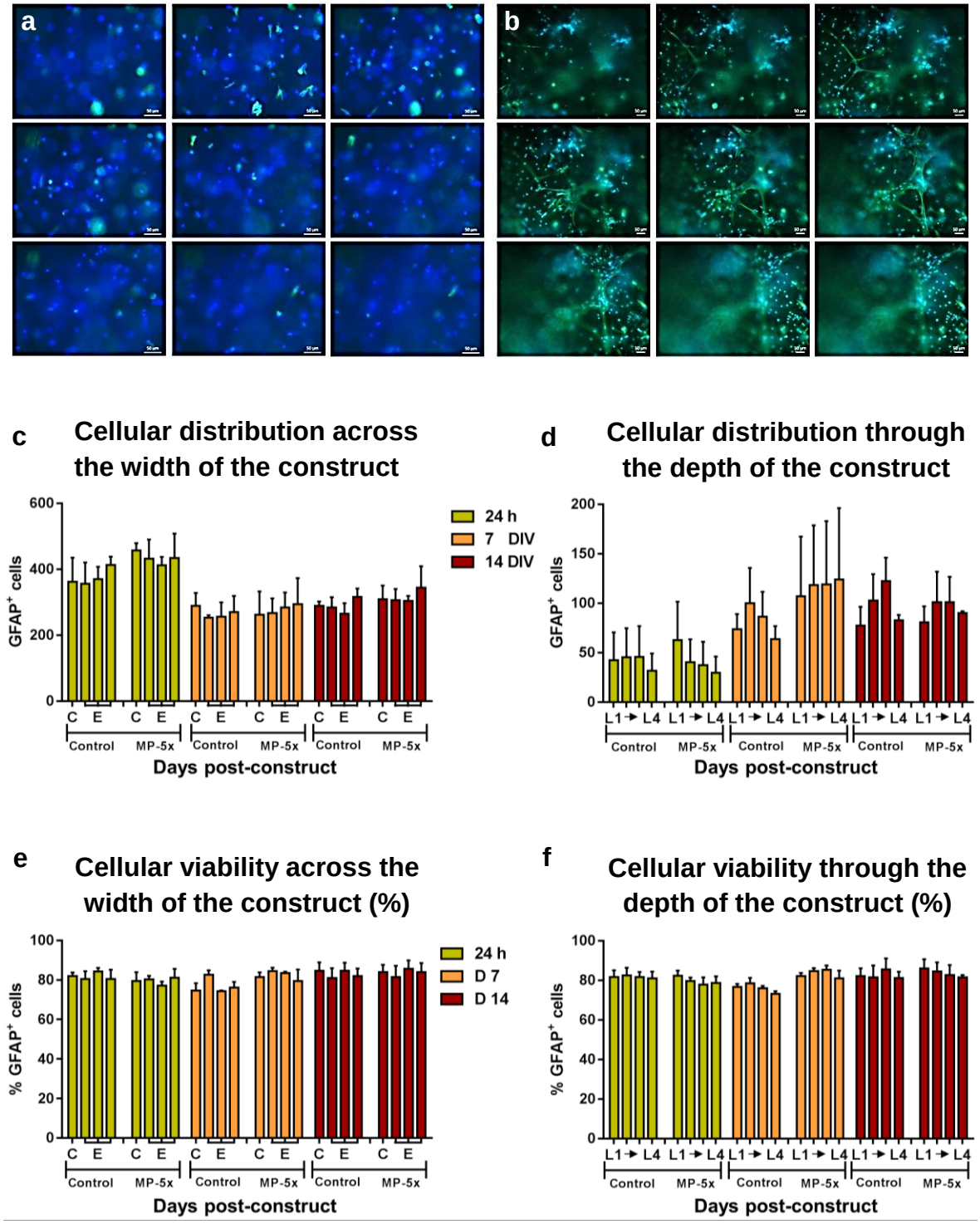

Figure 4.8 Safety assays show homogenous nature of cellular distribution in gels over time *Illustrative fluorescence images showing the homogenous cell distribution throughout the hydrogels at 24 h (a) and 14 days (b) post-construct (Supplementary Videos 2 & 3 – disc 1). Bar graphs show homogeneity in cellular distribution across (c) the width of the*

gel, and (d) throughout the depth of the gel in both control and MP-labelled gels. Bar graphs show homogeneity in cellular viability across (e) the width and (f) throughout the depth of the gel over 14 d. (n = 3) **C=centre; E=edge; L1 – L4=the layers through the depth of the gel where L1 = the base and L4 = the top of the gel.** *Results expressed as mean ± s.e.m.* **MP**: Magnetic particle

The collagen intraconstruct hydrogels showed significant contraction over time compared with their initial size at the time of construct (16 mm). A significant difference was seen in gel diameter within 3 h post-construct, reducing to *ca*. 9 mm at 14 d. Although the level of gel contraction appeared greatest within the first 24 h, the gel continued to show significant contraction over the 14 d. No difference in gel contraction was observed between control gels (cells, no particles) and MP-labelled gels (*Figure 4.9*).

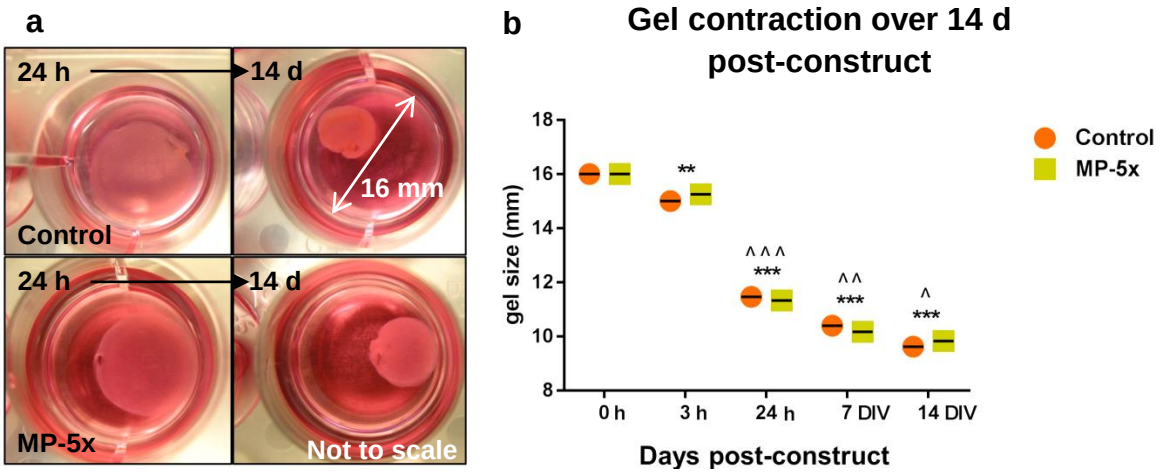

Figure 4.9 Gels show contraction of size over time *Representative photographs (a) of gels at 24 h and 14 d. The initial gel diameter was 16 mm (gel thickness ~ 1000 µm), gels having been cast within the well (a; white arrow). Note the difference in gel diameter between these two time frames. Graph (b) showing the significant reduction in gel diameter over the 14 d time frame compared with the initial gel diameter at the time of construct (***p < 0.001; **p < 0.01). Gels showed a significant level of contraction between each time point - 3 h vs. 24 h; 24 h vs. 7 d; 7 d vs. 14 d (^^^p < 0.001; ^^p < 0.01; ^ < 0.05). Images not to scale (n = 3). Results expressed as mean ± s.e.m.* **MP**: Magnetic particle

4.4.3 Characterisation of cellular and endocytotic features of cortical astrocytes within an intraconstruct hydrogel: comparison to astrocyte monolayers

A highly connective, complex cellular network was evident throughout the intraconstruct gels at 14 d post-construct, with similar levels of complexity observed in control gels and MP-5x labelled gels [*Figure 4.10 (a & b)*]. Networks of aligned astrocytic processes were evident throughout the gel [*Figure 4.10 (a)*]. Cell clumping was negligible (*ca.* < 1%). A high level of intracellular particle retention was observed in the MP-labelled cells [*Figure 4.10 (b & c)*] with peri-nuclear localisation of the particles still evident at this time-point [*Figure 4.10 (c)*].

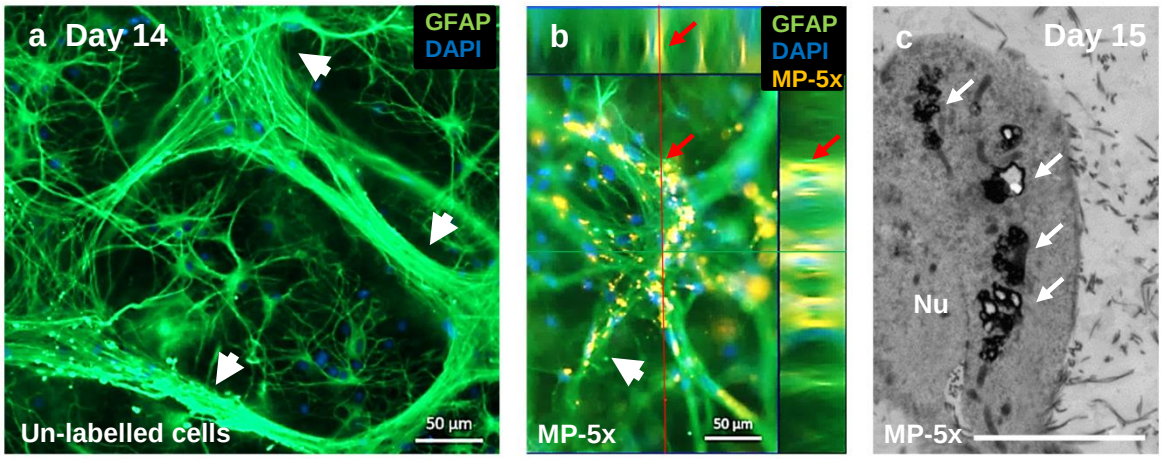

Figure 4.10 Intraconstruct hydrogels at 14 d post-construct *Fluorescence micrographs of (a) an intraconstruct hydrogel containing un- labelled cells (no MP-5x particles) and (b) MP-5x labelled cells. Note the complex cellular network, with dense "bundles" of aligned astrocytic processes evident throughout the gel (a & b; arrowhead). A high level of intracellular particle retention was evident (b; arrow). TEM micrograph of (c) an exogenous MP-labelled intraconstruct gel, at day 15. Note the high particle accumulation within the cell at this time point (arrow). Scale of images (a & b = 50 µm); (c = 5 µm) [Fig. 4.10 (a) replicate of Fig. 4.4 (a)]* **Nu:** Nucleus. **MP**: Magnetic particle

Cortical astrocytes grown within the 3-dimensional environment of intraconstruct hydrogels displayed a set of characteristics distinctly different to that of cortical astrocytes cultured as 2-dimensional monolayers on glass coverslips. The former are of a highly ramified nature, having a small soma and nucleus in comparison to the highly membranous, flattened morphology typical of astrocyte monolayers. They possess a high number of long, threadlike filopodia compared with the short, truncated processes of astrocytes cultured on glass [*Compare figure 4.11 (a and b)*].

A measure [*Figure 4.11 (c)*] to compare the cell shape (round *vs.* ramified) of cells grown in the 2- or 3-dimensional environment found no difference between the cells in either environment at 24 h, indicating the rounded nature of the cells in the 3-dimensional gels at this time point. At 14 d, the cells within the hydrogel showed a significant difference in cell shape - being more highly branched at this time point –in comparison to their morphology at 24 h and to the morphology of cells cultured as monolayers [*Figure 4.11 (d)*].

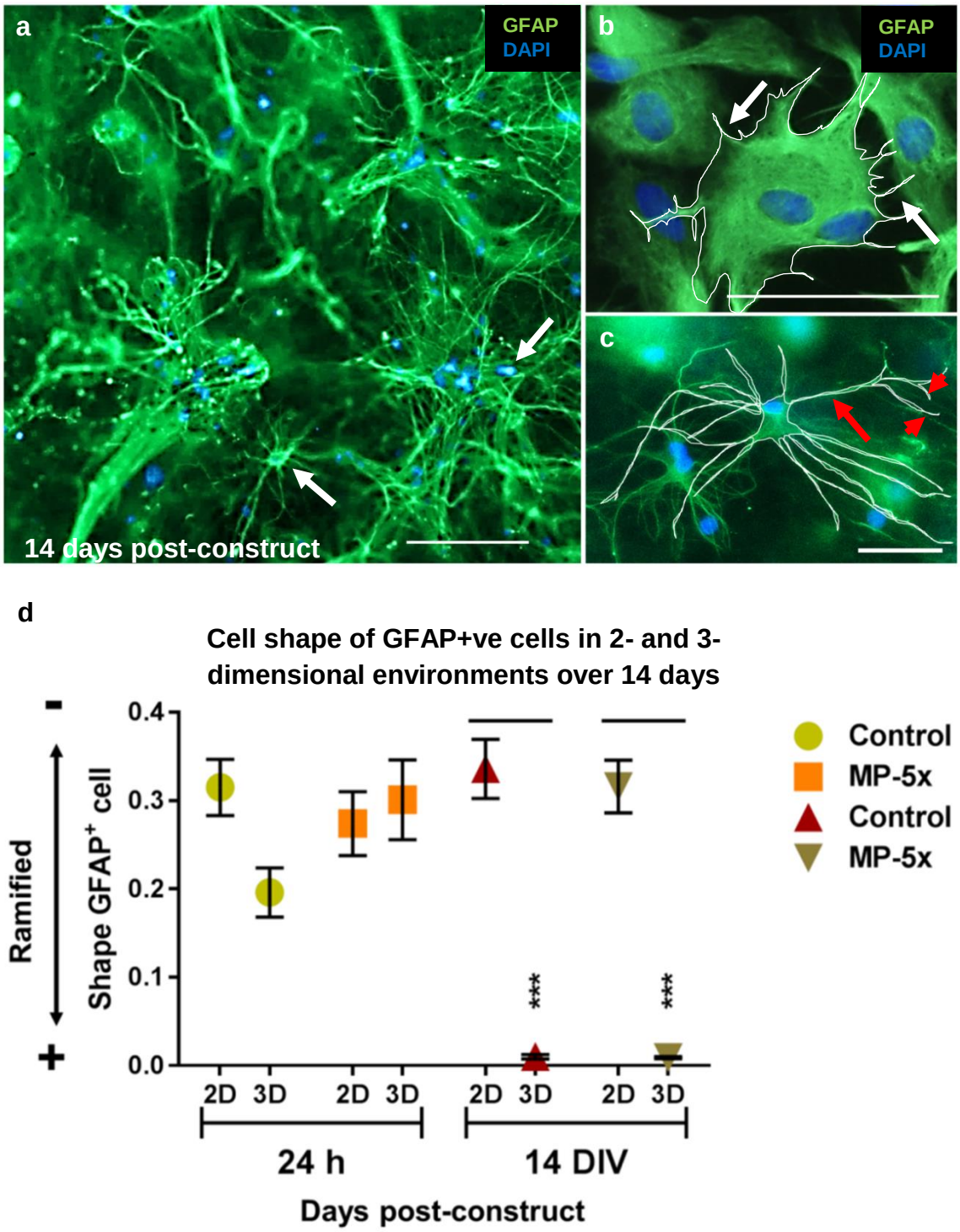

Figure 4.11 Cortical astrocytes grown within a 3-dimensional hydrogel show morphological characteristics different to that of astrocyte monolayers cultured on glass *Fluorescence micrographs at 14 d depict (a) the highly ramified morphology of cortical astrocytes grown within an intraconstruct hydrogel. Note the size of the cell soma and nucleus (a; arrows). Note the length and the overall complexity of the fine meshwork*

*of processes on these cells Compare this with (b) cortical astrocytes cultured as monolayers on glass. Note the larger size of the cell soma and nucleus and the highly membranous, flattened morphology of these cells. Note also the shorter, truncated filopodia extending from the astrocytes (b; arrows). By comparison (c) note the length of the primary processes of cells within intraconstruct gels (c; arrow) and their branched morphology (c; arrowhead). Representative fluorescence micrographs (b & c), illustrate how cells were measured to determine their shape (rounded or ramified). Graph (d) shows the rounded/ramified nature of cells grown within hydrogels or as monolayers on glass. (***p < 0.001). Scale of images (a; b & c = 50 µm) (n = 3) Results expressed as mean ± s.e.m.* **MP**: Magnetic particle

Comparative measures of cell morphology showed cells grown in intraconstruct hydrogels had a significantly smaller cell surface area at 24 h and at 14 d post-construct. It was notable that at 14 d, the reported difference in cell surface area between cells from the two environments, although significant for MP-labelled cells, was less than at 24 h. This is possibly indicative of the similarity in overall surface area at 14 d, taking into account the highly ramified nature, at this time point, of cells grown in hydrogels [*Figure 4.12 (a)*].

The average nuclear size of cells grown in gel constructs was significantly smaller at 14 d in comparison to cells cultured as monolayers. At 24 h, possibly due to the early time point, the reported difference was less with a significant difference reported between control cells [*Figure 4.12 (b)*].

The average number of primary processes was the same at 24 h, a finding supported by data showing similar measures of roundedness in cell shape at this time point. Cells in intraconstruct hydrogels showed a significantly higher number of processes at 14 d compared with cells grown as monolayers [*Figure 4.12 (c)*], indicating the level of complexity observed in these cells. Compared with cells cultured as monolayers, the average length ratio of primary processes was significantly higher in cells grown within hydrogels, indicating a significantly longer process length in relation to the size of the cell soma, and also being a further indicator of the smaller size cell soma of these cells [*Figure 4.12 (d)*].

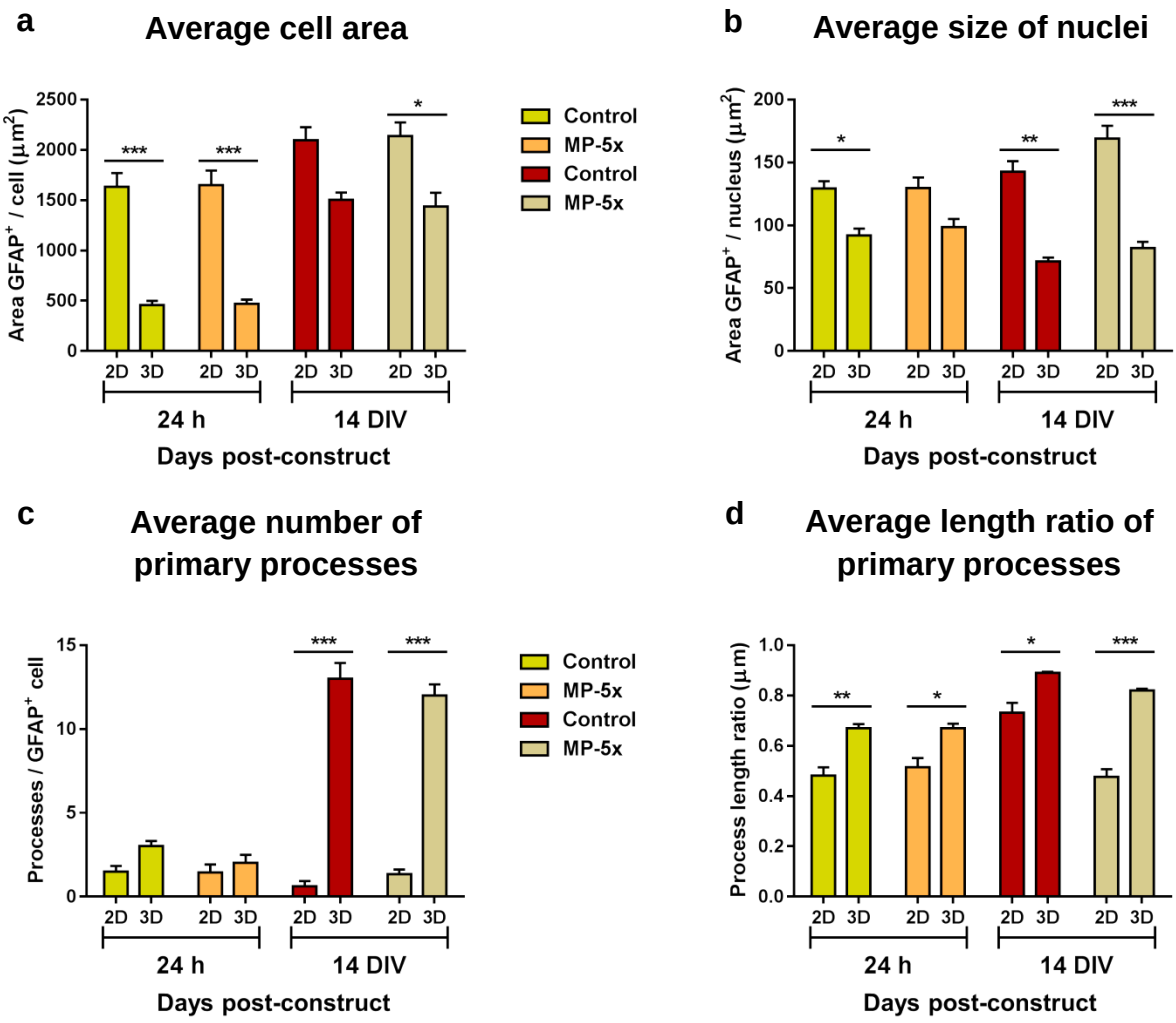

Figure 4.12 Comparative measures of cells grown in either a 2- or 3-dimensional environment show significant differences in morphology *Bar graphs showing the significant difference in (a) average cell area (µm^2) and (b) nucleus size (µm^2) between cells grown within a hydrogel vs. cells grown on glass. Bar graph (c) showing the average number of primary processes is significantly higher at 14 d for cells grown within a hydrogel. Bar graph (d) showing the average length ratio of primary processes is higher in cells grown within a gel compared with cells cultured on glass [process length was calculated as a length ratio of the cell size i.e. L/D where L=process length (µm) and D=distance from nucleus to process tip] (***p <0.001; **p <0.01; *p <0.05) (n = 3). Results expressed as mean ± s.e.m.* **MP**: Magnetic particle

4.4.4 Endocytotic features associated with particle uptake in an intraconstruct hydrogel

Ultrastructural membrane features visualised under FESEM

Cortical astrocytes are regarded as a highly endocytotic neural cell and are known to show avid particle uptake. In this regard, use of FESEM enabled visualisation of a number of ultrastructural membrane features associated with cellular endocytotic activity. Cell morphologies showed high levels of filopodia, membrane ruffling and pits; characteristics indicative of a highly endocytotic cell (*Figure 4.13*).

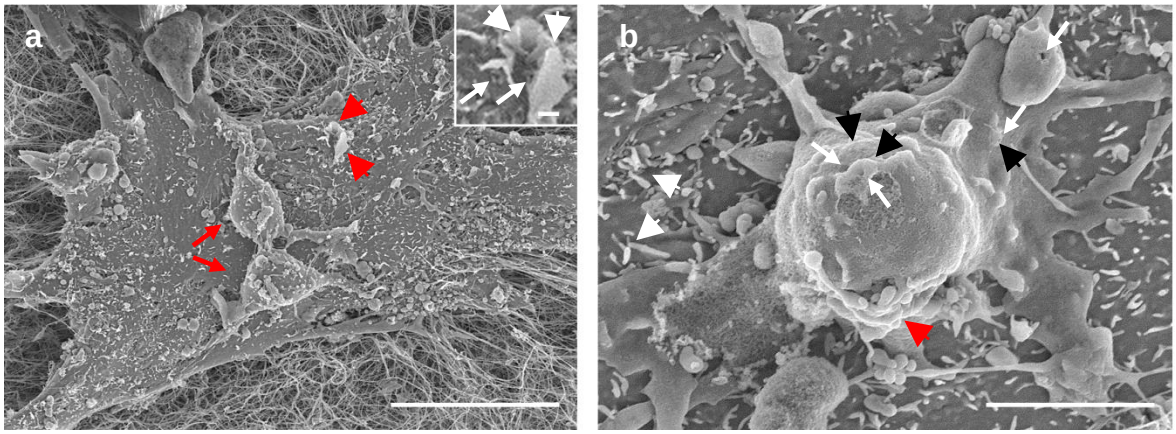

Figure 4.13 Ultrastructural membrane features of cortical astrocytes *FESEM micrographs displaying ultrastructural features associated with endocytotic activity. Supraconstruct gels showed differing morphologies between (a) areas of clumped cells and (b) individual cells. Cells were observed (b) on top of areas of highly connected astrocytes [also (a; red arrow)]. Cells displayed extensive levels of filopodia (b; white arrowhead) with membrane ruffling observable (a & b; red arrowhead). Pits were visible [(a; inset) and (b); white arrow). Note the membrane ruffling (a; inset; white arrowhead) and circular membrane nodule (b; black arrowhead) associated with the pits. Scale of images (a = 30 µm; inset = 3 µm); (b = 7.5 µm)* **FESEM**: Field Emission Scanning Electron Microscopy

Ultrastructural membrane and subcellular features visualised under TEM

Ultrastructural and subcellular observations of cortical astrocytes within intraconstruct hydrogels were facilitated by TEM microscopy. The cells were seen to be actively engaging with the collagen substrate, indicative of the remodelling of their environment. Together with a high level of membrane activity associated with the surrounding collagen fibrils [*Figure 4.14 (a & b)*], astrocytes displayed a number of typical endocytotic features pertinent to particle uptake and trafficking.

Invaginations and coated 'pits' were prominent features of the cell membrane. Both coated and non-coated invaginations were observed localised to areas of high membrane activity and may be membrane folding or ruffling associated with macropinocytosis [*Figure 4.14 (a and inset)*]. The coating observed on the invaginations/pits suggests a receptor-mediated endocytotic pathway which may be clathrin, although this was not verified [*Figure 4.14 (b & c)*].

High levels of MP-5x particle accumulation were observed within the cells at this time point, with the majority showing peri-nuclear localisation [*Figure 4.14 (a; b & inset)*]. Endosomal uptake of particles was also evident [*Figure 4.14 (d)*]. The high magnetite concentration particles were visualised as dark 'spheres' under TEM, with many displaying a small hollowed out core surrounded by a dense 'ring'; features that are consistent with the magnetite matrix composition of these particles [*Figure 4.14 (a – b & inset; d*).

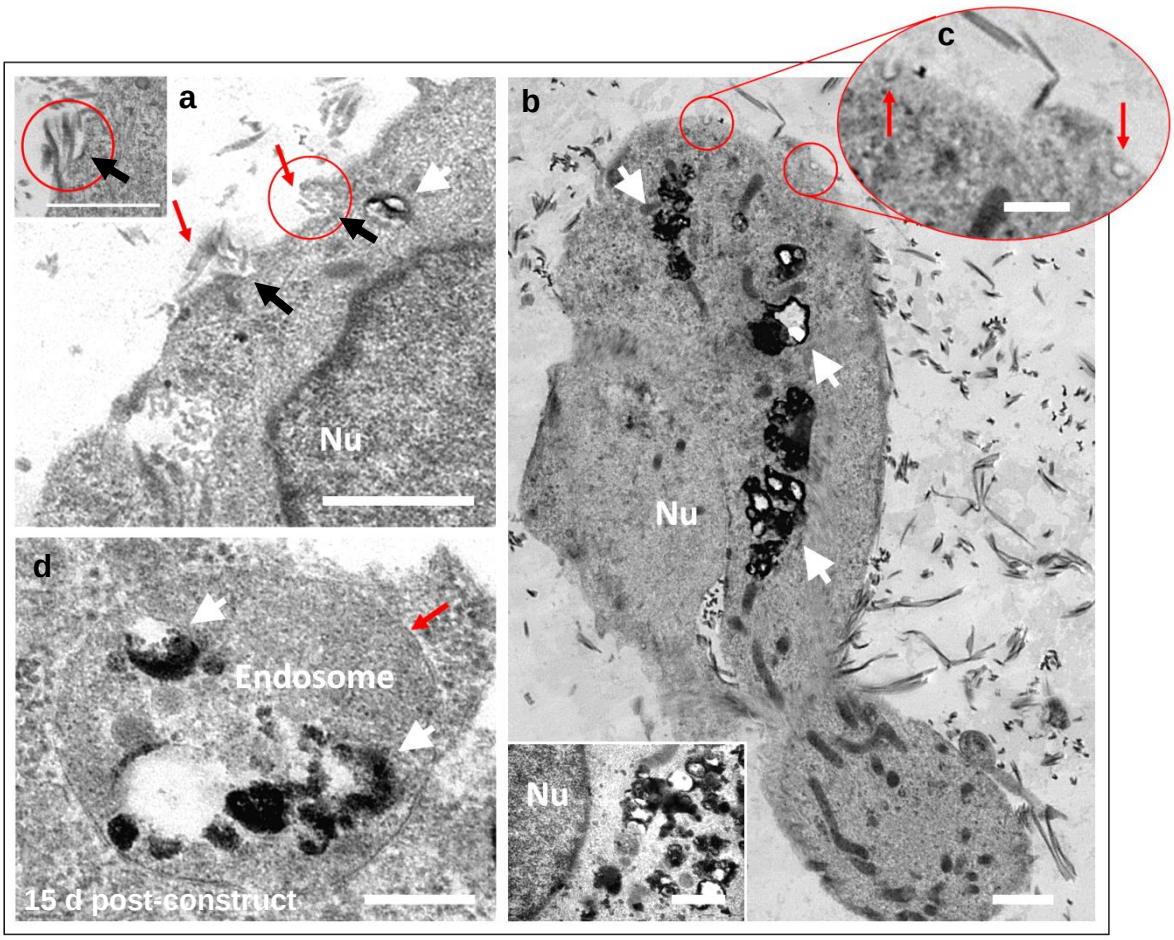

Figure 4.14 A number of endocytotic features were observed, associated with particle uptake and trafficking *TEM micrographs (a, b & c) at 15 d post-construct showing the highly active membrane of cortical astrocytes within a collagen construct. A high level of active engagement with collagen fibres was observed (a; red arrow and delineated in red) with the notable association of coated (a; inset – black arrow) and non-coated (a; black arrow) invaginations and membrane ruffling localised to this active area. A high number of coated pits were also evident (b & c; red arrow). Representative TEM micrograph (b) showing a high accumulation of MP-5x particles (a & b; white arrow) with the majority showing peri-nuclear localisation (b; inset). TEM micrograph (d) shows endosomal uptake (d; red arrow) of particles (d; white arrow). Note the appearance of the magnetite particle under TEM– a dark 'sphere' with a small hollowed out core surrounded by a dense 'ring',*

consistent with the high magnetite matrix composition of these particles (a – b, d; white arrow). Scale of images (a; a-inset & b = 1 µm); (b; inset = 0.25 µm); (c = 0.5 µm); (d = 0.25 µm) [Fig.4.14 (b) replicate of Fig. 4.10 (c)] **MP**: Magnetic particle; **Nu**: Nucleus; **TEM**: Transmission Electron Microscopy

4.4.5 Development of exogenous MP-labelled cellular intraconstruct hydrogel with the utility for non-invasive tracking of the neural cell population using MRI

At 24 h post-construct a high level of particle accumulation and co-localisation of particles with cells was noted, as was the homogenous distribution of the cells throughout the intraconstruct gel. A low level of free particles was observed at this time point suggesting loss of particles from cells during gel construct. Clumping of cells was not evident in these gels at this time [*Figure 4.15 (a)*].

MR imaging of these gels at 24 h showed a strong loss of signal (*hypointense*) from the MP-5x-labelled astrocytes within the gel [*Figure 4.15 (b)*]; loss of signal indicative of the presence of an effective contrast agent (i.e. MP-5x particles). By contrast, note the high level of MR signal (*hyperintense*) from the control gel (cells; no particles) [*Figure 4.15(c)*].

At 14 d there was a notable absence of particles from the extracellular space suggesting continued particle uptake by the cells within the gel construct [*Figure 4.15 (d)*]. MR imaging of these gels at 14 d recorded a hypointense signal from MP-5x labelled cells, with, by contrast, a hyperintense signal recorded from the control gel [*Figure 4.15 (e & f)*]. Networks of dense "bundles" of aligned astrocytic processes were evident within the cellular network at this time point. Cell clumping was negligible (*ca.* <1%).

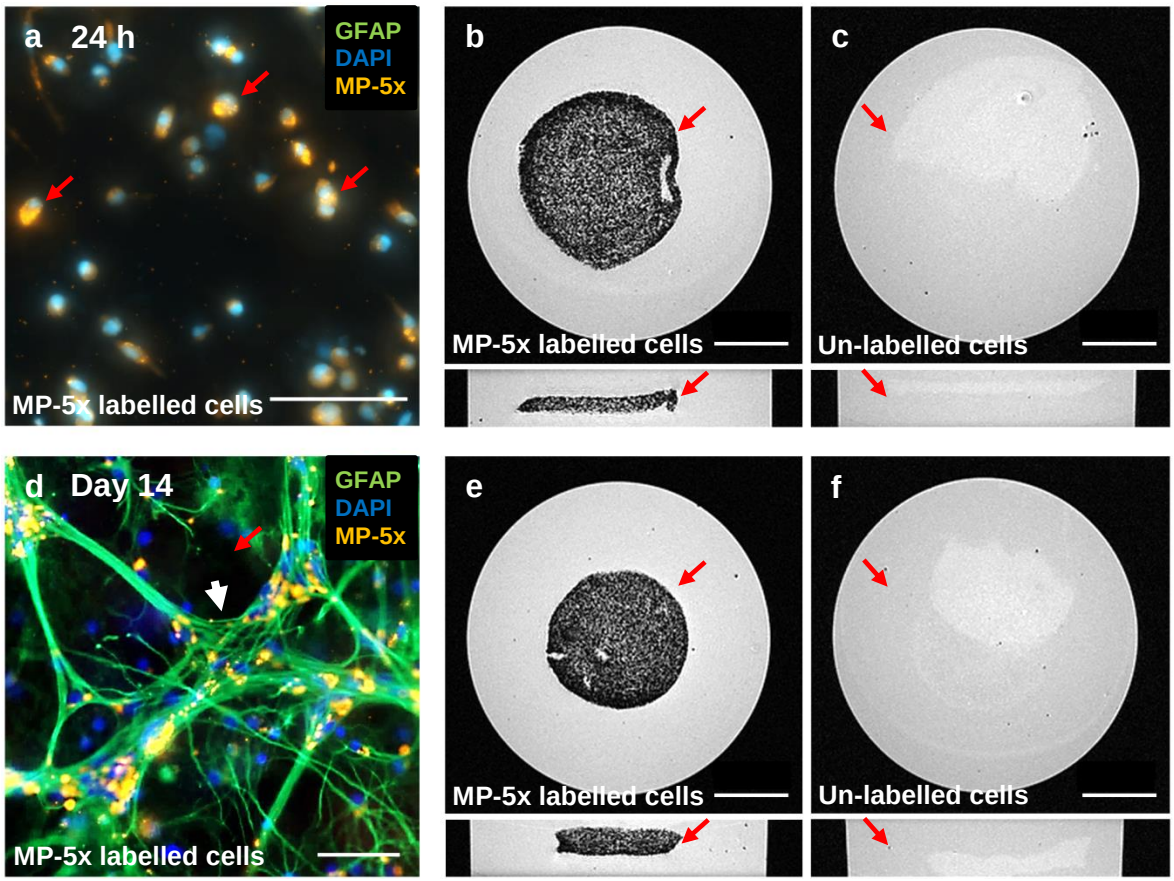

Figure 4.15 MP-5x labelled astrocytes within intraconstruct hydrogels provide a hypointense signal under MRI *Fluorescence micrograph of (a) an exogenous MP-5x labelled intraconstruct hydrogel at 24 h post-construct. Note the high level of particle accumulation (a; arrow). Comparable MR images showing (b) MP-5x labelled and (c) control (cells; no particles) intraconstruct gels at the same time-point (b & c; arrows – hydrogels indicated in orthogonal view). Fluorescence micrograph of (d) an exogenous MP-labelled intraconstruct gel at 14 d post-construct. Note the absence of particles in the extracellular space at this time-point (arrow). Networks of aligned astrocytic processes were evident throughout the cellular network (d; arrowhead). Comparable T^2-weighted MRI scans of (e) MP-5x labelled and (f) control gels at 14 d post-construct (arrow; hydrogel indicated in orthogonal view). Note the hypointense signal recorded from the MP-5x labelled cells within the gels (b & e) at both time-points with by contrast, the hyperintense signal recorded from the cells in the control gels (c & f). Scale of images (a*

= 100 µm); (b & c, e & f = 5 mm); (d = 50 µm) **MP**: Magnetic particle; **MR**: Magnetic resonance; **MRI**: Magnetic resonance imaging

Particle inheritance in daughter cells of dividing astrocytes

With use of dynamic time lapse imaging, cells were visualised to be dividing in real time [*Figure 4.16 (a – f)*]. The particles were inherited by the daughter cells [*Figure 4.16 (f)*], thereby retaining tracking capacity.

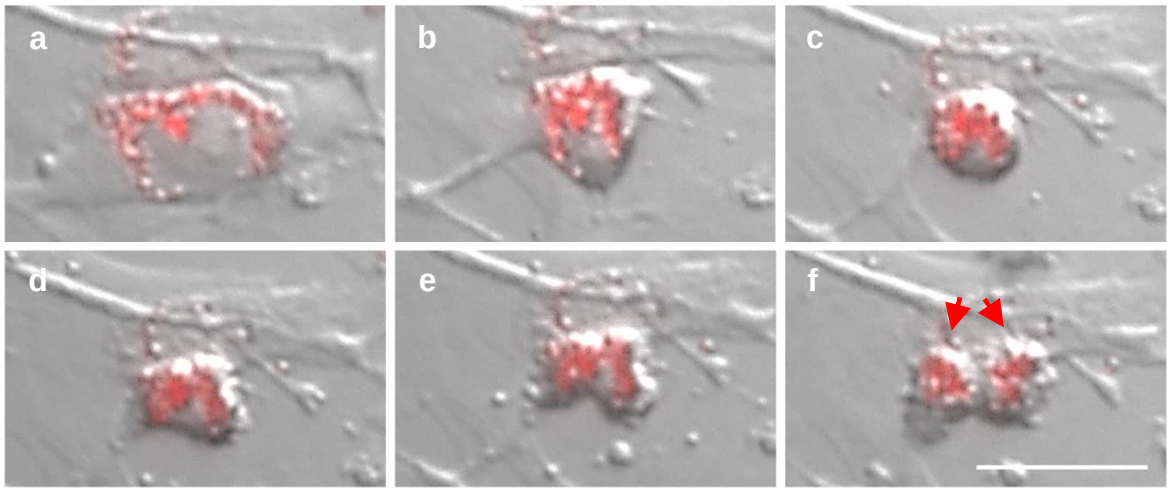

Figure 4.16 Particle inheritance between daughter cells of dividing astrocytes *Dynamic time-lapse still images showing (a – f) an MP-5x labelled cortical astrocyte undergoing division at 7 d post-construct (Please see Supplementary Video 4 – disc 1). The particles are inherited by the daughter cells (f; arrow head), thereby retaining their utility as a trackable cell population. Scale = 50 µm* **MP**: Magnetic particle

MP-labelled intraconstruct gel at 37 d post-construct

Intracellular particle retention was still visible in intraconstruct gels at 37 d post-construct. MR imaging of these gels showed a hypointense signal from the MP-labelled gel. The signal from these gels was observed as higher than that observed at 24 h and at day 14 indicating a lower level of particle accumulation within the cells at this time point. Hypointense localised signal was recorded from this gel. By contrast, a hyperintense signal was recorded from the comparable control gel (*Figure 4.17*).

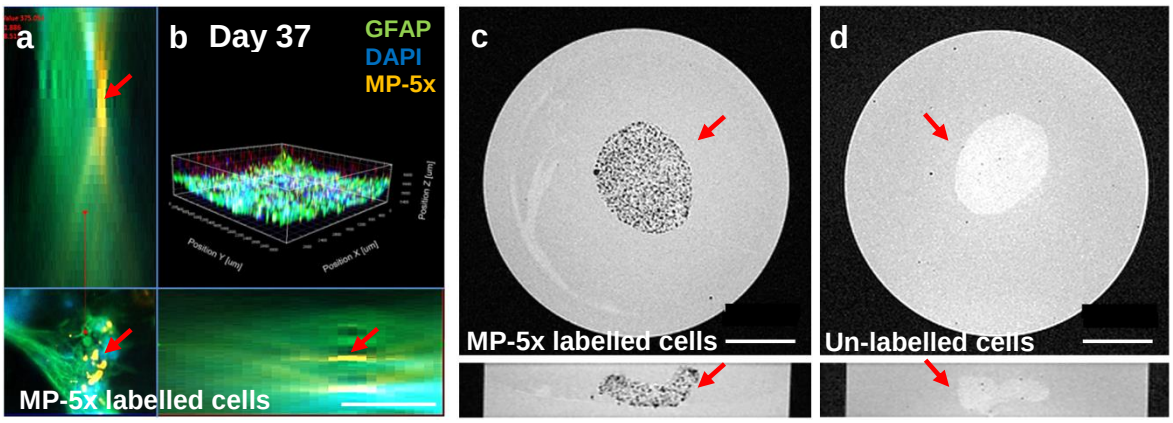

Figure 4.17 Hypointense signal recorded from MP-5x labelled cells within intraconstruct hydrogels at 37 d post-construct *Confocal fluorescence micrograph of (a & b) an MP-labelled intraconstruct hydrogel at 37 d post-construct (Please see Supplementary Video 5 – disc 1). Note the intracellular localisation of particles at this extended time-point (a; arrow). Comparable T^2-weighted MRI scans show (c) a hypointense signal from the MP-labelled cells within the gel (arrow – hydrogel indicated in orthogonal view) and (d) a hyperintense signal from the un-labelled cells within the control gel (arrow – hydrogel indicated in orthogonal view). Scale of images (a = 100 µm); (c & d = 5 mm)* **MP**: Magnetic particle; **MRI**: Magnetic resonance imaging

4.5 Discussion

Protective neural cell delivery systems offer a viable solution to the technical issues faced in cell transplant for spinal cord regenerative therapy. In order to develop such a system, there were a number of technical considerations in facilitating the development of a viable 3-dimensional neural cell construct with imaging potential for regenerative applications. Here the major challenges inherent to the development of such a construct have been addressed.

Exogenous MP-labelled intraconstruct hydrogels offered the most promising approach as a 3-dimensional construct, with collagen providing the ideal substrate (*as discussed previously; see section 1.5.2*). Its macroporous nature allowed the cells the opportunity to orient and remodel the fibres to support their growth; possessing the potential to mimic endogenous tissue (*Trappman & Chen, 2013; Wakatsuki & Elson, 2003*) and facilitating a highly viable complex cellular network throughout the gel. At 14 d post-construct, large networks of aligned "bundles" of astrocytic processes were evident throughout the cellular network. This suggests promise for the construct's utility as an implant, as cellular alignment offers a greater potential for guidance of ingrowing neuronal axons into the construct *in vivo* (*Winter et al., 2016*). In this regard, free-floating of the gel played a key role in promoting a homogenously distributed cell population, and one which possessed morphological characteristics closer to their *in vivo* counterparts – small cell soma, stellate morphology with a diffuse network of fine extensive processes (*Balasubramanian et al., 2016*). This in comparison to cortical astrocytes cultured as monolayers on glass (*Moshayedi et al., 2010*), or indeed cortical astrocytes grown within anchored gels, which are predominantly bipolar in shape and aligned to the tension exerted upon the gel (*East et al., 2010; Grinnel, 2000*).

The major challenge in clinic is lowered cellular viability, the cause *and* the effect of inhomogeneity of the transplanted cells (*Guest et al., 2011; Pearse et al., 2007*), and a major obstacle also realised within 3-dimensional constructs (*Unsworth et al., 2003*). Within the intraconstruct gels developed here, cellular distribution was homogenous throughout the breadth and depth of the constructs with cellular viability remaining consistently high across the time course.

In this respect, safety of the protocols was of paramount concern. The consistent cellular viability and the homogenous nature of cellular distribution and proliferation within the constructs suggested effective availability of oxygen and nutrients (*Malda et al., 2004*) and efficient removal of metabolic waste products from the hydrogel (*Mertens et al., 2014*). In each of these parameters, no significant difference was reported between MP-labelled and control hydrogels (cells, no particles) with similar levels of cellular viability and homogeneity of distribution and proliferation reported in both constructs over time. A drop in average cell numbers following 24 h post-construct was noticed within the gels, although cellular viability remained consistent at approximately 82% across the time period. A significant decrease in proliferative capacity was also recorded following 24 h and this, combined with the low level of cell death occurring over the time-span may account for this initial drop in cell number.

In respect of cellular proliferation, of critical importance to their utility within an implant is the growth curve of the cell transplant population (*as previously discussed within the main introduction*). Within intraconstruct hydrogels, following the significant reduction after the initial 24 h, proliferation remained consistently low across the time period studied, indicating a relatively quiescent population. In this respect, there is a wide body of evidence that reports the ECM proteins within collagen I regulate the proliferative capacity of cells (*Trappman & Chen, 2013*). This inhibition is mediated further following gel

contraction, whereby down regulation of extracellular signal regulated kinase (ERK) arrests cells in G_0 phase of the cell cycle (*Grinnel. 2000*). This interruption to the cell cycle may have further relevance to the level of relative quiescence observed within these gels in this particular neural cell, with studies reporting that of cell-cycle-arrested astrocytes, only 35% subsequently return to the cell cycle, either at any one time or if at all (*Murphy, 1990*).

As discussed previously cells, in establishing a connective, complex network, remodel the collagen fibrillar matrix and in so doing, contract and compress the gel. As reported extensively in other studies, gel contraction of free-floating gels is in direct relationship to the density of both the cell population and the collagen construct. Rapid contraction occurs within the first 12 h, the rate of which significantly decreases thereafter (*Brown, 2013*). The hydrogels in this study showed a similar rate of contraction, with no difference noted between MP-labelled and control gels. Safety assessments conducted over the time course showed gel contraction had no adverse effects on the viability of the intraconstruct hydrogels. The safety of the findings reported here were in line with many other cell:construct systems, whereby matrix-beneficial constructs have shown no significant adverse effects on cell viability (*Frampton et al., 2011*).

MP-5x particles were utilised in these gels due to the high level of uptake, accumulation and long-term retention previously observed with these particles in cortical astrocyte monolayers cultured on glass (*Tickle et al., 2016*). In respect of their utility as a contrast agent under MRI within the intraconstruct gel, the level of particle accumulation in these cells proved highly efficient in providing a hypointense signal at 24 h through 14 d to 37 d post-construct. The level of particle accumulation observed in the cells within the intraconstruct gel was lower than that typically observed in astrocyte monolayers; an interesting observation considering the cells were pre-labelled as a monolayer culture prior

to association with the hydrogel. Some particle loss was observed at 24 h post-construct. Although, the level of free particles noticeably decreased from approximately 48 h onwards, suggesting continued cellular uptake of the particles from within the gel. A probable explanation for lower intracellular particle accumulation may be due to their significantly smaller cell soma. The extent of particle loading within a cell is typically considered as being relational to their surface area and endocytotic activity i.e. comparison between astrocytes and NSCs *(Tickle et al., 2016*). However, it could be postulated that particle loading may also be directly associated with the size of the cell soma. This presents itself as a key factor in consideration of the optimal cell:label combination for transplant. Be that as it may, in respect of the particle load in cortical astrocytes within the construct developed here, a hypointense signal was observed in these cells over an extended time period.

In respect to its application to regenerative therapies, a concern with MRI was the potential for false-positive signal over an extended time frame. Despite no observation of free particles at 14 d, they were observable within the ECM of the gel at day 37. There are opposing views on the role exocytosis plays in particle release, with either vesicle or lysosome secretion factoring in particle trafficking from the cell (*Oh & Park, 2014*). It is also argued that exocytosis does *not* play a role in particle release, but that particle dilution in cells is a result of cell division and the subsequent inheritance of the particles by the daughter cells (*Harrison et al., 2016; Kim et al., 2012*). With regards to these constructs, the mechanism remains unclear. Particle loss may occur during cell division, although this was not observed in this study, with particles remaining cell-bound throughout. In this context, proliferative capacity was significantly reduced from day 7 onwards, suggesting a higher level of particle retention over time. A reasonable proposition, therefore, for the extracellular particles observed at this time point may be the release of particles from

apoptotic cells – a feature observed with collagen encapsulated cells (*Wakatsuki & Elson, 2003*).

What does remain unclear was why a less hypointense signal was recorded from the intraconstruct gel at day 37 versus the earlier time points. This would suggest removal of the free particles from the gel into the media, which, given the macroporous nature of the collagen may be a possibility. This would not though, explain the high observance of free particles *within* the gel. Even so, while lower hypointensity overall was recorded at this extended time point, hypointense 'spots' were observed throughout the gel, suggesting localised particle retention in cells. This possibility was corroborated by fluorescence microscopy, thus verifying the construct's continued utility over an extended time frame.

In regards to the potential use of this construct as a protective delivery system, is the effect of construct contraction following implant into a spinal cord lesion. Within the limitations of this study, the possible outcomes remain unclear. Nevertheless, collagen constructs as an implant have reported sufficient axonal infiltration into the construct within three weeks post-implant, coincident with almost complete degradation of the collagen construct at this time point. Moreover, subsequent neuronal regeneration and restoration of locomotor function was reported (*Kaneko et al., 2015*). Thus, while the findings cannot be considered analogous to the constructs engineered within the present study, they offer promise.

In respect of characterisation of cortical astrocytes, much has already been discussed regarding the morphological differences observed in these cells dependent on their environment. The similarity in endocytotic function with regards to particle uptake was evident, with uptake, accumulation and long-term retention a prominent feature in these cells, irrespective of their environment. The physico-chemical properties of MPs in relation to uptake, have previously been elucidated (*please refer to Chapter 3; Tickle et al., 2016*)

so will not be addressed further here. However, the use of FESEM and TEM in this study offered some insight into the potential endocytotic mechanisms utilised by these cells.

The technical development of embedding the hydrogels within a resin carrier allowed effective use of TEM to study the morphologies, membrane features and intracellular particle localisation in soft matrices. This is a novel development of key importance to the understanding of cell characteristics within a 3-dimensional soft matrix environment. Within these intraconstruct gels, the high level of membrane interaction with the collagen matrix was a key feature. From this, it could be speculated that this mechanism is related to the cells' remodelling and (re)adapting of their environment.

A number of endocytotic features such as membrane ruffling, filopodia and pits were evident. Speculative association of these features with endocytotic mechanisms such as macropinocytosis and clathrin-mediated endocytosis corroborated previous findings (*Pickard et al., 2011*). Cell trafficking of the particles was indisputable, with peri-nuclear localisation a prominent feature. What was clearly evident within the cells was endosomal uptake of the particles. The particles used in this study are 254-280 nm in diameter. Given the reported diameters of clathrin-coated pits (*ca*. 100-150 nm) and caveolae invaginations (*ca*. 60 nm) this would suggest that macropinocytosis (> 0.5 μm) is the endocytotic mechanism employed here (*Zhu et al., 2013*). Although, clathrin-mediated uptake of 200 nm diameter particles has been reported (*Oh et al., 2009*), with particles of 500 nm diameter reported associated with caveolae-mediated endocytosis (*Rejman et al., 2004*), hence there may be a number of endocytotic pathways employed in uptake of these particular particles. What is incontrovertible is that particles (or at least, some) are trafficked via endosomes, which suggests, considering the peri-nuclear localisation, that a number of strategies for endosomal escape are being employed by (the majority of) the particles. It has been suggested that oscillating magnetic fields may alter the intracellular

processing of particles to facilitate endosomal escape (*Adams et al., 2013; Dobson, J., 2008; Fouriki et al., 2010; McBain et al., 2008; Pickard & Chari, 2010)*, although, this would not be a viable explanation here as these cells/particles have not been exposed to such a field. An alternative intracellular route has been associated with caveolar-mediated uptake, whereby stimulated caveolae uptake resulted in formation of "caveosomes" (multiple caveolae structures) that bypassed the endosome-lysosome route (*Kiss & Botos, 2009*). This 'recruiting' of multiple structures may explain how caveolar-mediated endocytosis has been associated with uptake of much larger particles, and thus, may offer a plausible explanation here. However, the strategies employed remain to be elucidated.

Further characterisation of these constructs is required. Taken together, the findings from this study suggest the protocols employed here are robust for the development of an exogenously MP-labelled intraconstruct hydrogel. Such a construct offers potential as a protective neural cell delivery system with the capability for non-invasive tracking under MRI.

Chapter 5
Influence of amplitude of oscillating magnetic fields on MNP-mediated gene transfer to astrocytes

5.1 Introduction

Magnetofection - as discussed previously within the main introduction (*Section 1.5*) - offers significant benefits for regenerative neurology applications. In this context, functionalized magnetic particles (MNPs) have high promise for regenerative therapies, both as a label for non-invasive tracking of transplant populations (*White & Jakeman., 2008*) and, for the purposes of this series of studies, as a transfection vector for genetic modification of neural cells (*Plank et al., 2011*).

Of key importance, a high level of safety is associated with this technology (*for example Plank et al., 2003*), although there remains significant technical knowledge gaps in respect of the parameters that govern the efficacy of magnetofection with neural cells. This is potentially a very useful technology to regenerative therapy and therefore it is pertinent to explore its possibilities with these neural cells. The use of a static magnetic device overcomes the spatial barrier between cells and particles (*Laurentt et al., 2011*), efficiently and rapidly delivering the nucleic acid to the target cells; the combination of magnetic field and superparamagnetic particles becoming a driving force in drawing the particles and the associated plasmid down to and across the cell membrane (*Huth et al., 2004; Ma et al., 2011; Plank et al., 2011*). In this regard, *Furlani* and colleagues reported that the space between the magnet and the cell chamber affected the rate of particle accumulation: an important consideration in gene transfection studies (*Furlani & Ng., 2008*).

A major disadvantage associated with static magnetic fields has been the focused particle accumulation at the centre of a cell culture chamber (*Furlani & Ng, 2008*). This homogeneity of particle sedimentation has the potential to cause a 'bottleneck' predicting uptake in only a small percentage of cells located at the 'hotspot'. The probable result of this is low particle uptake but with a high potential for toxicity. A recent innovation to

magnetofection to modulate this high particle load at the cell membrane, has been the use of dynamic magnetic fields (*Baryshev et al., 2011; Dahmani et al., 2013; McBain et al., 2008*), including devices that oscillate along an axis with programmable frequency and amplitude. Oscillating fields have yielded higher levels of transfection compared with static fields, in a range of major neural transplant cell types such as cortical astrocytes (*Pickard & Chari, 2010*); OPCs (*Jenkins et al., 2011*) and NSCs - generally held to be 'hard-to-transfect' (*Adams et al., 2013; Pickard et al., 2011*). The mechanisms by which oscillating fields elicit greater transfection efficiency are not fully understood. It is likely that the lateral motion imparted to the particles, increases the probability of particle-cell contact across the *whole* of the cell culture. It has also been suggested that the lateral motion of unattached particles across the cell membrane, or vibration of membrane-bound/internalised particles may mechanically stimulate endocytosis due to the shearing forces at the cell level (*Huth et al., 2004; Kamau et al., 2006; McBain et al., 2008; Pickard & Chari, 2010*). Considering the major obstacle in gene delivery is thought to be related to the endocytotic capability of the target cell (*Fernandes & Chari., 2014*), this stimulatory mechanism is a predictor of high levels of particle uptake. Likewise it has been suggested that oscillating fields may alter the intracellular processing of particles, for example by facilitating endosomal escape (*Adams et al., 2013; Dobson, J., 2008; Fouriki et al., 2010; McBain et al., 2008; Pickard & Chari, 2010*).

In the context of utilising oscillating magnetic fields, McBain *et al.* studied the correlation between oscillation amplitude and efficacy of gene delivery to a human airway epithelial cell line (*McBain et al., 2008*). Using cell size as a comparator, amplitude parameters were based on oscillations smaller than cell size (100 nm), larger than cell size (200 µm) and much larger (1 mm). Compared with static systems they found improved transfection efficiency in the presence of applied oscillating fields (frequency (F) = 2 Hz, amplitude =

200 µm). Based on their examination of a range of frequencies/amplitudes, the authors suggest that *'amplitude is of greater importance than frequency'* in enhancing gene transfer, at least in the frequency range tested (1-4 Hz). Conversely, studies investigating optimal frequency for gene transfer to astrocytes, used a fixed amplitude of 200 µm to test a range of frequencies (F = 1; 3; 5 Hz). Of these, 1 Hz was reported to be optimal for gene delivery and hence, suggested as being frequency-dependent (*Pickard & Chari, 2010*). This latter study indicates that frequency may play a greater role in enhancing gene transfer than was previously assumed, at least in neural cells. **However, it is still unclear whether the most effective identified frequency in a specific neural cell type can potentially yield better transfection outcomes, when *paired* with optimal oscillation amplitude.**

Additionally, in terms of further enhancing non-viral gene delivery using MNPs, repeat administration of MNP:plasmid complexes ("multifection") have been shown to enhance transfection efficiency in NSCs, both as neurospheres (*Pickard at al., 2011*) and as a monolayer culture (*Shah et al., 2013*). Both studies found that the combinatorial effects of multifection and application of a magnetic field (*termed* 'magneto-multifection') increased transfection efficiency in NSC cultures. Therefore employing *the optimal frequency and amplitude for astrocytes*, magneto-multifection may enhance transfection efficiency and/or the extent of transgene expression. This is based on a number of considerations. One, repeat administration of MNP:plasmid complex at 8 h intervals could increase the likelihood of plasmid DNA (pDNA) exposure to a greater proportion of target cells. Two, previous studies (*Pickard & Chari, 2010*) have observed *gfp* expression in astrocytes in as little as 4 h, indicating rapid intranuclear delivery and transgene expression in a small number of cells. Potentially, levels of *gfp* expression could be significantly enhanced in this same subpopulation, being subject to repeat exposure of MNP:plasmid complex over the short time interval employed.

An important, but often overlooked consideration in transfection studies utilising MNPs, is the correlation of particle uptake with transgene expression. The perceived expectation is that increased particle load will, in turn, increase delivery of the pDNA to the target cell. While use of magnetofection strategies have reported significantly increased transfection efficiencies (i.e. number of transfected cells) in a number of neural cell types (*i.e. Adams et al., 2013; Jenkins et al., 2011; Pickard & Chari, 2010; Pickard et al., 2011*), no study has, as far as can be ascertained, explored the correlation between particle load and transgene expression. This has specific consequences in the context of drug/gene delivery for clinical application. A high number of cells expressing a low level of transgene expression offer a different clinical outcome than that of a low number of cells showing high transgene expression.

To address the key aims of this study – investigating the effects of amplitude and magneto-multifection on transgene expression in astrocytes - two hypotheses are proposed

i) that the amplitude of the oscillating magnetic field can influence transfection outcomes in astrocytes and

ii) that the sequential application of transfection complexes/magnetic fields can enhance transfection outcomes in astrocytes.

In order to test these hypotheses, a number of parameters were assessed. Previous studies (*Pickard & Chari, 2010*) reported a frequency of 1 Hz to be optimal for gene transfer to astrocytes, and hence this informed the fixed frequency utilised for this present study. Following a similar rationale to McBain *et al.* the range of amplitudes tested here was based on measures of the cell type used i.e. astrocytes, rather than a generic cell measurement as utilised in the McBain study. In respect of the findings by *Furlani & Ng*,

the effect of increasing the distance through use of a coverslip in the well plate was also assessed.

5.2 Objectives

1) Investigate the influence of amplitude of oscillating magnetic fields on MNP-mediated gene transfer to astrocytes

2) Investigate if magneto-multifection modifies MNP-mediated gene transfer to astrocytes

3) Investigate the correlation between MNP uptake and transgene expression in astrocytes

5.3 Experimental procedures

5.3.1 Reagents and equipment: All reagents and equipment used are as described previously in sections *2.1; 2.2.3; 2.3 & 2.6*. For the NeuroMag and NeuroMag Fluo, the recommended concentration by Oz Biosciences for magnetofection of neurons is 7 µl/mL. However, lower concentrations of these particles have been required for safe transfection of neural stem cells (*Pickard et al., 2011*); indeed, previously conducted cytotoxicity studies investigating particle concentrations for gene transfer to astrocytes, reported the optimal NeuroMag concentration for routine magnetofection in astrocytes is one tenth the concentration that of neurons (0.7 µl/mL) (*Pickard & Chari, 2010*). With regards to the DNA binding efficiency of NeuroMag, this has previously been identified as maximal at a ratio of 3.5 µl NeuroMag to 1 µg DNA (*Pickard & Chari, 2010*). These then informed the NeuroMag concentration and MNP:plasmid ratio used in the present study.

5.3.2 Area and Feret's Diameter (FD) as representative measures of cell size: A similar rationale to McBain *et al.* (*2008*) was used in determining the range of amplitudes to be tested; namely cell size as a parameter for amplitude selection. Primary-derived astrocytes in culture exhibit two phenotypes which differ in shape and size and are widely referred to as type 1 and type 2. Type 1 exhibit a variable 'polygonal' morphology made up of a highly membranous cell body with truncated processes. Type 2 have a small soma and are highly branched. Therefore two measures were selected, FD and cell area, as being representative of both phenotypes and the variable morphology observed within this neural cell population.

Area was used as astrocytes in culture are highly membranous (type 1) or highly branched (type 2) and therefore much larger than a generic cell size *in vivo*. FD was used as a measure of cell size as it accounts for the varied polygonal morphology typical of type 1

and the highly branched morphology of type 2 measuring, as it does, the widest and the shortest diameters of the cell taking into account the 'projected' cross section from these measures. The term 'Feret' refers to a caliper diameter (width) of an object with the resulting value based on the maximum (XFmax) and minimum feret (XFmin) with the feret angle (XFmax90) used in calculation of the XFmin in increments of 0.5° steps. FD uses the following formula: - √ (XFmin * XFmax). It provides a measure of the distance between two parallel lines, tangent to the projected cross section of the maximum and minimum width of a cell, and as such reflects the varying morphologies seen in this cell population.

5.3.3 MNP-mediated gene (gfp) transfer: To investigate the influence of amplitude on gene transfer, astrocytes were routinely plated on PDL-coated coverslips in a 24-well and a 96-well plate with MNP-mediated gene (*gfp*) transfer protocols conducted at 24-48 h post-plating to allow for cell adherence and growth of processes (*please refer to 2.6.3 for detailed protocols on complex formation and subsequent addition of complex to cells*). Briefly, 60 ng of pmaxGFP plasmid was mixed with 0.21 µL NeuroMag or NeuroMag Fluo in a final volume of 75 µL DMEM, and for each well of the 96-well plate, 12 ng of pmaxGFP was mixed with 0.042 µL NeuroMag or NeuroMag Fluo in a final volume of 15 µL DMEM. These were allowed to complex for 20 mins before addition to the cells. In each separate magnetofection condition, cells were exposed for 30 min to a magnetic field set at a frequency of 1 Hz, with each condition having a different amplitude within the range of 100 µm – 1000 µm (*parameters described in detail below; section 5.4.1*). Addition of DMEM or DMEM plus plasmid was added to control wells. At 48 h post-particle addition, cells in the 24-well plates were fixed and prepared for imaging and analysis. Cells in the 96-well plates were immediately subjected to an MTS assay (*Section 2.6.3; 2.13.2 for further details*).

5.3.4 Investigating MNP uptake versus transgene expression: Alongside investigation of amplitude parameters on transfection efficiency, NeuroMag Fluo was used in a subset of experiments to reveal any potential relationship between extent of particle uptake and *gfp* expression. Transfection protocols were performed under the same experimental conditions as above.

5.3.5 Pilot study: Investigating effect of coverslip depth on gene (gfp) transfer: For the pilot study, astrocytes were plated in a PDL-coated 24-well plate, with or without a PDL-coated coverslip with cells exposed to the differing magnetofection conditions as described above (*section 5.3.3*) (*Figure 5.1*).

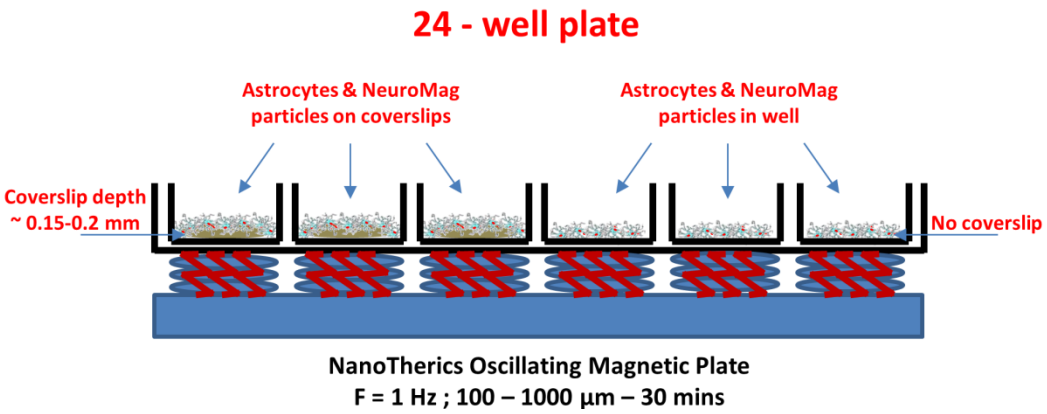

Figure 5.1 Schematic of experimental setup investigating effect of coverslip depth on gene transfer *Astrocytes were plated into a 24-well plate, with or without a coverslip. MNP-mediated gene transfer to the cells was conducted using transfection protocols with the cells exposed for 30 minutes to an oscillating magnetic field set at a frequency of F1 Hz, and a varied range of oscillation amplitude (100 µm – 1000 µm).*

Cells were fixed at 48 h post-transfection with quantification of transfection efficiency carried out from the coverslip and the well plate.

5.3.6 Magneto-multifection MNP-mediated gene (gfp) transfer: As for previous gene transfer experiments, astrocytes were routinely plated in a 24-well and a 96-well plate with MNP-mediated gene (*gfp*) transfer protocols conducted at 24-48 h post-plating (*as described above and detailed in 2.6.3*). Briefly, following addition of the MNP:plasmid complex, cells were exposed to the optimal magnetic field reported for astrocytes for 30 min, and then incubated in the absence of a magnetic field for 30 min, before being subject to 100% D10 medium refresh to remove any particles not already internalised. Cells were then incubated for a further 7 h before being subjected to a repeat gene transfer protocol as before (i.e. an interval of 8 h between repeat MNP:plasmid administration). Single transfection from each MNP:plasmid administration acted as controls [Time 1 (T1); Time 2 (T2)] for the magneto-multifection condition, allowing comparisons between this condition and T1 and T2 (*Figure 5.2*).

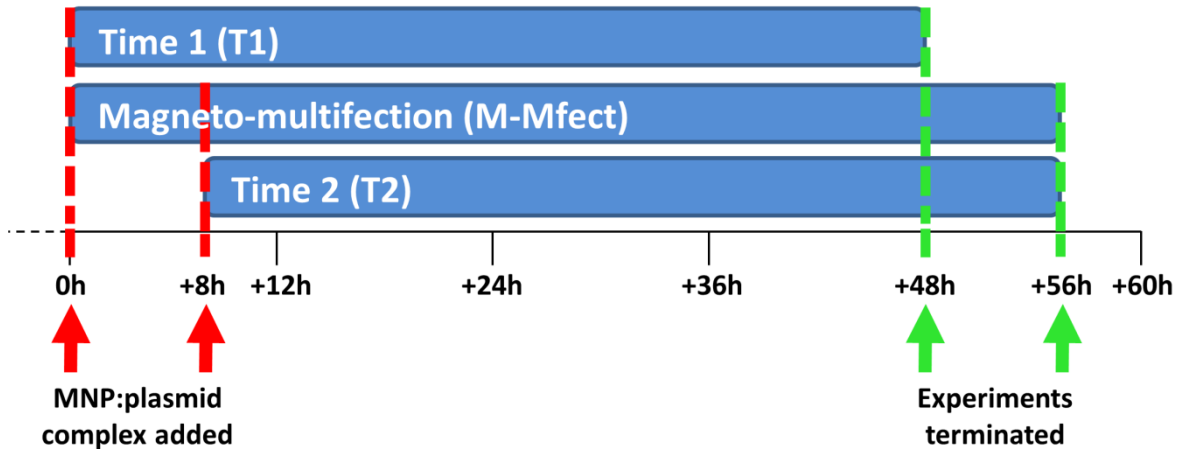

Figure 5.2 Schematic of time course of magneto-multifection protocol *Cells in the magneto-multifection condition were exposed to repeat transfection at T1 and T2 with an interval of 8 h. Controls for magneto-multifection were subjected to single transfection at T1 or T2. Cells in the T1 and T2 condition were terminated at 48 h following single transfection; cells in the magneto-multifection condition were terminated 48 h following repeat administration i.e. at 56 h.* **T1**:Time 1; **T2**: Time 2

5.3.7 Investigating proportions of cells showing repeat uptake: To investigate the proportion of cells transfected at each time point within the magneto-multifection condition, plasmids encoding for red fluorescent protein (*rfp*) and green fluorescent protein (*gfp*) were used at the different time points. It has been reported that use of *rfp* results in lower transfection efficiency than that seen with *gfp* due to the larger plasmid size of the former (4.6 kb *versus* 3.5 kb) (*Pickard et al., 2015*). Therefore experiments were duplicated with the use of *rfp* at T1 and *gfp* at T2, then the use of *gfp* at T1 and *rfp* at T2 (n=2; duplicates of each culture). Use of these two plasmids also enabled investigation of repeat transfection in individual cells (i.e. *rfp* and *gfp* co-expression).

Each condition was terminated 48 h following final MNP:plasmid administration. Control wells for the gene transfer protocol consisted of cells not exposed to MNP:plasmid complex. Cells plated in the 96-well plates were immediately subjected to an MTS assay (*detailed in section 2.6.3; 2.13.2*).

5.3.8 Immunocytochemistry: Immunolabelling of cells in gene (*gfp*) transfer experiments was as detailed in section *2.9.1*.

5.3.9 Imaging: Imaging of these experiments was conducted as detailed in section *2.10.1*

5.3.10 Analyses: Culture characteristics, cellular assays, transfection efficiency and extent of *gfp* expression were quantified from fluorescence micrographs (*detailed in section 2.11 & 2.12.2*). Transfection efficiency was determined as the percentage of GFAP+ve astrocytes co-expressing *gfp* expression, with the data normalised to the control amplitude condition (F = 1 Hz; 200 µm*)*. Extent of *gfp* expression was assessed using fluorescence intensity as a representative measure (*Section 2.12.2*). Analysis of MTS assays were as described previously (*Section 2.13.2*). For the MNP:plasmid M-Mfect experiments, transfection efficiency at T1 was determined as the percentage of GFAP+ve cells

exhibiting reporter protein expression. Co-expressing (*rfp* + *gfp*) cells were confirmed by coincident expression of red or green fluorescent protein on unmerged images, with the merged image exhibiting a combination of red and green fluorescent protein. Observations on the extent of NeuroMag Fluo uptake by astrocytes were estimated based on a previously described semi-quantitative method of low, medium or high particle accumulation within the cell (*Jenkins et al., 2013*).

5.3.11 Statistical analysis: Data were analysed as detailed previously (*Section 2.14*). The number of cultures used in this series of experiments was 3 ($n = 3$) unless otherwise noted, with each culture derived from a different rat litter.

5.4 Results

5.4.1 Measure of cell size to inform amplitude parameters

Using ImageJ software, fluorescence microscopy images were scaled to show measurements per micron (µm) with measures taken from 160 type 1 and type 2 astrocytes from three different control cultures. The formula for FD was applied to the values, the results averaged to show a mean FD of 98.3 µm (type 1) and 54.4 µm (type 2). The mean area of type 1 astrocytes measured was 1277.8 µm^2 with 309.7 µm^2 recorded for type 2 **(***Figure 5.3***).**

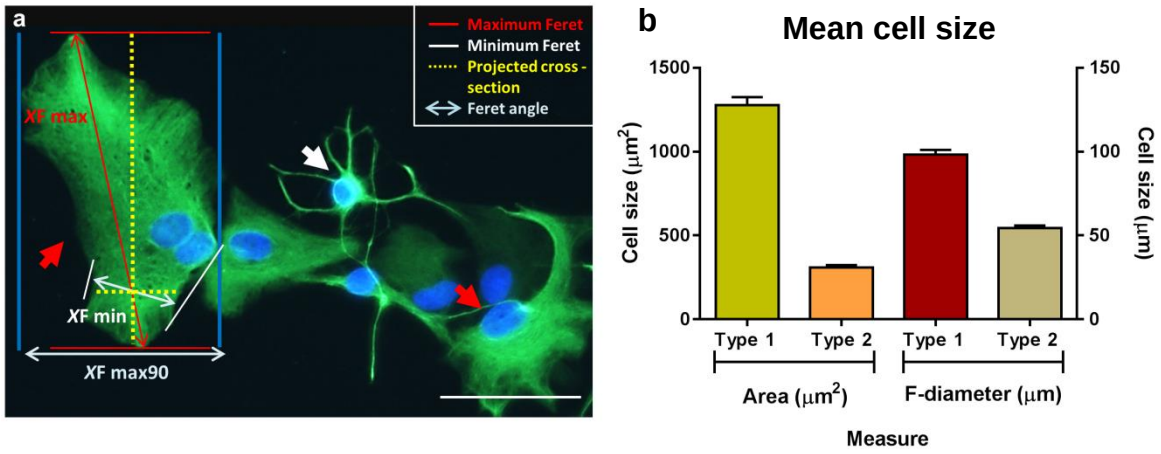

Figure 5.3 Measure of cell size *Representative fluorescence image (a) depicting schematic of the parameters utilised to calculate Feret's diameter [**FD** = √ (XFmin * XFmax)]*. Note *the polygonal morphology characteristic of astrocytes in culture. Note also the heterogeneity in morphology within this primary-derived cell population (arrows). Type 1 phenotype is highly membranous with a flattened morphology and truncated processes and shows a high level of variability in size (red arrows). In comparison, type 2 phenotype has a small soma and is highly branched (white arrow). Bar graph (b) shows the mean cell size according to area (µm^2) and FD (µm). Scale of image = 50 µm Results expressed as mean ± s.e.m.*

These values proposed an overall range of cell measures from which amplitude could be tested; 100 µm (average measure of FD) - 1000 µm (average measure of area) with intermediate steps tested within that range i.e. 100, 200, 400, 700, 1000 µm in total. The most effective parameters reported for magnetofection of astrocytes, namely 200 µm; 1Hz, were used as a control condition **(***Adams et el., 2013; McBain et al., 2008; Pickard & Chari, 2010; Pickard et al., 2015; Jenkins et al., 2011*).

5.4.2 Pilot study: Investigating effect of coverslip depth on gene (gfp) transfer

It has been reported that the space between magnet and chamber has an effect on particle accumulation, raising the question that use of a coverslip in the well may affect MNP-mediated gene transfer. Microscopy observations from initial transfection studies showed high numbers of transfected cells at the edges of the coverslip (the well trough). From this, it could be postulated that the depth of a coverslip (*ca*. 0.15 - 0.2 mm) in the well plate may influence MNP-mediated gene transfer due to the increased space between magnet and cells. It could be argued that removal of the coverslip would address this. However, coverslips facilitate easier processing of the sample for microscopy purposes. The depth and, of key importance, the refraction from glass coverslips are far less than that of culture plastic, resulting in higher resolution images; a key feature for accurate visual analysis. Accordingly, prior to performing the experiments, a pilot study was conducted to investigate the effect of coverslip depth on gene transfer.

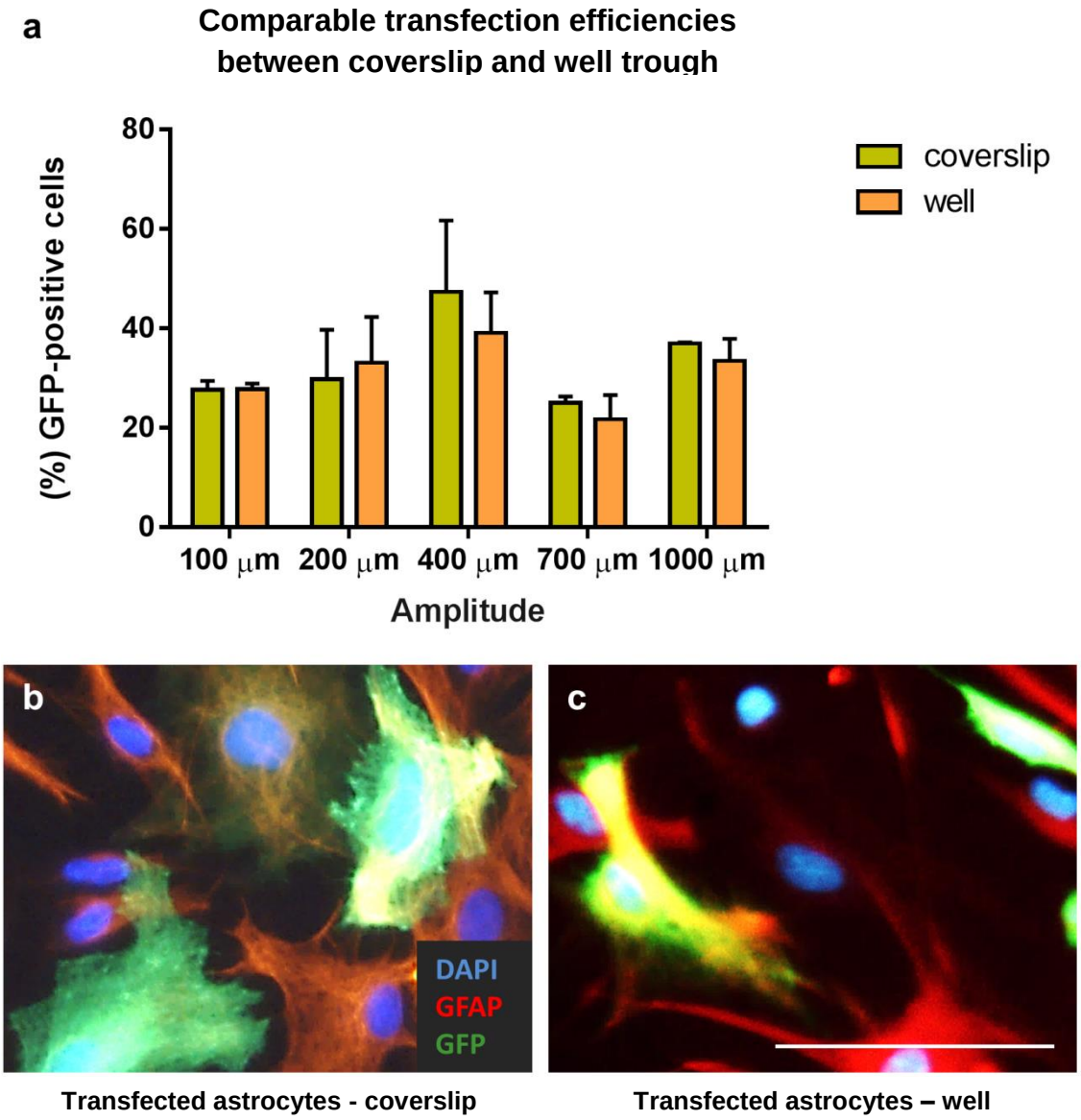

Figure 5.4 Effect of coverslip depth on gene (*gfp*) transfer *Bar graph showing (a) transfection efficiencies of cells plated on a coverslip and those plated directly into a well. Across all amplitude conditions, no differences were observed in transfection efficiency between coverslip and well. A trend towards increased transfection efficiency was noted at the higher amplitudes, peaking at 400 µm amplitude. Representative fluorescence images of transfected cells on (b) glass coverslips and (c) in a well illustrate the difference in resolution between glass and culture plastic. (n =2). Scale = 50 µm Results expressed as mean ± s.e.m. (Number of replicates = 3)*

The preliminary findings from this pilot study found that the depth of the coverslip did not adversely affect the efficiency of the magnetic field, with no obvious differences observed in transfection efficiencies between astrocytes plated on coverslips and those plated directly in a well [*Figure 5.4 (a)*]. Hence, as no adverse effect on transfection efficiency was found, the experiments were conducted using coverslips within the well. In this respect, use of coverslips resulted in higher resolution micrographs [*Figure 5.4 (b)*] compared with micrographs taken from cells within culture plastic [*Figure 5.4 (c)*].

Of further note from these results is the observed peak in transfection efficiency at 400 µm amplitude [*Figure 5.4 (a)*]. This preliminary finding suggests this amplitude may be optimal (at this frequency) for transfection efficiency in astrocytes.

5.4.3 Safety assessment of MNP-mediated gene (gfp) transfer to astrocytes

Safety was of prime concern with the use of these protocols. Astrocyte cultures were of high purity as judged by GFAP expression (99.3 ± 0.2%) [*Figure 5.5 (a)*]. The cells predominantly exhibited the membranous, flattened morphologies characteristic of type 1 astrocytes (92.6 ± 2.7% of GFAP+ve cells), with the morphological characteristics associated with type 2 (small soma, highly branched) accounting for 7.2 ± 2.7% of GFAP+ve cells. Proportions of astrocyte phenotype were similar across all conditions [*Figure 5.5 (b)*].

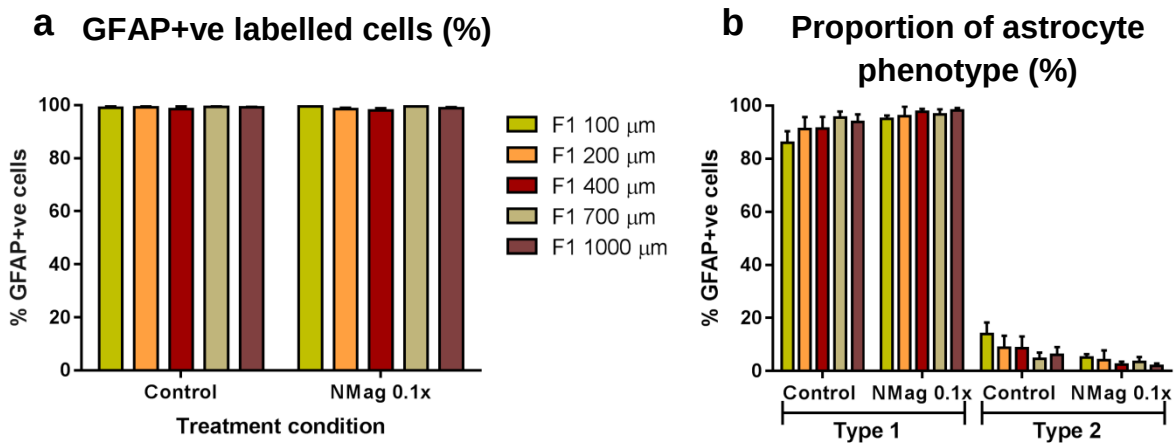

Figure 5.5 Influence of amplitude on proportions of astrocytes and on astrocyte phenotype *Bar graphs showing (a) the high purity of the cell population (99.3 ± 0.2%) expressing GFAP and (b) the mean proportions of the two astrocyte phenotypes represented within this cell population (92.6 ± 2.7%; 7.2 ± 2.7% - type 1 and type 2 respectively). No differences were seen between proportions of astrocytes or astrocyte phenotype. Results expressed as mean ± s.e.m. (Number of replicates = 3)*

Safety analyses revealed no acute toxicity, with cellular viability assays reporting no difference between the conditions with respect to cell counts or the percentage of pyknotic nuclei (*ca*. 1% across all conditions) [*Figure 5.6 (a) & (b) respectively*]. Cellular viability within this experiment was corroborated by MTS assays, where no alterations to metabolic function were detected for any of the experimental conditions [*Figure 5.6 (c)*]

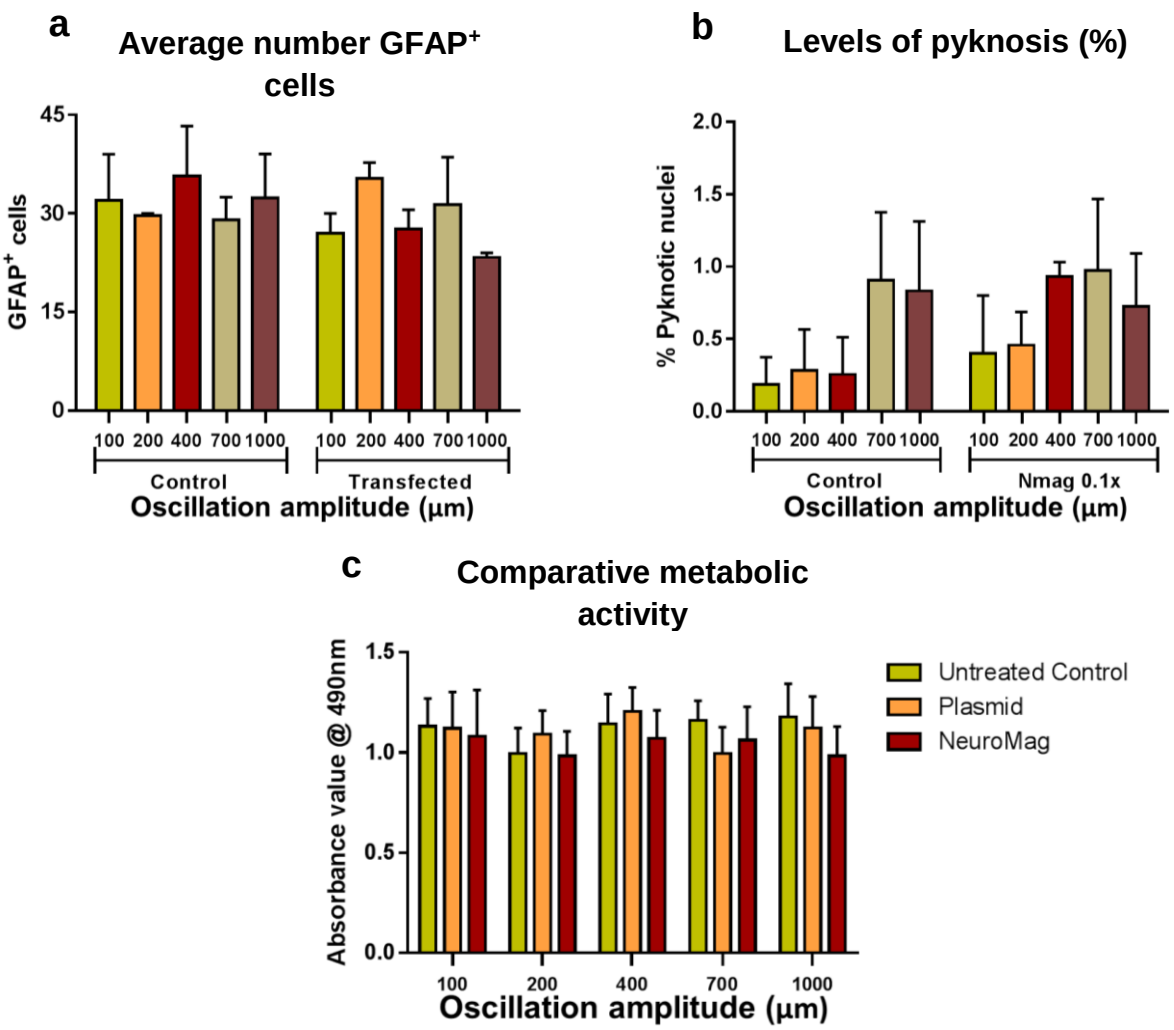

Figure 5.6 Cell viability analyses report no acute toxicity *No acute toxicity was reported with these protocols. Bar graphs of cellular viability assays reported (a) no differences in the average number of nuclei per microscopic field with (b) a low level of pyknosis (< 1%) across conditions. No differences in (c) metabolic activity were reported between conditions (MTS assay). Results expressed as mean ± s.e.m. (Number of replicates = 3)*

5.4.4 Influence of amplitude of oscillating magnetic fields on MNP-mediated gene (gfp) transfer to astrocytes

To investigate the influence of amplitude on gene transfer to astrocytes, utilising a fixed frequency of 1 Hz, a number of amplitudes were tested within a 100 – 1000 µm range, namely 100 µm; 200 µm; 400 µm; 700 µm; 1000 µm. Initial observation found no astrocytes exhibiting *gfp* expression in the plasmid-only control cultures. Of the transfected astrocytes, across all experimental conditions, analysis showed the overwhelming majority were identified phenotypically as type 1, with less than 2% exhibiting type 2 morphologies [*Figure 5.7 (a)*]. Therefore, analyses relating to transfection were restricted to type 1 astrocytes.

There was a tendency towards greater transfection efficiency at the higher amplitudes, peaking at an amplitude of 400 µm, with transfection efficiency at this amplitude being 2-fold greater than the control amplitude (200 µm), although no significant difference in transfection efficiency was found between the control amplitude and any of the 'test' amplitudes (100; 400-1000 µm) [*Figure 5.7 (b)*].

The extent of *gfp* expression in astrocytes (as evaluated by the measure of fluorescence intensity) was significantly elevated at an amplitude of 200 µm compared with amplitudes of 100 and 400 µm, with a notable trend towards higher values of *gfp* expression at amplitudes of 700 and 1000 µm [*Figure 5.7 (c) and (d)*]. Taken together, these findings show that transfection efficiency (i.e. numbers of transfected cells) is unaffected by amplitude but rather, amplitude plays a greater role than previously perceived in influencing the extent of transgene expression in individual cells.

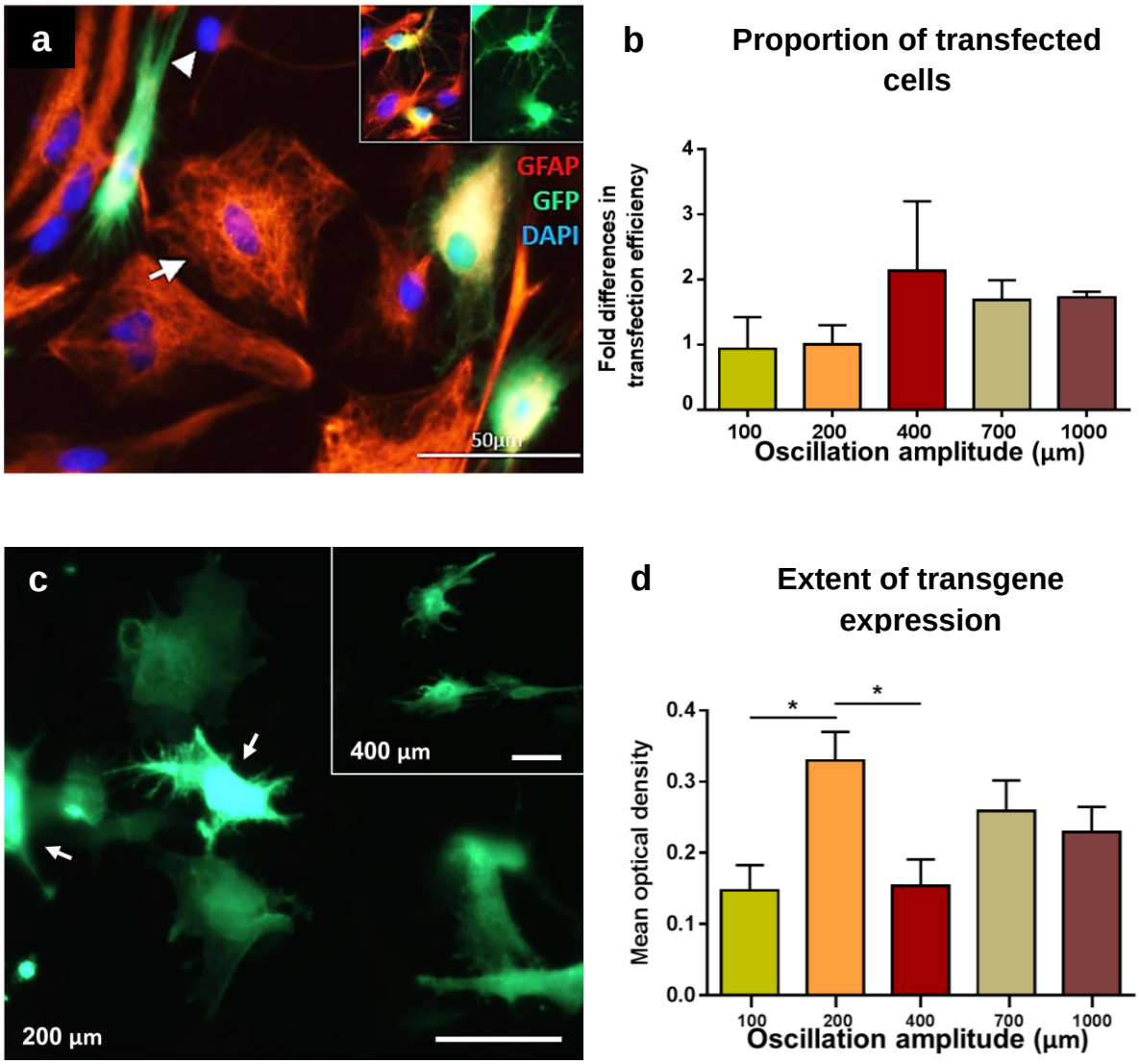

Figure 5.7 Influence of amplitude of oscillation on transfection efficiency and extent of transgene expression in astrocytes *Fluorescence micrograph (a) depicting the different phenotypes; type 1 (arrow) and type 2 (arrowhead) astrocytes. Small numbers of gfp+ve type 2 astrocytes were noted (inset shows counterpart micrographs). Bar graph (b) showing no significant difference in transfection efficiency between amplitudes, although a tendency towards increased efficiency at the greater amplitudes is noted, peaking at an amplitude of 400 µm; this amplitude reporting transfection efficiency as 2-fold greater than the control condition (200 µm). Representative fluorescence micrograph (c) showing differences in gfp expression between the 200 µm amplitude condition (main image) and*

*the 400 µm condition (inset); arrows indicating cells with high levels of gfp expression. Bar graph (d) showing extent of gfp expression (as measured by florescence intensity) was significantly elevated at 200 µm amplitude compared to 100 µm and 400 µm (Bonferroni's post-hoc tests; *p < 0.05), with a trend towards higher values with increased amplitude (700 – 1000 µm). Scale of images (a & b = 50 µm) Results expressed as mean ± s.e.m. (Number of replicates = 3).* **gfp**: green fluorescent protein

5.4.5 Safety assessment of magneto-multifection MNP-mediated gene (gfp) transfer to astrocytes

Of prime concern was the safety of the magneto-multifection protocol when used with astrocytes and to this end, a number of safety analyses was conducted. The percentage of cells expressing GFAP was consistent across all conditions (98.1 ± 0.5%) [*Figure 5.8 (a)*], and no difference was found in average cell number per microscopic field between control and experimental conditions [*Figure 5.8 (b)*]. Of astrocyte phenotype, type 1 astrocytes accounted for *ca.* 92% of GFAP+ve cells with type 2 accounting for *ca.* 8% [*Figure 5.8 (c)*]. Type 1 phenotype made up the majority of transfected cells (*ca.* 89% versus type 2; *ca.* 11%) [*Figure 5.8 (d)*]. Low levels of pyknosis were observed across all conditions (*ca.* 3% overall), with no difference reported in metabolic activity between cells exposed to plasmid only or MNP:plasmid complex across each of the experimental conditions [*Figure 5.8 (e) & (f), respectively*]. Thus, the high cellular viability reported within these experiments demonstrated the safety of the magneto-multifection protocols used.

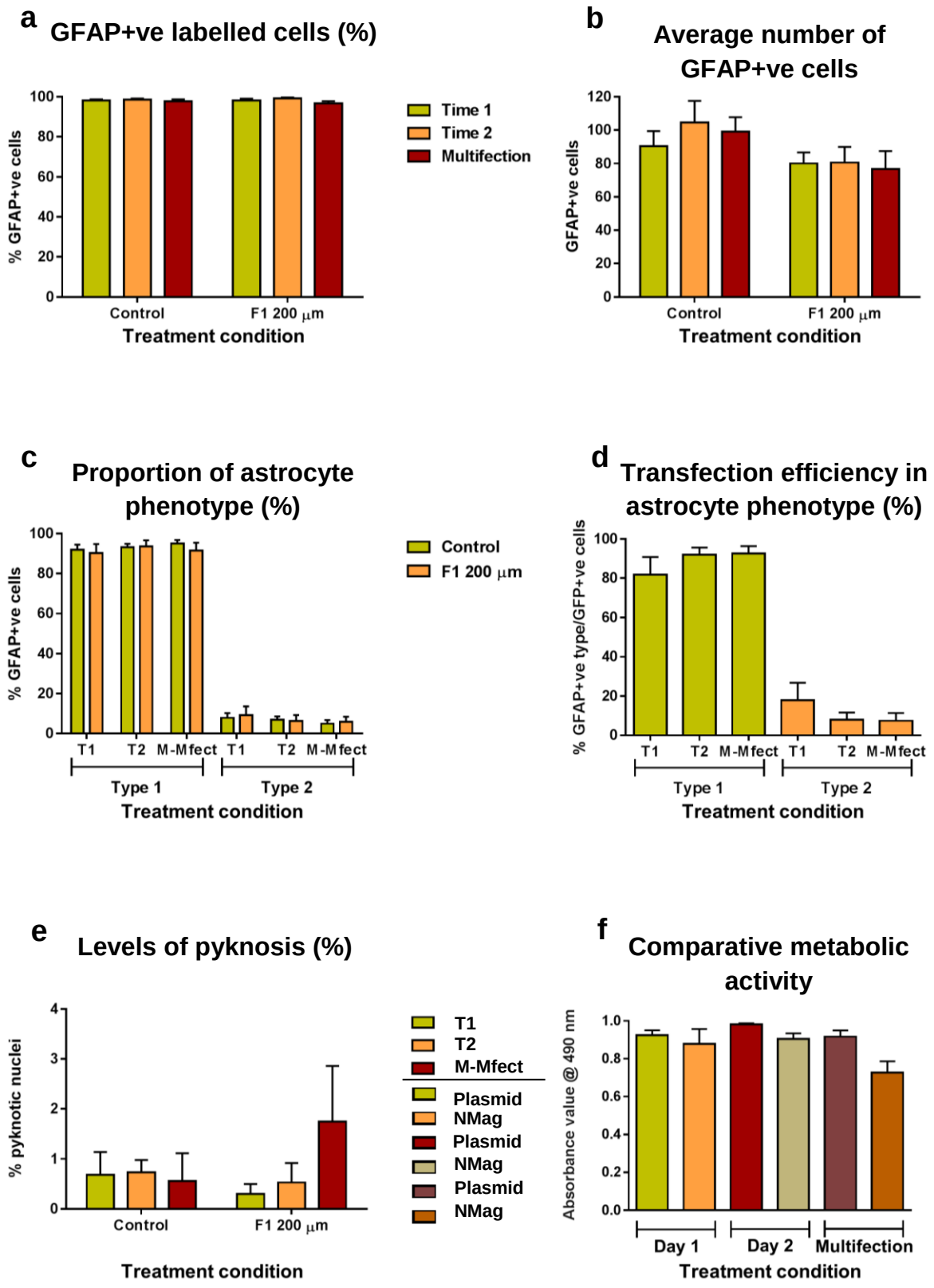

Figure 5.8 Safety assessment of magneto-multifection protocols *Bar graphs showing (a) the percentage of GFAP+ve labelled cells was consistent across all conditions with (b) no difference in average cell count. Bar graphs showing (c) proportion of astrocyte*

phenotype was predominantly type 1 (ca. 92% versus ca. 8% type 2) with (d) type 1 phenotype accounting for 89% of transfected cells versus 11% type 2 phenotype. Bar graphs showing (e) low levels of pyknosis across all conditions (ca. 3%) with (f) cellular viability assay showing no difference in comparative metabolic activity in the cells. Results expressed as mean ± s.e.m.

5.4.6 Magneto-multifection MNP-mediated gene (gfp) transfer

Repeat transfection has reported enhanced transfection efficiency in other neural cell populations. Having identified the optimal parameters (from those tested) for transfection of astrocytes, magneto-multifection was utilised to further enhance gene delivery to *this* neural cell.

For magneto-multifection, plasmids encoding for red fluorescent protein (*rfp*) and green fluorescent protein (*gfp*) were used to indicate transfection efficiency at the two time points [*Figure 5.9 (a)*] and investigate the level of co-expression [*Figure 5.9 (b)*]. Repeat administration significantly increased transfection efficiency compared with single MNP:plasmid dose at T1 or T2 alone [81.5 ± 1.9% (M-Mfect) *versus* 37.9 ± 8.8% (T1) and *versus* 43.7 ± 8.1% (T2)] [*Figure 5.9 (c)*]. Investigation of repeat exposure to individual cells revealed *ca*. 22% of cells showed co-expression of *rfp* and *gfp* [*Figure 5.9 (b; image and inset) & (d)*]. The majority of transfected cells exhibited *gfp* expression as opposed to *rfp* expression; this to some extent was anticipated due to the increased plasmid size encoding for *rfp* (*Pickard et al., 2015*) [*Figure 5.9(d)*].

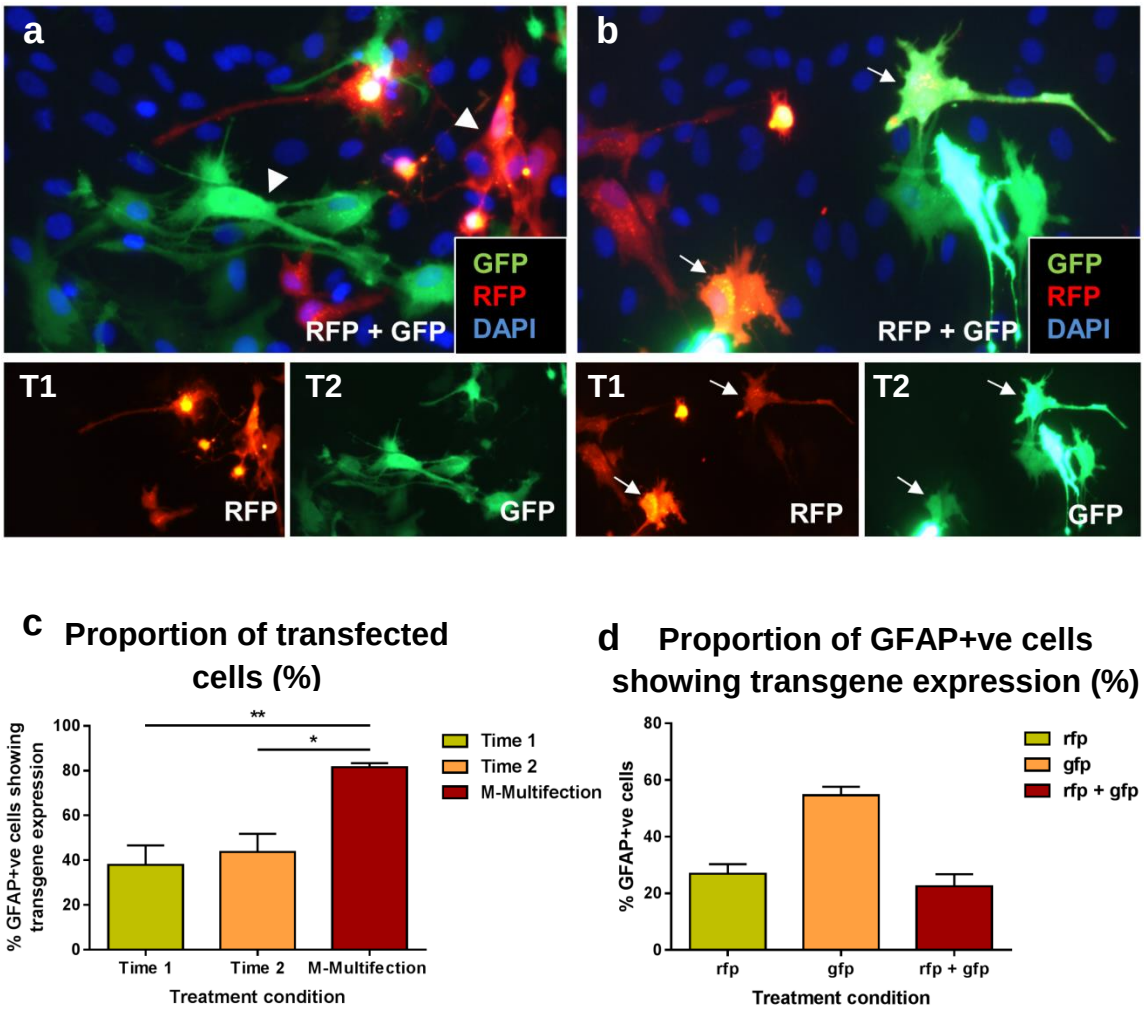

Figure 5.9 Magneto-multifection and transfection efficiency *Representative fluorescence micrographs illustrating (a) two different sub-populations of cells are transfected at T1 and T2; characterised respectively by rfp and gfp expression [arrowheads; main image (corresponding un-merged images showing rfp and gfp expressing cells)]. (b) The prevalence of a subpopulation of cells co-expressing rfp and gfp expression, indicating repeat uptake of MNP:plasmid complex [white arrows; main image (corresponding un-merged images showing coincident rfp and gfp expression)]. Bar graphs showing (c) repeat administration of MNP:plasmid complex significantly increased transfection efficiency compared with a single dose at T1 or T2 (**p < 0.01; *p < 0.05 respectively) and (d) a greater number of transfected cells exhibit gfp expression than exhibit rfp expression, with a subpopulation of cells exhibiting rfp and gfp co-expression.*

Results expressed as mean ± s.e.m. (Number of replicates = 3). **gfp**: green fluorescent protein; **rfp**: red fluorescent protein

5.4.7 Correlation between MNP-uptake and transgene expression

If the nanoparticles are DNA transporters, then is it reasonable to expect a dose relationship between nanoparticle uptake and gene expression? To explore this possibility, a subset of experiments was conducted using NeuroMag Fluo, a transfection-grade particle conjugated with a rhodamine fluorophore. This allowed observations of particle accumulation co-localised with *gfp* expression. Approximately 80% of cells exhibited NeuroMag Fluo labelling and of these only *ca*. 50% were transfected [*Figure 5.10 (a)*]. Type 1 astrocytes typically show 100% uptake; this lower level of uptake may be due to type 2 showing little or no uptake. Labelled cells showed low, moderate or high levels of particle accumulation as measured by a visual semi-quantitative analysis [*Figure 5.10 (b)*].

Investigation of the correlation between particle accumulation and transgene expression (as measured by fluorescence intensity) revealed an inverse relationship [*Figure 5.10 (c)*]. High transgene expression was associated with low levels of particle accumulation, whereas cells that were highly labelled exhibited (on the whole) a low extent of transgene expression. In this regard although low particle accumulation was always associated with reporter protein expression, the observed correlation between higher levels of particle accumulation and *gfp* expression was inconsistent. Higher levels of accumulation were observed in association with either high, moderate, low or no *gfp* expression [*Figure 5.10 (d)*], suggesting a highly complex relationship between particle uptake and protein expression, and the factors mediating this interaction.

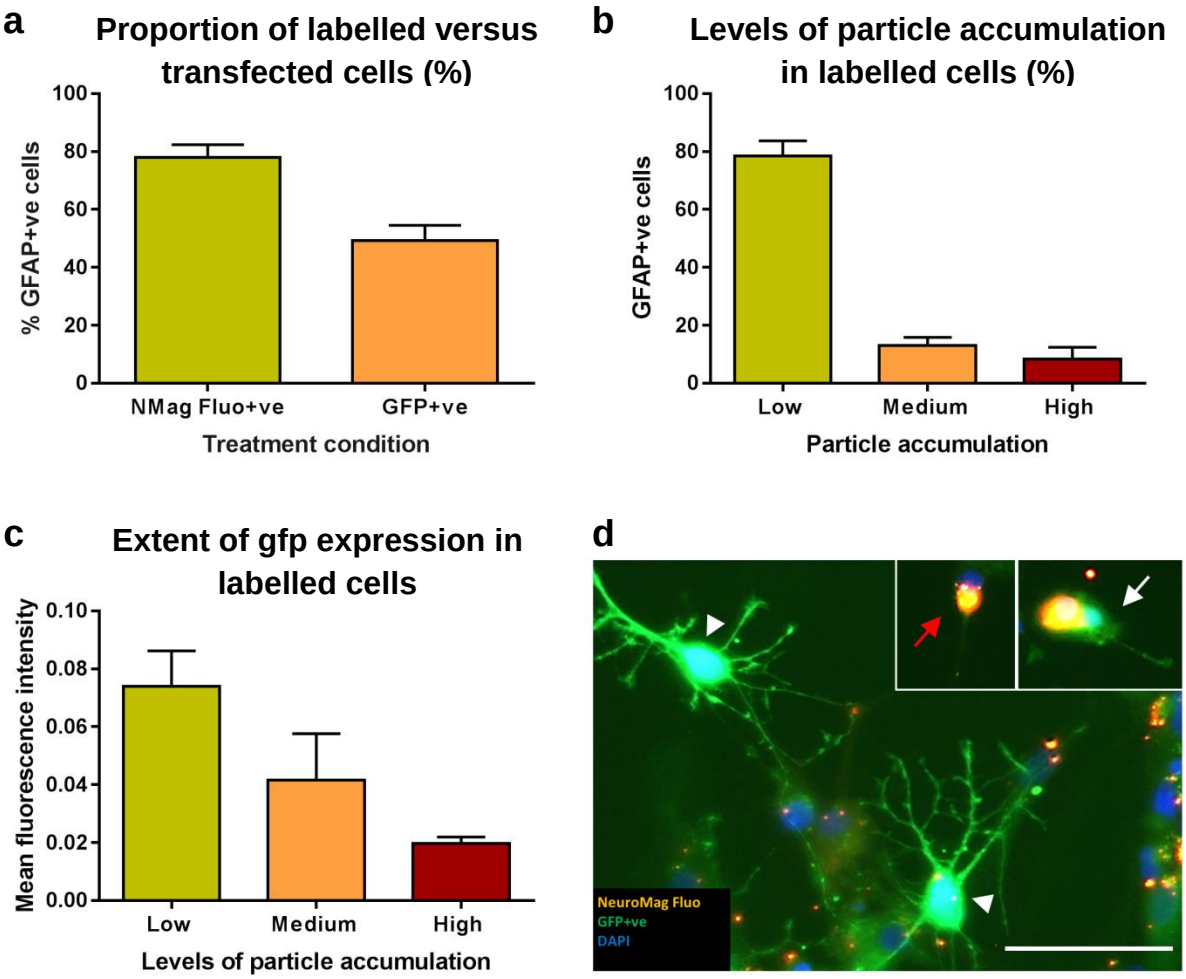

Figure 5.10 Relationship between particle uptake and transgene expression *Bar graphs showing (a) a discrepancy between the proportions of labelled cells and cells exhibiting gfp expression, with (b) labelled cells predominantly showing low levels of particle accumulation. Bar graph (c) shows an inverse relationship exists between particle accumulation and levels of gfp expression. Fluorescence micrograph (d) shows (i) high levels of gfp expression (white arrow head) in cells exhibiting low levels of particle uptake, (ii) extensive particle uptake coupled with negligible gfp expression (inset; red arrow) and conversely, high levels of gfp expression (inset; white arrow) (n = 2). Scale of main image = 50 µm Results expressed as mean ± s.e.m. (Number of replicates = 3).* **gfp**: green fluorescent protein

5.5 Discussion

Two key features of MNP-mediated gene transfer to astrocytes have been investigated. Firstly, the influence of varying amplitude of oscillation on MNP-mediated gene delivery and secondly, the use of a magneto-multifection strategy to investigate whether gene transfer could be enhanced further in this neural cell population. The findings from each study and their implications to regenerative neurology applications are addressed here.

One of the parameters to be assessed was the effect of coverslip depth on gene transfer to astrocytes. The findings here were in contrast to those reported by *Furlani & Ng.* This may be related to the strength of the magnets involved. The magnet utilised in this study exerted approximately half the magnetic field strength of the one utilised by *Furlani & Ng* (NdFeB magnet = 421 ± 20 mT *vs.* NdFeB magnet = 1 T, *respectively*). From this it could be postulated that distance would exert a greater adverse effect on particle accumulation in *this* study. However, this was not the case. The difference in distance between the two studies [1.0 mm (*Furlani & Ng*) compared with approximately. 0.15-0.2 mm - being the depth of the coverslip in this study] is a more likely explanation for the decrease in particle accumulation seen in the *Furlani & Ng* study, and why the shallow depth of the coverslip showed no such limitation.

In respect of the influence of amplitude on transfection efficiency, findings from the first study demonstrated that while amplitude of oscillation does not influence proportions of transfected cells, it does nevertheless modulate levels of transgene/protein expression within a cell. McBain *et al.* (*2008*) measured levels of transgene expression at three frequencies combined with four amplitudes, and concluded that "*perhaps the amplitude is more important than frequency*" (*McBain et al., 2008*), an observation broadly in accordance with the enhanced levels of transgene expression reported here. Although, it should be noted that McBain used a bioluminescence assay; its major limitation being its

inability to discriminate between higher proportions of transfected cells *versus* individual cells expressing higher transgene levels. By comparison, the methods employed in this study enabled separate quantification of proportions of transfected cells (transfection efficiency) and extent of transgene expression within a cell (*please refer to sections 2.12.2respectively for detailed methodology*).

The findings of this study reported no significant difference in proportions of transfected cells between 200 µm (the 'control' condition) and the 'test' amplitudes. Although, a trend towards increased transfection efficiency at the higher amplitudes was noted, peaking at an amplitude of 400 µm. However, quantification of *extent* of transgene expression reported a significant increase in *gfp* expression at an oscillating amplitude of 200 µm compared with 100 and 400 µm amplitude. Based on these findings, it could be proposed that oscillation *frequency* determines transfection efficiency (i.e. the proportions of transfected cells) (*Pickard & Chari, 2010*), but that it is *amplitude* that determines the *extent* of transgene expression in individual cells, at least in astrocytes; a novel finding in magnetofection studies and of potential importance to regenerative neurology applications. In this regard, before elucidating further, investigation of the relationship between MNP uptake and gene delivery is necessary to understand the potential mechanisms involved.

Primarily, particle uptake is dependent on the endocytotic activity of the target cell (*Adams et al., 2015; Fernandes & Chari, 2014; Treuel et al., 2013*), and in this respect primary-derived astrocytes possess a highly endocytotic membrane showing avid uptake of particles in both labelling and MNP-mediated gene transfer studies (*Jenkins et al., 2013; Pickard et al., 2011; Tickle et al., 2015; 2016*). In this present study use of MNPs that possessed both transfection *and* imaging capabilities enabled exploration of the relationship between MNP uptake and gene delivery. Of the 80% labelled cells, only approximately 50% exhibited transgene expression. Quantification of particle

accumulation co-localised with *gfp* expression revealed an inverse relationship between transgene expression and particle uptake. Interestingly, high transgene expression was associated with low particle uptake whereas cells that were highly labelled, for the most part exhibited a low extent of transgene expression. Taken together, these findings propose that high levels of transgene expression exhibited by a cell is inversely dependent on intracellular particle uptake, and in this respect, enhanced protein expression at the 200 µm amplitude may be due to *lower* uptake in individual cells. From this it could be postulated that a cell population with an overall low level of particle loading in individual cells, may offer potential for therapeutic transgene applications.

Understanding the mechanisms informing this complex relationship between uptake and transgene expression, is difficult to establish and requires further investigation. What is clear from these findings is that particle uptake *per se* is not the sole determinant of successful transfection, as was highlighted by the inconsistent particle:reporter protein association observed in highly labelled cells. Indeed for non-viral gene delivery, heterogeneity between uptake *versus* expression appears to be commonplace (*Akita et al., 2007; Tinsley et al., 2004; Wilke et al., 1996).* Although, the culture wide assays used to measure transgene expression in these studies did not allow for any particle:transgene relationship to be elucidated on a cell-by-cell basis, as has been undertaken here.

Nevertheless, in respect of this observed heterogeneity, it is not clear what accounts for these observations, but it may involve differences in intracellular processing of MNP:plasmid complexes. Intracellular particle clumping may have prevented DNA breaking away from the particles. Cultures derived from primary sources often exhibit heterogeneous behaviour (*Singhal et al., 2016*) and these differences may be related to individual cells (i) being at different stages of the cell cycle (*Kim et al., 2012; Tseng et al., 1999*) or (ii) belonging to subpopulations with differing intracellular processing

characteristics. For example, it is feasible that cells lacking transfection despite extensive particle uptake sequester the particles within intracellular vacuoles (*Tinsley et al., 2004*) or subject the plasmid to degradative processes.

In respect of cell cycle dynamics, this could offer a plausible explanation for the heterogeneity between particle uptake *versus* expression. The study of cell cycle dynamics in relation to gene transfer has reported a trafficking of the various elements – particle and pDNA - throughout the entire duration of the cell cycle. However, it has also clearly identified optimal timings ('hot spots') at different stages of the cell-cycle for uptake, delivery and subsequent transgene expression (*Akita et al., 2007*; *Brunner et al., 2002; Castro et al., 1997; James & Giorgio, 2000; Tseng et al., 1999) (Figure 5.11).* In this context it is of note that particle uptake and subsequent intracellular processing are not a continuous event but have been identified as a multi-stage process (*Pollard et al., 1998; Tinsley et al., 2004; Zabner et al., 1995*). This implies a longer time-course than has been previously supposed, and that the occurrence of one event does not necessarily confer the occurrence of a subsequent event. In respect of the findings from this current study, it could therefore be speculated that a high loading of particles into a cell may result in a longer trafficking time or 'held' at one stage of the process, offering a possible explanation for the inconsistency observed in highly labelled cells.

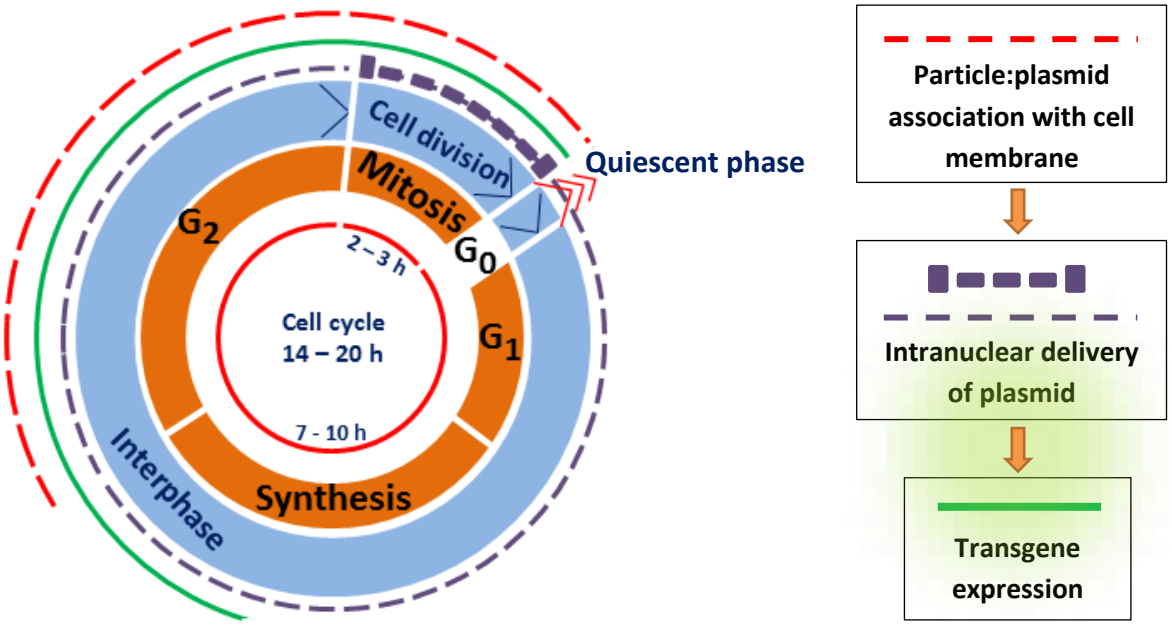

Figure 5.11 Schematic illustrating the putative interaction between cell cycle dynamics and MNP-mediated gene transfer *The cell cycle of astrocytes in culture is generally held to be ca. 14-20 h, with an M-phase of 2 -3 h and an S-phase of ca. 7 – 10 h. Particle uptake as a delivery vector for pDNA is reported as being greatest during the G2/M-phase, with intranuclear pDNA delivery reported as showing a comparable rate of delivery throughout the cell cycle, with potentially higher levels of uptake during mitosis. Subsequent transgene expression is understood to be dependent on mitotic events although significant increases have been reported throughout a larger proportion of the cell cycle prior to mitosis* (**G_0** - quiescent phase; **G_1-S-G_2** – interphase; **M** – cell division).

Single MNP-mediated gene transfer to astrocytes shows approximately 60% transfection efficiency (*Pickard et al., 2010; Tickle et al, 2015*). With regard to the use of a magneto-multifection strategy to further enhance gene transfer, the findings here show significantly increased transfection efficiency compared with single transfection protocols (> 80%

versus 60%). The results show that not only is a wider population of the target cells being transfected, but a subpopulation of those cells also show repeat transgene expression, indicative of repeat MNP:plasmid uptake.

Taken together, these overall findings have significant implications for tissue engineering and transplant mediated delivery of therapeutic biomolecules, offering a two-fold benefit for drug/gene delivery in regenerative therapy applications. For example, for clinical applications enhanced transgene expression would produce greater quantities of therapeutic biomolecules intended to promote neuroregenerative processes i.e. growth factors such as BDNF and FGF2 which promote nerve fibre regeneration (*for example, Deinhardt & Chao, 2014; Liang et al., 2010; Zagrebelsky & Korte, 2014*) and blood vessel growth respectively (*Gorin et al., 2016*). Hence a subpopulation of cells exhibiting high levels of gene expression could be more beneficial for slow release applications, due to the timeframe over which the transgene is diluted through proliferative processes. Conversely, a population containing a large proportion of transfected cells (albeit with low transgene expression per cell) can be advantageous for immediate 'one-step' release of a drug or growth protein.

Consequently, these findings emphasise the importance of identifying the most effective combinations of frequency and amplitude for use in magnetofection protocols, to optimise gene transfer to a particular neural cell population. However it is clear that more research is needed to fully elucidate the relevance of intracellular processing and cell cycle dynamics to gene transfer, and to firmly establish the mechanisms underlying magnetofection strategies. It is evident that the use of a magnetic field, at the optimal frequency and amplitude for each specific cell type, enhances transfection efficiency overall and, probably of key importance for regenerative applications, considerably enhances the extent of gene expression in individual cells. Of major importance, contrary to the widely held

belief that increased labelling is a precursor to enhanced transgene expression, the findings from this study would suggest that optimal transgene expression, at least in respect of astrocytes, may be due to *lower* particle uptake per cell – a novel finding in magnetolabelling studies.

Further detailed analyses of these processes using electron microscopy, lysotracker analyses and plasmid-tagging, in conjunction with cell cycle synchronisation, are warranted to elucidate the cellular mechanisms that contribute to successful MNP-mediated transfection in neural cells. Moreover, of key importance here is the bespoke optimisation of magnetofection strategies on a cell-specific basis.

Chapter 6
Future direction and concluding comments

6.1 Summary of key research findings

The research that comprises this thesis has studied three aspects of a combinatorial approach applicable to the delivery of primary-derived astrocytes as a cell transplant population; MNP-mediated gene transfer, MP-labelling for non-invasive cell tracking under MRI, and the development of a viable 3-dimensional hydrogel construct to act as a carrier for protective delivery of a neural cell transplant. The key research findings from each series of studies are summarised below.

Chapter 3 Endocytotic potential governs magnetic particle loading in dividing neural cells

Astrocytes are a highly endocytotic neural cell, and as such, showed rapid (4 h) uptake of high magnetite content particles (MP-5x). At 24 h post-particle exposure, MP-labelling efficiency was >98% for both MP-1x and MP-5x particles. Application of a magnetic field at both time points significantly promoted MP-5x particle accumulation within the cells. Despite the proliferative nature of these cells, the initial high loading of these particles facilitated long term retention over an extended time frame of 21 days. Dynamic time-lapse imaging showed particle dilution to be a result of particle inheritance to the daughter cells of dividing astrocytes. This inheritance was asymmetrical, resulting in a sub-population of cells with continued utility for tracking. Viability assays reported the high safety profile of these particles and the methodologies employed. A novel methodology was developed which provided an unbiased, robust quantifiable measure of particle accumulation on a cell-by-cell basis.

Chapter 4 Non-invasive tracking of neural cells in implantable materials

The substrate on which astrocytes were cultured differentially affected their morphological characteristics. Cells grown within a 3-dimensional hydrogel showed morphologies closer to that of their *in vivo* counterpart, having a small cell soma and being highly branched, and also possessing a stellate morphology. Use of a combinatorial approach, that of growing exogenously MP-labelled astrocytes within a 3-dimensional hydrogel construct, addresses the challenge presented with transplant of cell suspension into a lesion site. In this context, cellular distribution of MP-5x labelled astrocytes was homogenous throughout the width and the depth of the construct, with networked bundles of aligned astrocytic processes throughout the gel. The cells showed a more quiescent profile within the gel, consistent with other studies showing that collagen inhibited proliferation of encapsulated astrocytes. Safety assessments showed a high level of cell viability and safety of protocols over time. A novel approach was developed to investigate endocytotic features in astrocytes. This comprised the embedding of the gel within Spurr resin, facilitating visualisation of the subcellular features under TEM.

Chapter 5 Influence of amplitude of oscillating magnetic fields on MNP-mediated gene transfer to astrocytes

Transfection efficiency in astrocytes is not enhanced further by amplitude of oscillation, but rather, amplitude plays a greater role in influencing the extent of transgene expression in individual cells. A magneto-multifection strategy significantly increased transfection efficiency compared with single MNP:plasmid dose. Correlation between MNP uptake and transgene expression revealed an inverse relationship, in that high transgene expression was associated with low levels of particle accumulation. This would propose two different strategies for potential drug/gene delivery to the injury site. High numbers of transfected

cells would deliver a single efficient short term delivery of the therapeutic molecule, whereas a cell population with high levels of transgene expression could potentially deliver a steady longer term release of the therapeutic molecule to the target site.

6.2 Future direction

To have clear direction, it is necessary to have an understanding of the barriers to recovery, and matching these to a range of potential repair strategies *(Ahuja & Fehlings, 2016; Dunnett & Rosser, 2014; Xu & Onifer, 2009)* (*Table 6.1*).

Table 6.1 Barriers to recovery and proposed mechanism

Barriers to recovery	Proposed mechanism
Spinal cord loses its structural framework	Bridging the lesion gap with implants functionalised with neurotrophic factors and guidance channels
Glial scarring as a result of astrogliosis resulting in barrier to axonal ingrowth	A better understanding of the glial scar and how to incorporate this knowledge in promoting regeneration of SCI
Fibroblast infiltration results in dense fibrous scar binding growth inhibitory molecules	Reducing growth inhibitory molecules; Addition of neurotrophic and growth factors
Upregulation of CSPGs and cytokines further inhibit neurite outgrowth and axon regeneration	Use of chondroitinase ABC to reduce CSPG upregulation; elevating potential for axon capacity for regeneration
Loss of oligodendrocytes results in neuron demyelination leading to lack of myelin support and release of growth inhibitors from degrading myelin	Overcoming myelin-associated inhibitors; cell transplant of OPCs in implant to promote myelination; implant promotes axonal ingrowth
CSPGs activate the RHO-Rock cascade resulting in growth cone collapse and retraction	Downstream inhibition of EGFR inhibits RHO-Rock cascade; facilitate reinnervation of denervated targets
Syrinx formation prevents axonal ingrowth	Bridging the gap and enhancing directed axonal growth with guidance channels
No trophic or structural support to support ingrowing axons	Bridging the gap with functionalised implants
Infiltration of Schwann cells causes pain and spasticity	Protecting from secondary injury

Significant advances have been made in recent years in regeneration of the injured spinal cord which has translated to functional outcomes, in research and in the clinic. The challenges still to be met however cannot be addressed through the continued use of separate procedures. There is an array of factors that contribute to the damage inherent to a SCI, and therefore it is impractical to suppose that one therapeutic strategy alone will overturn the failure to regenerate and see successful functional recovery (*Xu & Onifer., 2009*). It is becoming increasingly clear that the way forward to recovery and regeneration of the injured spinal cord is that of a combinatorial approach. So what is the future direction for the research strategies developed within this project?

The findings of this research have been discussed extensively within each relevant chapter, and therefore will not be elucidated further here. However, based on these findings, there are a number of areas in which these approaches could be developed.

1). Cell cycle dynamics are a plausible explanation for the heterogeneity between particle uptake *versus* transgene expression in MNP-mediated gene transfer to astrocytes (*Chapter 5*). In this context, a number of 'hot spots' have been identified for each stage of particle uptake - from particle:plasmid association with the cell membrane, to intranuclear delivery of the pDNA, to subsequent transgene expression by the cell (*Akita et al., 2007*; *Brunner et al., 2002; Castro et al., 1997; James & Giorgio, 2000; Tseng et al., 1999*). What is unclear are the factors that govern these mechanisms. Bearing in mind that intracellular processing has been identified as a multi-stage process (*Pollard et al., 1998; Tinsley et al., 2004; Zabner et al., 1995*), do the dynamics of the cell cycle 'hold' particles at certain stages? A further question that arises from this is (how) are these dynamics influenced with application of a magnetic field? An important consideration with a study of this kind is that in stopping or synchronising the cell cycle, only approximately 35% of astrocytes subsequently rejoin the cell cycle, either overall or at any one time (*Murphy*,

1990). This has implications at an experimental level, as a large proportion of the cell population has effectively been removed. This would need addressing first, to be able to fully elucidate the findings in relation to the dynamics of the cell cycle.

2). The most effective combinations of frequency and amplitude (F1 Hz; 200 μm) for use in magnetofection protocols for astrocytes (*Chapter 5*) significantly increased transfection efficiency (>80%), and of key importance to regenerative applications, considerably enhanced the *extent* of gene expression in individual cells. An inverse relationship was found between particle uptake and transgene expression, in that high transgene expression was correlated with low particle uptake. As discussed within the relevant chapter, this offers a two-fold benefit for drug/gene delivery in regenerative therapy applications in respect of slow release or immediate 'one-step' release of a drug or growth protein. Thus, it is critical to further investigate the mechanisms underlying this to propose the opportunity of specifically engineering the desired transgene-expressing subpopulation. This understanding would prove highly applicable to gene/ drug delivery to promote recovery.

The use of a hydrogel construct in a combinatorial approach is an exciting, emerging field, and the findings from this project offer many opportunities for developing this further in respect of both basic and translational science.

3). Having developed and optimised the methodologies for a 3-dimensional hydrogel construct capable of supporting a viable MP-labelled astrocyte population, it would now be pertinent to use this combinatorial approach to form an intraconstruct gel with transgene (*gfp*) expressing astrocytes. Considering that application of optimal magnetofection parameters are required to enhance transfection efficiency and extent of transgene expression in these cells, an exogenous magnetofection approach would be required prior

to associating the cells with the collagen construct. Of particular interest here is that *gfp* expression in 2-dimensional culture (*Chapter 5*) peaks at approximately 48 h, being the timeframe over which this transgene is diluted through proliferative processes. Considering that substrate differentially affects astrocyte morphology and function (*Chapter 4*), how would the substrate (2-dimensional culture plastic *vs.* 3-dimensional gel) affect the timeframe of *gfp* expression?

4). The translational purpose of combining transgene-expressing astrocytes within a gel construct is to act as a carrier for delivery of a genetically engineered cell transplant to a target site. Thus, it is pertinent to investigate and elucidate both the time-frame and the mechanism of delivery from the construct to the lesion site. In reducing animal use, an *in vitro* 3-D organotypic slice model has been developed that replicates spinal cord cellular responses to *in vivo* SCI (*Weightman et al., 2014; 2016*). Use of this model could be proposed with these functionalised gels. Transplant of these gels into the lesion slice model would allow investigation and evaluation of time frame and mechanism of delivery, with the potential for findings analogous to *in vivo* SCI.

5). To fully realise a combinatorial approach applicable to clinical application, a magnetic particle is needed that offers high efficiency in gene delivery *and* high sensitivity as a contrast agent for non-invasive tracking with MRI. In this regard, a multifunctional magnetic particle has been trialled in NSCs that may offer promise to astrocytes (*Adams et al., 2016*). It showed high sensitivity with MRI, although transfection efficiency was low with these cells (<5%). NSCs are typically understood to be 'hard-to-label', therefore it would be interesting to trial this particle with astrocytes, a highly endocytotic cell. Use of a magnetic particle that had these dual capabilities could offer a full combinatorial approach for translational application. There are however, a number of considerations. To confer utility for cell tracking under MRI required initial high loading of a high magnetite content

particle (*Chapter 3 and Chapter 4*). In the same manner, the extent of transgene expression in astrocytes was determined by particle loading, with an inverse relationship found between transgene expression and particle uptake (*Chapter 5*). Thus, there would appear to be two different mechanisms at play here. Therefore, to find a particle that meets these disparate requirements requires an initial understanding of the mechanisms by which *i*) particle:pDNA is intracellularly processed and *ii*) oscillating magnetic fields influence uptake and intracellular processing. It is needful to elucidate the characteristics of each of the particles. It has to be realised that the optimal parameters for particle/particle:pDNA uptake *are specific to the cell and the particle used.* Trialling any new particle with this cell population will require systematic adjusting of each of the parameters.

6). There still remains a major challenge to be addressed in extrapolating the findings from rodent-based research to translational application in humans, not least because of the difference in astrocyte characteristics. To meet this challenge, replication of the methodologies developed here with human astrocytes would be highly interesting and of considerable value to translational application. The argument for *primary-derived* rodent neural cells is pertinent to rodent-based *in vitro* research, as there are a number of considerations that would preclude the use of primary human neural cells, most notably, ethical considerations and supply. Human astrocyte cell lines are available, although within ethical consent guidelines, human neural tissue that would otherwise be discarded is one possibility for use, with published protocols already in place (*Ridet et al., 1999; 2003*).

7). The need to improve cell survival is a pressing one. The benefits promised through cell transplant are being hampered by the lack of efficacy in surgical techniques – a challenge that has been extensively addressed within this project. However, cell survival is being hampered by the hostile environment into which they are transplanted and the lack of growth promoting factors. Therefore, it is here that the use of a combinatorial approach

becomes clear. Use of the construct developed within this thesis in conjunction with the 3D multicellular lesion slice model (*Weightman et al., 2016*) has considerable developmental potential as a biological model to assess tissue bioengineering in the injured spinal cord. The 3-dimensional carrier developed here acts as a vehicle to the lesion site; promising a number of advantages. It can be placed in the lesion site to provide a scaffold for growth. It can be functionalised with growth factors, neurotrophins, inhibitory molecules, anti-inflammatory molecules or drugs. It can transport an engineered cell transplant that can promote (re)myelination, growth and trophic support to the ingrowing axons. It can be engineered to act as a guidance channel. But, most importantly, this carrier offers two protective advantages. It acts as a protective delivery system for the encapsulated cell transplant, and continues to provide protection to the cell transplant and to the ingrowing axons when grafted into the hostile environment of the injured spinal cord. The findings from research such as this could be extrapolated to translational application.

6.3 Concluding comment

Research conducted at the bench is moving forward with an eye to translational application. The future direction to overcome the barriers to regeneration and recovery is through systematic research, and a greater understanding of the mechanisms underlying the non-regenerative injured spinal cord. But the most promising route of mediating repair, recovery and regeneration within the injured spinal cord is that of a combinatorial approach.

References

(AISA). *American Spinal Injury Association classification criteria* [Online]. http://boneandspine.com/what-is-asia-score-and-how-it-helps-in-classification-of-spinal-injury/. [Accessed 09-09 2016].
(ASTERIAS BIOTHERAPEUTICS, I., 2016). *ClinicalTrials.gov Identifier: NCT02302157* [Online]. https://clinicaltrials.gov/ct2/show/NCT02302157 [Accessed 09-09 2016].
(NINDS). *National Institute of Neurological Disorders and Stroke* [Online]. http://www.ninds.nih.gov/disorders/sci/detail_sci.htm: National Institute of Neurological Disorders and Stroke (NINDS). [Accessed 04-09 2016].
(UPMC). *UPMC Life Changing Medicine* [Online]. http://www.upmc.com/Services/rehab/rehab-institute/conditions/spinal-cord-injury/education-spinal-injury/Pages/bowel-bladder-and-sexual-function.aspx: University of Pittsburgh Medical Center. [Accessed 12-09 2016].
(WHO). *World Health Organisation* [Online]. http://www.who.int/mediacentre/factsheets/fs384/en/. [Accessed 23-08 2016].
ABBOTT, N. J., RONNBACK, L. & HANSSON, E. 2006. Astrocyte-endothelial interactions at the blood-brain barrier. *Nat Rev Neurosci,* 7**,** 41-53.
ADAMS, C., ISRAEL, L. L., OSTROVSKY, S., TAYLOR, A., POPTANI, H., LELLOUCHE, J. P. & CHARI, D. 2016. Development of Multifunctional Magnetic Nanoparticles for Genetic Engineering and Tracking of Neural Stem Cells. *Adv Healthc Mater,* 5**,** 841-9.
ADAMS, C. F., PICKARD, M. R. & CHARI, D. M. 2013. Magnetic nanoparticle mediated transfection of neural stem cell suspension cultures is enhanced by applied oscillating magnetic fields. *Nanomedicine,* 9**,** 737-41.
ADAMS, C. F., RAI, A., SNEDDON, G., YIU, H. H., POLYAK, B. & CHARI, D. M. 2015. Increasing magnetite contents of polymeric magnetic particles dramatically improves labeling of neural stem cell transplant populations. *Nanomedicine,* 11**,** 19-29.
AHUJA, C. S., MARTIN, A. R. & FEHLINGS, M. 2016. Recent advances in managing a spinal cord injury secondary to trauma. *F1000Res,* 5.
AKITA, H., ITO, R., KAMIYA, H., KOGURE, K. & HARASHIMA, H. 2007. Cell cycle dependent transcription, a determinant factor of heterogeneity in cationic lipid-mediated transgene expression. *J Gene Med,* 9**,** 197-207.
AL AHMAD, A., TABOADA, C. B., GASSMANN, M. & OGUNSHOLA, O. O. 2011. Astrocytes and pericytes differentially modulate blood-brain barrier characteristics during development and hypoxic insult. *J Cereb Blood Flow Metab,* 31**,** 693-705.
ALEXIS, F., PRIDGEN, E., MOLNAR, L. K. & FAROKHZAD, O. C. 2008. Factors affecting the clearance and biodistribution of polymeric nanoparticles. *Mol Pharm,* 5**,** 505-15.
ALOVSKAYA, A., ALEKSEEVA, T., PHILLIPS, J. B., KING, V. & BROWN, R. A. 2007. Fibronectin, Collagen, Fibrin - Components of Extracellular Matrix for Nerve Regeneration. *Topics in Tissue Engineering,* 3.
ANDERSON, M. A., BURDA, J. E., REN, Y., AO, Y., O'SHEA, T. M., KAWAGUCHI, R., COPPOLA, G., KHAKH, B. S., DEMING, T. J. & SOFRONIEW, M. V. 2016. Astrocyte scar formation aids central nervous system axon regeneration. *Nature,* 532**,** 195-200.
ASGHARIAN, A., BANAN, M. & NAJMABADI, H. 2014. Optimizing A Lipocomplex-Based Gene Transfer Method into HeLa Cell Line. *Cell J,* 15**,** 372-7.
ASHER, R. A., MORGENSTERN, D. A., SHEARER, M. C., ADCOCK, K. H., PESHEVA, P. & FAWCETT, J. W. 2002. Versican is upregulated in CNS injury and is a product of oligodendrocyte lineage cells. *J Neurosci,* 22**,** 2225-36.
ASSUNCAO-SILVA, R. C., GOMES, E. D., SOUSA, N., SILVA, N. A. & SALGADO, A. J. 2015. Hydrogels and Cell Based Therapies in Spinal Cord Injury Regeneration. *Stem Cells Int,* 2015**,** 948040.
AU, C., MUTKUS, L., DOBSON, A., RIFFLE, J., LALLI, J. & ASCHNER, M. 2007. Effects of nanoparticles on the adhesion and cell viability on astrocytes. *Biol Trace Elem Res,* 120**,** 248-56.
AZIZI, S. A. & KRYNSKA, B. 2013. Derivation of neuronal cells from fetal normal human astrocytes (NHA). *Methods Mol Biol,* 1078**,** 89-96.

BALASUBRAMANIAN, S., PACKARD, J. A., LEACH, J. B. & POWELL, E. M. 2016. Three-Dimensional Environment Sustains Morphological Heterogeneity and Promotes Phenotypic Progression During Astrocyte Development. *Tissue Eng Part A,* 22**,** 885-98.

BARRY, D. & MCDERMOTT, K. 2005. Differentiation of radial glia from radial precursor cells and transformation into astrocytes in the developing rat spinal cord. *Glia,* 50**,** 187-97.

BARYSHEV, M., VAINAUSKA, D., KOZIREVA, S. & KARPOVS, A. 2011. New Device for Enhancement of Liposomal Magnetofection Efficiency of Cancer Cells. *International Journal Of Medical, Health, Biomedical, Bioengineering and Pharmaceutical Engineering,* 5**,** 469-472.

BEHRMAN, A. L. & HARKEMA, S. J. 2000. Locomotor training after human spinal cord injury: a series of case studies. *Phys Ther,* 80**,** 688-700.

BERNSEN, M. R., GUENOUN, J., VAN TIEL, S. T. & KRESTIN, G. P. 2015. Nanoparticles and clinically applicable cell tracking. *Br J Radiol,* 88**,** 20150375.

BERNSTEIN, J. J. & GOLDBERG, W. J. 1991. Grafted fetal astrocyte migration can prevent host neuronal atrophy: comparison of astrocytes from cultures and whole piece donors. *Restor Neurol Neurosci,* 2**,** 261-70.

BLITS, B. & BUNGE, M. B. 2006. Direct gene therapy for repair of the spinal cord. *J Neurotrauma,* 23**,** 508-20.

BO, X., WU, D., YEH, J. & ZHANG, Y. 2011. Gene Therapy Approaches for Neuroprotection and Axonal Regeneration after Spinal Cord and Spinal Root Injury. *Current Gene Therapy,* 11**,** 101-115.

BRACKEN, M. B. 2012. Steroids for acute spinal cord injury (Review). *Cochrane Database of Systematic Reviews.*

BRADLEY, W. G. 1990. Critical review of ganglioside and thyrotropin-releasing hormone in peripheral neuromuscular diseases. *Muscle Nerve,* 13,833-842.

BROWN, R. A. 2013. In the beginning there were soft collagen-cell gels: towards better 3D connective tissue models? *Exp Cell Res,* 319**,** 2460-9.

BRUNNER, S., FURTBAUER, E., SAUER, T., KURSA, M. & WAGNER, E. 2002. Overcoming the nuclear barrier: cell cycle independent nonviral gene transfer with linear polyethylenimine or electroporation. *Mol Ther,* 5**,** 80-6.

BULTE, J. W., DOUGLAS, T., WITWER, B., ZHANG, S. C., STRABLE, E., LEWIS, B. K., ZYWICKE, H., MILLER, B., VAN GELDEREN, P., MOSKOWITZ, B. M., DUNCAN, I. D. & FRANK, J. A. 2001. Magnetodendrimers allow endosomal magnetic labeling and in vivo tracking of stem cells. *Nat Biotechnol,* 19**,** 1141-7.

BULTE, J. W. & KRAITCHMAN, D. L. 2004. Iron oxide MR contrast agents for molecular and cellular imaging. *NMR Biomed,* 17**,** 484-99.

BULTE, J. W., ZHANG, S., VAN GELDEREN, P., HERYNEK, V., JORDAN, E. K., DUNCAN, I. D. & FRANK, J. A. 1999. Neurotransplantation of magnetically labeled oligodendrocyte progenitors: magnetic resonance tracking of cell migration and myelination. *Proc Natl Acad Sci U S A,* 96**,** 15256-61.

BUXBOIM, A., RAJAGOPAL, K., BROWN, A. E. & DISCHER, D. E. 2010. How deeply cells feel: methods for thin gels. *J Phys Condens Matter,* 22**,** 194116.

CANTON, I. & BATTAGLIA, G. 2012. Endocytosis at the nanoscale. *Chem Soc Rev,* 41**,** 2718-39.

CAO, Q., HE, Q., WANG, Y., CHENG, X., HOWARD, R. M., ZHANG, Y., DEVRIES, W. H., SHIELDS, C. B., MAGNUSON, D. S., XU, X. M., KIM, D. H. & WHITTEMORE, S. R. 2010. Transplantation of ciliary neurotrophic factor-expressing adult oligodendrocyte precursor cells promotes remyelination and functional recovery after spinal cord injury. *J Neurosci,* 30**,** 2989-3001.

CASTRO, M. G., GOYA, R. G., SOSA, Y. E., ROWE, J., LARREGINA, A., MORELLI, A. & LOWENSTEIN, P. R. 1997. Expression of transgenes in normal and neoplastic anterior pituitary cells using recombinant adenoviruses: long term expression, cell cycle dependency, and effects on hormone secretion. *Endocrinology,* 138**,** 2184-94.

CEN, L., NEOH, K. G., SUN, J., HU, F., LIU, W., CUI, L. & CAO, Y. 2009. Labeling of Adipose-Derived Stem Cells by Oleic-Acid-Modified Magnetic Nanoparticles. *Advanced Functional Materials,* 19**,** 1158-1166.

CERQUEIRA, S. R., OLIVEIRA, J. M., SILVA, N. A., LEITE-ALMEIDA, H., RIBEIRO-SAMY, S., ALMEIDA, A., MANO, J. F., SOUSA, N., SALGADO, A. J. & REIS, R. L. 2013. Microglia response and in vivo therapeutic potential of methylprednisolone-loaded dendrimer nanoparticles in spinal cord injury. *Small,* 9**,** 738-49.

CHAUDHURI, A., BATTAGLIA, G. & GOLESTANIAN, R. 2011. The effect of interactions on the cellular uptake of nanoparticles. *Phys Biol,* 8**,** 046002.

CHEN, A., XU, X. M., KLEITMAN, N. & BUNGE, M. B. 1996. Methylprednisolone administration improves axonal regeneration into Schwann cell grafts in transected adult rat thoracic spinal cord. *Exp Neurol,* 138**,** 261-76.

CHEN, J., HUANG, N., MA, B., MAITZ, M. F., WANG, J., LI, J., LI, Q., ZHAO, Y., XIONG, K. & LIU, X. 2013. Guidance of stem cells to a target destination in vivo by magnetic nanoparticles in a magnetic field. *ACS Appl Mater Interfaces,* 5**,** 5976-85.

CHEN, Y. & SWANSON, R. A. 2003. Astrocytes and brain injury. *J Cereb Blood Flow Metab,* 23**,** 137-49.

CHU, T., ZHOU, H., LI, F., WANG, T., LU, L. & FENG, S. 2014. Astrocyte transplantation for spinal cord injury: current status and perspective. *Brain Res Bull,* 107**,** 18-30.

COLE, R. & DE VELLIS, J. 2001. Preparation of astrocyte, oligodendrocyte, and microglia cultures from primary rat cerebral cultures. *In:* FEDEROFF, S. & RICHARDSON, A. (eds.) *Protocols for Neural Cell Culture.* 3rd. Ed. ed. Totowa, NJ: Humana Press, Inc.

COLOMBO, J. A., QUINN, B. & PUISSANT, V. 2002. Disruption of astroglial interlaminar processes in Alzheimer's disease. *Brain Res Bull,* 58**,** 235-42.

COLOMBO, J. A. & REISIN, H. D. 2004. Interlaminar astroglia of the cerebral cortex: a marker of the primate brain. *Brain Res,* 1006**,** 126-31.

COLOMBO, J. A., REISIN, H. D., JONES, M. & BENTHAM, C. 2005. Development of interlaminar astroglial processes in the cerebral cortex of control and Down's syndrome human cases. *Exp Neurol,* 193**,** 207-17.

CORTI, S., NIZZARDO, M., SIMONE, C., FALCONE, M., DONADONI, C., SALANI, S., RIZZO, F., NARDINI, M., RIBOLDI, G., MAGRI, F., ZANETTA, C., FARAVELLI, I., BRESOLIN, N. & COMI, G. P. 2012. Direct reprogramming of human astrocytes into neural stem cells and neurons. *Exp Cell Res,* 318**,** 1528-41.

COSTANTINI, L. C., BAKOWSKA, J. C., BREAKEFIELD, X. O. & ISACSON, O. 2000. Gene therapy in the CNS. *Gene Ther,* 7**,** 93-109.

COUMANS, J. V., LIN, T. T., DAI, H. N., MACARTHUR, L., MCATEE, M., NASH, C. & BREGMAN, B. S. 2001. Axonal regeneration and functional recovery after complete spinal cord transection in rats by delayed treatment with transplants and neurotrophins. *J Neurosci,* 21**,** 9334-44.

CROMPTON, K. E., TOMAS, D., FINKELSTEIN, D. I., MARR, M., FORSYTHE, J. S. & HORNE, M. K. 2006. Inflammatory response on injection of chitosan/GP to the brain. *J Mater Sci Mater Med,* 17**,** 633-9.

DAHMANI, C., MYKHAYLYK, O., HELLING, F., GOTZ, S., WEYH, T., HERZOG, H. & PLANJ, C. 2013. Rotational magnetic pulses enhance the magnetofection efficiency in vitro in adherent and suspension cells. *Journal of Magnetism and Magnetic Materials,* 332**,** 163-171.

DAI, G., LIU, X., ZHANG, Z., YANG, Z., DAI, Y. & XU, R. 2013. Transplantation of autologous bone marrow mesenchymal stem cells in the treatment of complete and chronic cervical spinal cord injury. *Brain Res,* 1533**,** 73-9.

DANBOLT, N. C. 2001. Glutamate uptake. *Prog Neurobiol,* 65**,** 1-105.

DAVIES, J. E., HUANG, C., PROSCHEL, C., NOBLE, M., MAYER-PROSCHEL, M. & DAVIES, S. J. 2006. Astrocytes derived from glial-restricted precursors promote spinal cord repair. *J Biol,* 5**,** 7.

DAVIES, J. E., PROSCHEL, C., ZHANG, N., NOBLE, M., MAYER-PROSCHEL, M. & DAVIES, S. J. 2008. Transplanted astrocytes derived from BMP- or CNTF-treated glial-restricted precursors have opposite effects on recovery and allodynia after spinal cord injury. *J Biol,* 7**,** 24.

DAVIES, P. F. & ROSS, R. 1980. Growth-mediated, density-dependent inhibition of endocytosis in cultured arterial smooth muscle cells. *Exp Cell Res,* 129**,** 329-36.

DAVIES, S. J., SHIH, C. H., NOBLE, M., MAYER-PROSCHEL, M., DAVIES, J. E. & PROSCHEL, C. 2011. Transplantation of specific human astrocytes promotes functional recovery after spinal cord injury. *PLoS One,* 6**,** e17328.

DE LIMA, M. C., DA CRUZ, M. T., CARDOSO, A. L., SIMOES, S. & DE ALMEIDA, L. P. 2005. Liposomal and viral vectors for gene therapy of the central nervous system. *Curr Drug Targets CNS Neurol Disord,* 4**,** 453-65.

DE PAUL, M. A., PALMER, M., LANG, B. T., CUTRONE, R., TRAN, A. P., MADALENA, K. M., BOGAERTS, A., HAMILTON, J. A., DEANS, R. J., MAYS, R. W., BUSCH, S. A. & SILVER, J. 2015. Intravenous multipotent adult progenitor cell treatment decreases inflammation leading to functional recovery following spinal cord injury. *Sci Reports,* 5, 16795, DOI: 10.1038/srep16795.

DI LULLO, G. A., SWEENEY, S. M., KORKKO, J., ALA-KOKKO, L., ALA-KOKKO, S. A. & JAMES, D. 2002. Mapping the ligand-binding sites and disease-associated mutations on the most abundant protein in the human, type I collagen. *J Biol Chem,* 277 (6), 4223-4231.

DEINHARDT, K. & CHAO, M. V. 2014. Shaping neurons: Long and short range effects of mature and proBDNF signalling upon neuronal structure. *Neuropharmacology,* 76 Pt C**,** 603-9.

DISCHER, D. E., JANMEY, P. & WANG, Y. L. 2005. Tissue cells feel and respond to the stiffness of their substrate. *Science,* 310**,** 1139-43.

DOBSON, J. 2008. Remote control of cellular behaviour with magnetic nanoparticles. *Nat Nanotechnol,* 3**,** 139-43.

DRINKUT, A., TERESHCHENKO, Y., SCHULZ, J. B., BAHR, M. & KUGLER, S. 2012. Efficient gene therapy for Parkinson's disease using astrocytes as hosts for localized neurotrophic factor delivery. *Mol Ther,* 20**,** 534-43.

DUNNETT, S. B. & ROSSER, A. E. 2014. Challenges for taking primary and stem cells into clinical neurotransplantation trials for neurodegenerative disease. *Neurobiol Dis,* 61**,** 79-89.

DUNNING, M. D., LAKATOS, A., LOIZOU, L., KETTUNEN, M., FFRENCH-CONSTANT, C., BRINDLE, K. M. & FRANKLIN, R. J. 2004. Superparamagnetic iron oxide-labeled Schwann cells and olfactory ensheathing cells can be traced in vivo by magnetic resonance imaging and retain functional properties after transplantation into the CNS. *J Neurosci,* 24**,** 9799-810.

EAST, E., DE OLIVEIRA, D. B., GOLDING, J. P. & PHILLIPS, J. B. 2010. Alignment of astrocytes increases neuronal growth in three-dimensional collagen gels and is maintained following plastic compression to form a spinal cord repair conduit. *Tissue Eng Part A,* 16**,** 3173-84.

EAST, E., GOLDING, J. P. & PHILLIPS, J. B. 2009. A versatile 3D culture model facilitates monitoring of astrocytes undergoing reactive gliosis. *J Tissue Eng Regen Med,* 3**,** 634-46.

EAST, E., GOLDING, J. P. & PHILLIPS, J. B. 2012. Engineering an integrated cellular interface in three-dimensional hydrogel cultures permits monitoring of reciprocal astrocyte and neuronal responses. *Tissue Eng Part C Methods,* 18**,** 526-36.

ECCLESTON, P. A., MIRSKY, R. & JESSEN, K. R. 1989. Type I collagen preparations inhibit DNA synthesis in glial cells of the peripheral nervous system. *Exp Cell Res,* 182**,** 173-85.

EL-SAYED, A. & HARASHIMA, H. 2013. Endocytosis of gene delivery vectors: from clathrin-dependent to lipid raft-mediated endocytosis. *Mol Ther,* 21**,** 1118-30.

ERICSON, C., WICTORIN, K. & LUNDBERG, C. 2002. Ex vivo and in vitro studies of transgene expression in rat astrocytes transduced with lentiviral vectors. *Exp Neurol,* 173**,** 22-30.

ERRINGTON, R. J., BROWN, M. R., SILVESTRE, O. F., NJOH, K. L., CHAPPELL, S. C., KHAN, I. A., REES, P., WILKS, S. P., SMITH, P. J. & SUMMERS, H. D. 2010. Single cell nanoparticle tracking to model cell cycle dynamics and compartmental inheritance. *Cell Cycle,* 9**,** 121-30.

FAN, C., ZHENG, Y., CHENG, X., QI, X., BU, P., LUO, X., KIM, D. H. & CAO, Q. 2013. Transplantation of D15A-expressing glial-restricted-precursor-derived astrocytes improves anatomical and locomotor recovery after spinal cord injury. *Int J Biol Sci,* 9**,** 78-93.

FAULKNER, J. R., HERRMANN, J. E., WOO, M. J., TANSEY, K. E., DOAN, N. B. & SOFRONIEW, M. V. 2004. Reactive astrocytes protect tissue and preserve function after spinal cord injury. *J Neurosci,* 24**,** 2143-55.

FAWCETT, J. W. & ASHER, R. A. 1999. The glial scar and central nervous system repair. *Brain Res Bull,* 49**,** 377-91.

FELLIN, T. & CARMIGNOTO, G. 2004. Neurone-to-astrocyte signalling in the brain represents a distinct multifunctional unit. *J Physiol,* 559**,** 3-15.

FERNANDES, A. R., ADAMS, C. F., FURNESS, D. N. & CHARI, D. M. 2015. Early Membrane Responses to Magnetic Particles are Predictors of Particle Uptake in Neural Stem Cells. *Particle & Particle Systems Characterization,* 32**,** 661-667.

FERNANDES, A. R. & CHARI, D. M. 2014. A multicellular, neuro-mimetic model to study nanoparticle uptake in cells of the central nervous system. *Integr Biol (Camb),* 6**,** 855-61.

FILOUS, A. R., MILLER, J. H., COULSON-THOMAS, Y. M., HORN, K. P., ALILAIN, W. J. & SILVER, J. 2010. Immature astrocytes promote CNS axonal regeneration when combined with chondroitinase ABC. *Dev Neurobiol,* 70**,** 826-41.

FINK, K. L. & CAFFERTY, W. B. J. 2016. Reorganization of intact descending motor circuits to replace lost connections after injury. *Neurotherapeutics,* 13, 370-381.

FITZHARRIS, M., CRIPPS, R. A. & LEE, B. B. 2014. Estimating the global incidence of traumatic spinal cord injury. *Spinal Cord,* 52**,** 117-22.

FOURIKI, A., FARROW, N., CLEMENTS, M. A. & DOBSON, J. 2010. Evaluation of the magnetic field requirements for nanomagnetic gene transfection. *Nano Rev,* 1.

FRAMPTON, J. P., HYND, M. R., SHULER, M. L. & SHAIN, W. 2011. Fabrication and optimization of alginate hydrogel constructs for use in 3D neural cell culture. *Biomed Mater,* 6**,** 015002.

FRANKLIN, R. J., CRANG, A. J. & BLAKEMORE, W. F. 1991. Transplanted type-1 astrocytes facilitate repair of demyelinating lesions by host oligodendrocytes in adult rat spinal cord. *J Neurocytol,* 20**,** 420-30.

FREITAS-ANDRADE, M. & NAUS, C. C. 2016. Astrocytes in neuroprotection and neurodegeneration: The role of connexin43 and pannexin1. *Neuroscience,* 323**,** 207-21.

FURLANI, E. P. & NG, K. C. 2008. Nanoscale magnetic biotransport with application to magnetofection. *Phys Rev E Stat Nonlin Soft Matter Phys,* 77**,** 061914.

GALANDIUK, S., RAQUE, G., APPEL, S. & POLK, H. C. Jr. 1993. The two-edged sword of large-dose steroids for spinal cord trauma. *Ann Surg,* 218 (4), 419-425.

GE, S. & PACHTER, J. S. 2006. Isolation and culture of microvascular endothelial cells from murine spinal cord. *J Neuroimmunol,* 177**,** 209-14.

GEPPERT, M., HOHNHOLT, M. C., NURNBERGER, S. & DRINGEN, R. 2012. Ferritin up-regulation and transient ROS production in cultured brain astrocytes after loading with iron oxide nanoparticles. *Acta Biomater,* 8**,** 3832-9.

GIULIANO, F., HULTLING, C., EL MASRY, W. S., SMITH, M. D., OSTERLOH, I. H., ORR, M. & MAYTOM, M. 1999. Randomized trial of sildenafil for the treatment of erectile dysfunction in spinal cord injury. Sildenafil Study Group. *Ann Neurol,* 46**,** 15-21.

GOETZ, L. L. & MUMMANEMI, R. 2014. *Posttraumatic syringomyelia* [Online]. http://emedicine.medscape.com/article/322348-overview. [Accessed 04-09 2016].

GORIN, C., ROCHEFORT, G. Y., BASCETIN, R., YING, H., LESIEUR, J., SADOINE, J., BECKOUCHE, N., BERNDT, S., NOVAIS, A., LESAGE, M., HOSTEN, B., VERCELLINO, L., MERLET, P., LE-DENMAT, D., MARCHIOL, C., LETOURNEUR, D., NICOLETTI, A., VITAL, S. O., POLIARD, A., SALMON, B., MULLER, L., CHAUSSAIN, C. & GERMAIN, S. 2016. Priming Dental Pulp Stem Cells With Fibroblast Growth Factor-2 Increases Angiogenesis of Implanted Tissue-

Engineered Constructs Through Hepatocyte Growth Factor and Vascular Endothelial Growth Factor Secretion. *Stem Cells Transl Med,* 5**,** 392-404.
GRANGER, N., BLAMIRES, H., FRANKLIN, R. J. & JEFFERY, N. D. 2012. Autologous olfactory mucosal cell transplants in clinical spinal cord injury: a randomized double-blinded trial in a canine translational model. *Brain,* 135**,** 3227-37.
GRATTON, S. E., NAPIER, M. E., ROPP, P. A., TIAN, S. & DESIMONE, J. M. 2008. Microfabricated particles for engineered drug therapies: elucidation into the mechanisms of cellular internalization of PRINT particles. *Pharm Res,* 25**,** 2845-52.
GRINNELL, F. 2000. Fibroblast-collagen-matrix contraction: growth-factor signalling and mechanical loading. *Trends Cell Biol,* 10**,** 362-5.
GUEST, J., BENAVIDES, F., PADGETT, K., MENDEZ, E. & TOVAR, D. 2011. Technical aspects of spinal cord injections for cell transplantation. Clinical and translational considerations. *Brain Res Bull,* 84**,** 267-79.
GUO, Z., YANG, N. S., JIAO, S., SUN, J., CHENG, L., WOLFF, J. A. & DUNCAN, I. D. 1996. Efficient and sustained transgene expression in mature rat oligodendrocytes in primary culture. *J Neurosci Res,* 43**,** 32-41.
HAAS, C. & FISCHER, I. 2013. Human astrocytes derived from glial restricted progenitors support regeneration of the injured spinal cord. *J Neurotrauma,* 30**,** 1035-52.
HAASE, A., ROTT, S., MANTION, A., GRAF, P., PLENDL, J., THUNEMANN, A. F., MEIER, W. P., TAUBERT, A., LUCH, A. & REISER, G. 2012. Effects of silver nanoparticles on primary mixed neural cell cultures: uptake, oxidative stress and acute calcium responses. *Toxicol Sci,* 126**,** 457-68.
HAIDET-PHILLIPS, A. M., ROYBON, L., GROSS, S. K., TUTEJA, A., DONNELLY, C. J., RICHARD, J. P., KO, M., SHERMAN, A., EGGAN, K., HENDERSON, C. E. & MARAGAKIS, N. J. 2014. Gene profiling of human induced pluripotent stem cell-derived astrocyte progenitors following spinal cord engraftment. *Stem Cells Transl Med,* 3**,** 575-85.
HAN, Q., JIN, W., XIAO, Z., NI, H., WANG, J., KONG, J., WU, J., LIANG, W., CHEN, L., ZHAO, Y., CHEN, B. & DAI, J. 2010. The promotion of neural regeneration in an extreme rat spinal cord injury model using a collagen scaffold containing a collagen binding neuroprotective protein and an EGFR neutralizing antibody. *Biomaterials,* 31**,** 9212-20.
HANNILA, S. S. & FILBIN, M. T. 2008. The role of cyclic AMP signaling in promoting axonal regeneration after spinal cord injury. *Exp Neurol,* 209**,** 321-32.
HANS, M. L. & LOWMAN, A. M. 2002. Biodegradeable nanoparticles for drug delivery and targeting. *Current Opinion in Solid State and Materials Science,* 6**,** 319-327.
HARRISON, R., MARKIDES, H., MORRIS, R. H., RICHARDS, P., EL HAJ, A. J. & SOTTILE, V. 2016. Autonomous magnetic labelling of functional mesenchymal stem cells for improved traceability and spatial control in cell therapy applications. *J Tissue Eng Regen Med*.
HARUSH-FRENKEL, O., DEBOTTON, N., BENITA, S. & ALTSCHULER, Y. 2007. Targeting of nanoparticles to the clathrin-mediated endocytic pathway. *Biochem Biophys Res Commun,* 353**,** 26-32.
HAWKINS, B. T., GREGO, S. & SELLGREN, K. L. 2015. Three-dimensional culture conditions differentially affect astrocyte modulation of brain endothelial barrier function in response to transforming growth factor beta1. *Brain Res,* 1608**,** 167-76.
HAWRYLUK, G. W., ROWLAND, J., KWON, B. K. & FEHLINGS, M. G. 2008. Protection and repair of the injured spinal cord: a review of completed, ongoing, and planned clinical trials for acute spinal cord injury. *Neurosurg Focus,* 25**,** E14.
HAYASHI, K., HASHIMOTO, M., KODA, M., NAITO, A. T., MURATA, A., OKAWA, A., TAKAHASHI, K. & YAMAZAKI, M. 2011. Increase of sensitivity to mechanical stimulus after transplantation of murine induced pluripotent stem cell-derived astrocytes in a rat spinal cord injury model. *J Neurosurg Spine,* 15**,** 582-93.

HE, C., HU, Y., YIN, L., TANG, C. & YIN, C. 2010. Effects of particle size and surface charge on cellular uptake and biodistribution of polymeric nanoparticles. *Biomaterials,* 31**,** 3657-66.
HEJCL, A., LESNY, P., PRADNY, M., MICHALEK, J., JENDELOVA, P., STULIK, J. & SYKOVA, E. 2008. Biocompatible hydrogels in spinal cord injury repair. *Physiological Research,* 57**,** S121-S132.
HEYMER, A., HADDAD, D., WEBER, M., GBURECK, U., JAKOB, P. M., EULERT, J. & NOTH, U. 2008. Iron oxide labelling of human mesenchymal stem cells in collagen hydrogels for articular cartilage repair. *Biomaterials,* 29**,** 1473-83.
HILL, C. E., BEATTIE, M. S. & BRESNAHAN, J. C. 2001. Degeneration and sprouting of identified descending supraspinal axons after contusive spinal cord injury in the rat. *Exp Neurol,* 171**,** 153-69.
HILL, C. E., HURTADO, A., BLITS, B., BAHR, B. A., WOOD, P. M., BARTLETT BUNGE, M. & OUDEGA, M. 2007. Early necrosis and apoptosis of Schwann cells transplanted into the injured rat spinal cord. *Eur J Neurosci,* 26**,** 1433-45.
HILL, C. E., PROSCHEL, C., NOBLE, M., MAYER-PROSCHEL, M., GENSEL, J. C., BEATTIE, M. S. & BRESNAHAN, J. C. 2004. Acute transplantation of glial-restricted precursor cells into spinal cord contusion injuries: survival, differentiation, and effects on lesion environment and axonal regeneration. *Exp Neurol,* 190**,** 289-310.
HIRANO, M. & GOLDMAN, J. E. 1988. Gliogenesis in rat spinal cord: evidence for origin of astrocytes and oligodendrocytes from radial precursors. *J Neurosci Res,* 21**,** 155-67.
HOEHN, M., KUSTERMANN, E., BLUNK, J., WIEDERMANN, D., TRAPP, T., WECKER, S., FOCKING, M., ARNOLD, H., HESCHELER, J., FLEISCHMANN, B. K., SCHWINDT, W. & BUHRLE, C. 2002. Monitoring of implanted stem cell migration in vivo: a highly resolved in vivo magnetic resonance imaging investigation of experimental stroke in rat. *Proc Natl Acad Sci U S A,* 99**,** 16267-72.
HOFMANN-AMTENBRINK, M., HOFMANN, H. & MONTET, X. 2010. Superparamagnetic nanoparticles - a tool for early diagnostics. *Swiss Med Wkly,* 140**,** w13081.
HOHNHOLT, M. C. & DRINGEN, R. 2013. Uptake and metabolism of iron and iron oxide nanoparticles in brain astrocytes. *Biochem Soc Trans,* 41**,** 1588-92.
HOHNHOLT, M. C., GEPPERT, M., LUTHER, E. M., PETTERS, C., BULCKE, F. & DRINGEN, R. 2013. Handling of iron oxide and silver nanoparticles by astrocytes. *Neurochem Res,* 38**,** 227-39.
HOSSAIN, M. A., FRAMPTON, A. E. & BAGUL, A. 2014. Challenges facing in vivo tracking of mesenchymal stem cells used for tissue regeneration. *Expert Rev Med Devices,* 11**,** 9-13.
HU, W. W., WANG, Z., ZHANG, S. S., JIANG, L., ZHANG, J., ZHANG, X., LEI, Q. F., PARK, H. J., FANG, W. J. & CHEN, Z. 2014. Morphology and functions of astrocytes cultured on water-repellent fractal tripalmitin surfaces. *Biomaterials,* 35**,** 7386-97.
HURLBERT, R. J. 2000. Methylprednisolone for acute spinal cord injury: an appropriate standard of care. *J Neurosurg,* 93 (1 Suppl), 1-7.
HUSSAIN, S., GARANTZIOTIS, S., RODRIGUES-LIMA, F., DUPRET, J. M., BAEZA-SQUIBAN, A. & BOLAND, S. 2014. Intracellular signal modulation by nanomaterials. *Adv Exp Med Biol,* 811**,** 111-34.
HUTH, S., LAUSIER, J., GERSTING, S. W., RUDOLPH, C., PLANK, C., WELSCH, U. & ROSENECKER, J. 2004. Insights into the mechanism of magnetofection using PEI-based magnetofectins for gene transfer. *J Gene Med,* 6**,** 923-36.
HWANG, D. H., KIM, B. G., KIM, E. J., LEE, S. I., JOO, I. S., SUH-KIM, H., SOHN, S. & KIM, S. U. 2009. Transplantation of human neural stem cells transduced with Olig2 transcription factor improves locomotor recovery and enhances myelination in the white matter of rat spinal cord following contusive injury. *BMC Neurosci,* 10**,** 117.
ITO, A., SHINKAI, M., HONDA, H. & KOBAYASHI, T. 2005. Medical application of functionalized magnetic nanoparticles. *J Biosci Bioeng,* 100**,** 1-11.

JAMES, M. B. & GIORGIO, T. D. 2000. Nuclear-associated plasmid, but not cell-associated plasmid, is correlated with transgene expression in cultured mammalian cells. *Mol Ther,* 1**,** 339-46.
JENDELOVA, P., HERYNEK, V., URDZIKOVA, L., GLOGAROVA, K., KROUPOVA, J., ANDERSSON, B., BRYJA, V., BURIAN, M., HAJEK, M. & SYKOVA, E. 2004. Magnetic resonance tracking of transplanted bone marrow and embryonic stem cells labeled by iron oxide nanoparticles in rat brain and spinal cord. *J Neurosci Res,* 76**,** 232-43.
JENKINS, S. I., PICKARD, M. R., FURNESS, D. N., YIU, H. H. & CHARI, D. M. 2013. Differences in magnetic particle uptake by CNS neuroglial subclasses: implications for neural tissue engineering. *Nanomedicine (Lond),* 8**,** 951-68.
JENKINS, S. I., PICKARD, M. R., GRANGER, N. & CHARI, D. M. 2011. Magnetic nanoparticle-mediated gene transfer to oligodendrocyte precursor cell transplant populations is enhanced by magnetofection strategies. *ACS Nano,* 5**,** 6527-38.
JENKINS, S. I., YIU, H. H. P., ROSSEINSKY, M. J. & CHARI, D. M. 2014. Magnetic nanoparticles for oligodendrocyte precursor cell transplantation therapies: progress and challenges. *Molecular Cellular Therapy,* 2**,** 23.
JIN, H., HELLER, D. A., SHARMA, R. & STRANO, M. S. 2009. Size-dependent cellular uptake and expulsion of single-walled carbon nanotubes: single particle tracking and a generic uptake model for nanoparticles. *ACS Nano,* 3**,** 149-58.
JIN, Y., NEUHUBER, B., SINGH, A., BOUYER, J., LEPORE, A., BONNER, J., HIMES, T., CAMPANELLI, J. T. & FISCHER, I. 2011. Transplantation of human glial restricted progenitors and derived astrocytes into a contusion model of spinal cord injury. *J Neurotrauma,* 28**,** 579-94.
JOHN, G. R., LEE, S. C. & BROSNAN, C. F. 2003. Cytokines: Powerful Regulators of Glial Cell Activation. *The Neuroscientist,* 9**,** 10-22.
JOHNSON, B., TOLAND, B., CHOKSHI, R., MOCHALIN, V., KOUTZAKI, S. & POLYAK, B. 2010. Magnetically responsive paclitaxel-loaded biodegradable nanoparticles for treatment of vascular disease: preparation, characterization and in vitro evaluation of anti-proliferative potential. *Curr Drug Deliv,* 7**,** 263-73.
JONES, L. L., OUDEGA, M., BUNGE, M. B. & TUSZYNSKI, M. H. 2001. Neurotrophic factors, cellular bridges and gene therapy for spinal cord injury. *J Physiol,* 533**,** 83-9.
JOOSTEN, E. A. & GRIBNAU, A. A. 1989. Immunocytochemical localization of cell adhesion molecule L1 in developing rat pyramidal tract. *Neurosci Lett,* 100**,** 94-8.
JOOSTEN, E. A., VELDHUIS, W. B. & HAMERS, F. P. 2004. Collagen containing neonatal astrocytes stimulates regrowth of injured fibers and promotes modest locomotor recovery after spinal cord injury. *J Neurosci Res,* 77**,** 127-42.
KABU, S., GAO, Y., KWON, B. K. & LABHASETWAR, V. 2015. Drug delivery, cell-based therapies, and tissue engineering approaches for spinal cord injury. *J Control Release,* 219**,** 141-54.
KAMAU, S. W., HASSA, P. O., STEITZ, B., PETRI-FINK, A., HOFMANN, H., HOFMANN-AMTENBRINK, M., VON RECHENBERG, B. & HOTTIGER, M. O. 2006. Enhancement of the efficiency of non-viral gene delivery by application of pulsed magnetic field. *Nucleic Acids Res,* 34**,** e40.
KAMBER, D., EREZ, H. & SPIRA, M. E. 2009. Local calcium-dependent mechanisms determine whether a cut axonal end assembles a retarded endbulb or competent growth cone. *Exp Neurol,* 219**,** 112-25.
KANDEL, E. R., SCHWARTZ, J. H. & JESSELL, T. M. 1991. *Principles of Neuroscience,* NY, USA, McGraw-Hill, New York.
KANEKO, A., MATSUSHITA, A. & SANKAI, Y. 2015. A 3D nanofibrous hydrogel and collagen sponge scaffold promotes locomotor functional recovery, spinal repair, and neuronal regeneration after complete transection of the spinal cord in adult rats. *Biomed Mater,* 10**,** 015008.
KARAOZ, E., KABATAS, S., DURUKSU, G., OKCU, A., SUBASI, C., AY, B., MUSLUMAN, M. & CIVELEK, E. 2012. Reduction of lesion in injured rat spinal cord and partial functional recovery of

motility after bone marrow derived mesenchymal stem cell transplantation. *Turk Neurosurg,* 22**,** 207-17.
KATIYAR, K. S., WINTER, C. C., STRUZYNA, L. A., HARRIS, J. P. & CULLEN, D. K. 2016. Mechanical elongation of astrocyte processes to create living scaffolds for nervous system regeneration. *J Tissue Eng Regen Med*.
KEIRSTEAD, H. S., NISTOR, G., BERNAL, G., TOTOIU, M., CLOUTIER, F., SHARP, K. & STEWARD, O. 2005. Human embryonic stem cell-derived oligodendrocyte progenitor cell transplants remyelinate and restore locomotion after spinal cord injury. *J Neurosci,* 25**,** 4694-705.
KERSTETTER, A. E. & MILLER, R. H. 2012. Isolation and culture of spinal cord astrocytes. *Methods Mol Biol,* 814, 93-104.
KETTLER, K., VELTMAN, K., VAN DE MEENT, D., VAN WEZEL, A. & HENDRIKS, A. J. 2014. Cellular uptake of nanoparticles as determined by particle properties, experimental conditions, and cell type. *Environ Toxicol Chem,* 33**,** 481-92.
KHORRAMI, M. H., JAVID, A., MOSHTAGHI, D., NOURIMAHDAVI, K., MORTAZAVI, A. & ZIA, H. R. 2010. Sildenafil efficacy in erectile dysfunction secondary to spinal cord injury depends on the level of cord injuries. *Int J Androl,* 33**,** 861-4.
KIM, J. A., ABERG, C., SALVATI, A. & DAWSON, K. A. 2012. Role of cell cycle on the cellular uptake and dilution of nanoparticles in a cell population. *Nat Nanotechnol,* 7**,** 62-8.
KIRCHER, M. F., GAMBHIR, S. S. & GRIMM, J. 2011. Noninvasive cell-tracking methods. *Nat Rev Clin Oncol,* 8**,** 677-88.
KISS, A. L. & BOTOS, E. 2009. Endocytosis via caveolae: alternative pathway with distinct cellular compartments to avoid lysosomal degradation? *J Cell Mol Med,* 13**,** 1228-37.
KLIOT, M., SMITH, G. M., SIEGAL, J. D. & SILVER, J. 1990. Astrocyte-polymer implants promote regeneration of dorsal root fibers into the adult mammalian spinal cord. *Exp Neurol,* 109**,** 57-69.
KOFUJI, P. & NEWMAN, E. A. 2004. Potassium buffering in the central nervous system. *Neuroscience,* 129**,** 1045-56.
KOU, L., SUN, J., ZHAI, Y. & HE, Z. 2013. The endocytosis and intracellular fate of nanomedicines: Implication for rational design. *Asian Journal of Pharmaceutical Sciences,* 8**,** 1-10.
KRUEGER, W. H., MADISON, D. L. & PFEIFFER, S. E. 1998. Transient transfection of oligodendrocyte progenitors by electroporation. *Neurochem Res,* 23**,** 421-6.
KUSHCHAYEV, S. V., GIERS, M. B., HOM ENG, D., MARTIROSYAN, N. L., ESCHBACHER, J. M., MORTAZAVI, M. M., THEODORE, N., PANITCH, A. & PREUL, M. C. 2016. Hyaluronic acid scaffold has a neuroprotective effect in hemisection spinal cord injury. *J Neurosurg Spine,* 25**,** 114-24.
LACOMBLEZ, L., BOUCHE, P., BENSIMON, G. & MEININGER. 1989. A double-blind, placebo-controlled trial of high doses of gangliosides in amyotrophic lateral sclerosis. *Neurology,* 39,1635-1637.
LAI, J. C., LAI, M. B., JANDHYAM, S., DUKHANDE, V. V., BHUSHAN, A., DANIELS, C. K. & LEUNG, S. W. 2008. Exposure to titanium dioxide and other metallic oxide nanoparticles induces cytotoxicity on human neural cells and fibroblasts. *Int J Nanomedicine,* 3**,** 533-45.
LAMKOWSKY, M. C., GEPPERT, M., SCHMIDT, M. M. & DRINGEN, R. 2012. Magnetic field-induced acceleration of the accumulation of magnetic iron oxide nanoparticles by cultured brain astrocytes. *J Biomed Mater Res A,* 100**,** 323-34.
LAURENTT, N., SAPET, C., LE GOURRIEREC, L., BERTOSIO, E. & ZELPHATI, O. 2011. Nucleic acid delivery using magnetic nanoparticles: the Magnetofection technology. *Ther Deliv,* 2**,** 471-82.
LEE, B. B., CRIPPS, R. A., FITZHARRIS, M. & WING, P. C. 2014. The global map for traumatic spinal cord injury epidemiology: update 2011, global incidence rate. *Spinal Cord,* 52**,** 110-6.

LEE, W., MALARKEY, E. B., REYES, R. C. & PARPURA, V. 2008. Micropit: A New Cell Culturing Approach for Characterization of Solitary Astrocytes and Small Networks of these Glial Cells. *Front Neuroeng,* 1**,** 2.

LENTZ, T. B., GRAY, S. J. & SAMULSKI, R. J. 2012. Viral vectors for gene delivery to the central nervous system. *Neurobiol Dis,* 48**,** 179-88.

LESNIAK, A., SALVATI, A., SANTOS-MARTINEZ, M. J., RADOMSKI, M. W., DAWSON, K. A. & ABERG, C. 2013. Nanoparticle adhesion to the cell membrane and its effect on nanoparticle uptake efficiency. *J Am Chem Soc,* 135**,** 1438-44.

LI, G., CHE, M. T., ZHANG, K., QIN, L. N., ZHANG, Y. T., CHEN, R. Q., RONG, L. M., LIU, S., DING, Y., SHEN, H. Y., LONG, S. M., WU, J. L., LING, E. A. & ZENG, Y. S. 2016. Graft of the NT-3 persistent delivery gelatin sponge scaffold promotes axon regeneration, attenuates inflammation, and induces cell migration in rat and canine with spinal cord injury. *Biomaterials,* 83**,** 233-48.

LI, K., JAVED, E., HALA, T. J., SANNIE, D., REGAN, K. A., MARAGAKIS, N. J., WRIGHT, M. C., POULSEN, D. J. & LEPORE, A. C. 2015b. Transplantation of glial progenitors that overexpress glutamate transporter GLT1 preserves diaphragm function following cervical SCI. *Mol Ther,* 23**,** 533-48.

LI, K., JAVED, E., SCURA, D., HALA, T. J., SEETHARAM, S., FALNIKAR, A., RICHARD, J. P., CHORATH, A., MARAGAKIS, N. J., WRIGHT, M. C. & LEPORE, A. C. 2015a. Human iPS cell-derived astrocyte transplants preserve respiratory function after spinal cord injury. *Exp Neurol,* 271**,** 479-92.

LI, N. & LEUNG, G. K. 2015. Oligodendrocyte Precursor Cells in Spinal Cord Injury: A Review and Update. *Biomed Res Int,* 2015**,** 235195.

LI, Y., CARLSTEDT, T., BERTHOLD, C. H. & RAISMAN, G. 2004. Interaction of transplanted olfactory-ensheathing cells and host astrocytic processes provides a bridge for axons to regenerate across the dorsal root entry zone. *Exp Neurol,* 188**,** 300-8.

LI, Y., DECHERCHI, P. & RAISMAN, G. 2003. Transplantation of olfactory ensheathing cells into spinal cord lesions restores breathing and climbing. *J Neurosci,* 23**,** 727-31.

LI, Y., FIELD, P. M. & RAISMAN, G. 1998. Regeneration of adult rat corticospinal axons induced by transplanted olfactory ensheathing cells. *J Neurosci,* 18**,** 10514-24.

LIANG, W., HAN, Q., JIN, W., XIAO, Z., HUANG, J., NI, H., CHEN, B., KONG, J., WU, J. & DAI, J. 2010. The promotion of neurological recovery in the rat spinal cord crushed injury model by collagen-binding BDNF. *Biomaterials,* 31**,** 8634-41.

LIBERTO, C. M., ALBRECHT, P. J., HERX, L. M., YONG, V. W. & LEVISON, S. W. 2004. Pro-regenerative properties of cytokine-activated astrocytes. *J Neurochem,* 89**,** 1092-100.

LIU, R., WANG, Z., GOU, L. & XU, H. 2015. A cortical astrocyte subpopulation inhibits axon growth in vitro and in vivo. *Mol Med Rep,* 12**,** 2598-606.

LIUZZI, F. J. & LASEK, R. J. 1987. Astrocytes block axonal regeneration in mammals by activating the physiological stop pathway. *Science,* 237, 642-645.

LOMBARDI, G., NELLI, F., CELSO, M., MENCARINI, M. & DEL POPOLO, G. 2012. Treating erectile dysfunction and central neurological diseases with oral phosphodiesterase type 5 inhibitors. Review of the literature. *J Sex Med,* 9**,** 970-85.

MA, Y., ZHANG, Z., WANG, X., XIA, W. & GU, H. 2011. Insights into the mechanism of magnetofection using MNPs-PEI/pDNA/free PEI magnetofectins. *Int J Pharm,* 419**,** 247-54.

MACAYA, D. & SPECTOR, M. 2012. Injectable hydrogel materials for spinal cord regeneration: a review. *Biomed Mater,* 7**,** 012001.

MACAYA, D. J., HAYAKAWA, K., ARAI, K. & SPECTOR, M. 2013. Astrocyte infiltration into injectable collagen-based hydrogels containing FGF-2 to treat spinal cord injury. *Biomaterials,* 34**,** 3591-602.

MACDONALD, C., BARBEE, K. & POLYAK, B. 2012. Force dependent internalization of magnetic nanoparticles results in highly loaded endothelial cells for use as potential therapy delivery vectors. *Pharm Res,* 29**,** 1270-81.

MAGISTRETTI, P. J. & PELLERIN, L. 1999. Cellular mechanisms of brain energy metabolism and their relevance to functional brain imaging. *Philos Trans R Soc Lond B Biol Sci,* 354**,** 1155-63.

MALATESTA, P., APPOLLONI, I. & CALZOLARI, F. 2008. Radial glia and neural stem cells. *Cell Tissue Res,* 331**,** 165-78.

MALDA, J., WOODFIELD, T. B., VAN DER VLOODT, F., KOOY, F. K., MARTENS, D. E., TRAMPER, J., VAN BLITTERSWIJK, C. A. & RIESLE, J. 2004. The effect of PEGT/PBT scaffold architecture on oxygen gradients in tissue engineered cartilaginous constructs. *Biomaterials,* 25**,** 5773-80.

MARAGAKIS, N. J. & ROTHSTEIN, J. D. 2006. Mechanisms of Disease: astrocytes in neurodegenerative disease. *Nat Clin Pract Neurol,* 2**,** 679-89.

MARTIN, J. H. 2016. Harnessing neural activity to promote repair of the damaged corticospinal system after spinal cord injury. *Neural Regen Res,* 11 (9), 1389-1391.

MATSUMOTO, T., TAMAKI, T., KAWAKAMI, M., YOSHIDA, M., ANDO, M. & YAMADA, H. 2001. Early complications of high-dose methylprednisolone sodium succinate treatment in the follow-up of acute cervical spinal cord injury. *Spine (Phila Pa 1976),* 26 (4), 426-430.

MAXWELL, W. L. 1996. Histopathological changes at central nodes of Ranvier after stretch-injury. *Microsc Res Tech,* 34**,** 522-35.

MAYER-PROSCHEL, M., KALYANI, A. J., MUJTABA, T. & RAO, M. S. 1997. Isolation of lineage-restricted neuronal precursors from multipotent neuroepithelial stem cells. *Neuron,* 19**,** 773-85.

MCBAIN, S. C., GRIESENBACH, U., XENARIOU, S., KERAMANE, A., BATICH, C. D., ALTON, E. W. & DOBSON, J. 2008. Magnetic nanoparticles as gene delivery agents: enhanced transfection in the presence of oscillating magnet arrays. *Nanotechnology,* 19**,** 405102.

MEGIAS, L., GUERRI, C., FORNAS, E., AZORIN, I., BENDALA, E., SANCHO-TELLO, M., DURAN, J. M., TOMAS, M., GOMEZ-LECHON, M. J. & RENAU-PIQUERAS, J. 2000. Endocytosis and transcytosis in growing astrocytes in primary culture. Possible implications in neural development. *Int J Dev Biol,* 44**,** 209-21.

MEIJS, M. F., TIMMERS, L., PEARSE, D. D., TRESCO, P. A., BATES, M. L., JOOSTEN, E. A., BUNGE, M. B. & OUDEGA, M. 2004. Basic fibroblast growth factor promotes neuronal survival but not behavioral recovery in the transected and Schwann cell implanted rat thoracic spinal cord. *J Neurotrauma,* 21**,** 1415-30.

MELCHELS, F. P., BARRADAS, A. M., VAN BLITTERSWIJK, C. A., DE BOER, J., FEIJEN, J. & GRIJPMA, D. W. 2010. Effects of the architecture of tissue engineering scaffolds on cell seeding and culturing. *Acta Biomater,* 6**,** 4208-17.

MERIENNE, N., LE DOUCE, J., FAIVRE, E., DEGLON, N. & BONVENTO, G. 2013. Efficient gene delivery and selective transduction of astrocytes in the mammalian brain using viral vectors. *Front Cell Neurosci,* 7**,** 106.

MERTENS, M. E., FRESE, J., BOLUKBAS, D. A., HRDLICKA, L., GOLOMBEK, S., KOCH, S., MELA, P., JOCKENHOVEL, S., KIESSLING, F. & LAMMERS, T. 2014a. FMN-coated fluorescent USPIO for cell labeling and non-invasive MR imaging in tissue engineering. *Theranostics,* 4**,** 1002-13.

MERTENS, M. E., HERMANN, A., BUHREN, A., OLDE-DAMINK, L., MOCKEL, D., GREMSE, F., EHLING, J., KIESSLING, F. & LAMMERS, T. 2014b. Iron Oxide-labeled Collagen Scaffolds for Non-invasive MR Imaging in Tissue Engineering. *Adv Funct Mater,* 24**,** 754-762.

MIRON-MENDOZA, M., KOPPAKA, V., ZHOU, C. & PETROLL, W. M. 2013. Techniques for assessing 3-D cell-matrix mechanical interactions in vitro and in vivo. *Exp Cell Res,* 319**,** 2470-80.

MITSUI, T., SHUMSKY, J. S., LEPORE, A. C., MURRAY, M. & FISCHER, I. 2005. Transplantation of neuronal and glial restricted precursors into contused spinal cord improves bladder and motor functions, decreases thermal hypersensitivity, and modifies intraspinal circuitry. *J Neurosci,* 25**,** 9624-36.

MOLOFSKY, A. V., KRENICK, R., ULLIAN, E., TSAI, H., DENEED, B., RICHARDSON, W. D., BARRES, B. A. & ROWITCH, D.H. 2012. Astrocytes and disease: A neurodevelopmental perspective. *Genes & Development,* 26, 891-907

MOOS, T. 2002. Brain iron homeostasis. *Dan Med Bull,* 49**,** 279-301.

MOOS, T., ROSENGREN NIELSEN, T., SKJORRINGE, T. & MORGAN, E. H. 2007. Iron trafficking inside the brain. *J Neurochem,* 103**,** 1730-40.

MOSHAYEDI, P., COSTA LDA, F., CHRIST, A., LACOUR, S. P., FAWCETT, J., GUCK, J. & FRANZE, K. 2010. Mechanosensitivity of astrocytes on optimized polyacrylamide gels analyzed by quantitative morphometry. *J Phys Condens Matter,* 22**,** 194114.

MUKHOPADHYAY, G., DOHERTY, P., WALSH, F. S., CROCKER, P. R. & FILBIN, M. T. 1994. A novel role for myelin-associated glycoprotein as an inhibitor of axonal regeneration. *Neuron,* 13**,** 757-67.

MURAKAMI, M. & KUDO, I. 2002. Phospholipase A2. *J Biochem,* 131**,** 285-92.

MURPHY, S. 1990. Generation of Astrocyte Cultures from Normal and Neoplastic Central Nervous System. *In:* CONN, P. M. (ed.) *Methods in Neurosciences: Cell Culture.* Academic Press Inc.

MYER, D. J., GURKOFF, G. G., LEE, S. M., HOVDA, D. A. & SOFRONIEW, M. V. 2006. Essential protective roles of reactive astrocytes in traumatic brain injury. *Brain,* 129**,** 2761-72.

MYKHAYLYK, O., ANTEQUERA, Y. S., VLASKOU, D. & PLANK, C. 2007. Generation of magnetic nonviral gene transfer agents and magnetofection in vitro. *Nat Protoc,* 2**,** 2391-411.

NAGAI, Y., MOMOI, T., SAITO, M., MITSUZAWA, E. & OBTANI, S. 1976. Ganglioside syndrome, a new autoimmune neurologic disorder, experimentally induced with brain gangliosides. *Neurosci Lett,* 2, 107-111.

NAGY, J. I. & RASH, J. E. 2000. Connexins and gap junctions of astrocytes and oligodendrocytes in the CNS. *Brain Res Brain Res Rev,* 32**,** 29-44.

NAKAGAWA, H., NINOMIYA, T., YAMASHITA, T. & TAKADA, M. 2015. Reorganization of corticospinal tract fibers after spinal cord injury in adult macaques. *Nat/Sci Reports,* 5,11986, DOI: 10.1038/srep11986.

NAKAMURA, M. & OKANO, H. 2013. Cell transplantation therapies for spinal cord injury focusing on induced pluripotent stem cells. *Cell Res,* 23**,** 70-80.

NAM, K., KIMURA, T., FUNAMOTO, S. & KISHIDA, A. 2010. Preparation of a collagen/polymer hybrid gel for tissue membranes. Part II: in vitro and in vivo biological properties of the collagen gels. *Acta Biomater,* 6**,** 409-17.

NICAISE, C., MITRECIC, D., FALNIKAR, A. & LEPORE, A. C. 2015. Transplantation of stem cell-derived astrocytes for the treatment of amyotrophic lateral sclerosis and spinal cord injury. *World J Stem Cells,* 7**,** 380-98.

NIU, W., ZANG, T., ZOU, Y., FANG, S., SMITH, D. K., BACHOO, R. & ZHANG, C. L. 2013. In vivo reprogramming of astrocytes to neuroblasts in the adult brain. *Nat Cell Biol,* 15**,** 1164-75.

NOBLE, M., DAVIES, J. E., MAYER-PROSCHEL, M., PROSCHEL, C. & DAVIES, S. J. 2011. Precursor cell biology and the development of astrocyte transplantation therapies: lessons from spinal cord injury. *Neurotherapeutics,* 8**,** 677-93.

NORENBERG, M. D., SMITH, J. & MARCILLO, A. 2004. The pathology of human spinal cord injury: defining the problems. *J Neurotrauma,* 21**,** 429-40.

NOUT, Y. S., CULP, E., SCHMIDT, M. H., TOVAR, C. A., PROSCHEL, C., MAYER-PROSCHEL, M., NOBLE, M. D., BEATTIE, M. S. & BRESNAHAN, J. C. 2011. Glial restricted precursor cell transplant with cyclic adenosine monophosphate improved some autonomic functions but resulted in a reduced graft size after spinal cord contusion injury in rats. *Exp Neurol,* 227**,** 159-71.

O'SHAUGHNESSY, T. J., LIN, H. J. & MA, W. 2003. Functional synapse formation among rat cortical neurons grown on three-dimensional collagen gels. *Neuroscience Letters,* 340**,** 169-172.
OBERHEIM, N. A., TAKANO, T., HAN, X., HE, W., LIN, J. H., WANG, F., XU, Q., WYATT, J. D., PILCHER, W., OJEMANN, J. G., RANSOM, B. R., GOLDMAN, S. A. & NEDERGAARD, M. 2009. Uniquely hominid features of adult human astrocytes. *J Neurosci,* 29**,** 3276-87.
OBERHEIM, N. A., WANG, X., GOLDMAN, S. & NEDERGAARD, M. 2006. Astrocytic complexity distinguishes the human brain. *Trends Neurosci,* 29**,** 547-53.
OGATA, K. & KOSAKA, T. 2002. Structural and quantitative analysis of astrocytes in the mouse hippocampus. *Neuroscience,* 113**,** 221-33.
OGAWA, Y., SAWAMOTO, K., MIYATA, T., MIYAO, S., WATANABE, M., NAKAMURA, M., BREGMAN, B. S., KOIKE, M., UCHIYAMA, Y., TOYAMA, Y. & OKANO, H. 2002. Transplantation of in vitro-expanded fetal neural progenitor cells results in neurogenesis and functional recovery after spinal cord contusion injury in adult rats. *J Neurosci Res,* 69**,** 925-33.
OH, J. M., CHOI, S. J., LEE, G. E., KIM, J. E. & CHOY, J. H. 2009. Inorganic metal hydroxide nanoparticles for targeted cellular uptake through clathrin-mediated endocytosis. *Chem Asian J,* 4**,** 67-73.
OH, N. & PARK, J. H. 2014. Endocytosis and exocytosis of nanoparticles in mammalian cells. *Int J Nanomedicine,* 9 Suppl 1**,** 51-63.
OUDEGA, M. & PEREZ, M. A. 2012. Corticospinal reorganization after spinal cord injury. *J Physiol,* 590 (16), 3647-3663.
PANDYA, K. A., WEANT, K. A. & COOK, A. M. 2010. High-dose methylprednisolone in acute spinal cord injuries: Proceed with caution. *Orthopedics,* 33,(5), 327-331
PEARSE, D. D., PEREIRA, F. C., MARCILLO, A. E., BATES, M. L., BERROCAL, Y. A., FILBIN, M. T. & BUNGE, M. B. 2004. cAMP and Schwann cells promote axonal growth and functional recovery after spinal cord injury. *Nat Med,* 10**,** 610-6.
PEARSE, D. D., SANCHEZ, A. R., PEREIRA, F. C., ANDRADE, C. M., PUZIS, R., PRESSMAN, Y., GOLDEN, K., KITAY, B. M., BLITS, B., WOOD, P. M. & BUNGE, M. B. 2007. Transplantation of Schwann cells and/or olfactory ensheathing glia into the contused spinal cord: Survival, migration, axon association, and functional recovery. *Glia,* 55**,** 976-1000.
PEDRAM, A., RAZANDI, M., HU, R. M. & LEVIN, E. R. 1998. Astrocyte progression from G1 to S phase of the cell cycle depends upon multiple protein interaction. *J Biol Chem,* 273**,** 13966-72.
PENCALET, P., SERGUERA, C., CORTI, O., PRIVAT, A., MALLET, J. & GIMENEZ Y RIBOTTA, M. 2006. Integration of genetically modified adult astrocytes into the lesioned rat spinal cord. *J Neurosci Res,* 83**,** 61-7.
PERALE, G., BIANCO, F., GIORDANO, C., MATTEOLI, M., MASI, M. & CIGADA, A. 2008. Engineering injured spinal cord with bone marrow derived stem cells and hydrogel based matrices : a glance at the state of art. *Journal of Applied Biomaterials & Biomechanics,* 6**,** 1-8.
PERALE, G., ROSSI, F., SUNDSTROM, E., BACCHIEGA, S., MASI, M., FORLONI, G. & VEGLIANESE, P. 2011. Hydrogels in spinal cord injury repair strategies. *ACS Chem Neurosci,* 2**,** 336-45.
PETTERS, C., THIEL, K. & DRINGEN, R. 2016. Lysosomal iron liberation is responsible for the vulnerability of brain microglial cells to iron oxide nanoparticles: comparison with neurons and astrocytes. *Nanotoxicology,* 10**,** 332-42.
PHILLIPS, J. B. & BROWN, R. A. 2011. Micro-structured Materials and Mechanical Cues in 3D Collagen Gels. *In:* HAYCOCK, J. W. (ed.) *3D Cell Culture: Methods and Protocols, Methods in Molecular Biology.* London, UK: Springer Science+Business Media LLC.
PICKARD, M. R., ADAMS, C. F., BARRAUD, P. & CHARI, D. M. 2015. Using magnetic nanoparticles for gene transfer to neural stem cells: stem cell propagation method influences outcomes. *J Funct Biomater,* 6**,** 259-76.

PICKARD, M. R., BARRAUD, P. & CHARI, D. M. 2011a. The transfection of multipotent neural precursor/stem cell transplant populations with magnetic nanoparticles. *Biomaterials,* 32**,** 2274-84.

PICKARD, M. R. & CHARI, D. M. 2010. Robust uptake of magnetic nanoparticles (MNPs) by central nervous system (CNS) microglia: implications for particle uptake in mixed neural cell populations. *Int J Mol Sci,* 11**,** 967-81.

PICKARD, M. R., JENKINS, S. I., KOLLER, C. J., FURNESS, D. N. & CHARI, D. M. 2011b. Magnetic nanoparticle labeling of astrocytes derived for neural transplantation. *Tissue Eng Part C Methods,* 17**,** 89-99.

PLACONE, A. L., MCGUIGGAN, P. M., BERGLES, D. E., GUERRERO-CAZARES, H., QUINONES-HINOJOSA, A. & SEARSON, P. C. 2015. Human astrocytes develop physiological morphology and remain quiescent in a novel 3D matrix. *Biomaterials,* 42**,** 134-43.

PLANK, C., SCHILLINGER, U., SCHERER, F., BERGEMANN, C., REMY, J. S., KROTZ, F., ANTON, M., LAUSIER, J. & ROSENECKER, J. 2003. The magnetofection method: using magnetic force to enhance gene delivery. *Biol Chem,* 384**,** 737-47.

PLANK, C., ZELPHATI, O. & MYKHAYLYK, O. 2011. Magnetically enhanced nucleic acid delivery. Ten years of magnetofection-progress and prospects. *Adv Drug Deliv Rev,* 63**,** 1300-31.

POLLARD, H., REMY, J. S., LOUSSOUARN, G., DEMOLOMBE, S., BEHR, J. P. & ESCANDE, D. 1998. Polyethylenimine but not cationic lipids promotes transgene delivery to the nucleus in mammalian cells. *J Biol Chem,* 273**,** 7507-11.

RAINETEAU, O. & SCHWAB, M. E. 2001. Plasticity of motor systems after incomplete spinal cord injury. *Nat Rev Neurosci*, 2,263-273.

RAMON-CUETO, A., CORDERO, M. I., SANTOS-BENITO, F. F. & AVILA, J. 2000. Functional recovery of paraplegic rats and motor axon regeneration in their spinal cords by olfactory ensheathing glia. *Neuron,* 25**,** 425-35.

REES, P., WILLS, J. W., BROWN, M. R., TONKIN, J., HOLTON, M. D., HONDOW, N., BROWN, A. P., BRYDSON, R., MILLAR, V., CARPENTER, A. E. & SUMMERS, H. D. 2014. Nanoparticle vesicle encoding for imaging and tracking cell populations. *Nat Methods,* 11**,** 1177-81.

REJMAN, J., OBERLE, V., ZUHORN, I. S. & HOEKSTRA, D. 2004. Size-dependent internalization of particles via the pathways of clathrin- and caveolae-mediated endocytosis. *Biochem J,* 377**,** 159-69.

RENAULT-MIHARA, F., OKADA, S., SHIBATA, S., NAKAMURA, M., TOYAMA, Y. & OKANO, H. 2008. Spinal cord injury: emerging beneficial role of reactive astrocytes' migration. *Int J Biochem Cell Biol,* 40**,** 1649-53.

RIDET, J. L., CORTI, O., PENCALET, P., HANOUN, N., HAMON, M., PHILIPPON, J. & MALLET, J. 1999. Toward autologous ex vivo gene therapy for the central nervous system with human adult astrocytes. *Hum Gene Ther,* 10**,** 271-80.

RIDET, J. L., SARKIS, C., SERGUERA, C., ZENNOU, V., CHARNEAU, P. & MALLET, J. 2003. Transplantation of human adult astrocytes: efficiency and safety requirements for an autologous gene therapy. *J Neurosci Res,* 72**,** 704-8.

RIEGLER, J., WELLS, J. A., KYRTATOS, P. G., PRICE, A. N., PANKHURST, Q. A. & LYTHGOE, M. F. 2010. Targeted magnetic delivery and tracking of cells using a magnetic resonance imaging system. *Biomaterials,* 31**,** 5366-71.

ROUACH, N., KOULAKOFF, A. & GIAUME, C. 2004. Neurons set the tone of gap junctional communication in astrocytic networks. *Neurochem Int,* 45**,** 265-72.

RUBIO, N., RODRIGUEZ, R. & AREVALO, M. A. 2004. In vitro myelination by oligodendrocyte precursor cells transfected with the neurotrophin-3 gene. *Glia,* 47**,** 78-87.

RUFF, C. A., WILCOX, J. T. & FEHLINGS, M. G. 2012. Cell-based transplantation strategies to promote plasticity following spinal cord injury. *Exp Neurol,* 235**,** 78-90.

RUOSLAHTI, E., BHATIA, S. N. & SAILOR, M. J. 2010. Targeting of drugs and nanoparticles to tumors. *J Cell Biol,* 188**,** 759-68.

RYAN, D. A. & FEDEROFF, H. J. 2007. Translational considerations for CNS gene therapy. *Expert Opin Biol Ther,* 7**,** 305-18.

SABERI, H., FIROUZI, M., HABIBI, Z., MOSHAYEDI, P., AGHAYAN, H. R., ARJMAND, B., HOSSEINI, K., RAZAVI, H. E. & YEKANINEJAD, M. S. 2011. Safety of intramedullary Schwann cell transplantation for postrehabilitation spinal cord injuries: 2-year follow-up of 33 cases. *J Neurosurg Spine,* 15**,** 515-25.

SABERI, H., MOSHAYEDI, P., AGHAYAN, H. R., ARJMAND, B., HOSSEINI, S. K., EMAMI-RAZAVI, S. H., RAHIMI-MOVAGHAR, V., RAZA, M. & FIROUZI, M. 2008. Treatment of chronic thoracic spinal cord injury patients with autologous Schwann cell transplantation: an interim report on safety considerations and possible outcomes. *Neurosci Lett,* 443**,** 46-50.

SANDHU, M. S., ROSS, H. H., LEE, K. Z., ORMEROD, B. K., REIER, P. J. & FULLER, D. D. 2016. Intraspinal transplantation of subventricular zone-derived neural progenitor cells improves phrenic motor output after high cervical spinal cord injury. *Exp Neurol*.

SANDROW-FEINBERG, H. R. & HOULE, J. D. 2015. Exercise after spinal cord injury as an agent for neuroprotection, regeneration and rehabilitation. *Brain Res,* 1619**,** 12-21.

SATTLER, R. & TYMIANSKI, M. 2001. Molecular mechanisms of glutamate receptor-mediated excitotoxic neuronal cell death. *Mol Neurobiol,* 24**,** 107-29.

SCEMES, E. SUADICANI, S. O. & SPRAY, D. C. 2000. Intercellular communication in spinal cord astrocytes: Fine tuning between gap junctions and P2 nucleotide receptors in calcium wave propagation. *J Neurosci,* 20 (4), 1435-1445.

SCHIPKE, C. G. & KETTENMANN, H. 2004. Astrocyte responses to neuronal activity. *Glia,* 47**,** 226-32.

SEEDS, N. W., SICONOLFI, L. B. & HAFFKE, S. P. 1997. Neuronal extracellular proteases facilitate cell migration, axonal growth, and pathfinding. *Cell Tissue Res,* 290**,** 367-70.

SELKIRK, S. M., GREENBERG, S. J., PLUNKETT, R. J., BARONE, T. A., LIS, A. & SPENCE, P. O. 2002. Syngeneic central nervous system transplantation of genetically transduced mature, adult astrocytes. *Gene Ther,* 9**,** 432-43.

SEO, T. B., CHANG, I. A., LEE, J. H. & NAMGUNG, U. 2013. Beneficial function of cell division cycle 2 activity in astrocytes on axonal regeneration after spinal cord injury. *J Neurotrauma,* 30**,** 1053-61.

SERGUERA, C., SARKIS, C., RIDET, J. L., COLIN, P., MOULLIER, P. & MALLET, J. 2001. Primary adult human astrocytes as an ex vivo vehicle for beta-glucuronidase delivery in the brain. *Mol Ther,* 3**,** 875-81.

SETOGUCHI, T., NAKASHIMA, K., TAKIZAWA, T., YANAGISAWA, M., OCHIAI, W., OKABE, M., YONE, K., KOMIYA, S. & TAGA, T. 2004. Treatment of spinal cord injury by transplantation of fetal neural precursor cells engineered to express BMP inhibitor. *Exp Neurol,* 189**,** 33-44.

SEYEDHASSANTEHRANI, N., LI, Y. & YAO, L. 2016. Dynamic behaviors of astrocytes in chemically modified fibrin and collagen hydrogels. *Integr Biol (Camb),* 8**,** 624-34.

SHAH, B., YIN, P. T., GHOSHAL, S. & LEE, K. B. 2013. Multimodal magnetic core-shell nanoparticles for effective stem-cell differentiation and imaging. *Angew Chem Int Ed Engl,* 52**,** 6190-5.

SHARP, J., FRAME, J., SIEGENTHALER, M., NISTOR, G. & KEIRSTEAD, H. S. 2010. Human embryonic stem cell-derived oligodendrocyte progenitor cell transplants improve recovery after cervical spinal cord injury. *Stem Cells,* 28**,** 152-63.

SHIH, C. H., LACAGNINA, M., LEUER-BISCIOTTI, K. & PROSCHEL, C. 2014. Astroglial-derived periostin promotes axonal regeneration after spinal cord injury. *J Neurosci,* 34**,** 2438-43.

SIEBERT, J. R., EADE, A. M. & OSTERHOUT, D. J. 2015. Biomaterial Approaches to Enhancing Neurorestoration after Spinal Cord Injury: Strategies for Overcoming Inherent Biological Obstacles. *Biomed Res Int,* 2015**,** 752572.

SILVA, N. A., SOUSA, N., REIS, R. L. & SALGADO, A. J. 2014. From basics to clinical: a comprehensive review on spinal cord injury. *Prog Neurobiol,* 114**,** 25-57.

SINGHAL, P. K., SASSI, S., LAN, L., AU, P., HALVORSEN, S. C., FUKUMURA, D., JAIN, R. K. & SEED, B. 2016. Mouse embryonic fibroblasts exhibit extensive developmental and phenotypic diversity. *Proc Natl Acad Sci U S A,* 113**,** 122-7.

SOENEN, S. J., HIMMELREICH, U., NUYTTEN, N., PISANIC, T. R., 2ND, FERRARI, A. & DE CUYPER, M. 2010. Intracellular nanoparticle coating stability determines nanoparticle diagnostics efficacy and cell functionality. *Small,* 6**,** 2136-45.

SOFRONIEW, M. V. 2015. Astrocyte barriers to neurotoxic inflammation. *Nature Rev Neurosci,* 16, 249-263.

SOFRONIEW, M. V., HOWE, C. L. & MOBLEY, W. C. 2001. Nerve growth factor signaling, neuroprotection, and neural repair. *Annu Rev Neurosci,* 24**,** 1217-81.

SOFRONIEW, M. V. & VINTERS, H. V. 2010. Astrocytes: biology and pathology. *Acta Neuropathol,* 119, 7-35

SONG, W., AMER, A., RYAN, D. & MARTIN, J. H. 2016. Combined motor cortex and spinal cord neuromodulation promotes corticospinal system functional and structural plasticity and motor function after injury. *Exp Neurol,* 277, 46-57.

SPURR, A. R. 1969. A low-viscosity epoxy resin embedding medium for electron microscopy. *J Ultrastruct Res,* 26**,** 31-43.

STEWARD, O., SHARP, K. G. & MATSUDAIRA YEE, K. 2014. Long-distance migration and colonization of transplanted neural stem cells. *Cell,* 156**,** 385-7.

STICHEL, C. C., HERMANNS, S., LUHMANN, H. J., LAUSBERG, F., NIERMANN, H., D'URSO, D., SERVOS, G., HARTWIG, H.-G. & MÜLLER, H. W. 1999. Inhibition of collagen IV deposition promotes regeneration of injured CNS axons. *European Journal of Neuroscience,* 11**,** 632-646.

SUBERVIOLA, B., GONZALEZ-CASTRO, A., LLORCA, J., ORTIZ-MELON, F. & MINAMBRES, E. 2008. Early complications of high-dose methylprednisolone in acute spinal cord injury patients. *Injury,* 39 (7), 748-752.

SUBRAMANIAN, M., LIM, J. & DOBSON, J. 2013. Enhanced nanomagnetic gene transfection of human prenatal cardiac progenitor cells and adult cardiomyocytes. *PLoS One,* 8**,** e69812.

SUMMERS, H. D., BROWN, M. R., HOLTON, M. D., TONKIN, J. A., HONDOW, N., BROWN, A. P., BRYDSON, R. & REES, P. 2013. Quantification of nanoparticle dose and vesicular inheritance in proliferating cells. *ACS Nano,* 7**,** 6129-37.

SUN, T. S., REN, J. X. & SHI, J. G. 2005. [Repair of acute spinal cord injury promoted by transplantation of olfactory ensheathing glia]. *Zhongguo Yi Xue Ke Xue Yuan Xue Bao,* 27**,** 143-7.

SUN, Z., YATHINDRANATH, V., WORDEN, M., THLIVERIS, J. A., CHU, S., PARKINSON, F. E., HEGMANN, T. & MILLER, D. W. 2013. Characterization of cellular uptake and toxicity of aminosilane-coated iron oxide nanoparticles with different charges in central nervous system-relevant cell culture models. *Int J Nanomedicine,* 8**,** 961-70.

SYKOVA, E. & JENDELOVA, P. 2005. Magnetic resonance tracking of implanted adult and embryonic stem cells in injured brain and spinal cord. *Ann N Y Acad Sci,* 1049**,** 146-60.

SYKOVA, E., JENDELOVA, P., URDZIKOVA, L., LESNY, P. & HEJCL, A. 2006. Bone marrow stem cells and polymer hydrogels--two strategies for spinal cord injury repair. *Cell Mol Neurobiol,* 26**,** 1113-29.

TABAKOW, P., RAISMAN, G., FORTUNA, W., CZYZ, M., HUBER, J., LI, D., SZEWCZYK, P., OKUROWSKI, S., MIEDZYBRODZKI, R., CZAPIGA, B., SALOMON, B., HALON, A., LI, Y., LIPIEC, J., KULCZYK, A. & JARMUNDOWICZ, W. 2014. Functional regeneration of supraspinal connections in a patient with transected spinal cord following transplantation of bulbar olfactory ensheathing cells with peripheral nerve bridging. *Cell Transplant,* 23**,** 1631-55.

TAKAMI, T., OUDEGA, M., BATES, M. L., WOOD, P. M., KLEITMAN, N. & BUNGE, M. B. 2002. Schwann cell but not olfactory ensheathing glia transplants improve hindlimb locomotor

performance in the moderately contused adult rat thoracic spinal cord. *J Neurosci,* 22**,** 6670-81.
TATE, M. C., SHEAR, D. A., HOFFMAN, S. W., STEIN, D. G. & LAPLACA, M. C. 2001. Biocompatibility of methylcellulose-based constructs designed for intracerebral gelation following experimental traumatic brain injury. *Biomaterials,* 22**,** 1113-23.
TENG, F. Y., HOR, C. H. & TANG, B. L. 2009. Emerging cues mediating astroglia lineage restriction of progenitor cells in the injured/diseased adult CNS. *Differentiation,* 77**,** 121-7.
THOMPSON, W. G. 1890. Successful Brain Grafting. *New York Medical Journal***,** 1-4.
TIAN, W. M., HOU, S. P., MA, J., ZHANG, C. L., XU, Q. Y., LEE, I. S., LI, H. D., SPECTOR, M. & CUI, F. Z. 2005. Hyaluronic acid-poly-D-lysine-based three-dimensional hydrogel for traumatic brain injury. *Tissue Eng,* 11**,** 513-25.
TICKLE, J. A., JENKINS, S. I., PICKARD, M. R. & CHARI, D. M. 2015. Influence of Amplitude of Oscillating Magnetic Fields on Magnetic Nanoparticle-Mediated Gene Transfer to Astrocytes. *Nano LIFE,* 05**,** 1450006.
TICKLE, J. A., JENKINS, S. I., POLYAK, B., PICKARD, M. R. & CHARI, D. M. 2016. Endocytotic potential governs magnetic particle loading in dividing neural cells: studying modes of particle inheritance. *Nanomedicine (Lond),* 11**,** 345-58.
TINSLEY, R. B., VESEY, M. J., BARATI, S., RUSH, R. A. & FERGUSON, I. A. 2004. Improved non-viral transfection of glial and adult neural stem cell lines and of primary astrocytes by combining agents with complementary modes of action. *J Gene Med,* 6**,** 1023-32.
TOY, D. & NAMGUNG, U. 2013. Role of glial cells in axonal regeneration. *Exp Neurobiol,* 22**,** 68-76.
TRAPPMANN, B. & CHEN, C. S. 2013. How cells sense extracellular matrix stiffness: a material's perspective. *Curr Opin Biotechnol,* 24**,** 948-53.
TREUEL, L., JIANG, X. & NIENHAUS, G. U. 2013. New views on cellular uptake and trafficking of manufactured nanoparticles. *J R Soc Interface,* 10**,** 20120939.
TSENG, W. C., HASELTON, F. R. & GIORGIO, T. D. 1999. Mitosis enhances transgene expression of plasmid delivered by cationic liposomes. *Biochim Biophys Acta,* 1445**,** 53-64.
UNSWORTH, J. M., ROSE, F. R., WRIGHT, E., SCOTCHFORD, C. A. & SHAKESHEFF, K. M. 2003. Seeding cells into needled felt scaffolds for tissue engineering applications. *J Biomed Mater Res A,* 66**,** 425-31.
VAN DEN BOSCH, L. & ROBBERECHT, W. 2008. Crosstalk between astrocytes and motor neurons: what is the message? *Exp Neurol,* 211**,** 1-6.
VATER, C., LODE, A., BERNHARDT, A., REINSTORF, A., HEINEMANN, C. & GELINSKY, M. 2010. Influence of different modifications of a calcium phosphate bone cement on adhesion, proliferation, and osteogenic differentiation of human bone marrow stromal cells. *J Biomed Mater Res A,* 92**,** 1452-60.
VERMA, A. & STELLACCI, F. 2010. Effect of surface properties on nanoparticle-cell interactions. *Small,* 6**,** 12-21.
VIAPIANO, M. S. & MATTHEWS, R. T. 2006. From barriers to bridges: chondroitin sulfate proteoglycans in neuropathology. *Trends Mol Med,* 12**,** 488-96.
VRIEND, R. A. & GEISSINGER, H. D. 1980. An improved direct intermicroscopic (LM leads to SEM leads to TEM) correlative procedure for the examination of mammalian skeletal muscle. *J Microsc,* 120**,** 53-64.
WAKATSUKI, T. & ELSON, E. L. 2003. Reciprocal interactions between cells and extracellular matrix during remodeling of tissue constructs. *Biophys Chem,* 100**,** 593-605.
WALZ, W. 2000. Role of astrocytes in the clearance of excess extracellular potassium. *Neurochem Int,* 36**,** 291-300.
WANG, J. J., CHUAH, M. I., YEW, D. T., LEUNG, P. C. & TSANG, D. S. 1995. Effects of astrocyte implantation into the hemisected adult rat spinal cord. *Neuroscience,* 65**,** 973-81.
WANG, L. C., BAIRD, D. H., HATTEN, M. E. & MASON, C. A. 1994. Astroglial differentiation is required for support of neurite outgrowth. *J Neurosci,* 14**,** 3195-207.

WANG, P. C. & SHAN, L. 2012. Essential Elements to Consider for MRI Cell Tracking Studies with Iron Oxide-based Labeling Agents. *J Basic Clin Med,* 1**,** 1-6.
WEIGHTMAN, A. P., JENKINS, S. I. & CHARI, D. M. 2016. Using a 3-D multicellular simulation of spinal cord injury with live cell imaging to study the neural immune barrier to nanoparticle uptake. *Nano Research,* 9**,** 2384-2397.
WEIGHTMAN, A. P., PICKARD, M. R., YANG, Y. & CHARI, D. M. 2014. An in vitro spinal cord injury model to screen neuroregenerative materials. *Biomaterials,* 35**,** 3756-65.
WELLS, M. R., KRAUS, K., BATTER, D. K., BLUNT, D. G., WEREMOWITZ, J., LYNCH, S. E., ANTONIADES, H. N. & HANSSON, H. A. 1997. Gel matrix vehicles for growth factor application in nerve gap injuries repaired with tubes: a comparison of biomatrix, collagen, and methylcellulose. *Exp Neurol,* 146**,** 395-402.
WHETSTONE, W. D., HSU, J. Y., EISENBERG, M., WERB, Z. & NOBLE-HAEUSSLEIN, L. J. 2003. Blood-spinal cord barrier after spinal cord injury: relation to revascularization and wound healing. *J Neurosci Res,* 74**,** 227-39.
WHITE, R. E. & JAKEMAN, L. B. 2008. Don't fence me in: harnessing the beneficial roles of astrocytes for spinal cord repair. *Restor Neurol Neurosci,* 26**,** 197-214.
WILCOX, J. T., CADOTTE, D. & FEHLINGS, M. G. 2012. Spinal cord clinical trials and the role for bioengineering. *Neurosci Lett,* 519**,** 93-102.
WILKE, M., FORTUNATI, E., VAN DEN BROEK, M., HOOGEVEEN, A. T. & SCHOLTE, B. J. 1996. Efficacy of a peptide-based gene delivery system depends on mitotic activity. *Gene Ther,* 3**,** 1133-42.
WILLERTH, S. M. & SAKIYAMA-ELBERT, S. E. 2008. Cell therapy for spinal cord regeneration. *Adv Drug Deliv Rev,* 60**,** 263-76.
WILLIAMS, R. R., HENAO, M., PEARSE, D. D. & BUNGE, M. B. 2015. Permissive Schwann cell graft/spinal cord interfaces for axon regeneration. *Cell Transplant,* 24**,** 115-31.
WILLITS, R. K. & SKORNIA, S. L. 2004. Effect of collagen gel stiffness on neurite extension. *J Biomater Sci Polym Ed,* 15**,** 1521-31.
WINTER, C. C., KATIYAR, K. S., HERNANDEZ, N. S., SONG, Y. J., STRUZYNA, L. A., HARRIS, J. P. & CULLEN, D. K. 2016. Transplantable living scaffolds comprised of micro-tissue engineered aligned astrocyte networks to facilitate central nervous system regeneration. *Acta Biomater,* 38**,** 44-58.
WOERLY, S., PLANT, G. W. & HARVEY, A. R. 1996. Cultured rat neuronal and glial cells entrapped within hydrogel polymer matrices: a potential tool for neural tissue replacement. *Neurosci Lett,* 205**,** 197-201.
WU, L., LI, J., CHEN, L., ZHANG, H., YUAN, L. & DAVIES, S. J. 2013. Combined transplantation of GDAs(BMP) and hr-decorin in spinal cord contusion repair. *Neural Regen Res,* 8**,** 2236-48.
XIE, X. M., SHI, L. L., SHEN, L., WANG, R., QI, Q., WANG, Q. Y., ZHANG, L. J., LU, H. Z. & HU, J. G. 2016. Co-transplantation of MRF-overexpressing oligodendrocyte precursor cells and Schwann cells promotes recovery in rat after spinal cord injury. *Neurobiol Dis,* 94**,** 196-204.
XU, X. M., CHEN, A., GUENARD, V., KLEITMAN, N. & BUNGE, M. B. 1997. Bridging Schwann cell transplants promote axonal regeneration from both the rostral and caudal stumps of transected adult rat spinal cord. *J Neurocytol,* 26**,** 1-16.
XU, X. M. & ONIFER, S. M. 2009. Transplantation-mediated strategies to promote axonal regeneration following spinal cord injury. *Respir Physiol Neurobiol,* 169**,** 171-82.
XU, X. M., ZHANG, S. X., LI, H., AEBISCHER, P. & BUNGE, M. B. 1999. Regrowth of axons into the distal spinal cord through a Schwann-cell-seeded mini-channel implanted into hemisected adult rat spinal cord. *Eur J Neurosci,* 11**,** 1723-40.
YAMAMOTO, M., RAISMAN, G., LI, D. & LI, Y. 2009. Transplanted olfactory mucosal cells restore paw reaching function without regeneration of severed corticospinal tract fibres across the lesion. *Brain Res,* 1303**,** 26-31.

YAMANAKA, S. 2009. A fresh look at iPS cells. *Cell,* 137**,** 13-7.
YAMEEN, B., CHOI, W. I., VILOS, C., SWAMI, A., SHI, J. & FAROKHZAD, O. C. 2014. Insight into nanoparticle cellular uptake and intracellular targeting. *J Control Release,* 190**,** 485-99.
YANAI, A., HAFELI, U. O., METCALFE, A. L., SOEMA, P., ADDO, L., GREGORY-EVANS, C. Y., PO, K., SHAN, X., MORITZ, O. L. & GREGORY-EVANS, K. 2012. Focused magnetic stem cell targeting to the retina using superparamagnetic iron oxide nanoparticles. *Cell Transplant,* 21**,** 1137-48.
YANG, D., PENG, C., LI, X., FAN, X., LI, L., MING, M., CHEN, S. & LE, W. 2008. Pitx3-transfected astrocytes secrete brain-derived neurotrophic factor and glial cell line-derived neurotrophic factor and protect dopamine neurons in mesencephalon cultures. *J Neurosci Res,* 86**,** 3393-400.
YAWO, H. & KUNO, M. 1985. Calcium dependence of membrane sealing at the cut end of the cockroach giant axon. *J Neurosci,* 5**,** 1626-32.
YOSHII, S., OKA, M., SHIMA, M., TANIGUCHI, A., TAKI, Y. & AKAGI, M. 2004. Restoration of function after spinal cord transection using a collagen bridge. *J Biomed Mater Res A,* 70**,** 569-75.
YU, A. C., DREJER, J., HERTZ, L. & SCHOUSBOE, A. 1983. Pyruvate carboxylase activity in primary cultures of astrocytes and neurons. *J Neurochem,* 41**,** 1484-7.
YUKI, N., SATO, S., MIYATAKE, T., SUGIYAMA, K., KATAGIRI, T. & SASAKI, H. 1991. Moto-neuron-disease-like disorder after ganglioside therapy. *Lancet,* 337,1109-1110.
ZABNER, J., FASBENDER, A. J., MONINGER, T., POELLINGER, K. A. & WELSH, M. J. 1995. Cellular and molecular barriers to gene transfer by a cationic lipid. *J Biol Chem,* 270**,** 18997-9007.
ZAGREBELSKY, M. & KORTE, M. 2014. Form follows function: BDNF and its involvement in sculpting the function and structure of synapses. *Neuropharmacology,* 76 Pt C**,** 628-38.
ZHANG, Y., SLOAN, S. A., CLARKE, L. E., CANEDA, C., PLAZA, C. A., BLUMENTHAL, P. D., VOGEL, H., STEINBERG, G. K., EDWARDS, M. S., LI, G., DUNCAN, J. A., 3RD, CHESHIER, S. H., SHUER, L. M., CHANG, E. F., GRANT, G. A., GEPHART, M. G. & BARRES, B. A. 2016. Purification and Characterization of Progenitor and Mature Human Astrocytes Reveals Transcriptional and Functional Differences with Mouse. *Neuron,* 89**,** 37-53.
ZHAO, F., ZHAO, Y., LIU, Y., CHANG, X., CHEN, C. & ZHAO, Y. 2011. Cellular uptake, intracellular trafficking, and cytotoxicity of nanomaterials. *Small,* 7**,** 1322-37.
ZHU, M., NIE, G., MENG, H., XIA, T., NEL, A. & ZHAO, Y. 2013. Physicochemical properties determine nanomaterial cellular uptake, transport, and fate. *Acc Chem Res,* 46**,** 622-31.

Appendices

Appendix 1

Click-iT® EdU (5-ethynyl-2´-deoxyuridine) cell proliferation assay protocol

Click-iT® EdU Imaging Kits

Search the handbook

Buy Now

Table 1. Contents and storage information.

Material	C10337	C10338	C10339	C10340	Concentration	Storage*
EdU (Component A)	5 mg	5 mg	5 mg	5 mg	NA	• 2–6˚C • Desiccate • Protect from light • DO NOT FREEZE
Alexa Fluor® azide (Component B)	1 vial (Alexa Fluor® 488)	1 vial (Alexa Fluor® 555)	1 vial (Alexa Fluor® 594)	1 vial (Alexa Fluor® 647)	NA	
Dimethylsulfoxide (DMSO, Component C)	4 mL	4 mL	4 mL	4 mL	NA	
Click-iT® EdU reaction buffer (Component D)	4 mL	4 mL	4 mL	4 mL	10X solution containing Tris-buffered saline	
$CuSO_4$ (Component E)	1 vial	1 vial	1 vial	1 vial	100 mM aqueous solution	
Click-iT® EdU buffer additive (Component F)	400 mg	400 mg	400 mg	400 mg	NA	
Hoechst 33342 (Component G)	35 µL	35 µL	35 µL	35 µL	10 mg/mL in water	

*These storage conditions are appropriate when storing the entire kit upon receipt. For optimal storage conditions for each component, see labels on the vials. When stored as directed, this kit is stable for 1 year.
NA = Not applicable.

Number of assays: Sufficient material is supplied for 50 coverslips based on the protocol below.

Approximate fluorescence excitation/emission maxima, in nm: Alexa Fluor® 488 azide**:** 495/519; Alexa Fluor® 555 azide**:** 555/565; Alexa Fluor® 594 azide: 590/615; Alexa Fluor® 647 azide: 650/670; Hoechst 33342: 350/461, bound to DNA.

Introduction

Measuring a cell's ability to proliferate is a fundamental method for assessing cell health, determining genotoxicity, and evaluating anti-cancer drugs. The most accurate method of doing this is by directly measuring DNA synthesis. Initially this was performed by incorporation of radioactive nucleosides[3] (for example, H-thymidine). This method was replaced by antibody-based detection of the nucleoside analog bromo-deoxyuridine (BrdU). The Click-iT® EdU Assay from Invitrogen is a novel alternative to the BrdU assay. EdU (5-ethynyl-2´-deoxyuridine) provided in the kit is a nucleoside analog of thymidine and is incorporated into DNA during active DNA synthesis.[1] Detection is based on a click reaction,[2-5] a copper-catalyzed covalent reaction between an azide and an alkyne. In this

application, the EdU contains the alkyne and the Alexa Fluor® dye contains the azide. The advantages of the Click-iT® EdU labeling are readily evident while performing the assay. The small size of the dye azide allows for efficient detection of the incorporated EdU using mild conditions. Standard aldehyde-based fixation and detergent permeabilization are sufficient for the Click-iT® detection reagent to gain access to the DNA. This is in contrast to BrdU assays that require DNA denaturation (typically using HCl or heat or digestion with DNase) to expose the BrdU so that it may be detected with an anti-BrdU antibody (Figure 1).

The denaturation step in the BrdU protocol can disrupt dsDNA integrity, which can affect nuclear counterstaining, and can also destroy cell morphology and antigen recognition sites. In contrast, the EdU assay kit is not only easy to use, but is fully compatible with DNA staining, including dyes for cell cycle analysis. The EdU assay kit can also be multiplexed with surface and intracellular marker detection using antibodies (see Table 2 for details). Finally, unlike the BrdU assay, which relies upon antibodies which can exhibit nonspecific binding, the Click-iT® EdU assay uses bioorthogonal (biologically unique) moieties, producing low backgrounds and high detection sensitivities.

The kit contains all of the components needed to label and detect the incorporated EdU as well as perform cell cycle analysis on samples from adherent cells (Figure 2). For cell cycle analysis, the kit is supplied with blue fluorescent Hoechst 33342 dye. The kit includes sufficient reagents for labeling 50, 18 × 18 coverslips using 500 µL of reaction buffer per test. For the latest information on Click-iT® EdU, visit www.lifetechnologies.com.

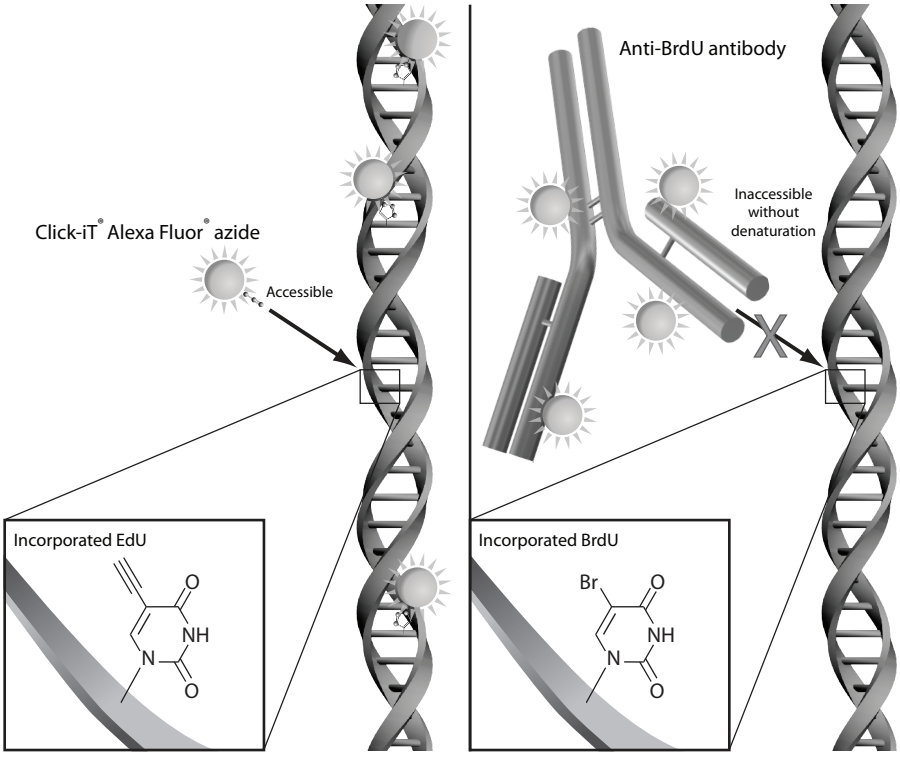

Figure 1. Detection of the incorporated EdU with the Alexa Fluor® azide versus incorporated BrdU with an anti-BrdU antibody. The small size of the Alexa Fluor® azide eliminates the need to denature the DNA for the EdU detection reagent to gain access to the nucleotide.

Table 2. Click-iT® detection reagent compatibility.

Molecule	Compatibility*
Qdot® nanocrystals	Use Qdot® nanocrystals **after** the Click-iT® detection reaction.
Fluorescent proteins such as Green Fluorescent Protein (GFP)	Use organic dye-based reagents, such as TC-FlAsH™ or TC-ReAsH™ reagents, for protein expression detection or anti-GFP rabbit or chicken antibodies **before** the Click-iT® detection reaction.
Organic dyes such as Alexa Fluor® dyes, fluorescein (FITC)	**Completely compatible** with the Click-iT® detection reaction.
TC-FlAsH™ or TC-ReAsH™ reagents	Detect the tetracysteine (TC) tag with FlAsH™ or ReAsH™ reagents **before** the Click-iT® detection reaction.
Phalloidin	Phalloidin staining is **not compatible** with the Click-iT® detection reaction. Use antibodies against other proteins, such as anti-α-tubulin, for visualization of the cytoskeleton.
Horseradish peroxidase (HRP)	Use HRP **after** the Click-iT® detection reaction.
R-phycoerythrin (R-PE) and R-PE-tandems such as Alexa Fluor® 680-R-PE	Use R-PE and R-PE tandems **after** the Click-iT® detection reaction.
Allophycocyanin (APC) and APC-tandems	**Completely compatible** with the Click-iT® detection reaction.
*Compatibility indicates whether the fluorescent molecule itself or the detection method involves components that are unstable in the presence of copper catalyst used for the Click-iT® detection reaction.	

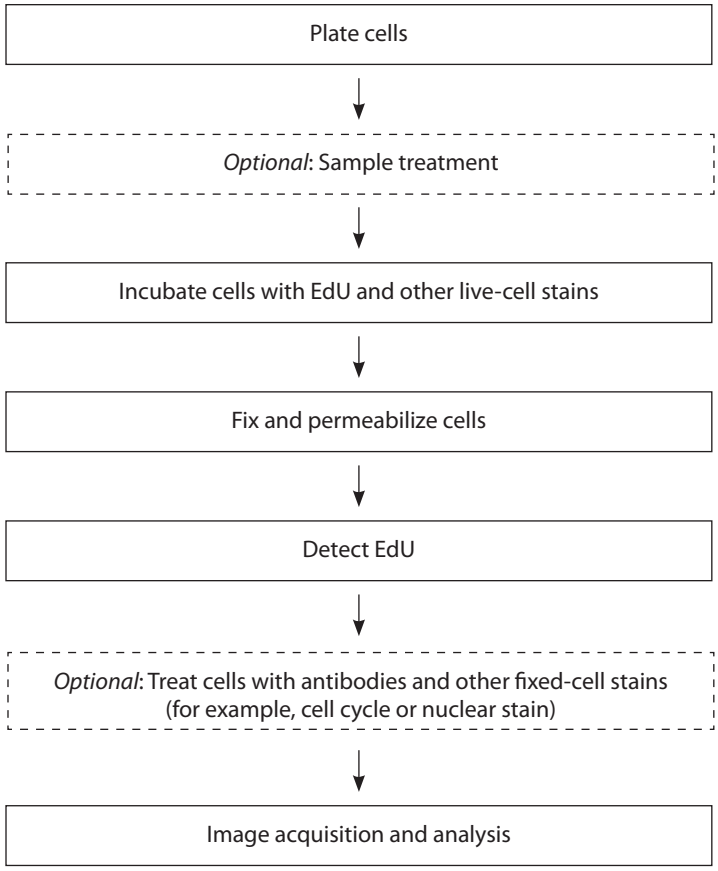

Figure 2. Workflow diagram for the Click-iT® EdU Imaging Assay.

Before You Begin

Materials required but not provided

- Phosphate-buffered saline (PBS, pH 7.2–7.6)
- Fixative (for example, 3.7% Formaldehyde in PBS)
- Permeabilization reagent (for example, 0.5% Triton® X-100 in PBS)
- 3% Bovine serum albumin (BSA) in PBS (3% BSA in PBS), pH 7.4
- Deionized water
- 18 × 18-mm coverslips
- *Optional*: 6-well microplate

Cautions

Hoechst 33342 (Component G) is a known mutagen. Use the dye with appropriate precautions.

DMSO (Component C), provided as a solvent in this kit, is known to facilitate the entry of organic molecules into tissues. Handle reagents containing DMSO using equipment and practices appropriate for the hazards posed by such materials. Dispose of the reagents in compliance with all pertaining local regulations.

Preparing the stock solutions

1.1 Allow the vials to warm to room temperature before opening.

1.2 Prepare a 10-mM stock solution of EdU (Component A): Add 2 mL of DMSO (Component C) or an aqueous solution (for example, buffer, saline) to EdU (Component A), then mix well.

After use, store any remaining stock solution at ≤–20°C. When stored as directed, this stock solution is stable for up to 1 year.

1.3 Prepare a working solution of the Alexa Fluor® azide (Component B): Add 70 µL of DMSO (Component C) to Component B, then mix well.

After use, store any remaining working solution at ≤–20°C. When stored as directed, this working solution is stable for up to 1 year.

1.4 Prepare a working solution of 1X Click-iT® EdU reaction buffer (Component D): Transfer all of the solution (4 mL) in the Component D bottle to 36 mL of deionized water. Rinse the Component D bottle with some of the diluted Click-iT™ EdU reaction buffer to ensure the transfer of all of the 10X concentrate.

To make smaller amounts of 1X Click-iT® EdU reaction buffer, dilute volumes from the Component D bottle 1:10 with deionized water. After use, store any remaining 1X solution at 2–6˚C. When stored as directed, this 1X solution is stable for up to 6 months.

1.5 To make a 10X stock solution of the Click-iT® EdU buffer additive (Component F): Add 2 mL of deionized water to the vial, then mix until fully dissolved. After use, store any remaining stock solution at ≤–20°C.

When stored as directed, this stock solution is stable for up to 1 year. If the solution develops a brown color, it has degraded and should be discarded.

Labeling cells with EdU

The following protocol was developed with A549, HeLa, and NIH/3T3 cells with an optimized EdU concentration of 10 µM, but it can be adapted for any adherent cell type. Growth medium, cell density, cell type variations, and other factors may influence labeling. In initial experiments, we recommend testing a range of EdU concentrations to determine the optimal concentration for your cell type and experimental conditions. Although sufficient material is included with the kit for standard dose response, additional EdU (Cat. nos. A10044, E10187) is available. If you are currently using a BrdU-based assay for cell proliferation, a similar concentration to BrdU is a good starting concentration for EdU.

2.1 Plate the cells on coverslips at the desired density, then allow them to recover overnight before additional treatment.

2.2 Prepare a 2X working solution of EdU (Component A) in complete medium from the 10-mM stock solution. A suggested starting concentration is 10 µM.

2.3 Prewarm the 2X EdU solution, then add an equal volume of the 2X EdU solution to the volume of media containing cells to be treated to obtain a 1X EdU solution. (For example, for a final concentration of 10 µM, replace half of the media with fresh media containing 20 µM of EdU). We do not recommend replacing all of the media, because this could affect the rate of cell proliferation.

2.4 Incubate the cells for the desired length of time under conditions optimal for the cell type. The time of EdU exposure to the cells allows for direct measurement of cells synthesizing DNA. The choice of time points and the length of time depends on the cell growth rate. Pulse labeling of cells by brief exposures to EdU permits studies of cell-cycle kinetics.

2.5 Incubate under conditions optimal for the cell type for the desired length of time. The time of EdU exposure to the cells allows for the direct measurement of cells synthesizing DNA. The choice of time points and length of time for pulsing depends on the cell growth rate.

2.6 Proceed immediately to **Cell fixation and permeabilization** (steps 3.1–3.3), followed by **EdU detection** (steps 4.1–4.7).

Cell fixation and permeabilization

Note: This protocol is optimized with a fixation step using 3.7% formaldehyde in PBS, followed by a 0.5% Triton® X-100 permeabilization step. However, this protocol is also amenable to other fixation/permeabilization reagents, such as methanol and saponin.

Transfer the coverslips into a 6-well plate for convenient processing, such that each well contains a single coverslip.

3.1 After incubation, remove the media and add 1 mL of 3.7% formaldehyde in PBS to each well containing the coverslips. Incubate for 15 minutes at room temperature.

3.2 Remove the fixative and wash the cells in each well twice with 1 mL of 3% BSA in PBS.

3.3 Remove the wash solution. Add 1 mL of 0.5% Triton® X-100 in PBS to each well, then incubate at room temperature for 20 minutes.

EdU detection

Note: This protocol uses 500 µL of Click-iT® reaction cocktail per coverslip. A smaller volume can be used as long as the remaining reaction components are maintained at the same ratios.

4.1 Prepare 1X Click-iT® EdU buffer additive (see Table 3) by diluting the 10X solution (prepared in step 1.5) 1:10 in deionized water. Prepare this solution **fresh** and use the solution on the same day.

4.2 Prepare Click-iT® reaction cocktail according to Table 3. It is important to add the ingredients in the order listed in the table; otherwise, the reaction will not proceed optimally. Use the Click-iT® reaction cocktail within 15 minutes of preparation.

Table 3. Click-iT® reaction cocktails.

Reaction components*	Number of coverslips						
	1	2	4	5	10	25	50
1X Click-iT® reaction buffer (prepared in step 1.4)	430 µL	860 µL	1.8 mL	2.2 mL	4.3 mL	10.7 mL	21.4 mL
$CuSO_4$ (Component E)	20 µL	40 µL	80 µL	100 µL	200 µL	500 µL	1 mL
Alexa Fluor® azide (prepared in step 1.3)	1.2 µL	2.5 µL	5 µL	6 µL	12.5 µL	31 µL	62 µL
Reaction buffer additive (prepared in step 4.1)	50 µL	100 µL	200 µL	250 µL	500 µL	1.25 mL	2.5 mL
Total volume	500 µL	1 mL	2 mL	2.5 mL	5 mL	12.5 mL	25 mL

*__Note__: Add the ingredients in the order listed in the table.

4.3 Remove the permeabilization buffer (step 3.3), then wash the cells in each well twice with 1 mL of 3% BSA in PBS. Remove the wash solution.

4.4 Add 0.5 mL of Click-iT® reaction cocktail to each well containing a coverslip. Rock the plate briefly to insure that the reaction cocktail is distributed evenly over the coverslip.

4.5 Incubate the plate for 30 minutes at room temperature, **protected from light**.

4.6 Remove the reaction cocktail, then wash each well once with 1 mL of 3% BSA in PBS. Remove the wash solution.

For nuclear staining, proceed to **DNA staining**. If no additional staining is desired, proceed to **Imaging and analysis**.

4.7 *Optional*: Perform antibody labeling of the samples at this time, following the recommendations from the manufacturer of the primary and secondary antibody. It is important to keep the samples **protected from light** during incubations.

DNA staining

5.1 Wash each well with 1 mL of PBS. Remove the wash solution.

5.2 Dilute the Hoechst 33342 (Component G) solution 1:2000 in PBS to obtain a 1X Hoechst 33342 solution (the final concentration is 5 µg/mL).

Note: A range between 2–10 µg/mL of Hoechst 33342 has been shown to work.

5.3 Add 1 mL of 1X Hoechst 33342 solution per well. Incubate for 30 minutes at room temperature, **protected from light**. Remove the Hoechst 33342 solution.

5.4 Wash each well twice with 1 mL of PBS. Remove the wash solution.

Imaging and analysis

Click-iT® EdU cells are compatible with all methods of slide preparation, including wet mount or prepared mounting media. See Table 4 for the approximate fluorescence excitation/emission maxima for Alexa Fluor® dyes and Hoechst 33342 dye bound to DNA.

Table 4. Approximate fluorescence excitation/emission maxima.

Fluorophore	Excitation (nm)	Emission (nm)
Alexa Fluor® 488	495	519
Alexa Fluor® 555	555	565
Alexa Fluor® 594	590	615
Alexa Fluor® 647	650	670
Hoechst 33342, bound to DNA	350	461

References

1. Proc Natl Acad Sci USA 105, 2415 (2008); **2.** ChemBioChem 4, 1147 (2003); **3.** J Am Chem Soc 125, 3192 (2003); **4.** Angew Chem Int Ed Engl 41, 2596 (2002); **5.** Angew Chem Int Ed Engl 40, 2004 (2001).

Product List **Current prices may be obtained from our website or from our Customer Service Department.**

	Cat No.	Product Name	Unit Size
Buy Now	C10337	Click-iT® EdU Alexa Fluor® 488 Imaging Kit *for 50 coverslips*	1 kit
Buy Now	C10338	Click-iT® EdU Alexa Fluor® 555 Imaging Kit *for 50 coverslips*	1 kit
Buy Now	C10339	Click-iT® EdU Alexa Fluor® 594 Imaging Kit *for 50 coverslips*	1 kit
Buy Now	C10340	Click-iT® EdU Alexa Fluor® 647 Imaging Kit *for 50 coverslips*	1 kit
	Related Products		
Buy Now	C10289	Click-iT® AHA Alexa Fluor® 488 Protein Synthesis HCS Assay	1 kit
Buy Now	C10327	Click-iT® RNA Alexa Fluor® 488 HCS Assay *2-plate size*	1 kit
Buy Now	C10328	Click-iT® RNA Alexa Fluor® 594 HCS Assay *2-plate size*	1 kit
Buy Now	C10329	Click-iT® RNA Alexa Fluor® 488 Imaging Kit *for 25 coverslips*	1 kit
Buy Now	C10330	Click-iT® RNA Alexa Fluor® 594 Imaging Kit *for 25 coverslips*	1 kit
Buy Now	C10350	Click-iT® EdU Alexa Fluor® 488 HCS Assay *2-plate size*	1 kit
Buy Now	C10351	Click-iT® EdU Alexa Fluor® 488 HCS Assay *10-plate size*	1 kit
Buy Now	C10352	Click-iT® EdU Alexa Fluor® 555 HCS Assay *2-plate size*	1 kit
Buy Now	C10353	Click-iT® EdU Alexa Fluor® 555 HCS Assay *10-plate size*	1 kit
Buy Now	C10354	Click-iT® EdU Alexa Fluor® 594 HCS Assay *2-plate size*	1 kit
Buy Now	C10355	Click-iT® EdU Alexa Fluor® 594 HCS Assay *10-plate size*	1 kit
Buy Now	C10356	Click-iT® EdU Alexa Fluor® 647 HCS Assay *2-plate size*	1 kit
Buy Now	C10357	Click-iT® EdU Alexa Fluor® 647 HCS Assay *10-plate size*	1 kit
Buy Now	A10044	EdU (5-ethynyl-2´-deoxyuridine)	50 mg
Buy Now	E10187	EdU (5-ethynyl-2´-deoxyuridine)	500 mg
Buy Now	E10415	EdU (5-ethynyl-2´-deoxyuridine)	5 g
Buy Now	H3570	Hoechst 33342, trihydrochloride, trihydrate *10 mg/mL solution in water*	10 mL

Contact Information

Corporate Headquarters
5791 Van Allen Way
Carlsbad, CA 92008
USA
Phone: +1 760 603 7200
Fax: +1 760 602 6500
Email: techsupport@lifetech.com

European Headquarters
Inchinnan Business Park
3 Fountain Drive
Paisley PA4 9RF
UK
Phone: +44 141 814 6100
Toll-Free Phone: 0800 269 210
Toll-Free Tech: 0800 838 380
Fax: +44 141 814 6260
Tech Fax: +44 141 814 6117
Email: euroinfo@invitrogen.com
Email Tech: eurotech@invitrogen.com

Japanese Headquarters
LOOP-X Bldg. 6F
3-9-15, Kaigan
Minato-ku, Tokyo 108-0022
Japan
Phone: +81 3 5730 6509
Fax: +81 3 5730 6519
Email: jpinfo@invitrogen.com

Additional international offices are listed at **www.lifetechnologies.com.**

These high-quality reagents and materials must be used by, or directly under the supervision of, a technically qualified individual experienced in handling potentially hazardous chemicals. Read the Safety Data Sheet provided for each product; other regulatory considerations may apply.

Obtaining Support
For the latest services and support information for all locations, go to **www.lifetechnologies.com**.

At the website, you can:

- Access worldwide telephone and fax numbers to contact Technical Support and Sales facilities
- Search through frequently asked questions (FAQs)
- Submit a question directly to Technical Support (techsupport@lifetech.com)
- Search for user documents, SDSs, vector maps and sequences, application notes, formulations, handbooks, certificates of analysis, citations, and other product support documents
- Obtain information about customer training
- Download software updates and patches

SDS
Safety Data Sheets (SDSs) are available at **www.lifetechnologies.com/sds**.

Certificate of Analysis
The Certificate of Analysis provides detailed quality control and product qualification information for each product. Certificates of Analysis are available on our website. Go to **www.lifetechnologies.com/support** and search for the Certificate of Analysis by product lot number, which is printed on the product packaging (tube, pouch, or box).

Limited Warranty
Invitrogen (a part of Life Technologies Corporation) is committed to providing our customers with high-quality goods and services. Our goal is to ensure that every customer is 100% satisfied with our products and our service. If you should have any questions or concerns about an Invitrogen product or service, contact our Technical Support Representatives.
All Invitrogen products are warranted to perform according to specifications stated on the certificate of analysis. The Company will replace, free of charge, any product that does not meet those specifications. This warranty limits the Company's liability to only the price of the product. No warranty is granted for products beyond their listed expiration date. No warranty is applicable unless all product components are stored in accordance with instructions. The Company reserves the right to select the method(s) used to analyze a product unless the Company agrees to a specified method in writing prior to acceptance of the order.
Invitrogen makes every effort to ensure the accuracy of its publications, but realizes that the occasional typographical or other error is inevitable. Therefore the Company makes no warranty of any kind regarding the contents of any publications or documentation. If you discover an error in any of our publications, please report it to our Technical Support Representatives.
Life Technologies Corporation shall have no responsibility or liability for any special, incidental, indirect or consequential loss or damage whatsoever. The above limited warranty is sole and exclusive. No other warranty is made, whether expressed or implied, including any warranty of merchantability or fitness for a particular purpose.

Limited Use Label License: Research Use Only
The purchase of this product conveys to the purchaser the limited, non-transferable right to use the purchased amount of the product only to perform internal research for the sole benefit of the purchaser. No right to resell this product or any of its components is conveyed expressly, by implication, or by estoppel. This product is for internal research purposes only and is not for use in commercial services of any kind, including, without limitation, reporting the results of purchaser's activities for a fee or other form of consideration. For information on obtaining additional rights, please contact outlicensing@lifetech.com or Out Licensing, Life Technologies Corporation, 5791 Van Allen Way, Carlsbad, California 92008.

For research use only. Not intended for any animal or human therapeutic or diagnostic use.

Appendix 2

Tickle et al., 2015

Influence of amplitude of oscillating magnetic fields on magnetic nanoparticle mediated gene transfer to astrocytes

- This publication contains data from Chapter 5 which has been licensed for use in this thesis by Elsevier

Nano LIFE
Vol. 5, No. 1 (2015) 1450006 (6 pages)

DOI: 10.1142/S1793984414500068

World Scientific
www.worldscientific.com

Influence of Amplitude of Oscillating Magnetic Fields on Magnetic Nanoparticle-Mediated Gene Transfer to Astrocytes

Jacqueline A. Tickle, Stuart I. Jenkins, Mark R. Pickard and Divya M. Chari*
Cellular and Neural Engineering Group
Institute for Science and Technology in Medicine
Keele University, Keele, Staffordshire, ST5 5BG, UK
**d.chari@keele.ac.uk*

Received 8 April 2014
Accepted 16 June 2014
Published 7 August 2014

Functionalized magnetic nanoparticles (MNPs) are emerging as a major nanoplatform for regenerative neurology, particularly as transfection agents for gene delivery. Magnetic assistive technology, particularly the recent innovation of applied oscillating magnetic fields, can significantly enhance MNP-mediated gene transfer to neural cells. While transfection efficiency varies with oscillation frequency in various neural cell types, the influence of oscillation amplitude has not yet been investigated. We have addressed this issue using cortical astrocytes that were transfected using MNPs functionalized with plasmid encoding a reporter protein. Cells were exposed to a range of oscillation amplitudes (100–1000 μm), using a fixed oscillation frequency of 1 Hz. No significant differences were found in the proportions of transfected cells at the amplitudes tested, but GFP-related optical density measurements (indicative of reporter protein expression) were significantly enhanced at 200 μm. Safety data show no amplitude-dependent toxicity. Our data suggest that the amplitude of oscillating magnetic fields influences MNP-mediated transfection, and a tailored combination of amplitude and frequency may further enhance transgene expression. Systematic testing of these parameters in different neural subtypes will enable the development of a database of neuro-magnetofection protocols — an area of nanotechnology research where little information currently exists.

Keywords: Astrocytes; magnetic nanoparticles; magnetofection; nonviral transfection; gene delivery.

1. Introduction

Functionalized magnetic nanoparticles (MNPs) have high promise for regenerative neurology both as labeling agents for noninvasive tracking of transplant populations[1] and as transfection vectors for genetic modification of neural cells.[2] A major area of research focus currently, is to devise strategies to enhance the efficacy of MNP-mediated gene transfer to various neural cell populations. In this regard, the major rate-limiting factor in gene delivery to cells is thought to be the uptake of particle-gene complexes by the cellular endocytotic machinery. An innovative strategy to overcome this bottleneck has been the deployment of static magnetic fields beneath cell monolayers to promote the sedimentation of particle-DNA complexes onto cells, thereby enhancing

complex interaction with and subsequent uptake by cells.[3] This process of magnetically assisted gene delivery is known as 'magnetofection'.[2]

A recent innovation to magnetofection has been the use of dynamic magnetic fields,[4–6] including devices that oscillate along an axis with programmable frequency and amplitude. Oscillating fields have yielded higher levels of transfection compared with static fields in a range of major neural transplant cell types such as neural stem cells (NSCs),[7] astrocytes,[8] and oligodendrocyte precursor cells (OPCs).[9] The mechanisms by which oscillating fields elicit greater transfection efficiency are not fully understood, but it is likely that lateral motion is imparted to the MNPs, increasing the probability of MNP-cell contact,[4,8] and possibly overcoming the accumulation biases predicted for static magnetic fields.[10] It has also been suggested that lateral motion of unattached MNPs across the cell membrane, or vibration of membrane-bound/internalized MNPs, may mechanically stimulate endocytosis, and/or the intracellular processing of MNPs may be altered, for example by facilitating endosomal escape.[4,7,8,11,12]

Despite the significant benefits for regenerative neurology offered by these systems, magnetic assistive technologies are only recently being exploited for neural transplant populations. Consequently, there is a significant current technical knowledge gap in respect of the parameters that govern the efficacy of magnetofection with neural cells. Such an understanding can aid the development of both robust experimental protocols, and state-of-the-art devices, to optimize the use of magnetic assistive technology with neural transplant cells.

In this context, McBain *et al.* studied the correlation between oscillation amplitude and efficacy of gene delivery to a human airway epithelial cell line, using cell size as a comparator to select oscillation amplitudes.[4] Compared with static systems they found improved transfection efficiency in the presence of applied oscillating fields [frequency $(F) = 2\,\text{Hz}$, amplitude $= 200\,\mu\text{m}$]. Based on their examination of a range of frequencies/amplitudes, the authors suggest that amplitude is of greater importance than frequency in enhancing gene transfer, at least in the frequency range tested (1–4 Hz). Conversely, using a fixed amplitude of $200\,\mu\text{m}$, our laboratory has shown frequency-dependent enhancement of MNP-mediated gene delivery in a range of neural cells.[8] This frequency-dependent effect indicates that frequency may play a greater role in enhancing gene transfer than was previously assumed. It is still unclear however, whether the most effective identified frequency in a specific neural cell type can potentially yield better transfection outcomes, when *paired* with an optimal oscillation amplitude.

To address this technical issue, the goal of the current study was to test the effects of systematically varying magnetic field oscillation amplitude (while maintaining a fixed oscillation frequency) on MNP-mediated gene transfer to astrocytes. The associated safety of the protocols used was assessed for all conditions. Astrocytes were selected as the test cell population given their major roles in regenerative neurology. Their expression of both regeneration promoting and inhibiting molecules[13,14] highlights astrocytes as endogenous therapeutic targets. Their ability to migrate, integrate, and survive post transplantation also make these cells excellent candidates as transplant populations for *ex vivo* gene delivery.[15]

2. Materials and Methods

The care and use of animals was in accordance with the Animals (Scientific Procedures) Act of 1986 (UK), and approved by local ethics committee.

2.1. *Cell culture*

Astrocytes were purified from mixed glial cultures derived from cerebral cortices of Sprague Dawley rats (postnatal day 1–3) using established procedures[8,16] and cultured in poly-D-lysine (PDL) coated flasks [D10 medium (DMEM with supplements: 2 mM glutaMAX-I, 1 mM sodium pyruvate, 50 U/ml penicillin, $50\,\mu\text{g}$/ml streptomycin and 10% fetal bovine serum); 95% humidified air/5% CO_2; 37°C] with 50% medium changes (2–3 d). Astrocytes were trypsinized and seeded (4×10^4 cells/cm^2; D10) on PDL-coated coverslips in 24-well plates ($300\,\mu\text{L}$) and PDL-coated 96-well plates ($70\,\mu\text{L}$).

2.2. *Magnetofection device*

The magnefect-nano device (nanoTherics Ltd., Stoke-on-Trent, UK) is composed of an array of high gradient neodymium iron boron (NdFeB) magnets which oscillates laterally with programmable amplitude and frequency beneath a culture

plate. The field strength at the magnet face was 421 ± 20 mT and 303 ± 5 mT (24 and 96 magnet arrays, respectively; nanoTherics, personal communication). The most effective parameters reported for magnetofection of astrocytes were used as a control condition (200 μm, 1 Hz)[8] within the range of amplitudes selected for testing (all at 1 Hz: 100, 200, 400, 700 and 1000 μm).

2.3. *Magnetofection protocols*

Transfection-grade MNPs were obtained from OZ Biosciences (France) in commercially available (NeuroMag; mean diameter 160 nm; range 140–200 nm)[8] and custom-synthesized (NeuroMag conjugated with the fluorophore rhodamine; termed herein $NMag^{Rhod}$) forms. As these are proprietary formulations, further physicochemical properties cannot be made available. The $NMag^{Rhod}$ MNPs allow MNP uptake and transgene expression to be compared within the same cells, potentially revealing relationships between oscillation amplitude, extent of nanoparticle uptake and transgene expression. Transfection was performed as described previously.[8] Briefly: one hour prior to transfection (24 h post-plating) D10 medium was refreshed (24 well, 225 μL; 96 well, 54 μL). Plasmid encoding green fluorescent protein (pmaxGFP; Amaxa Biosciences, Cologne, Germany) was incubated with MNPs in DMEM [serum-free; 20 min, room temperature (RT)], then added dropwise to cultures. Quantities of pmaxGFP:DMEM:NeuroMag added per well were 60 ng:75 μL:0.21 μL (24-well) and 12 ng:15 μL:0.042 μL (96-well); a constant MNP:plasmid ratio was used for all experiments. Controls were treated with plasmid in DMEM without NeuroMag. Plates were then placed on the magnefect-nano (preheated within the incubator; using 24 or 96 magnet array to match culture plate) for 30 min, incubated without a magnetic field for 30 min, then subject to a 100% medium change. The magnetic plate was allowed to cool for 30 min between each use. At peak transgene expression (48 h post-transfection)[8] cells in 24-well plates were washed twice (phosphate buffered saline, PBS), fixed (4% paraformaldehyde, 25 min, RT) and washed twice (PBS). Coverslips from Neuromag experiments were immunostained, then all coverslips were mounted with the nuclear stain 4′,6-diamidino-2-phenylindole (DAPI; Vector Laboratories, Peterborough, UK).

2.4. *Immunocytochemistry*

Washed, fixed coverslips were blocked (5% normal donkey serum in PBS, 0.3% Triton X-100, 30 min, RT), incubated overnight with primary antibody (polyclonal rabbit anti-GFAP, DakoCytomation, Ely, UK; 1:500 in blocker; 4°C), washed, blocked (30 min, RT), incubated with secondary antibody (Cy3-labeled donkey anti-rabbit IgG; 1:200 in blocker, 2 h, RT), washed and mounted.

2.5. *MTS assays*

Reduction of MTS reagent to formazan was used to assess the effects of transfection procedures on astrocyte metabolic activity (and consequently safety of the procedures). At 48 h post-magnetofection, medium was removed from astrocyte cultures in 96 well plates and replaced with 100 μL fresh D10 and 20 μL MTS reagent, then incubated for 3 h. Absorbance was measured at 490 nm ($VICTOR^2$ Multilabel Counter, PerkinElmer). Measurements from cell-free wells, containing medium or medium plus MNP–plasmid complexes as appropriate, were used as blanks.

2.6. *Microscopical analyses*

Fluorescence micrographs of cultures (fixed exposure times; Axio Scope A1 fluorescence microscope, Axio Cam ICc1 digital camera and Axiovision software; Carl Zeiss MicroImaging, GmbH, Germany) were double/triple merged as appropriate (Photoshop CS5, Adobe, USA). For each treatment condition, a minimum of four micrographs and 100 nuclei were analyzed. Culture purity was determined as the percentage of DAPI-stained healthy nuclei associated with GFAP expression. Transfection efficiency was determined as the percentage of $GFAP^+$ cells expressing GFP (normalized to the control amplitude, 200 μm). Complementary to the MTS assays, toxicity was assessed by determining (i) the percentage of pyknotic nuclei (pyknotic/pyknotic plus healthy), (ii) numbers of $GFAP^+$ cells per field, and (iii) proportions of type 1 and type 2 astrocytes (identified morphologically). Extent of transgene expression was assessed by optical density (OD) measurements. Calibration was performed using an OD step tablet. All green (GFP) channel images were converted to 8-bit grayscale and inverted, then GFP^+ type 1 cells (25 per condition)

were individually delineated for OD measurement (ImageJ software, NIH, USA). Mean OD was reported as level of reporter protein expression. The extent of $NMag^{Rhod}$ uptake by astrocytes was estimated based on a previously reported semi-quantitative method.[17]

2.7. *Statistical analyses*

All data are presented as mean ± standard error of the mean and were analyzed using one-way ANOVA (Prism software, GraphPad, CA, USA), with Bonferroni's multiple comparison test for post-hoc analysis. n = number of cultures, each derived from a separate litter.

3. Results

Astrocyte cultures were of high purity as judged by GFAP expression ($99.3 \pm 0.2\%$; $n = 3$). Cells predominantly exhibited flattened, unbranched morphologies characteristic of type 1 astrocytes ($92.6 \pm 2.7\%$ of $GFAP^+$ cells), with the complex, finely processed branching morphologies typical of type 2 astrocytes accounting for $7.2 \pm 2.7\%$ of $GFAP^+$ cells (Fig. 1). No transfected astrocytes were observed in plasmid-only control cultures. The overwhelming majority of $GFAP^+/GFP^+$ cells were identified phenotypically as type 1 astrocytes, with

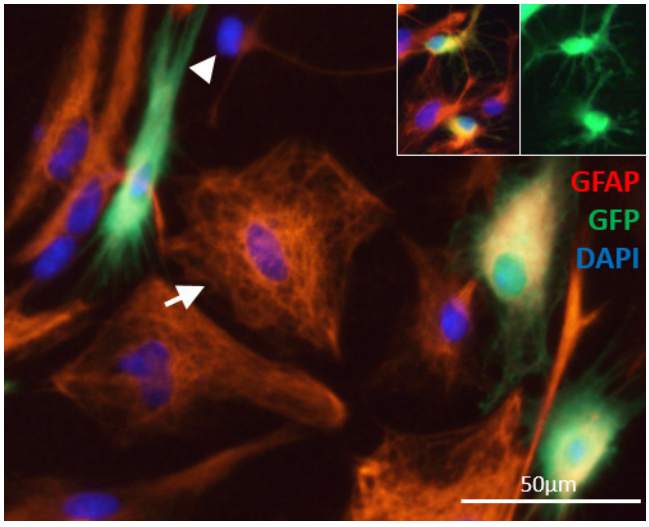

Fig. 1. MNPs mediate delivery of *gfp* plasmid to both type 1 and type 2 astrocytes. Fluorescence micrograph depicting the different morphologies of type 1 (arrow) and type 2 (arrowhead) astrocytes. GFP expression was predominantly observed in type 1 astrocytes. Small numbers of GFP^+ type 2 astrocytes were noted (inset shows counterpart micrographs).

$< 2\%$ of $GFAP^+/GFP^+$ cells exhibiting type 2 morphologies under any treatment condition (Fig. 1). Therefore, analyses were restricted to type 1 astrocytes.

Whilst there was a tendency towards greater transfection efficiency at higher amplitudes [Fig. 2(a)], no significant differences in astrocyte transfection efficiency were noted between the control amplitude (200 μm) and any of the 'test' amplitudes. However, GFP-related OD measurements (a proxy for levels of reporter protein expression) were elevated at an amplitude of 200 μm compared with amplitudes of 100 μm and 400 μm [Figs. 2(b) and 2(c)]. No differences were noted between treatment conditions with respect to cell counts [Fig. 2(d)], percentage of pyknotic nuclei ($< 1\%$), or the relative proportions of type 1 and type 2 astrocyte subtypes (data not shown). These findings were corroborated by MTS assays, where no alterations to metabolic function were detected for any treatment conditions [Fig. 2(e)].

Fluorescently labeled NeuroMag particles were employed to explore a correlation between extent of amplitude, MNP uptake and levels of transgene expression. Approximately 90% of $GFAP^+$ cells exhibited $NMag^{Rhod}$-labeling, with $\sim 40\%$ of these being GFP^+. However, no systematic relationship was apparent between *extent* of $NMag^{Rhod}$ accumulation and either success of transfection or levels of transgene expression for individual cells (Fig. 3).

4. Discussion

Here we have studied the influence of varying amplitude of oscillation (at a frequency previously identified as optimal for astrocyte transfection) on MNP-mediated gene delivery to a major transplant population — the astrocytes. To the best of our knowledge, our work is the first to systematically address the significant knowledge gap regarding optimal parameters for magnetofection of the diverse cells of the nervous system, particularly in the context of cells of primary origin.

Our methods allow for both proportions of transfected cells and extent of protein expression, extrapolated from quantitative imaging, to be separately quantified, unlike previous studies using bioluminescence measures of transgene expression. Our findings demonstrate for the first time that whilst amplitude of oscillation does not influence proportions of transfected cells, it nevertheless

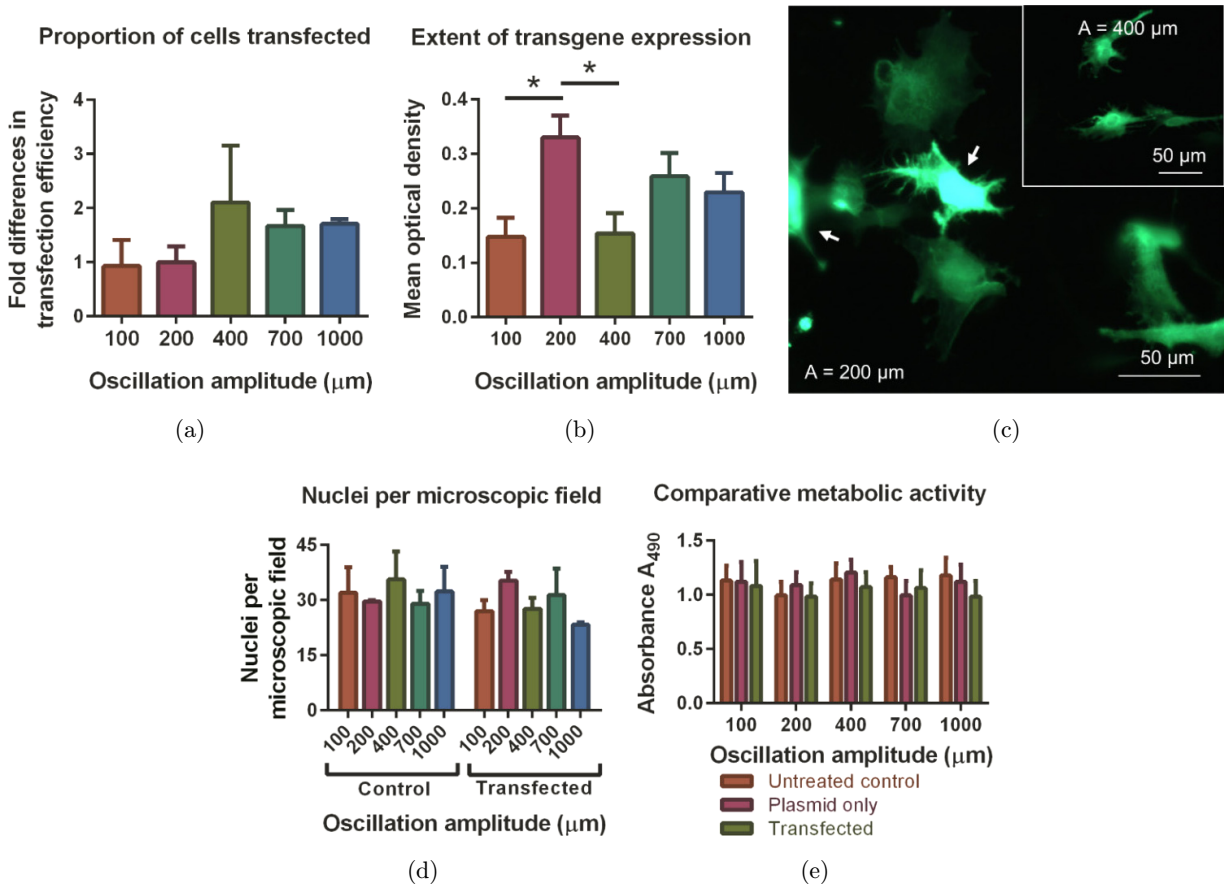

Fig. 2. Extent of transgene expression is influenced by amplitude of oscillation without acute cytotoxicity. Bar graphs show (a) No significant differences in transfection efficiency between amplitudes, although a tendency towards increased efficiency at the greater amplitudes is noted. (b) Greater levels of GFP expression (optical density) at 200 μm amplitude compared to 100 μm and 400 μm (Bonferroni's post-hoc tests; $*p < 0.05$). (c) Representative fluorescence micrographs showing differences in GFP expression between the 200 μm amplitude condition (main image) and 400 μm (inset), arrows showing cells with high levels of expression. (d) No differences in the average nuclei per microscopic field under any treatment conditions. (e) No differences in metabolic activity between treatment groups (MTS assay). $n = 3$ for all experiments.

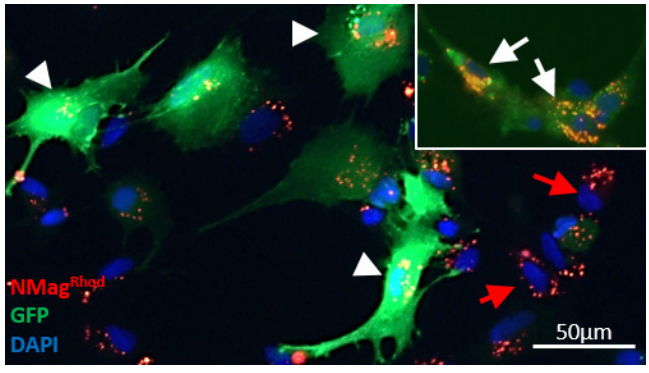

Fig. 3. Lack of correlation between MNP uptake and gfp transgene expression. This lack of consistency is illustrated by (i) high levels of GFP expression (arrow head) in cells exhibiting moderate levels of particle uptake, (ii) lack of GFP expression (red arrows) despite extensive particle uptake, and (iii) extensive particle uptake coupled with high levels of GFP expression (inset, white arrows).

modulates levels of transgene expression within a cell. Our protocols showed high safety and we consider these findings have significant implications for tissue engineering and transplant mediated delivery of therapeutic biomolecules. As an example, for clinical applications enhanced transgene expression would produce greater quantities of therapeutic biomolecules intended to promote neuroregenerative processes; for example, growth factors such as BDNF and FGF2 to promote nerve fiber regeneration and blood vessel growth, respectively. These findings emphasize the importance of identifying the most effective combinations of frequency and amplitude, for use in magnetofection protocols to optimize gene transfer to neural cell populations.

McBain *et al.* measured levels of transgene expression at three frequencies combined with four

amplitudes, and concluded that "*perhaps the amplitude is more important than frequency*"[4]; an observation broadly in accordance with the enhanced levels of transgene expression reported here. However, it should be noted that this study used a bioluminescence assay, and could not discriminate between higher proportions of transfected cells versus individual cells expressing higher transgene levels. Therefore, based on our findings, we can propose a scheme wherein oscillation frequency determines transfection efficiency[8] whereas amplitude determines the extent of transgene expression in individual cells, at least in astrocytes.

By using multimodal MNPs with both transfection and imaging capabilities, we were able to examine the relationship between MNP uptake and gene delivery. No relationship could be discerned between the extent of particle accumulation in cells and transgene expression, therefore we were unable to establish if enhanced protein expression at the 200 μm amplitude is due to increased MNP uptake. Our results further suggest that particle uptake alone is not sufficient for successful transfection. It is not clear what accounts for these observations, but it may involve differences in intracellular processing of MNP–plasmid complexes. Cultures derived from primary sources often exhibit heterogeneous behavior, and these differences may be related to individual cells (i) being at different stages of the cell cycle (mitosis-associated breakdown of the nuclear envelope being known to facilitate plasmid entry into the nucleus) or (ii) belonging to subpopulations with differing intracellular processing characteristics. For example, it is feasible that cells lacking transfection despite extensive particle uptake sequester the particles within intracellular vacuoles or subject the plasmid to degradative processes. Further detailed analyses of these processes using electron microscopy, lysotracker analyses and plasmid-tagging are warranted to elucidate the cellular mechanisms that contribute to successful transfection in neural cells. Our studies indicate that achieving MNP-labeling of cells, for example for imaging applications, is relatively simple compared with achieving efficient transfection, which shows a more complex relationship with MNP uptake. This emphasizes the need for advanced research at the interface between biological trafficking mechanisms, nanoparticle handling and gene delivery to facilitate the development of next generation transfection-grade particles.

Acknowledgment

Jacqueline A. Tickle and Stuart I. Jenkins contribute equally to this paper.

References

1. R. White and L. Jakeman, *Restor. Neurol. Neurosci.* **26**, 197 (2008).
2. C. Plank, O. Zelphati and O. Mykhaylyk, *Adv. Drug Deliv. Rev.* **63**, 1300 (2011).
3. N. Laurent, C. Sapet, L. Le Gourrierec, E. Bertosio and O. Zelphati, *Ther. Deliv.* **2**, 471 (2011).
4. S. C. McBain, U. Griesenbach, S. Xenariou *et al.*, *Nanotechnology* **19**, 405102 (2008).
5. M. Baryshev, D. Vainauska, S. Kozireva and A. Karpovs, *World Acad. Sci. Eng. Tech.* **58**, 306 (2011).
6. C. Dahmani, O. Mykhaylyk, F. Helling *et al.*, *J. Magn. Magn. Mater.* **332**, 163 (2013).
7. C. F. Adams, M. R. Pickard and D. M. Chari, *Nanomedicine* **9**, 737 (2013).
8. M. R. Pickard and D. M. Chari, *Nanomedicine (Lond.)* **5**, 217 (2010).
9. S. I. Jenkins, M. R. Pickard, N. Granger and D. M. Chari, *ACS Nano.* **5**, 6527 (2011).
10. E. P. Furlani and K. C. Ng, *Phys. Rev.* **77**, 061094 (2008).
11. A. Fouriki, N. Farrow, M. A. Clements and J. Dobson, *Nano Rev.* **1**, 1 (2010).
12. J. Dobson, *Nat. Nanotechnology.* **3**, 139 (2008).
13. C. M. Liberto, P. J. Albrecht, L. M. Herx, V. W. Yong and S. W. Levison, *J. Neurochem.* **89**, 1092 (2004).
14. G. R. John, S. C. Lee and C. F. Brosnan, *Neurosci.* **9**, 10 (2003).
15. S. J. A. Davies, C.-H. Shih, M. Noble, M. Mayer-Proschel, J. E. Davies and C. Proschel, *PLoS One* **6**, e17328 (2011).
16. K. D. McCarthy, J. de Vellis, *J. Cell Biol.* **85**, 890 (1980).
17. S. I. Jenkins, M. R. Pickard, D. N. Furness, H. H. P. Yiu and D. M. Chari, *Nanomedicine (Lond.)* **8**, 951 (2013).

Appendix 3

Tickle et al., 2016

Endocytotic potential governs magnetic particle loading in dividing neural cells: studying modes of particle inheritance

- This publication contains data from Chapter 3 which has been licensed for use in this thesis by Elsevier

Research Article

For reprint orders, please contact: reprints@futuremedicine.com

Nanomedicine

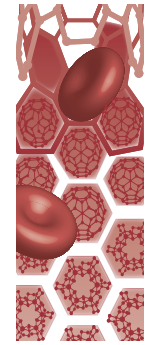

Endocytotic potential governs magnetic particle loading in dividing neural cells: studying modes of particle inheritance

Aim: To achieve high and sustained magnetic particle loading in a proliferative and endocytotically active neural transplant population (astrocytes) through tailored magnetite content in polymeric iron oxide particles. **Materials & methods:** MPs of varying magnetite content were applied to primary-derived rat cortical astrocytes ± static/oscillating magnetic fields to assess labeling efficiency and safety. **Results:** Higher magnetite content particles display high but safe accumulation in astrocytes, with longer-term label retention versus lower/no magnetite content particles. Magnetic fields enhanced loading extent. Dynamic live cell imaging of dividing labeled astrocytes demonstrated that particle distribution into daughter cells is predominantly 'asymmetric'. **Conclusion:** These findings could inform protocols to achieve efficient MP loading into neural transplant cells, with significant implications for post-transplantation tracking/localization.

Jacqueline A Tickle[1], Stuart I Jenkins[1], Boris Polyak[2], Mark R Pickard[1] & Divya M Chari*,[1]

[1]Institute for Science & Technology in Medicine, School of Medicine, David Weatherall Building, Keele University, Staffordshire, ST5 5BG, UK

[2]Department of Surgery & Department of Pharmacology & Physiology, Drexel University College of Medicine, Philadelphia, PA 19102, USA

*Author for correspondence:
Tel.: +44 1782 733314
Fax: +44 1782 734634
d.chari@keele.ac.uk

First draft submitted: 27 August 2015; **Accepted for publication:** 27 November 2015; **Published online:** 20 January 2016

Keywords: astrocytes • cell transplantation • label dilution • magnetite • magnetolabeling • polymeric particles

Deploying magnetic particles (MPs) with cell therapies for magnetic cell localization and imaging applications is paving the way for safe and efficient delivery of cell transplant populations to sites of pathology, and allowing for noninvasive monitoring of grafts [1–4]. A major emergent area for such applications, given the limited regenerative capacity of the central nervous system, is in neural cell transplantation for the repair of neurological injury and disease. Labeling cells prior to transplantation requires a cell–particle combination that results in rapid and safe particle uptake by the majority of (ideally all) cells. However, the regenerative capacity of most transplant populations relies partially on their proliferative capacity which results in rapid dilution of intracellular particle accumulations in labeled cells [5]. Particle loss can also occur via exocytosis, potentially compromising magnetic cell localization and imaging success [6]. Therefore, a further requirement for transplant cell labeling is long-term retention of sufficient particles per cell to confer utility, despite the proliferative nature of the cell, which could be achieved by high initial loading of label into graft cells.

In order to achieve this goal, we require a clear understanding of both the physicochemical and biological parameters that govern particle loading in transplant populations. However, there is a major knowledge gap regarding the factors that contribute to successful 'magnetolabeling' and label retention in neural cells. These issues are complicated by the complexity of the architecture of the nervous system wherein multiple cell types are present possessing distinct biological properties. These cell types vary greatly in terms of proliferative and endocytotic capacity, cell-specific modes of intracellular particle processing and susceptibility

Future Medicine part of fsg

to particle induced toxicity, requiring detailed characterizations on a cell-by-cell basis for neurological applications [7].

We recently proved that systematic tailored increases in the magnetite content of polymeric particles could significantly enhance cell labeling (>95% cells labeled) in the typically 'hard-to-label' transplant population of neural stem cells (NSCs) [8]. However, this study did not evaluate the longer-term retention of particles of different magnetite content by the labeled cells, or establish the pattern of 'inheritance' of particles by daughter NSCs post-proliferation. Furthermore, it is well established that uptake of nanoparticles is mediated via a range of endocytotic mechanisms [9–12]. In this context, it should be noted that NSCs have relatively small cell bodies, elaborate limited amounts of cell membrane and appear in ultrastructural observations to possess comparatively quiescent membranes [13]. How neural transplant cell populations with greater levels of endocytotic activity handle such high magnetite content MPs is unclear, but it can be postulated that such cell/MP combinations can result in greater enhancement of cell labeling for neural transplant applications.

In order to address these issues, we have applied particles with differing magnetite content to cortical astrocytes of primary origin. The astrocytes offer major promise as a transplant population [14–16] and also play key roles in lesion sites post-injury [17]; as such these are of great interest as a target cell population for nanotechnology studies. Astrocytes have major homeostatic functions in the CNS, for example in the maintenance of normal ionic concentrations and neurotransmitter levels in the extracellular space [18,19]. Consistent with these roles, astrocytes display high levels of membrane activity and can mediate nanoparticle uptake via a broad range of endocytotic mechanisms [19,20]. Indeed, in a recent ultrastructural study using an advanced and high-resolution scanning electron microscopy technique, we showed that astrocytes are the dominant neuroepithelial population in terms of particle uptake, displaying extensive membrane ruffling with numerous filopodia/membrane pits in line with greater particle uptake/transfection, relative to other major neural cell types such as neurons and oligodendrocytes [21]; MPs appear to be relatively stable (not degraded) within these cells [7]. Of relevance to the current study, these cells also have a relatively short cell cycle time (ca. 20 h) making these ideal for capture of cell division events and dynamic imaging studies of particle inheritance [22,23]. Polymeric particles with different levels of magnetite content deployed in this study were formulated using biocompatible and biodegradable components highlighting their translational potential and justifying their use in this study [8]. The main study goals were to investigate the influence of tailored particle magnetite content on astrocyte loading and particle retention, while evaluating the safety of the methods and to investigate the profiles of particle inheritance in the daughter cells of labeled astrocytes using dynamic time-lapse imaging.

Materials & methods

The care and use of animals were in accordance with the Animals (Scientific Procedures) Act of 1986 (UK), and approved by the local ethics committee.

Astrocyte cell culture

Disaggregated cerebral cortices from Sprague-Dawley rats (post-natal day 1–3) were used to establish mixed glial cultures. Following 7 days' culture in D10 medium (Dulbecco's modified Eagle's medium, 2 mM glutaMAX-I, 1 mM sodium pyruvate, 50 U/ml penicillin, 50 µg/ml streptomycin and 10% fetal bovine serum), sequential overnight shakes facilitated astrocyte purification [24]. Astrocytes were enzymatically detached (TrypLE synthetic trypsin, Life Technologies), plated on poly-D-lysine (PDL)-coated T75 flasks and maintained in D10 medium, as previously described [25]. Subconfluent cultures were enzymatically detached by addition of TrypLE and orbital shaking at 100 rpm, <5 min. Following centrifugation (1000 rpm; 4 min) and phosphate buffered saline (PBS) wash (800 µl), cells were resuspended in D10 for plating.

Magnetic particle characterization

Superparamagnetic, poly(lactic acid)/poly(vinyl alcohol) (PLA/PVA)-coated particles, with a fluorescent BODIPY® 564/570–PLA coating and of differing relative magnetite matrix loading, termed MP-0x (nonmagnetite), MP-1x and MP-5x, were prepared by the Boris Polyak Laboratory, Drexel University, Philadelphia, using published procedures [26]. These were formulated using biocompatible and biodegradable components (PLA, PVA, magnetite and oleic acid). Extensive characterization of these MPs has previously been undertaken [8,27]. In brief, the average sizes are similar for each particle type (hydrodynamic diameter 262–278 nm) with a slightly negative surface charge (-9.5 to -14.4 mV) The differing magnetite content of these particles alters magnetic responsiveness and weight ratio of the MPs, but not particle size or surface charge. Fourier transform IR spectroscopy confirmed similar organic composition of each particle type, with no alteration due to increased magnetite loading [8] (Table 1).

Table 1. Physical characterization of magnetic particles.

Magnetic particle	Magnetite content (w/w)	Hydrodynamic diameter (nm)	ζ-potential (mV)
MP-0x	Nonmagnetite	267 ± 0.65	-8.98 ± 0.16
MP-1x	11.5 ± 0.98	262 ± 9.56	-9.46 ± 0.14
MP-5x	46.0 ± 1.08	278 ± 1.62	-14.4 ± 0.34

Data taken from [8,26].

Magnetic particle labeling utilizing the magnefect-nano device

The MPs were evaluated for cellular labeling efficiency and extent of cellular accumulation over time. For particle uptake experiments, astrocytes were seeded onto PDL-coated glass coverslips in 24-well plates (0.4×10^5 cells/cm^2), and allowed to adhere for 24 h prior to addition of MPs, followed immediately by exposure to a magnetic field. Lyophilized MPs were resuspended in sterile water and added to D10 at a concentration of 13 µg (MP-0x), 15 µg (MP-1x) and 26.5 µg (MP-5x) per ml of fresh D10 medium; each corresponding to an identical concentration (particles per ml), as MP density increases with greater magnetite content [8].

Particles were added to cultures (0.3 ml per culture well), with control cultures receiving D10 without MPs. To enhance particle/cell interactions, a magnefect-nano device was used (high gradient neodymium iron boron [NdFeB] magnets with lateral oscillation capability and programmable frequency/amplitude; field strength at magnet face 421 ± 20 mT [24-magnet array] and 303 ± 5 mT [96-magnet array]; nanoTherics Ltd., Stoke-on-Trent, UK). The superparamagnetic nature of the particles allows for magnetic responsiveness only when particles are exposed to a magnetic field and field gradient. Therefore, deploying a magnetic field and field gradient (permanent NdFeB magnets in this study) beneath the culture plate attracts the particles down to the cell monolayer, while the application of an oscillating field/gradient (termed later as a magnetic field condition for simplicity) theoretically causes particles to move horizontally along the magnet's surface enhancing the likelihood of contact with cells, and/or oscillate *in situ* when attached to cell membrane, thus stimulating endocytotic mechanisms and enhancing cellular MP uptake [20,28–30]. Culture plates were exposed to a static magnetic field (frequency, F = 0 Hz), an oscillating field (F = 1 Hz; 200 µm amplitude) or no magnetic field (NF) for the first 30 min of the MP incubation period (either 4 or 24 h; 37°C, 5% CO_2/95% humidified air throughout). Then cells were washed twice with PBS to remove any particles not internalized by cells, and fixed with 4% paraformaldehyde (25 min at room temperature, RT).

Long-term particle retention

Particle retention, that is, percentage of cells labeled and the extent of MP accumulation were monitored over a 21 day period, together with assessment of particle safety. For these experiments, astrocytes were incubated with particles for 24 h, with exposure to magnetic field conditions for the first 30 min, as detailed above, followed by PBS washes (×2) to remove noninternalized particles, then fresh D10 medium was added. To facilitate continued proliferation of astrocytes over the long term, coverslips containing MP-loaded cells were transferred to PDL-coated 6-well plates at 96 h, cultured up to day 7 with the coverslip containing cells then transferred to a fresh well at 14 days and cultivated up to 21 days. Cells were maintained in D10 medium with 50% refresh every 2–3 days, with some cultures fixed (PBS wash x2; 4% paraformaldehyde, 25 min, RT) at day 1 and every 4 days thereafter up to day 21 (six time points in total).

Immunostaining

Cells were immunostained for GFAP to enable assessment of culture purity, morphological characteristics and intracellular localization of particles. Cells were incubated in blocker (5% normal donkey serum and 0.3% Triton X-100; 30 min at RT) followed by overnight incubation at 4°C in primary antibody, polyclonal rabbit anti-GFAP (Z0334; DakoCytomation, Ely, UK; 1:500 in blocker). Following two PBS washes (15 min/wash at RT), cells were incubated in blocker (30 min at RT) prior to incubation with secondary antibody (FITC-labeled donkey antirabbit, IgG; Jackson Laboratories, USA; 1:200 in blocker; 2–3 h at RT). Coverslips were washed with PBS (3 × 5 min) then mounted with the nuclear stain DAPI (4′,6-diamidino-2-phenylindole; Vector Laboratories, Peterborough, UK).

Fluorescence imaging

MP-labeling efficiency, extent of particle accumulation and MP intracellular localization, together with culture characteristics and safety assessment, were assessed using fluorescence micrographs. These consisted of four images – fluorescent channels (BODIPY 564/570-PLA MPs; FITC-GFAP$^+$ astrocytes; DAPI

stained nuclei) and phase image (Axio Scope A1 fluorescence microscope, AxioCam ICc1 digital camera and Axiovision software; Carl Zeiss MicroImaging, GmbH, Germany). A standardized exposure time was used for density quantification of BODIPY 564/570-PLA MPs. For each of the experimental conditions, at least four micrographs, encompassing a minimum of 100 nuclei, were quantified for statistical analyses.

Particle inheritance-dynamic time-lapse imaging

Dynamic time-lapse imaging allowed determination of the pattern of particle inheritance in daughter cells of dividing astrocytes (Axio Zoom V16 with AxioCam ICm1 camera and ZEN software [Blue Ed., v.1.1.1.0]; Carl Zeiss GmbH, Germany). Time-lapse images were acquired from transmitted light and BODIPY 564/570-relevant fluorescence channels for 48 h, post-addition of MPs. Visual observation of time-lapse imaging videos provided counts of symmetrical/nonsymmetrical particle inheritance events. A total of 30 mitotic events were recorded (60 daughter cells) and each was classified as 'symmetric' or 'asymmetric'. The total area occupied by MPs was determined for both daughters, and events were classed as symmetrical inheritance when each daughter cell contained 40–60% of this area, with nonsymmetrical defined as >60% in one daughter cell.

Histological analyses of culture properties

Fluorescence micrographs were triple-merged (Photoshop CS5 Extended, Version 12 x32; Adobe, CA, USA) and viewed using ImageJ (NIH USA) to allow quantification of culture and particle uptake characteristics and safety assessments across each experimental condition. Culture purity was determined as the percentage of DAPI-stained nuclei which were $GFAP^+$, with average cell counts determined from the number of nuclei per micrograph. To quantify astrocyte phenotype ratios, each astrocyte was classified based on morphological characteristics (Type 1 [flat, membranous, unbranched] or Type 2 [highly branched, complex cells]). For each experimental condition, average cell count, distribution of astrocyte phenotype and percentage of pyknotic nuclei (defined as shrunken, fragmenting nuclei) were quantified from fluorescence micrographs.

Integrated density-based technique for unbiased quantification of extent of cellular MP uptake

In terms of quantification of cellular particle uptake, taking average measures of fluorescence (using plate readers) across cultures or assessing iron uptake by quantitative (culture wide) iron assays, assumes an even particle distribution between cells, and while arguably appropriate for cell lines (which behave in a relatively homogenous and clonal manner in respect of particle uptake), this approach is not suitable for evaluating MP uptake in the astrocyte cultures used in our studies which are derived from primary cortical tissue and show extensive heterogeneity in uptake. Moreover, fluorescence measurements typically include substantial extracellular (membrane-bound) particles (notably, up to 50% of the signal for astrocytes [31]). In this context, a flow cytometry approach was also considered but rejected as particles adherent to the plasma membrane lead to 'false-positives'. Moreover, enzymatically detached cells provide few morphological features for analysis, features pertinent to the assessment of uptake and toxicity in specific astrocyte classes. MP-labeling efficiency (% labeled cells) and the extent of particle accumulation within cells, were quantified using triple-merges of DAPI, GFAP and particle images/channels. The dense accumulation of internalized particles prevented exact particle counts per cell, therefore particle accumulation per cell was quantified using integrated density (ID – a measure of pixel intensity) values (ImageJ software, NIH USA). Merged fluorescence micrographs were scaled and, for each MP-labeled astrocyte, the total area per cell occupied by intracellular MPs was outlined, with this outline then being transferred to the unmerged particle channel from which a raw cellular ID measure was obtained. Five background measures were taken from the same unmerged particle channel. The cellular ID values are presented as a corrected total cell fluorescence (CTCF) measure, where:

CTCF = ID - (area of selected cell × mean fluorescence of background readings)

Therefore, the resulting CTCF value represents the fluorescence intensity of the internalized particles (having corrected for any background fluorescence) and as such provides a quantifiable and unbiased measure of particle accumulation within the cell.

Statistical analyses

Data were analyzed by one-way ANOVA, with Bonferroni's *post hoc* multiple comparison test (Prism software, version 6.03; GraphPad, CA, USA). All data are expressed as mean ± standard error of the mean with 'n' referring to the number of different cultures, each derived from a different rat litter.

Results

Astrocyte uptake characteristics for particles with differing proportions of magnetite

Astrocyte cultures used in our study were of high purity as judged by expression of the astrocyte marker

GFAP (99.4 ± 0.2% of cells were GFAP$^+$, n = 6). Cells displayed healthy morphologies typical of Type 1 and Type 2 astrocytes (Figure 1A), with Type 1 cells dominating (92.4 ± 1.0% of GFAP$^+$ cells). Both perinuclear and cytoplasmic distributions of MPs were observed post-labeling (Figure 1A–C). Visual analysis showed widespread cellular uptake throughout cultures for all three particle types, and revealed cellular heterogeneity in terms of relative particle accumulation showing low, medium or high uptake (Figure 1A–C).

Particle uptake was rapid, and for magnetite-loaded cells a substantial proportion (ca. 50%) of cells were MP-labeled at 4 h post-particle exposure; MP-5x particles showed significantly increased labeling efficiency versus the other particle types, and in turn, MP-1x showed significantly increased MP-labeling versus MP-0x (Figure 1D). By contrast, magnetic field application had no effect on labeling efficiency with MP-0x or MP-1x particles at 4 h. Further, magnetic fields had no effect on the proportion of cells labeled with the MP-5x particles, which was very high (>90%) even under the no magnetic field condition. With regard to the extent of particle accumulation at 4 h, cells labeled with MP-5x particles showed significantly higher particle accumulation compared with MP-0x and MP-1x particles for both magnetic field conditions (Figure 1E); fields also resulted in significantly greater accumulation of MP-5x particles versus the no field condition (Figure 1E).

At 24 h, a greater proportion of cells were MP-labeled versus 4 h for all particle types (compare Figure 1D & F). Notably, for MP-1x and MP-5x particles, virtually all (>98%) astrocytes were MP-labeled (Figure 1F); magnetic field application at both frequencies was without effect at this time point. The extent of particle accumulation was also much greater at 24 h compared with 4 h for all magnetite containing particles (compare Figure 1E & G; please note scale difference of y-axes), with particle accumulation significantly higher versus MP-0x (Figure 1G). Further, for MP-5x particles magnetic field application promoted particle accumulation (Figure 1G) but the effect was not observed for MP-1x.

Long-term particle retention analysis

Long-term particle retention was studied for magnetite containing particles with applied oscillating fields, which yield optimal MP loading using our protocols. For both MP-1x and MP-5x, substantial label retention (>50%) was evident over 21 days. For MP-1x particles, approximately 92% of cells were labeled at day 1 and this value declined significantly by day 17 to ca. 51% of cells (Figure 2A). For MP-5x particles, in contrast, a greater labeling efficiency (ca. 99% of cells) was obtained at day 1, which declined significantly by day 21, albeit with >78% of cells remaining labeled at this time point (Figure 2B). A steady reduction in particle retention was noted over the 21-day time period, with considerable heterogeneity observed over cells in terms of extent of particle retention. Visual observations over time for MP-1x showed a clear transition from perinuclear clustering of particles (Figure 2C, inset) to a more cytoplasmic distribution (Figure 2C, main image) suggesting reverse trafficking of particles. While a similar pattern was seen overall with MP-5x (Figure 2D, inset), it was noticeable that a subpopulation of astrocytes retained large particle accumulations clustered around the nucleus even at 21 days (Figure 2D, main image). Extent of particle retention was lower for MP-1x than MP-5x particles (compare Figure 2E & F: please note scale difference of y-axes).

Safety assessment of long-term particle retention

Long-term retention of the particles did not impair the proliferative capacity of astrocytes, with average cell numbers showing a significant increase by day 9 for both MP-1x and MP-5x particles and for both magnetic field conditions, with no significant differences compared with untreated controls at 21 days (Figure 3A & B). Culture purity remained at >99% over the 21 days (Figure 3C & D). There was no effect of either particles or magnetic field condition on astrocyte phenotype distribution (84.6 ± 0.7% Type 1 compared with 15.4 ± 0.7% Type 2, average across all conditions; Figure 3E & F). A small proportion (<2%) of nuclei were pyknotic across all time points; pyknosis was associated with aberrant intense GFAP staining indicative of membrane detaching from the substrate (Figure 4A & B). By contrast, using histological analyses, the majority of labeled cells showed no obvious aberrations in GFAP staining or in astrocyte morphologies compared with controls.

Live cell imaging of particle inheritance in dividing astrocytes

To gain further insight into the pattern of particle distribution into daughter cells, astrocytes labeled with MP-5x particles were studied using dynamic time-lapse imaging of proliferating cells (Figure 5; see Supplementary Video). This revealed that daughter cells exhibited a predominantly asymmetric profile of particle inheritance (from 30 mitotic events, 21 were asymmetric compared with 9 showing symmetrical inheritance; Figure 5A). Distribution of particles within the parent cell prior to division (Figure 5B & F) was predictive of the inheritance profile in daughter cells. Parent cells exhibiting a symmetric perinuclear distribution of particles (Figure 5B–D) gave rise to

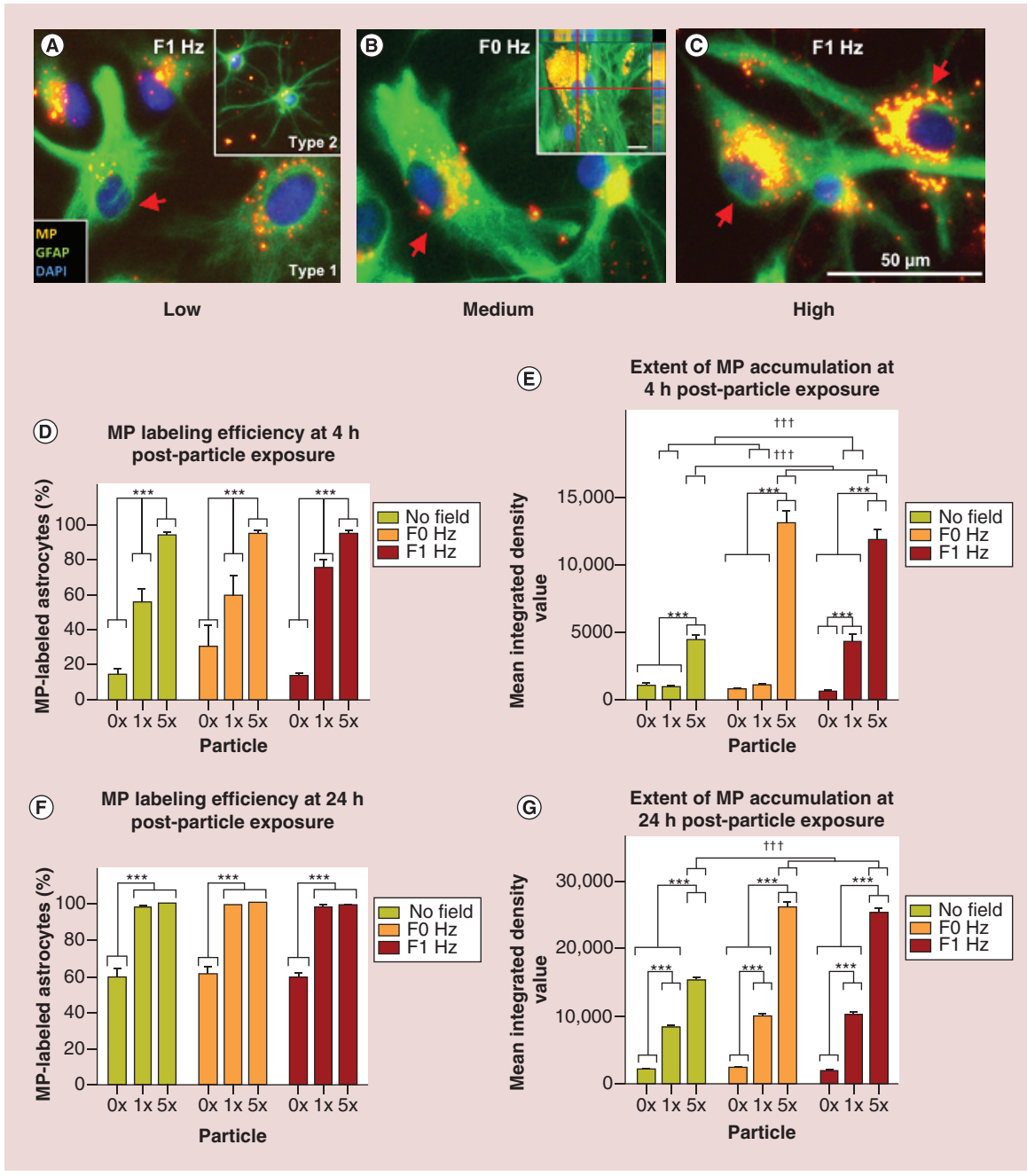

Figure 1. Magnetic particle labeling of astrocytes at 4 h and 24 h post-particle exposure, with and without magnetic field application. **(A–C)** Representative triple-merged images of MP-5x uptake in Type 1 and Type 2 (**[A]**, inset) astrocytes (24 h). Arrows indicate **(A)** 'low', **(B)** 'medium' and **(C)** 'high' levels of intracellular particle accumulation. (**[B]**, inset) Z-stack micrograph demonstrating intracellular localization of particles. **(D)** Bar chart displaying MP-labeling efficiency in astrocytes at 4 h. **(E)** Bar chart showing extent of particle accumulation across magnetic fields at 4 h. **(F)** Bar chart showing MP-labeling efficiency at 24 h. **(G)** Bar chart showing extent of particle accumulation across magnetic fields at 24 h. Differences are indicated in terms of magnetic field ($^{\dagger\dagger\dagger}p < 0.001$) and particle (*$p < 0.05$; **$p < 0.01$; ***$p < 0.001$). All graphs: n = 6.
MP: Magnetic particle.

daughter cells with symmetric inheritance of particles (Figure 5E), and mitosis of parent cells with asymmetrically distributed particles resulted in asymmetric inheritance (Figure 5I).

Discussion

Here, we have investigated the interaction between the physicochemical properties (specifically, magnetite content) of polymeric iron oxide particles and a highly

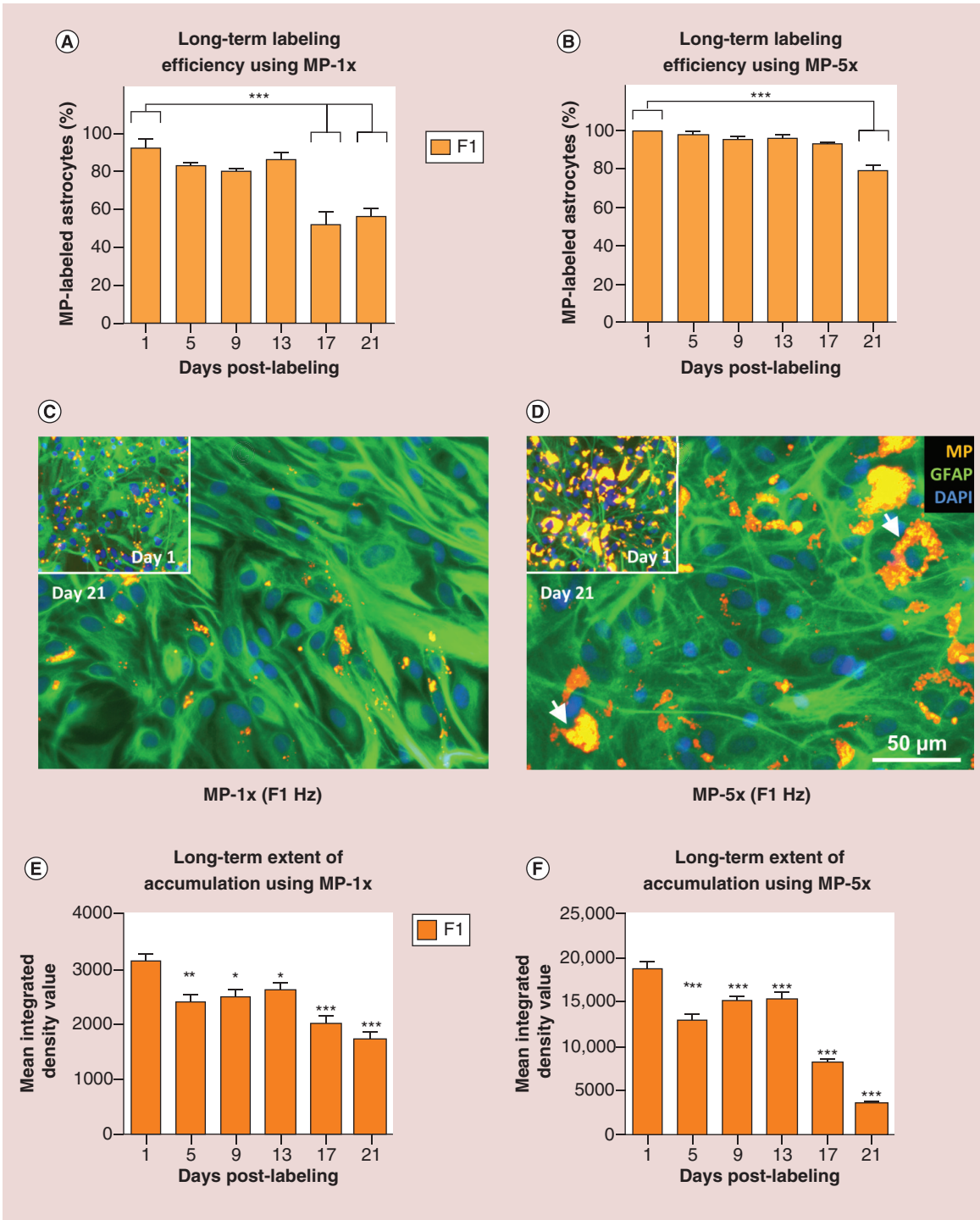

Figure 2. Long-term particle retention following 30-min application of an oscillating magnetic field. Bar charts showing proportions of labeled cells post-exposure to **(A)** MP-1x and **(B)** MP-5x particles (***p < 0.001). **(C & D)** Representative triple-merged images showing differences in levels of particle accumulation seen at day 1 (insets) and day 21 (main images) post-labeling with **(C)** MP-1x and **(D)** MP-5x particles. Arrows indicate 'high' levels of perinuclear labeling at day 21 with MP-5x particles. Bar charts displaying levels of **(E)** MP-1x and **(F)** MP-5x particle accumulation over 21 days following exposure to oscillating magnetic field. Within each particle condition versus day 1 (*p < 0.05; **p < 0.01; ***p < 0.001). All graphs: n = 3.
MP: Magnetic particle.

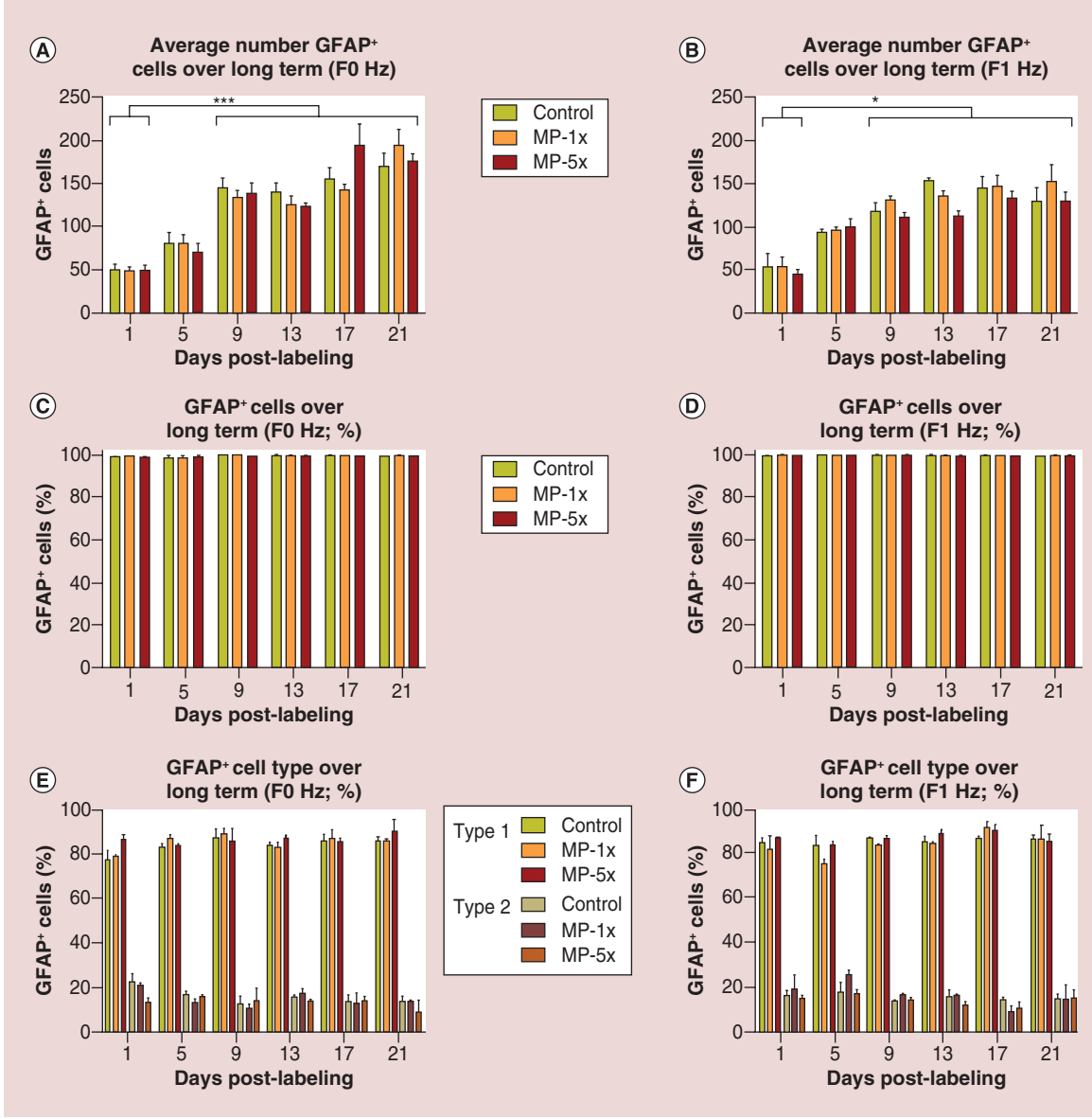

Figure 3. Safety assessment of long-term particle retention. Bar charts displaying astrocyte number per microscopic field post-labeling under **(A)** static and **(B)** oscillating magnetic field conditions (*p < 0.05; ***p < 0.001 vs day 1). Bar charts displaying proportions of GFAP+ cells post-labeling under **(C)** static field and **(D)** oscillating field conditions. Bar charts showing the distribution of astrocyte phenotypes post-labeling under **(E)** static field and **(F)** oscillating field conditions. All graphs: n = 3.

endocytotic neural cell (the astrocyte). When trying to achieve intracellular particle uptake by transplant populations, two delivery routes can be considered. Either intrinsic 'engulfing' behaviors of cells can be exploited or the membrane can be temporarily disrupted (e.g., by electroporation or ultrasound bubble stimulation [32]). As the former approach relies on natural biological mechanisms, it can be argued that this offers a safer and more attractive labeling approach, particularly when long-term safety (e.g., post-transplantation into host tissue) is a critical consideration [33,34]. Generally speaking however, the relative endocytotic behaviors of major neural transplant populations have been poorly documented. In turn, the combinatorial interactions of such engulfing mechanisms with the physicochemical properties of particles have received little attention, but remain an important issue when developing neural transplant labeling methods. It can be predicted that the effectiveness of different labeling approaches may vary depending on the cell type and particle deployed, and protocols will need to be tailored for individual cell/particle combinations.

As far as we are aware, the integrated density-based approach that we have utilized has never been

applied for quantification of nanoparticle uptake in cells, providing an unbiased, objective approach at the single-cell level while allowing for simultaneous evaluation of cellular morphological features and subcellular particle localization. We demonstrate that enhanced magnetite concentration in particles leads to greater particle loading in highly endocytotically active cells. This is associated with longer particle retention (≥21 days) versus cells loaded with particles of lower/no magnetite content. Greater labeling efficiency with high magnetite particles within a short time frame is likely attributable to accelerated gravitational particle sedimentation onto cells (due to the increased particle density), similar to the mechanism by which applied magnetic fields enhance transfection-grade MP-mediated gene transfer to target cells ('magnetofection'). This technique is now an established experimental procedure, used widely in laboratories in genetic modification protocols [35], but the compatibility of this approach with a wider range of MPs (e.g., clinical contrast agents or polymeric particles for drug delivery/magnetic cell targeting) is still relatively unexplored. With the MPs studied here, application of static or oscillating fields did not influence the proportions of cells labeled, but significantly enhanced the extent of intracellular particle accumulation. Together, our data suggest that a tailored combination of magnetic field application, high magnetite content particles and longer particle exposure times operate synergistically allowing for greater labeling efficiencies to be achieved. The prolonged retention of higher magnetite content particles is of high relevance for translational applications, where proliferative dilution/exocytosis and label loss are known to be major challenges [5,36]. It is possible that the longer retention is simply related to higher initial loading into cells, but we cannot rule out effects such as slower exocytosis of higher magnetite content particles. The combination of high survival of our transplant populations post-labeling in conjunction with such slower excretion, may serve to reduce the instance of 'false-positive' signals, due to secondary uptake by cell populations such as the resident astrocytes and microglial cells in host tissue.

The overall trend in labeling was similar to that seen in NSCs, although magnetic field application did significantly enhance labeling efficiency with low magnetite content particles in the latter [8]. We can speculate that the higher levels of endocytotic activity in astrocytes result in rapid particle uptake and outweigh the benefits of field application, particularly for higher magnetite content particles with more rapid sedimentary profiles. Further, microscopic observations reveal that for a given condition, the intracellular label per cell is greater in astrocytes versus NSCs. The reasons for this may be related to the morphological features and relative endocytotic profiles of the cells. For example, scanning electron micrographs show broad, flattened morphologies for astrocytes with elaboration of large amounts of cell membrane, and surface features suggestive of high cellular membrane activity (Figure 6A). By contrast, NSCs are bipolar cells with smaller cell

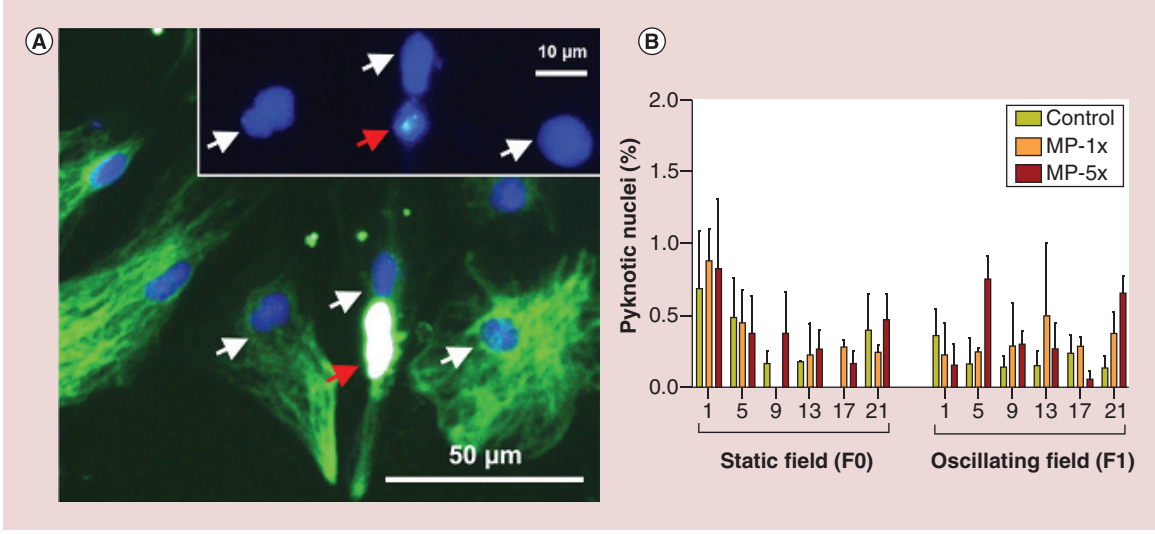

Figure 4. Identification of pyknotic cells in astrocyte cultures. **(A)** The viability of astrocyte cultures was assessed by identifying cells with fragmenting and condensing nuclei, frequently associated with aberrant glial fibrillary acidic protein staining and evidence of membrane detachment from the substrate, all features indicative of pyknosis (red arrows indicate same pyknotic cell in main image and inset). Healthy nuclei were associated with adherent cells and normal GFAP staining (white arrows indicate same cells in main image and inset). **(B)** The percentage of pyknotic nuclei did not vary across conditions or time points ($p > 0.05$). All graphs: $n = 3$.

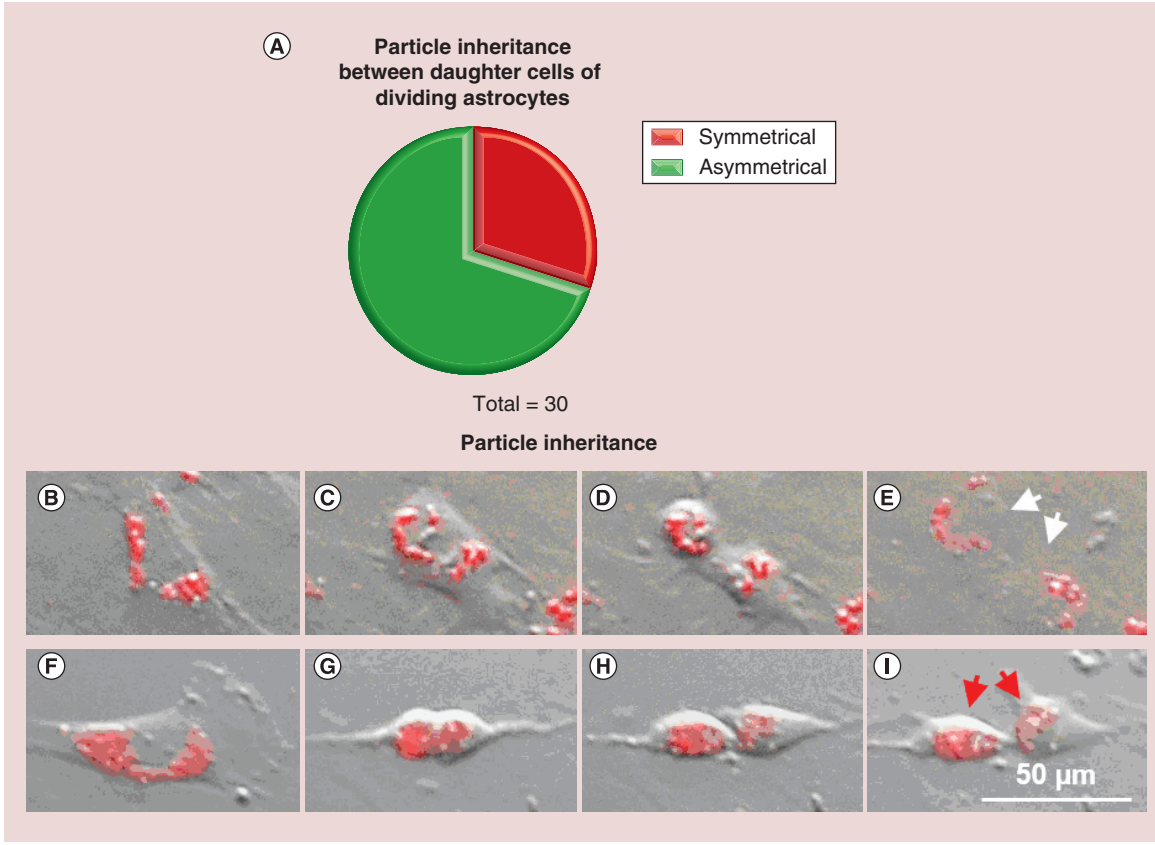

Figure 5. Particle inheritance in labeled astrocytes. (A) Pie chart displaying quantification of particle inheritance profiles in MP-labeled astrocytes. **(B–I)** Representative sequential still images from dynamic time-lapse imaging (Supplementary Data) of dividing astrocytes post-labeling with MP-5x particles without a magnetic field, showing examples of **(B–E)** symmetric and **(F–I)** asymmetric particle inheritance between daughter cells (arrows).
MP: Magnetic particle.

bodies, relatively quiescent membranes and less surface area available for particle uptake (Figure 6B); additionally label loss appeared to occur rapidly from NSCs (within 1 week, unpublished observations). Taken together, our findings highlight the importance of studying the interactions of neural cell type and endocytotic behaviors in conjunction with particle tailoring strategies.

They also indicate the potential benefits of 'endocytosis prestimulation' strategies in enhancing particle uptake, although such strategies are not routinely used currently in labeling protocols. These could include serum starvation [37], growth factor stimulation [38] or mechanical stimulation (as deforming or shear forces may stimulate endocytosis [28]). A less obvious point to note here is the importance of controlling cell densities for such work; in some populations containing actively dividing cells, there is a density-dependent inhibition of endocytosis which could negatively impact particle uptake processes [39]. The majority of neural transplant populations are highly proliferative and are usually propagated under growth factor drive, so the optimal cell densities for each cell type must be established and cellular confluence carefully monitored prior to particle addition in labeling protocols for biomedical applications.

The safety of the procedures utilized here was of paramount concern, given the combined variation of multiple parameters (particle properties, magnetic field application and duration of particle exposure). The procedures did not result in acute or long-term alterations in magnetolabeled cells, as determined by a spectrum of safety assays assessing survival, proliferative capacity and cell phenotype. This finding parallels our previous observations in NSCs, highlighting the neurocompatibility of the particles used [8]. The safety profile of these MPs could be attributable to the slow degradation profile of the PLA matrix component (limiting the rate at which iron leaches from degrading particles; rapid leaching is a major correlate of MP toxicity [40,41]), and is also consistent with the observed stability of intracellular MPs in astrocytes [7]. We have used histological analyses to evaluate particle safety, however astrocytes participate in complex signaling pathways and secrete several biomolecules needed for homeostatic function [16,18,19].

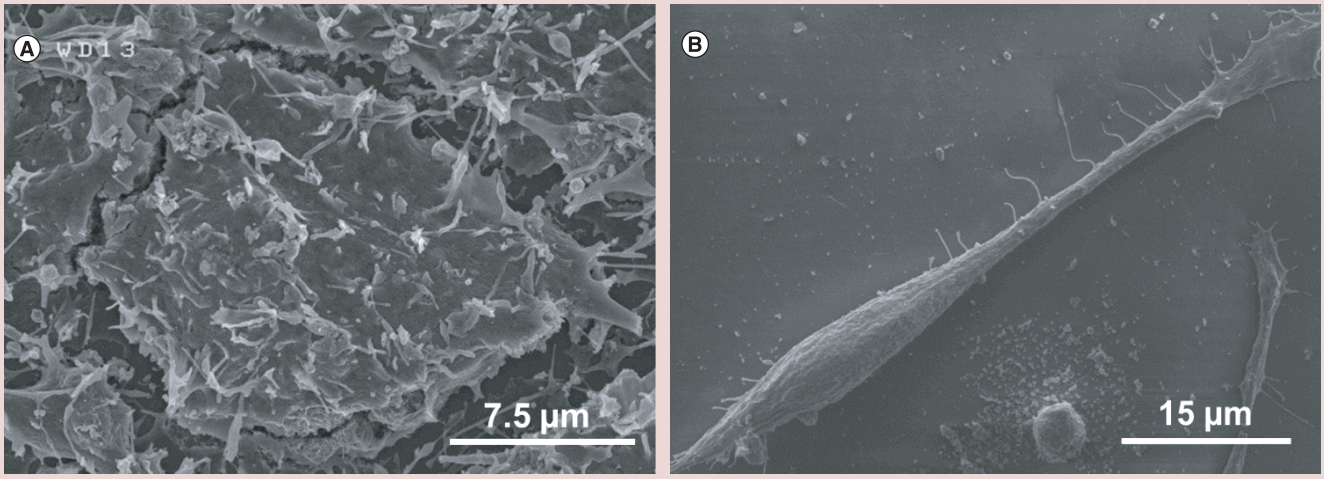

Figure 6. Cellular membrane activity features. Scanning electron micrographs of **(A)** an astrocyte, and **(B)** a neural stem cell, for comparison of typical morphological characteristics. Note the differences between the two cell types in terms of both quantity of membrane available for particle interactions, and the quantity of specific membraneous features associated with endocytotic activity, such as processes, filopodia and ruffles. Electron microscopy and neural stem cell culture methods published previously [21].

More detailed readouts of safety will require combined proteomic and bioinformatic pathway analyses of potential dysregulated processes in magnetolabeled astrocytes, to establish if particular secretory mechanisms or individual proteins involved in regenerative processes or signaling pathways are perturbed by the labeling procedures.

As far as we are aware, our study is the first to use a dynamic, live cell imaging approach to study the distribution (inheritance) of MPs into the progeny of neural cells derived from primary cultures. Our observations that particle inheritance is largely asymmetric (in that particle distributions are uneven between daughter cells, post-proliferation) are consistent with previ-

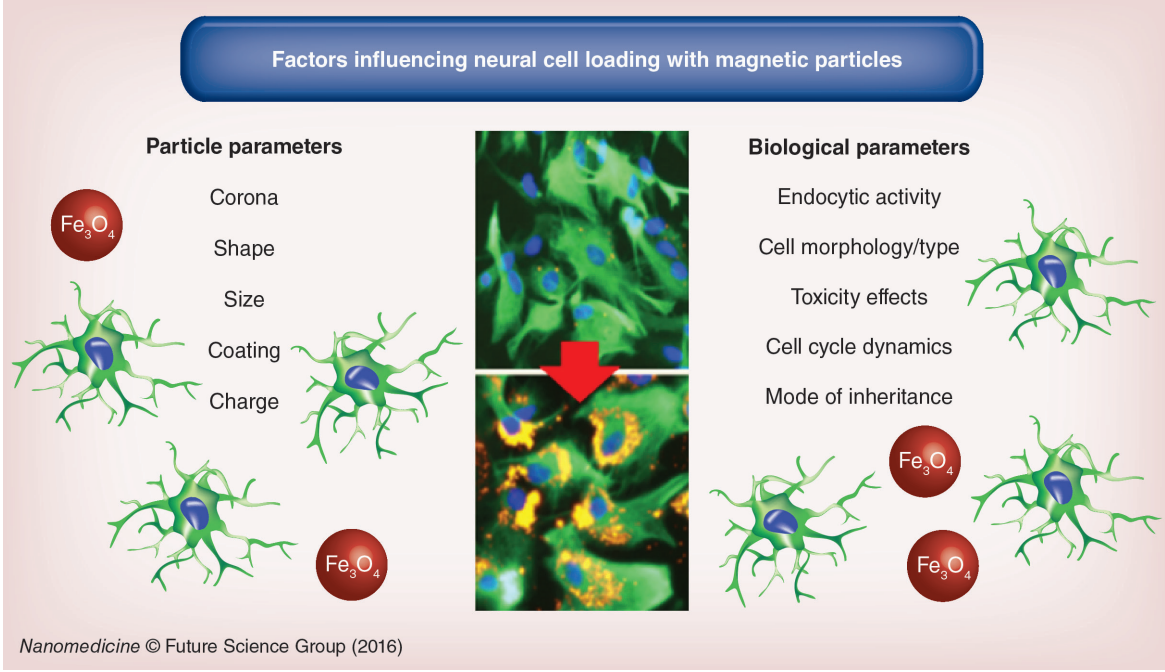

Figure 7. Factors influencing cellular particle uptake. Schematic diagram showing factors that influence cell loading with particles, illustrating the combined dynamics of the physicochemical characteristics of magnetic particles and the biological function of the cell. Micrograph shows MP-5x labeled astrocytes.
MP: Magnetic particle.

ous observations in cell lines wherein particle uptake and redistribution to daughter cells after mitosis, is a 'random' and asymmetric process [5,36,42,43]. The reasons for this uneven inheritance are unclear, but may relate to nonuniform distribution of MPs around the nuclear poles, which we consistently observed in the majority (ca. 75%) of labeled astrocytes. In turn, the reasons for this polarized initial distribution are unknown. Nonetheless, we consider that our findings do have significant implications for the use of the MP platform for biomedical applications involving astrocytes, and indeed other proliferative neural transplant populations. Label loss with cell division contributes to reduced efficacy of particle labeling for imaging/targeting applications; however our results indicate that not all transplant cells would be affected similarly in this regard. Unequal inheritance would imply that with each division, the utility of the intracellular MP label would exponentially diminish for a subpopulation of daughter cells. On the other hand, useful levels of labeling would persist in a larger subpopulation for a longer period of time (than would be predicted with symmetric inheritance) resulting in the ability to track overall biodistribution of the cellular graft, even if some cells are lost to the imaging process. Consequently, we believe that an understanding/characterization of the specific modes of particle inheritance in the progeny of a given labeled transplant population is an important parameter contributing to particle detection and must be taken into consideration in studies aiming to optimize MP labeling for neural cell therapies. In summary, a wide range of biological and chemical parameters exert an influence on the utility of the MP platform for neural transplantation therapies (Figure 7) but require systematic investigation. A detailed understanding of the relative importance of each of these parameters will allow for the tailored development of optimal labeling protocols for translational applications.

Conclusion

We show that initial greater MP cell loading achieved using high-magnetite-content polymeric particles in highly endocytotic neural cells, leads to enhanced cellular particle retention. The inheritance of particles into daughter cells, studied using dynamic live cell imaging, is predominantly asymmetric/unequal which we consider will have significant implications for tracking of labeled cells in imaging applications.

Supplementary data

To view the supplementary data that accompany this paper, please visit the journal website at: www.futuremedicine.com/doi/full/10.2217/NNM.15.202

Supporting information available: Video 1

Time-lapse micrographs of astrocyte culture 8 h post-addition of MP-5x particles. Arrows indicate two mitotic events, with examples of both asymmetric (red arrow, upper half, occurring at time point ~01:50; 70:30 inheritance split) and symmetric (white arrow, lower half, occurring at time point ~01:32; 50:50 inheritance split) MP inheritance.

Executive summary

Effective tracking of neural transplant populations using magnetic particles requires efficient cell labeling

- This involves high initial cellular loading and effective particle retention for clinically relevant periods in labeled populations.
- The synergistic interactions of biological properties such as cellular endocytotic capacity and physicochemical properties such as particle magnetite content in neural cells are not known.

Tailored nanoparticle & protocol design can increase the efficacy of transplant cell labeling

- Rapid and efficient particle uptake is achieved using particles with high magnetite content versus those with low/no magnetite.
- Higher magnetite particles are also associated with longer-term particle retention in cells.
- Applied magnetic fields/gradients did not affect cell labeling efficiency, but did increase extent of cell loading for higher magnetite particles.

Most neural transplant populations are proliferative & cell division dilutes particle label limiting tracking capacity

- Few studies have investigated the pattern of particle 'inheritance' into daughter cells post-division.
- Mitosis typically results in asymmetric particle distribution: daughter cells do not inherit equal proportions of particles.
- The implications for such unequal particle distribution remain to be established with complementary MRI studies.

Conclusion

- Our data can provide valuable information to transplantation biologists and materials chemists to develop effective protocols for labeling cell transplant populations.

Acknowledgements

Electron micrographs used with kind permission of AR Fernandes (Figure 3A), and CF Adams (Figure 3B); both Keele University.

Financial & competing interests disclosure

This work was supported by grants from the BBSRC (DM Chari), USA Award Number R01HL107771 from the National Heart, Lung and Blood Institute and Drexel University College of Medicine Clinical & Translational Research Institute, CTRI (B Polyak). SI Jenkins was supported by an EPSRC E-TERM Landscape Fellowship (EP/I017801/1). The authors have no other relevant affiliations or financial involvement with any organization or entity with a financial interest in or financial conflict with the subject matter or materials discussed in the manuscript apart from those disclosed.

No writing assistance was utilized in the production of this manuscript.

Ethical conduct of research

The authors state that they have obtained appropriate institutional review board approval or have followed the principles outlined in the Declaration of Helsinki for all human or animal experimental investigations. In addition, for investigations involving human subjects, informed consent has been obtained from the participants involved.

References

Papers of special note have been highlighted as:
• of interest; •• of considerable interest

1 Jenkins SI, Yiu HHP, Rosseinsky MJ, Chari DM. Magnetic nanoparticles for oligodendrocyte precursor cell transplantation therapies: progress and challenges. *Mol. Cell. Ther.* 2(1), 23 (2014).

• **Review of magnetic particle use for neural transplantation.**

2 Yanai A, Häfeli UO, Metcalfe AL *et al.* Focused magnetic stem cell targeting to the retina superparamagnetic iron oxide nanoparticles. *Cell Transplant.* 21(6), 1137–1148 (2012).

3 Chen J, Huang N, Maitz MF *et al.* Guidance of stem cells to a target destination *in vivo* by magnetic nanoparticles in a magnetic field. *ACS Appl. Mater. Interfaces* 5, 5976–5985 (2013).

4 Riegler J, Wells JA, Kyrtatos PG, Price AN, Pankhurst QA, Lythgoe MF. Targeted magnetic delivery and tracking of cells using a magnetic resonance imaging system. *Biomaterials* 31(20), 5366–5371 (2010).

5 Kim JA, Åberg C, Salvati A, Dawson KA. Role of cell cycle on the cellular uptake and dilution of nanoparticles in a cell population. *Nat. Nanotechnol.* 7(1), 62–68 (2012).

6 Jin H, Heller DA, Sharma R, Strano MS. Size-dependent cellular uptake and expulsion of single-walled carbon nanotubes: single particle tracking and a generic uptake model for nanoparticles. *ACS Nano* 3(1), 149–158 (2009).

7 Jenkins SI, Pickard MR, Furness DN, Yiu HHP, Chari DM. Differences in magnetic particle uptake by CNS neuroglial subclasses: implications for neural tissue engineering. *Nanomedicine (Lond.)* 8(6), 951–68 (2013).

8 Adams CF, Rai A, Sneddon G, Yiu HHP, Polyak B, Chari DM. Increasing magnetite contents of polymeric magnetic particles dramatically improves labeling of neural stem cell transplant populations. *Nanomedicine* 11(1), 19–29 (2015).

• **Examines influence of particle magnetite content on neural stem cell labeling.**

9 Yameen B, Choi W Il, Vilos C, Swami A, Shi J, Farokhzad OC. Insight into nanoparticle cellular uptake and intracellular targeting. *J. Control. Release* 190, 485–499 (2014).

10 Canton I, Battaglia G. Endocytosis at the nanoscale. *Chem. Soc. Rev.* 41, 2718–2739 (2012).

11 Verma A, Stellacci F. Effect of surface properties on nanoparticle–cell interactions. *Small* 6(1), 12–21 (2010).

12 Kou L, Sun J, Zhai Y, He Z. The endocytosis and intracellular fate of nanomedicines: implication for rational design. *Asian J. Pharm. Sci.* 8(1), 1–8 (2013).

13 Fernandes AR, Adams CF, Furness DN, Chari DM. Early membrane responses to magnetic particles are predictors of particle uptake in neural stem cells. *Particle & Particle Systems Characterization* 32(6), 661–667 (2015).

14 Davies SJA, Shih C-H, Noble M, Mayer-Proschel M, Davies JE, Proschel C. Transplantation of specific human astrocytes promotes functional recovery after spinal cord injury. *PLoS ONE* 6(3), e17328 (2011).

•• **Demonstrates utility of astrocytes as neural transplant population.**

15 Davies JE, Huang C, Proschel C, Noble M, Mayer-Proschel M, Davies SJA. Astrocytes derived from glial-restricted precursors promote spinal cord repair. *J. Biol.* 5(3), 7 (2006).

16 Chu T, Zhou H, Li F, Wang T, Lu L, Feng S. Astrocyte transplantation for spinal cord injury: current status and perspective. *Brain Res. Bull.* 107, 18–30 (2014).

•• **Reviews utility of astrocytes as neural transplant population.**

17 Barnett SC, Linington C. Myelination: do astrocytes play a role? *Neuroscientist* 19(5), 442–450 (2013).

18 Abbott NJ, Rönnbäck L, Hansson E. Astrocyte–endothelial interactions at the blood–brain barrier. *Nat. Rev. Neurosci.* 7, 41–53 (2006).

19 Walz W. Role of astrocytes in the clearance of excess extracellular potassium. *Neurochem. Int.* 36(4–5), 291–300 (2000).

20 Pickard MR, Jenkins SI, Koller C, Furness DN, Chari DM. Magnetic nanoparticle labelling of astrocytes derived for neural transplantation. *Tissue Eng. Part C* 17(1), 89–99 (2011).

21 Fernandes AR, Chari DM. A multicellular, neuro-mimetic model to study nanoparticle uptake in cells of the central nervous system. *Integr. Biol.* 6(9), 855–861 (2014).

22 Környei Z, Czirók A, Vicsek T, Madarász E. Proliferative and migratory responses of astrocytes to *in vitro* injury. *J. Neurosci. Res.* 61(4), 421–429 (2000).

23 Morrison RS, de Vellis J, Magoun HW. Growth of purified astrocytes in a chemically defined medium. *Proc. Natl Acad. Sci. USA* 78(11), 7205–9 (1981).

24 McCarthy KD, de Vellis J. Preparation of separate astroglial and oligodendroglial cell cultures from rat cerebral tissue. *J. Cell Biol.* 85(3), 890–902 (1980).

25 Pickard MR, Chari DM. Enhancement of magnetic nanoparticle-mediated gene transfer to astrocytes by "magnetofection": effects of static and oscillating fields. *Nanomedicine (Lond.)* 5(2), 217–232 (2010).

26 MacDonald C, Barbee K, Polyak B. Force dependent internalization of magnetic nanoparticles results in highly loaded endothelial cells for use as potential therapy delivery vectors. *Pharm. Res.* 29(5), 1270–81 (2012).

27 Johnson B, Toland B, Chokshi R, Mochalin V, Koutzaki S, Polyak B. Magnetically responsive paclitaxel-loaded biodegradable nanoparticles for treatment of vascular disease: preparation, characterization and in-vitro evaluation of anti-proliferative potential. *Curr. Drug Deliv.* 7, 263–273 (2010).

28 McBain SC, Griesenbach U, Xenariou S *et al.* Magnetic nanoparticles as gene delivery agents: enhanced transfection in the presence of oscillating magnet arrays. *Nanotechnology* 19(40), 405102 (2008).

29 Adams CF, Pickard MR, Chari DM. Magnetic nanoparticle mediated transfection of neural stem cell suspension cultures is enhanced by applied oscillating magnetic fields. *Nanomedicine* 9(6), 737–41 (2013).

30 Fouriki A, Farrow N, Clements MA, Dobson J. Evaluation of the magnetic field requirements for nanomagnetic gene transfection. *Nano Rev.* 1, 1–5 (2010).

31 Geppert M, Hohnholt MC, Thiel K *et al.* Uptake of dimercaptosuccinate-coated magnetic iron oxide nanoparticles by cultured brain astrocytes. *Nanotechnology* 22(14), 145101 (2011).

32 Chaudhuri A, Battaglia G, Golestanian R. The effect of interactions on the cellular uptake of nanoparticles. *Phys. Biol.* 8(4), 046002 (2011).

33 Krueger WHH, Madison DL, Pfeiffer SE. Transient transfection of oligodendrocyte progenitors by electroporation. *Neurochem. Res.* 23(3), 421–426 (1998).

34 Guo Z, Yang N-S, Jiao S *et al.* Efficient and sustained transgene expression in mature rat oligodendrocytes in primary culture. *J. Neurosci. Res.* 43, 32–41 (1996).

35 Plank C, Zelphati O, Mykhaylyk O. Magnetically enhanced nucleic acid delivery. Ten years of magnetofection-progress and prospects. *Adv. Drug Deliv. Rev.* 63(14–15), 1300–1331 (2011).

•• **Comprehensive review of magnetically assisted magnetic particle delivery.**

36 Errington RJ, Brown MR, Silvestre OF *et al.* Single cell nanoparticle tracking to model cell cycle dynamics and compartmental inheritance. *Cell Cycle* 9(1), 121–130 (2010).

37 Geppert M, Petters C, Thiel K, Dringen R. The presence of serum alters the properties of iron oxide nanoparticles and lowers their accumulation by cultured brain astrocytes. *J. Nanoparticle Res.* 15(1), 1349 (2013).

38 Kerr MC, Teasdale RD. Defining macropinocytosis. *Traffic* 10, 364–371 (2009).

39 Davies PF, Ross R. Growth-mediated, density-dependent inhibition of endocytosis in cultured arterial smooth muscle cells. *Exp. Cell Res.* 129, 329–336 (1980).

40 Petters C, Thiel K, Dringen R. Lysosomal iron liberation is responsible for the vulnerability of brain microglial cells to iron oxide nanoparticles: comparison with neurons and astrocytes. *Nanotoxicology* (2015) (Epub ahead of print).

41 Soenen SJH, Himmelreich U, Nuytten N, Pisanic TR 2nd, Ferrari A, De Cuyper M. Intracellular nanoparticle coating stability determines nanoparticle diagnostics efficacy and cell functionality. *Small* 6(19), 2136–2145 (2010).

42 Rees P, Wills JW, Brown MR *et al.* Nanoparticle vesicle encoding for imaging and tracking cell populations. *Nat. Methods* 11(11), 1177–1181 (2014).

43 Summers HD, Brown MR, Holton MD *et al.* Quantification of nanoparticle dose and vesicular inheritance in proliferating cells. *ACS Nano* 7(7), 6129–6137 (2013).

• **Investigates particle distribution into progeny of dividing cells.**